AN ABSTRACT OF THE THESIS OF

Leanne Renee Heck for the dual degree of Master of Science in Civil Engineering and Forest Products presented on November 6, 1997. Title: Evaluation of the Torsion Test for Determining the Shear Strength of Structural Lumber.

Redacted for privacy

Abstract approved: _____
Thomas H. Miller

Redacted for privacy

Abstract approved: _____
Rakesh Gupta

The torsion test was evaluated as a method for determining the shear strength of full-size structural lumber. The evaluation involved an experimental length study, an experimental depth study, and a finite element study.

The length study consisted of fifty nominal 2x4 specimens, ten specimens for each length, and ten American Society for Testing and Materials (ASTM) shear blocks. One 14 foot long board yielded one specimen for each length: (a) 21.0", (b) 28.5", (c) 32.0", (d) 35.5", (e) 39.0", and (f) an ASTM D143-94 shear block. The statistical analysis revealed no evidence that the length affected the shear strength.

The depth study consisted of fifty specimens, ten specimens for each depth: (a) 2x4, (b) 2x6, (c) 2x8, (d) 2x10, and (e) 2x12. In addition, fifty ASTM shear blocks, one block for each specimen, were tested. The statistical study

did not reveal convincing evidence of a depth effect on shear strength, even after accounting for specific gravity and shear span as covariates.

Failure modes for the torsion samples involved a longitudinal shear crack at the mid-point of the longest side, which propagated toward the ends of the specimen and through the cross section perpendicular to the growth rings.

The finite element model revealed that uniform shear stress occurs within the shear span, which begins and ends a distance of approximately two times the depth plus the grip distance away from each end of the member. In addition, torsion theory verified that the experimental shear failure plane that occurs within the shear span is parallel to the grain and the shear slippage is also parallel to the grain, similar to the known shear failure in specimens subjected to bending loads.

Based on the results of this study, the torsion test is the best practical method to determine the pure shear strength of full-size structural lumber, because the test yields 100% shear failures and the specimen is in a state of pure shear stress.

Evaluation of the Torsion Test for Determining the Shear Strength of Structural Lumber

by

Leanne Renee Heck

A THESIS

submitted to

Oregon State University

in partial fulfillment of
the requirements for the
degree of

Master of Science

Presented November 6, 1997
Commencement June 1998

Master of Science thesis of Leanne Renee Heck presented on November 6, 1997

APPROVED:

Redacted for privacy

Co-Major Professor, representing Civil Engineering

Redacted for privacy

Co-Major Professor, representing Forest Products

Redacted for privacy

Head of Department of Civil, Construction, and Environmental Engineering

Redacted for privacy

Head of Department of Forest Products

Redacted for privacy

Dean of Graduate School

I understand that my thesis will become part of the permanent collection of Oregon State University libraries. My signature below authorizes release of my thesis to any reader upon request.

Redacted for privacy

Leanne Renee Heck, Author

Acknowledgments

I would like to thank my major professors, Dr. Thomas Miller and Dr. Rakesh Gupta for the opportunity to research the shear strength of structural lumber at Oregon State University and for their guidance during the project. I also appreciated my three other committee members, Dr. Barbara Gartner, Dr. Solomon Yim, and Dr. Timothy Kennedy for their contributions and advice on this project. In addition, I acknowledge Dr. Willie Rochefort for his participation as the graduate school representative, and Dr. Robert Leichti for additional research advice.

I also thank the Oregon State University Forest Products Department for providing the funding for this project.

To make the electronic recording torsion system possible, I recognize two other staff members, Andy Brickman and Milo Clauson, who shared their knowledge and provided assistance.

Finally, I would especially like to thank God, my family, and my close friends, who provided the unlimited emotional support and confidence in my abilities as an engineer.

Table of Contents

Table of Contents (Continued)

Table of Contents (Continued)

List of Figures

List of Figures (Continued)

List of Figures (Continued)

List of Figures (Continued)

List of Tables

List of Tables (Continued)

List of Appendices

List of Appendices Figures

Dedication

I would like to dedicate my thesis to my Savior, who is the true strength behind all my accomplishments, who answers my requests in ways I can never imagine, and who fills me with incomprehensible peace. But most importantly, I praise Him for His sacrifice so that I would live.

> *Be anxious for nothing, but in everything by prayer and supplication with thanksgiving let your requests be made known to God. And the peace of God, which surpasses all comprehension, shall guard your hearts and your minds in Christ Jesus.*
>
> *Philippians 4: 6 and 7*

In addition, I would also like to dedicate my thesis to my best friend, who provided humor to brighten even an ugly day, to my sisters, who encouraged me in my never ending profession as a student, and to my Mother and Father, who sacrificed so much for me. All of them are truly gifts from God and provide daily unconditional love, unlimited emotional support, and immeasurable encouragement.

Evaluation of the Torsion Test for Determining the Shear Strength of Structural Lumber

1. Introduction

As with other materials used in design, the structural properties of wood must be known in order to design wood structures or structural components. The properties of wood must be determined with an understanding of the material's mechanics which include stiffnesses and strengths in bending, compression parallel and perpendicular to grain, tension, and shear. Historically these properties have been determined using small clear blocks of wood with straight grain and free from defects. The current National Design Specification for Wood Construction (AFPA, 1991) provides design values for strengths in bending, compression parallel to the grain, and tension parallel to the grain based on testing large scale specimens of structural sizes. Although compression perpendicular to the grain and shear strengths remain based on small blocks, shear strength testing of full-size structural lumber is gaining more attention. For shear strength testing of structural sizes, shear failures can be achieved using short and deep beams under bending loads or using any size beam under torsion loads. Structural lumber specimens provide additional insights to effects on mechanical properties due to grain slope and defects that small clear blocks may not provide.

Although other mechanical failures, such as bending failures or compression parallel to the grain failures, are more common than shear failures, shear failures do occur in service and must be accounted for in design. Shear failure occurs when the material is unable to continue resisting internal slipping of parallel planes relative to one another and a split occurs between these planes (Wood Handbook, 1987).

Shear strength of wood has been examined by several researchers (Riyanto and Gupta, 1997; Rammer et al., 1996; Riyanto, 1996; Asselin et al., 1995; Longworth, 1977), and the studies imply that (1) the shear strength obtained from small blocks of wood without defects is not representative of the shear strength of structural lumber with defects, (2) the shear strength is dependent upon the method of testing, and (3) the shear strength is affected by the size of the specimen. The current standard used to determine the allowable shear strength of structural lumber is based on a small block with straight grain and without defects (ASTM, 1996a). Other testing methods have been used to determine the shear strength of structural lumber to compare to the shear strength of the small block.

For bending specimens, the shear stress is uniform across the width (fore example 1.5 inches for a nominal 2x4 beam), but as the specimen is failing in shear there are interactions of compressive stress parallel to the grain, compressive stress perpendicular to the grain, and tensile stress. However, for a specimen subjected to torsion, the specimen experiences pure shear, but the stress is not uniform across the width or the depth of the specimen. This

research examines the shear strength of structural lumber specimens subjected to torsion. The specific objectives for this study are the following:

- Evaluate the torsion test as a method to determine shear strength of structural lumber with experimental studies examining
    - length effects on shear strength,
    - depth effects on shear strength, and
    - differences between the ASTM (1996a) clear block shear strength and the torsion test shear strength.
- Develop a finite element model to represent a 2x4 and 2x12 wood beam experiencing torsion that will
    - enhance the understanding of torsion theory applied to these beams,
    - determine shear stress distribution for torsion specimens and compare it with the known shear stress distribution of bending specimens, and
    - determine the distance from the beam ends where the shear stress distribution becomes uniform.

2. Literature Review

Historically, mechanical properties for wood were determined using small clear wood specimens. Recently, bending strength, compression strength parallel to the grain, and tensile strength parallel to the grain have been determined using full size structural lumber specimens (Green, 1989). Shear strength, however, is still based on a small clear block.

There are two types of specimens that could be used to determine mechanical properties of wood materials: (1) small, clear specimens without defects and (2) large specimens with defects, similar in size and shape used in design as structural components. When using small, clear specimens, the material mechanical property determined reflects ideal material conditions specifically homogeneity. However, when testing a larger specimen of structural component size, the mechanical properties determined more accurately reflect material with all the natural characteristics and design conditions.

Diverse methods for various materials have been employed to determine the shear strength of the material. Examining some of these methods will provide insights to a reliable method to determine the shear strength of wood.

2.1 Steel

Several methods have been used to determine the shear strength of steel. Some of these methods include experimental testing or theoretical analysis or a combination of both.

A common way to determine shear strength for steel is the theoretical analysis using strength failure theories. The strength failure theories are used to determine allowable stresses for complicated stress conditions for practical design by predicting failures under combined stresses using simple tension or compression test results obtained from the material under investigation (Timoshenko, 1956).

Four strength theories are used to evaluate strength properties for design in many materials, (1) maximum normal stress theory, (2) maximum strain theory, (3) maximum shear stress theory, and (4) maximum distortion energy theory (Timoshenko, 1956). The latter two theories are the most common strength theories applied to designs using steel. The maximum shear stress theory, which agrees better with experimental results for ductile materials, determines failure by assuming that yielding occurs when the maximum shear stress equals half the tension yield stress (Timoshenko, 1956). Maximum distortion energy theory assumes that yielding will occur when the distortion energy reaches a critical value (Timoshenko, 1956).

When considering steel, with a Poisson's ratio of 0.3, subjected to pure shear, the maximum shear theory and the maximum distortion energy theory

yield Equation 2.1, where τ_{yp}= shear stress at the yield point and σ_{yp}= normal stress at the yield point (Timoshenko, 1956).

Maximum shear theory

$$\tau_{yp} = 0.5\sigma_{yp} \tag{2.1a}$$

Maximum distortion energy theory

$$\tau_{yp} = 0.62\sigma_{yp} \tag{2.1b}$$

The maximum distortion energy theory has been recommended, and is currently used, when designing with steel; therefore the shear yield stress for steel is $0.6\sigma_{yp}$ (Gaylord et al., 1992; McGuire, 1968; AISC, 1994). As a result, for common A-36 steel, the allowable shear strength is 21.6 ksi.

Often, steel is used to fabricate various shapes to use as components in a structure, for example, I-beams, T-beams, channel sections, and angles; each component type may react differently under shear failures. When designing with steel, the maximum shear value, $0.6\sigma_{yp}$, is used. However, laboratory testing of full-size steel members is often performed to understand how the member reacts under a given loading condition. To test the shear strength of large specimens, the three point and four point flexure methods are often used (Elgaaly et al., 1996; Roberts et al., 1995; AISI, 1969). In addition, the torsion test has been used to determine the shear stress distribution in a full-size member (Lyse and Johnston, 1936).

Elgaaly et al. (1996) researched the shear strength of steel beams with corrugated webs--a method of reinforcement by shaping the steel web into

parallel grooves and ridges for out-of-plane stiffness and buckling strength without the use of vertical stiffeners. The three point flexure method was used to test the corrugated webs for shear strength. Five different shear ratios were examined (half the shear span divided by the depth of the specimen, 1:1, 1.5:1, 2:1, 1:1.5, 1:2). Through this study, the effects of corrugated webs, which are not considered in the theories discussed previously, the shear strength of the member could be determined (Elgaaly, et. al., 1996). The results indicated that the buckling stress formulas for flat isotropic or orthotropic plates adequately predicted the shear strength observed of the experimental study.

The three point flexure method was also used for the shear strength testing of plate girders with longitudinal stiffeners (AISI, 1969). In this case, the shear ratio was 3.0, and the shear strength was found to increase as a result of the stiffeners from 6% to 38% compared to theoretical strengths of similar non-stiffened girders (AISI, 1969). The theoretical strengths determined for the non-stiffened girders is not related to the strength theories discussed previously. This research also determined that neither buckling theory nor beam theory can be used to predict the shear strength of longitudinally stiffened plate girders (AISI, 1969). The torsion test has been used to test standard steel H-sections and I-sections to furnish a reliable basis for the design of structural members subjected to torsion loads (Lyse and Johnston, 1936). Although the main objective of this research was to determine the torsional rigidity of the member, small specimens were used to determine the tensile strength and the shear strength of the material by standard tensile tests, round bar torsion tests, and

slotted plate shear tests. In addition, with the torsional rigidity constant developed through the experimental studies in conjunction with the shear stress equations developed through theoretical analysis, the shear stress in the flanges and the in the web could be calculated (Lyse and Johnston, 1936).

2.2 Concrete

Several types of methods have been used in the shear testing of concrete materials. Some experiments required small size specimens while other methods required full-size beams.

In one research study three different shear tests for concrete were performed: (1) the indirect shear test, (2) the direct double surface shear test, and the Iosipescu shear test (Horiguchi, et. al., 1988). The samples used were small in size with the largest dimension of 400 millimeters. The shear values appeared to vary using each of these test methods. On average, the direct double surface shear test values, 1565 psi (coefficient of variation of 32.2%), were 83% higher than those from the indirect method, 895 psi (coefficient of variation of 35.5%) , and the Iosipescu shear test, 1880 psi (coefficient of variation of 32.9%), values were 123% higher than those from the indirect method. This research implies that shear strength may be affected by the testing method.

In some cases reinforcing materials, such as steel fibers, can be incorporated into the concrete mixture and then be examined for their effect on shear strength using small specimens. However, small specimens are often too small to accommodate reinforcing bars; in this case, the concrete is tested as a large specimen. In other cases, unique shapes, such as deep beams or corbels, are tested as full-size specimens. Small specimens cannot be used alone to predict shear capacities for unique shapes used in design, but rather these small specimens focus on the shear strength independent of specimen size. When testing large specimens the interactions of the concrete and reinforcing must be observed and quantified when the member fails in shear.

In one study (Rebeiz et al., 1995), a resin binder made of plastic waste was used in the concrete mixture rather than the normal water and cement binder. In addition, steel reinforcement was used in the specimens. Using a shear ratio, in this study the shear ratio was defined as the shear span divided by depth, range from 1 to 3.6, concrete beams were tested using the four point flexure test. Several modes of failure occurred, but none of the modes exhibited a pure shear failure. The most common of the failures was a shear-tension failure where the initial failure was shear and the final catastrophic failure was the splitting of the concrete along the reinforcing steel near the support (Rebeiz, et al., 1995). Shear-compression, diagonal tension, crushing of the concrete with shear cracks, and flexure summarize the remaining failure modes. Small

specimens using the concrete mixture with the plastic resin material with or without steel reinforcement were not tested.

Other factors can affect the shear strength of concrete. The three point flexure method was used to test the shear capacity of steel-reinforced deep concrete beams near 1 to 1.5 shear ratio (Zielinski et al., 1995). Most failure modes showed an initial flexural crack between the supports and an inclined crack following the initial crack. This inclined crack then propagated toward the shear interface. By testing the large beams, the effects of the steel reinforcement and geometry of the beam can be observed for various concrete beam shapes often used in design.

Additional studies have used the four point flexure test method to determine the shear capacity of concrete (Rebeiz et al., 1995; Siao, 1995; Sharma, 1986; Rajagopalan and Ferguson, 1968; Salandra et al., 1989; Elzanaty et al., 1986). Although not as common as the four point flexure test, other studies have used the three point flexure test method to determine the shear capacity of concrete (Yuliang et al., 1994; MacLeod and Houmsi, 1994). Yuliang et. al. (1994) noticed that the mode of failure and the shear strength were influenced by the shear span to depth ratio.

Bending tests are often used to determine the shear capacity of a concrete specimen (Rebeiz et al., 1995; Siao, 1995; Sharma, 1986; Rajagopalan and Ferguson, 1968; Salandra et al., 1989; Elzanaty et al., 1986), and torsion tests are often used to determine the torsional behavior of concrete beams (Bakhsh et al., 1990). Bakhsh et al. (1990) tested high strength concrete

rectangular beams in torsion to study the torsional behavior of the beam and correlate the torsional strength to the modulus of rupture and the spitting tensile strength. The relationships observed compared well with other research results discussed in the study (Bakhsh et al., 1990) suggesting the torsion test is an excellent method to use to investigate the torsional strength. However, no suggestion indicated that the torsion test would be effective to determine the shear strength of concrete beams.

2.3 Plastics and composites

Most of the literature indicated that plastics and composites were tested for shear strength using small specimens. No information was found which reported the use of large size structural component testing for plastics or composite materials.

To determine the shear strength of plastics, ASTM has approved a standard using a punch tool (ASTM, 1996d; ASTM, 1958). This method uses a small specimen with thickness no greater than one half of an inch. The force measured to punch out a circular section in the middle of the specimen is used to calculate the shear strength of the specimen.

Although Goldenberg et al. (1959) studied shear strength of plastics, they outlined four general requirements, independent of the tested material, for a shear strength test method: (1) deformations should result from pure shear stress, (2) load application should yield pure shear, (3) shear stress distribution

should be uniform to decrease the influence of stress concentration points, and (4) specimen shape should yield results equal to all other practical cases in which the material is subjected to shear stress. After experimental research with various specimen shapes, an arrow shape, which provides double shearing, was proposed as an improved method over the ASTM (1958) standard. Goldenberg et al. (1959) found that at the failure cross section, the stress was nearly uniformly distributed pure shear, the specimen did not require a special testing apparatus, and the specimen could be quickly clamped and tested. These findings were positive advantages over the 1958 ASTM (1958) specifications.

Goldenberg's comparison of shear strength values from his shape and the ASTM (1958) shape indicated a 20% higher shear strength for his shape. Since the current ASTM (1996d) specification requires the same shear tool, the same specimen dimensions, and the same shear calculations as the previous standard, Goldenberg's results apply to today's standard as well. Thus, Goldenberg's comparison study implied that the shear strength of plastic is dependent on the method of testing.

Another ASTM (1996i) specification provided guidelines for obtaining horizontal shear strength of pultruded reinforced plastic rods using the short beam method. For this test, a small, plastic specimen with reinforcement was subjected to a three point load to test for shear strength. The diameter depended upon the span length provided by the loading apparatus. ASTM D 4475-85 (1996i) recommended that the shear ratio (shear span to diameter)

range from three to six. The standard also indicated that research showed that shear strength was a function of support span to specimen diameter ratio for most materials; therefore, the shear strength obtained was the "apparent horizontal shear strength" since it is not based on a state of pure shear stress (ASTM, 1996i).

Composites relate more closely to wood than some other materials mentioned previously in that composites are often anisotropic or orthotropic; similarly, wood is orthotropic. As a result, shear tests used for composites may be applicable for wood shear testing, but the only literature available used small composite specimens rather than large specimens.

Several methods to determine the shear strength of anisotropic and orthotropic composite materials, for example boron/aluminum and graphite/epoxy have been researched (Gipple and Hoyns, 1994; Odom et. al., 1994; Morton et. al., 1992; Pindera et al., 1990; Pindera, 1989; Yen et al., 1988; Lee and Munro, 1986; Arcan, 1984; Walrath and Adams, 1983; Novak, 1969). The various methods include, the Iosipescu method, the Arcan method, the three and four point bending methods, and the torsion method. The Iosipescu uses a small beam about 2 inches long and 0.1 inch thick with two 90° notches, one on the top of the beam and one on the bottom of the beam. The Arcan method uses a butterfly shaped specimen with a height of 3.5 inches and a thickness near 1 inch. Small size beams, of approximate dimensions 0.1 inch thick and 0.25 inch wide, are used for the short beam three- and four- point bending tests. All of the

specimens used in these methods were small specimens and determined the in-plane shear strength and/or the shear modulus of the material. Each of these methods have advantages and disadvantages when determining shear strength.

A cost effective method to test for shear strength, and the method most accepted is the Iosipescu shear test because of the pure shear state of stress and fabrication ease (Gipple and Hoyns, 1994; Odom et. al., 1994; Morton et. al., 1992; Pindera et al., 1990; Pindera, 1989; Arcan, 1984; Walrath and Adams, 1983). Although the specimen is subjected to pure shear at the line of failure, the Iosipescu test has disadvantages. Morton et al. (1992) identified that the shear stress was not uniform in the specimen. They showed that the fixture set up and orthotropic material influenced the shear strain measurements while the main objective of Odem et al. (1994) was to identify how the fixture interacted with the shear specimen. Two main disadvantages of the fixture were the lack of asymmetric loading caused by unequal compliance between the two halves of the fixture and possible fixture misalignment which could cause substantial effects in the modulus measurements.

The Arcan method allows for uniform pure shear stress to occur at a section of the test specimen. However, instability, grip failure, adhesive, and specimen thickness requirement problems may provide inaccurate results (Yen et. al., 1988).

Not only have the three and four point flexure test methods been used for obtaining the shear strength of wood, but these flexure tests have also been used to obtain the shear strengths of composites using small specimens (Adams and Lewis, 1995; Whitney and Browning, 1985). The flexure methods showed that the shear strength was "strongly influenced" by the support span to specimen thickness ratio and the specimen thickness (Adams and Lewis, 1995). To a "lesser extent" the specimen width to thickness ratio and diameter of the loading cylinder influenced the shear strength (Adams and Lewis, 1995). The trend showed a decrease in shear strength as the support span to specimen thickness ratio increased (Adams and Lewis, 1995). Although shear failures were observed in most specimens, the transverse compressive stresses, caused by the support and load cylinders, could have suppressed the shear failures as the distance between the load points and the support points decreased (Adams and Lewis, 1995).

Due to specialized fabrication techniques that increased the specimen fabrication costs, torsion specimens were not often used to determine the shear strength of anisotropic or orthotropic composites (Pindera, 1989; Walrath and Adams, 1983). Although specimens were difficult and expensive to fabricate, the in-plane and out-of-plane shear moduli were determined for two composite materials, graphite/epoxy and silicon carbide/glass ceramic (Tsai and Daniel, 1990) using solid circular specimens in torsion. Previous research had opted for circular tube specimens (Lee and Munro, 1986). Using a circular tube, rather than a solid cylinder, allowed the wall of the tube to be thin enough, when

compared to the radius, so that the shear stress was assumed uniform (Lee and Munro, 1986). In other research, Novak (1969) tested solid circular rods (1/4 inch in diameter and 4.5 inches long) in torsion to determine the shear strength of graphite reinforced epoxy composites. Novak (1969) also investigated the filament-epoxy bond response to a shear failure.

2.4 Wood

The shear strength design values found in the National Design Specification (AFPA, 1991) are based on small, clear block specimens tested according to ASTM (1996a) standards. Several researchers have shown that this ASTM block yields different shear strength values than other methods (Rammer et al., 1996; Riyanto, 1996; Longworth, 1977; Ylinen, 1963).

The shear strength value obtained from the ASTM test is multiplied by various factors to determine allowable shear strength: (1) duration of load (2) checks and (3) factor of safety, which includes but is not limited to ring angle, seasoning, and fabrication errors (Ethington et al., 1979). The resulting factor of 4.1 (Ethington et al., 1979) is applied to the shear stress determined by the ASTM (1996a) standard, the final shear stress is known as the allowable shear strength. After obtaining the allowable shear strength, which is the shear strength divided by the 4.1 factor, a strength ratio based on ASTM D245-93

(1996c) is also applied to the allowable shear strength to account for strength reductions due to knots, slope of grain, end splits, and checks.

Other methods to determine the shear strength of wood have been examined, such as Arcan (Liu, 1984; Liu and Floeter, 1984), notched beam, (Hilbrand, 1964; Ylinen, 1963; Radcliffe and Suddarth, 1955), modified block shear specimen (Ylinen , 1963; Radcliffe and Suddarth, 1955), double shear specimen (Ylinen, 1963), shear specimen with oblique grain (Ylinen, 1963), panel shear specimen (Norris, 1957), and torsion (Ylinen, 1963). In general, the shear strength appeared to be dependent upon the method of testing (Liu, 1984).

Ylinen (1963) performed a comparison of his torsion test to the British standard cube test and the ASTM block shear test; he observed that "wood possesses a substantially higher shearing strength" when his torsion test is followed. His data of Finnish pine (*Pinus silvestris*) (Ylinen, 1963) indicated that the torsion test using a solid circular specimen yielded a 32% and 27% higher shear strength than the ASTM (1996a) shear block and the British cube respectively. However, Noris (1957) performed a study using a panel of wood which yielded shear strength values similar to the ASTM (1996a) shear block test. Hilbrand's study (1964) involved testing equipment that used roller bases and non-roller bases; the roller test arrangements included the notch beam test and the non-roller test arrangements included the ASTM (1996a) shear block test. The results of the study implied that testing equipment may also affect the

shear strength values: the non-roller test showed a higher shear strength value when compared to the roller equipped apparatus. For example, Hilbrand's (1964) study of southern yellow pine showed a 27% higher the tangential shear strength for a non-roller test set up using the ASTM (1996a) shear block compared to a roller test set up using the ASTM(1996a) shear block; the same comparison of shear tests was made using overcup oak and the tangential shear strength was only 17% higher for the respective tests. Although Ylinen (1963) and Hibrand (1964) observed different shear strength results by employing different shear strength test equipment Noris (1957) observed a percentage as low as 5% to as high as 25% difference between the Douglas-fir shear strength obtained by his panel test and the standard ASTM (1996a) shear block test suggesting that the panel test may report shear strength values comparable with the ASTM (1996a) shear strength test.

Ylinen (1963) observed a difference between the shear strength from the ASTM standard method when compared to other methods. One method examined in the comparison was the torsion test. In his torsion test specimens, the longitudinal shear followed a plane of weakness and shear failure occurred in the light spring wood tissue tangential to the growth rings. This type of failure confirmed that shearing strength determined by a Ylinen's (1963) torsion test was not identical with the shear strength parallel to the grain in a tangential plane, as determined by other tests such as the British standard cube test (Ylinen, 1963). As will be discussed in Chapter 6, Analytical Results and

Discussion, the failures observed in the current study occurred along a plane of weakness with shear strength parallel to grain in a transverse plane, and the failures are identical to the shear failures seen in bending specimens.

The contradiction between Ylinen's (1963) torsion specimen failures and the current study's torsion specimen failures may be due to the geometry of the specimen used for both tests and, as a result, the distribution of shear stress. For Ylinen's (1963) circular specimen, the shear stress is maximum along the outer edge of the circle for every radii in the cross section of the circle, as discussed in Chapter 3, Torsion Theory. Ylinen's (1963) cylindrical specimen experiences identical shear stress along the tangential-longitudinal (TL) plane and along the radial longitudinal (RL) plane. As a result of equal stresses along two different planes, failure should occur in the weakest plane. In the case of Ylinen's (1963) specimens, failure occurred along the TL plane: tangent to the growth rings along the longitudinal axis.

The current study's specimen, a rectangular specimen, experiences a maximum shear stress at the middle point of the rectangle's long side along the longitudinal axis and a smaller shear stress at the middle point of the rectangle's short side. If the beam is quarter sawn or flat sawn similar to the typical beam shown in Figure 3.2, then the maximum shear stress will cause a failure in the RL plane: perpendicular to the growth rings along the longitudinal axis. If the wood was weak enough to fail along the TL plane due to the smaller shear

stress, failure would then occur along the middle point of the short side and would be similar to Ylinen's observations with his specimens.

Because the small specimens used in the testing methods mentioned previously did not contain natural characteristics, the shear strength values may not be representative of wood materials used in design.

Riyanto (1996) used four test methods in addition to the small clear block ASTM (1996a) method; they included the three point, four point, and five point flexure tests, and the torsion test. Based on results from this study, the shear strength was dependent upon the method of testing since each method reported different shear values for the same type of wood (Riyanto, 1997). If structural lumber should be tested under loading conditions most similar to real-life flexural applications, Riyanto (1996) recommended that the three point flexure test be used to obtain the shear strength of wood since the three point flexure method resulted in more shear failures than did the four or five point flexure methods. However, if structural lumber should be tested under pure shear stress conditions, then the torsion test should be used since 100% of the failures were shear parallel to grain (Riyanto, 1996).

Until Riyanto's (1996) research and this current study, previous research examined the shear strength of wood using structural lumber specimens subjected to bending, such as in the three point, four point, and five point flexure tests. Although Riyanto (1996) did not test for a size effect on shear strength, prior research indicated that wood shear strength may be affected by the shear

area or possibly by the shear volume (Rammer et al., 1996; Asselin et. al., 1995; Rammer and Soltis, 1994; Foschi and Barrett, 1975; Keenan, 1974; Keenan and Selby, 1973). In general, the studies reported a convincing size effect on shear strength: an increase in beam size correlated to a decrease in shear strength. None of the studies indicated that the interaction between bending stress, compressive stress, and tensile stress, which occurs in the bending specimens, has any effect on this reported size effect on shear strength in research by Rammer et al.(1996), Asselin et al. (1995), Rammer and Soltis (1994), Foschi and Barret (1975), Keenan (1974), and Keenan and Selby (1973).

In a finite element study of the three- and five- point bending test method (Cofer et al., 1997), the size effect apparent in the experimental studies (Rammer et al., 1996; Asselin et. al., 1995; Rammer and Soltis, 1994; Foschi and Barrett, 1975; Keenan, 1974; Keenan and Selby, 1973), was not reproduced. Since the finite element model did not contain any natural wood characteristics and did not show a size effect on shear strength, Cofer et al., (1997) suggested that the reason for the decrease in shear strength due to an increase in size is mainly because a larger beam has a higher likelihood of structural flaws, which are also referred to as natural characteristics of wood.

Since the ASTM (1996a) shear block tests are not able to account for differences in lumber size or natural wood defects, the clear block may not yield shear strength values representative of structural lumber (Longworth, 1977). Longworth verified, using a four point bending test method, that different

specimen widths suggested different shear stress-shear area relationships. He also noticed that the beam shear strength was lower than the shear strength from the ASTM (1996a) block. Riyanto (1996) showed this same trend in his study of the four point bending test, but the shear strength for the five point bending test for 2x4 beams indicated a 40% higher shear strength value than that from the ASTM (1996a) shear blocks. In another study, Rammer et al. (1996) tested 2x4 beams, and larger, with the five point bending test. The results of this study indicated that the shear strength from the 2x4 beams was 11% higher than the shear strength from the ASTM (1996a) method, but the shear strengths for the 2x10, 4x8, 4x12, and 4x14 beams were 30% to 50% lower than those from the ASTM (1996a) method. The difference between the small 2x4 beams and the larger beams was that the five point bending test suggested a shear strength decrease based on an increased beam size (Rammer et al., 1996). Equation 2.2 was proposed by Rammer et al. (1996) to convert the ASTM (1996a) small clear block shear strength to bending shear strength using τ=shear strength as determined from bending tests, C_f=stress concentration factor at the re-entrant corner of the ASTM (1996a) specimen, τ_{ASTM}=shear strength as determined from the ASTM (1996a) standard, and A=the shear area, which is the product of the shear span and the width of the beam. However, this equation may yield misrepresented results because the possible stress interactions associated with bending tests, in addition to wood natural characteristic effects, have not been quantified.

$$\tau = \frac{1.3 C_f \tau_{ASTM}}{A^{1/5}} \qquad (2.2)$$

This size effect found in shear strength is similar to the reported size effect on bending strength (Bohannan, 1966). Currently, the National Design Specification (AFPA, 1991) requires a strength modification factor for beam size applied not only to bending, but also to tensile strength perpendicular to grain, and compressive strength parallel to grain design values. Similar to the shear strength-beam size relationship identified in recent studies, a decrease in beam size results in an increase in bending and tensile strengths (AFPA, 1991).

Although Rammer et al., (1996a) did not look at stress interactions between bending, tensile, compressive, and shear stresses, the interaction may be important, as well as the frequency and type of natural characteristics of wood. Because bending and tensile stress may be interacting with the shear stress, the related size effect found for shear strength may be a result of the size effect based on the bending and tensile properties as opposed to only the shear property. In addition, as suggested by Cofer et al. (1997) the beam size effect on shear strength may be related to the frequency and the size of the natural characteristics of wood.

2.5 Recommendations for an ideal shear strength test method

After Ylinen (1963) examined various shear strength testing methods, he recommended the following characteristics for an ideal shear test method:

- Distribution of shearing stress in the shearing plane must be
    - Exactly determinable,
    - Uniformly distributed, and
    - Independent of the wood elastic constants.
- Normal stresses must not appear in the shearing plane.
- If other stresses occur in the shearing plane, then their effect must be determined.
- Plastic deformations must not appear in the specimen at loading sites.
- Specimen must be small.

In later research, Keenan (1974) and Keenan & Selby (1973) recommended that allowing a specimen to seek a plane of weakness may provide a better indication of shear strength for the specimen. Due to application of loads and the configuration of the specimens the ASTM (1996a) shear block test forces the shear failure along a particular plane in the cube specimen, but the torsion test may allow the shear failure to occur along a plane of weakness in the specimen easier than the bending test.

2.6 Evaluation of other shear test methods for wood

Some of the shear test methods previously described can be used for a variety of materials; for example, the Iosipescu shear test can be used to determine the shear strengths for concrete, composites, and wood. However, for wood, some of these methods may not yield representative shear strength values because the specimens are small. As a result, they do not account for any size effect on shear strength or natural wood characteristic effects on shear strength.

The methods to determine shear strength of a material, as described previously, include theoretical analysis, three-, four-, and five- point flexure, torsion, Iosipescu, direct double surface, indirect, punching, "Arrow" double shear shape, Arcan, and ASTM (1996a) wood block methods. The latter six methods require small size specimens for testing. Using these tests for wood would neglect possible effects from natural characteristic or size effects on the shear strength of the wood. As for applying theoretical analysis in a manner similar to that used for steel, this method would not account for size or natural defects in the wood specimen such as knots, checks, and ring angle and additional shear strength reduction factors would be necessary to account for the natural characteristics. The remaining methods, flexure and torsion testing, are possible options for determining the shear strength of full-size lumber. Unfortunately, flexure test methods do not result in one hundred percent shear failures due to interactions from other stresses in the beam and possible

apparatus effects. While torsion specimens provide a pure shear stress, non-uniform shear stress across the width and depth of a rectangular specimen, and availability of a torsion machine may hinder shear strength research using the torsion test.

2.7 Torsion test as a shear test method

The torsion test has been considered by some researchers to be "the most appropriate method for determining the shear stress-shear strain relationship because a pure shear stress can be applied to the material" (Yoshihara and Ohta, 1997, 1996, 1995a, 1995b, 1993). Because tensile and compressive stresses are not induced on the specimen, a more accurate value of the shear strength can be determined (Hancox, 1972).

As will be shown in Chapter 3, Torsion Theory, flexure test methods and the torsion test allow the shear failure to seek a plane of weakness in the specimen, unlike the current ASTM (1996a) standard. However, the distribution of the shear stresses in the shear plane differs between the flexure, the torsion, and the ASTM (1996a) shear block method. The stress concentration at the re-entrant corner of the ASTM (1996a) shear block does not allow for a uniform stress distribution or an exactly determinable shear stress distribution. The shear stresses determined with the torsion test are theoretically based and may require knowledge of the elastic constants to account for the orthotropic nature of wood, if the assumption of isotropic behavior of wood does not determine the

shear strength correctly (Lekhnitskii, 1981). However, for the current study using Douglas-fir (*Pseudotsuga menziesii*), using the ASTM (1996b) standard torsion formulas which relates applied torque to the shear stress, the elastic constants are not necessary to determine the shear strength of wood (Trayer and March, 1929). These torsion formulas from the ASTM (1996b) standard are based on the isotropic assumption of wood, but the difference in shear strength results using the orthotropic nature of wood (Lekhnitskii, 1981) is negligible (0.9%) for the Douglas-fir specimens tested in this study.

A rectangular torsion specimen only has uniform shear stress distribution along the length but does not have a uniform shear stress distribution across the width or the depth. Although the torsion tests has not been recognized as a possible shear strength test based on this non-uniform stress distribution (Youngquist and Kuenzi, 1961), the torsion specimen is subjected to pure shear stresses that are determinable. On the contrary, the rectangular bending specimen also have determinable shear stresses which are uniform across the width, but bending specimens experience compressive and tensile stresses as well as shear stresses. The effect of these additional stresses have been studied briefly through finite element modeling (Cofer et al., 1997), and have implied that the stress interaction may not be causing the apparent size effect on shear strength observed in other studies (Rammer et al., 1996; Asselin et. al., 1995; Rammer and Soltis, 1994; Foschi and Barrett, 1975; Keenan, 1974; Keenan and Selby, 1973).

Since the shear span, which is used indirectly to determine shear strength, is the middle portion of the specimen and does not consider the ends where the torque is applied, plastic deformation due to the necessary compression of the wood at the grips should not affect the shear strength.

In most studies using the torsion test to determine the shear strength of a material, small specimens were used. Although Ylinen (1963) did not elaborate on why a small specimen should be used, small specimens provide more clear wood material to determine the wood strength without the natural characteristics. Specific equipment was required when testing small specimens in torsion and the specimens varied in shape (Pindera, 1989; Walrath and Adams, 1983). For example, torsion specimens may be solid cylinders, circular tubes, or solid cylinders with square ends (Pindera, 1989; Walrath and Adams, 1983; Novak, 1969). The expense for testing increases dramatically when the specimen must be specially fabricated, for example, into circular tubes or solid cylinders with square ends. If these shapes are to be used in testing, significant costs are associated with special torsion testing equipment and special fabrication of the torsion shapes. As a result, the torsion test is not always a practical method of testing (Pindera, 1989; Walrath and Adams, 1983). However, for the torsion test used in the current study, larger specimens are used to test the effects of natural characteristics on wood shear strength. Also, since the full-size rectangular piece of lumber is tested in torsion, no extra fabrication costs are

associated with this torsion test since the available torsion machine accommodates rectangular torsion specimens.

After examining other test methods frequently used to determine the shear strength used for other materials as well as wood, the torsion test was recognized as a test with the most potential to yield representative shear strength values for full-size lumber.

3. Torsion Theory

Torsion is the twisting of a member of any cross sectional shape when it is loaded by force couples; these couples produce rotation about the member's longitudinal axis (Gere and Timoshenko, 1984). During rotation, if one end is fixed and the other end of the member is allowed to rotate, the longitudinal sides of the member do not change in length (Gere and Timoshenko, 1984). However, the straight longitudinal axis of the member will deform into a helical curve (Boresi et al., 1993). The member, regardless of its material symmetry, is in a state of pure shear stress--a stress that acts parallel to the surface of the material (Gere and Timoshenko, 1984). In a state of pure shear, the member sees only shear stresses--as opposed to the interaction of compressive, tensile, and shear stresses in the case of bending specimen.

Due to the geometry of circular prismatic bars, the torsion theory is less complex than for rectangular prismatic bars. Although, structural lumber is manufactured in rectangular shapes, torsion theory for circular prismatic bars will be explored first, followed by the torsion theory for rectangular prismatic bars.

3.1 Circular prismatic bars

Circular bars have a geometric advantage over rectangular bars: due to the radial symmetry of the circular cross section and because cross sections rotate about the longitudinal axis as rigid bodies, plane cross sections of the

torsion member normal to the longitudinal axis remain plane after deformation and all radii remain straight (Boresi et al., 1993).

The main assumptions for circular rods necessary for the development of useful relationships between the torque and shear stress values include (Boresi et al., 1993):

- Straight torsion member with constant cross section
- Small displacements
- Plane sections remain plane after torsion loading is applied
- Rotation varies linearly along the longitudinal axis
- Homogeneous material
- Obeys Hooke's law
- Isotropic materials

With these assumptions, Equation 3.1 was developed using equations of equilibrium (Gere and Timoshenko, 1984). Equation 3.1 yields the transverse shear stress for a circular cross section where $\tau_{maximum}$=the maximum shear stress, T=applied torque, r=radius of the circular cross section, J=polar moment of inertia.

$$\tau_{Maximum} = \frac{Tr}{J} \tag{3.1a}$$

$$\text{Where } J = \pi \frac{r^4}{2} \tag{3.1b}$$

To maintain equilibrium, equal shear stresses always occur on mutually perpendicular planes, and as a result, the transverse shear stress is identical in value to the longitudinal shear stress (Gere and Timoshenko, 1984). This concept can be illustrated with a solid wood cylinder: since wood is generally weaker in shear along the longitudinal plane, the first cracks due to shear failure will occur along the longitudinal plane as opposed to along the transverse plane (Gere and Timoshenko, 1984). Figure 3.1 shows the point of maximum shear stress and the stress distribution for a circular member.

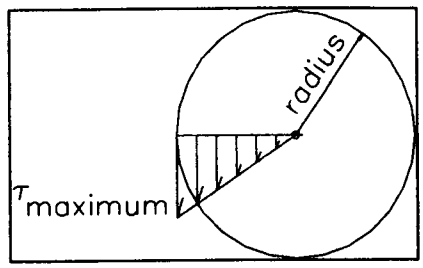

Figure 3.1: Shear stress distribution for a solid circular cross section (Gere and Timoshenko, 1984).

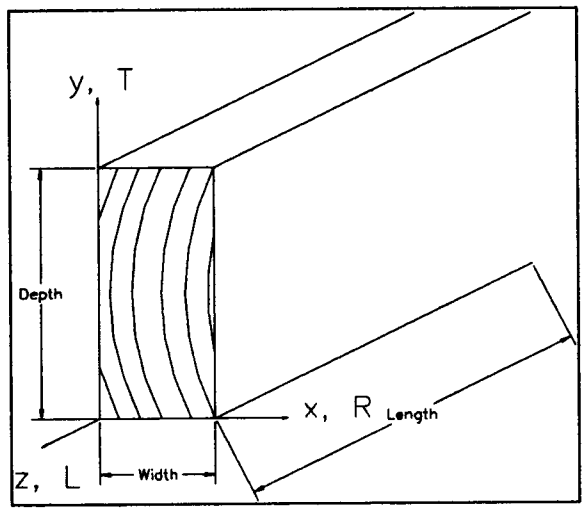

Figure 3.2 Rectangular wood beam

3.2 Rectangular prismatic bars

For rectangular prismatic bars, such as the bar shown in Figure 3.2 where L=longitudional direction, T=transverse direction, and R=radial direction for a wood specimen, the assumption that plane sections remain plane is not valid. Warping does occur after applying a torque. Thus, the theory needs to account

for warping; in other words, various points in the cross section displace differently in the longitudinal axis. In addition, experimental evidence showed that warping of each cross section is identical (Boresi et al., 1993). Other assumptions are necessary for the torsion analysis of rectangular members (Boresi et al., 1993).

- Straight torsion member with constant cross section
- Each cross section rotates approximately as a rigid body
- Rotation of each cross section varies linearly along the longitudinal axis
- Small displacements
- Warping of each cross section is identical
- Homogeneous material
- Obeys Hooke's law
- Isotropic materials

Because plane sections do not remain plane during torsion loading of a rectangular bar, the theory increases in complexity from the theory for a circular bar. To account for warping, the resulting geometric compatibility condition, Equation 3.2, to be satisfied for the torsion problem considers distortion of each section from its plane, and the displacements in the plane of the cross section caused by the rotation (Boresi et al., 1993). In Equation 3.2, θ, the rotation of the torsion member, is related to the partial derivatives with respect to y and x of γ_{xz}, engineering shear strain between the two line elements initially parallel to the xz axis, and γ_{yz}, engineering shear strain between the two line elements initially

parallel to the yz axis, respectively. Engineering shear strains are twice the shear strain.

$$\frac{\delta \gamma_{xz}}{\delta y} - \frac{\delta \gamma_{yz}}{\delta x} = -2\theta \tag{3.2}$$

Applying Hooke's law, the torsion compatibility equation becomes Equation 3.3 (Boresi et al, 1993). This equation relates the product of the shear modulus, G, and the rotation of the specimen, θ, to the second derivatives with respect to x and y for the Prandtl stress function, ϕ. The Prandtl stress function is related to the geometry of the member under torsion and the manner in which the cross section warps (Boresi et al, 1993). This stress function has three requirements it must satisfy in order to provide a torsion solution (Boresi et al, 1993).

$$\frac{\delta^2 \phi}{\delta x^2} + \frac{\delta^2 \phi}{\delta y^2} = -2G\theta \tag{3.3}$$

The first requirement is based on the stress condition that all normal stresses and one shear stress equal zero for torsion members composed of isotropic materials, Equation 3.4. where σ_x, σ_y, and σ_z equal the normal stresses in the x, y, and z direction and τ_{xy} equals the shear stress in the xy direction (Boresi et al, 1993).

$$\sigma_x = \sigma_y = \sigma_z = \tau_{xy} = 0 \tag{3.4}$$

The stress function must also satisfy torsion equilibrium equations, Equation 3.5, which was developed from the stress condition in Equation 3.4 and equilibrium equations from statics (Boresi et al, 1993). Differentiating the shear stress in the xz direction, τ_{xz}, with respect to z and differentiating the shear stress in the yz direction, τ_{yz}, with respect to z both equal zero. This indicates that the shear stresses are independent of z, the longitudinal axis (Boresi et al., 1993). The summation of the differential of τ_{yz} with respect to y and τ_{xz} with respect to x equal zero.

$$\frac{\delta \tau_{xz}}{\delta z} = 0 \tag{3.5a}$$

$$\frac{\delta \tau_{yz}}{\delta z} = 0 \tag{3.5b}$$

$$\frac{\delta \tau_{yz}}{\delta y} + \frac{\delta \tau_{xz}}{\delta x} = 0 \tag{3.5c}$$

The summation equation, Equation 3.5c, is a required condition for the existence of a stress function, ϕ, where τ_{xz} is given as the differential of the stress function with respect to y and τ_{yz} is given as the negative differential of the stress function with respect to x, Equation 3.6 (Boresi et al, 1993).

$$\tau_{xz} = \frac{\delta \phi}{\delta y} \tag{3.6a}$$

$$\tau_{yz} = \frac{\delta \phi}{\delta x} \tag{3.6b}$$

The final requirement is the boundary condition: the lateral surface of a torsion member is free from applied stress (Boresi et al, 1993). Therefore, as shown through statics, the resultant shear stress, in the cross section at the boundary, must be directed tangent to the boundary. Statics proves then that the stress function along the boundary is a constant (Boresi et al, 1993). Theory has arbitrarily established this constant as zero, resulting in Equation 3.7, the stress function is zero along the boundary of the cross section of the shape subjected to torsion (Boresi et al, 1993). Applying this boundary condition to the stress function, the shear stress relationship to the applied torque and the angle of rotation relationship to the applied torque can be determined.

$$\phi = 0 \tag{3.7}$$

For a rectangular beam, the stress function is shown as Equation 3.8 (Boresi and Chong, 1987)

$$\phi = -G\beta\left(b^2 - x^2\right) - \frac{32G\beta b^2}{\pi^3} \sum_{n=1,3,5,\ldots}^{n=\infty} \frac{(-1)^{(n-1)/2} \cos\frac{n\pi x}{2b} \cosh\frac{n\pi y}{2b}}{n^3 \cosh\frac{n\pi h}{2b}} \tag{3.8}$$

Using this stress function, the torque-shear stress and the torque-rotation relationships can be solved as Equation 3.9 (Trayer and March, 1929). The maximum shear stress at the middle point of the long side, τ_l, is a function of the applied torque, T; beam depth, 2h; beam width, 2b; and geometric factors, μ and γ, as numerically defined in Table 4.3 (Trayer and March, 1929) of Chapter 4,

Materials and Methods. The maximum shear stress at the middle point of the short side, τ_s, is a function of the applied torque, T; beam width, 2b; and geometric factors, μ and γ_1, as numerically defined in Table 4.3 (Trayer and March, 1929) of Chapter 4, Materials and Methods. The applied torque, T, is related to beam depth, 2h; beam width, 2b; shear modulus of the material tested, G; shear span length, L; specimen rotation angle, θ; and geometric factor, λ, (Trayer and March, 1929). The geometric constants, γ, μ, γ_1, λ, are determined by the ratio of the rectangle's depth to width; these factors are required in order to solve Equation 3.9. Equation 3.9a was used in this study to determine the maximum shear stress in the lumber specimens using the recorded dimensions and torque at failure.

$$\tau_l = \frac{\gamma T}{\mu h b^2} \tag{3.9a}$$

$$\tau_s = \frac{\gamma_1 T}{\mu b^3} \tag{3.9b}$$

$$T = hb^3\left(\frac{16}{3}\lambda\frac{b}{h}\right)G\frac{\theta}{L} \tag{3.9c}$$

3.3 Prandtl's membrane analogy

Due to the complexity of the theoretical derivation of the shear stress relationships, the stress distribution is often difficult to visualize. To illustrate the

stress distribution of any cross section under torsion loads, Prandtl's soap film membrane analogy is used.

An analogy was developed by Prandtl in 1903 (Boresi et al., 1993) which states that the equilibrium equation for a homogeneous membrane subjected to a pressure is equivalent to the compatibility equation for a torsion member (Boresi et al., 1993).

Consider a rigid edge supporting a homogeneous membrane stretched across a hole in the shape of a thin rectangular cross section (Figure 3.3a). The size of the hole does not affect the results of the theory (Ugural et al., 1995). The homogeneous material, such as a soap film, is stretched over the hole (Figure 3.3b). The base provides edge support for the soap film, which will be subjected to a uniform pressure on one side of the film (Ugural et al., 1995).

The uniform pressure causes the film/membrane, to deflect outward and away from the base/edge support. The deflected membrane is a curved surface, and Figure 3.3b shows the deflected film in the plane perpendicular to the x-axis (Figure 3.3bi) and in the plane perpendicular to the y-axis (Figure 3.3bii), after the pressure has been applied. The equilibrium equation of the lateral displacement in the z direction for the defected membrane, Equation 3.10 is equivalent to the compatibility equation for a torsion member, Equation 3.3, but is repeated here as Equation 3.11 for convenience.

Equilibrium Equation

$$\frac{\delta^2 z}{\delta x^2} + \frac{\delta^2 z}{\delta y^2} = -\frac{P}{S} \tag{3.10}$$

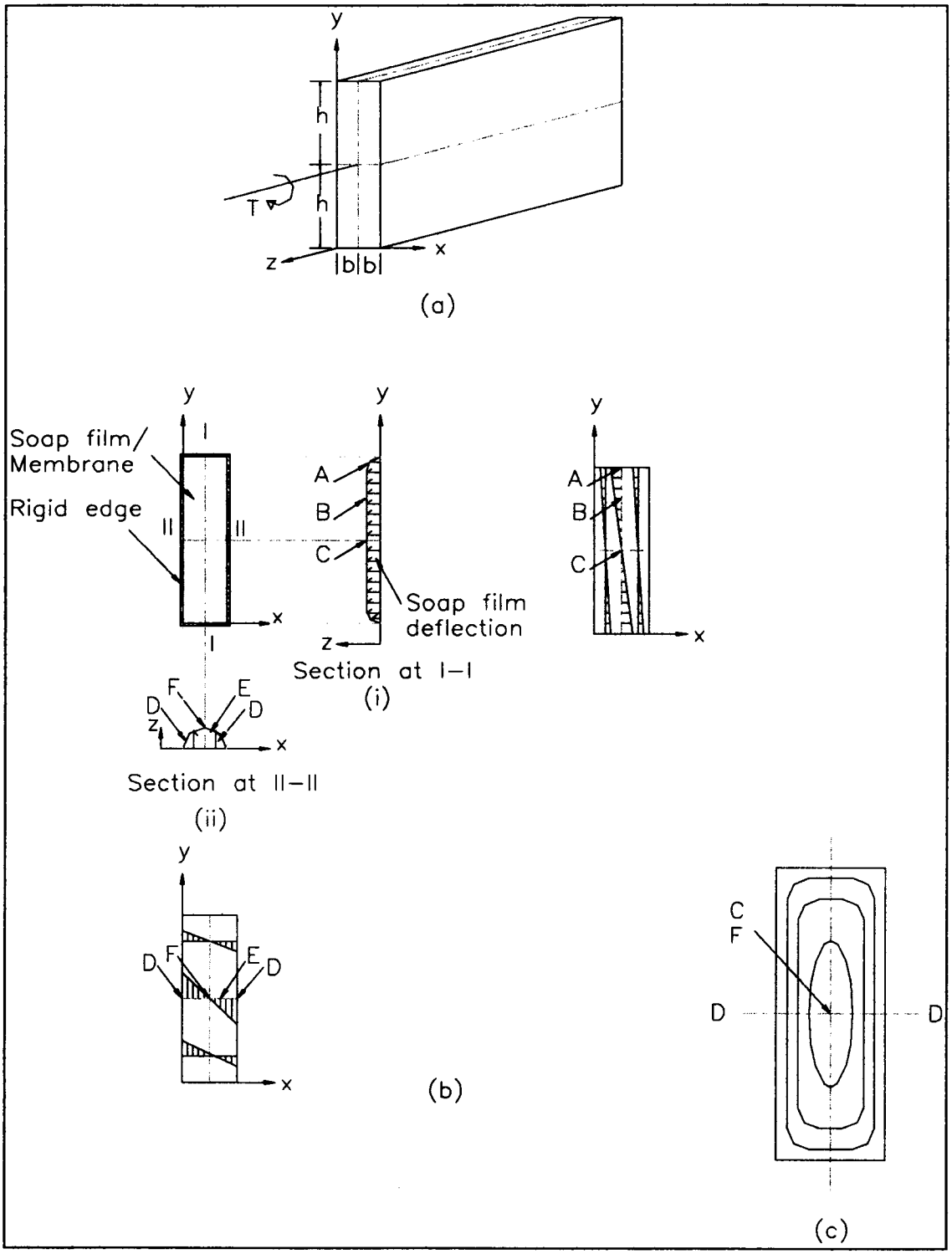

Figure 3.3: Prandtl's membrane analogy (a) member subjected to torque, T, (b) soap film deflection, (c) soap film contour lines (Boresi et al., 1993; McGuire, 1968; Timoshenko, 1956)

Torsion Compatibility Equation

$$\frac{\delta^2 \phi}{\delta x^2} + \frac{\delta^2 \phi}{\delta y^2} = -2G\theta \qquad (3.11)$$

Comparing Equation 3.10 to Equation 3.11 yields that the membrane displacement, z, is proportional to the Prandtl stress function, ϕ (Boresi et al., 1993). Substituting Equation 3.6 into Equation 3.11 yields Equation 3.12. Comparing Equation 3.12 with the membrane equilibrium equation, Equation 3.10, the slope of the membrane at any point in the cross section is proportional to the stress components at these same points (Boresi et al., 1993).

$$\frac{\delta \tau_{yz}}{\delta x} + \frac{\delta \tau_{xz}}{\delta y} = -2G\theta \qquad (3.12)$$

By examining the deflected membranes at the centerlines of the cross section in Figure 3.3b (line I-I for Figure 3.3bi and line II-II for Figure 3.3bii), the shear stress component distributions can be identified. Figure 3.3bi shows the deflected soap film along line, I-I, as if viewing the rigid plate in the yz plane along the long side of the rectangular hole. In this direction, the stress distribution for the shear in the xz direction, τ_{xz} can be visualized (Figure 3.3bi). The large slope at point A of the deflected membrane at either end of he rectangle indicates that the τ_{xz} is large at A. Comparing point A to point B, the slope at point B is smaller than at point A; therefore τ_{xz} is also smaller at point B. Also point C on the membrane shows a zero slope, which indicates a zero shear

stress value in the middle of the cross section along line I-I. The same analogy can be used to determine the stress distribution for the shear in the yz direction, τ_{yz}, by viewing the flat plate in the xz plane along the short side of the rectangle, Figure 3.3i, which shows the deflected membrane along line II-II. The slope at point D is large than the slope at point E, indicating that τ_{yz} at D is lager than at E. The shear stress τ_{yz} is zero at the exact center of the cross section, point F, where the membrane shows a zero slope. The largest τ_{xz}, from Figure 3.3bi, occurs at point A, and the largest τ_{yz}, from Figure 3.3bii occurs at point D. Comparing the slopes at these two points, A and D, Figure 3.3b shows that point D has a larger slope. Consequently, the largest shear stress is τ_{yz}, and occurs at the middle point of the long side, point D in Figure 3.3b.

The analogy can also be useful when considering the contour lines of the deflected membrane. If the contour lines in Figure 3.3c represent the deflected membrane, then the shear stress magnitude is inversely proportional to the spacing between the contour lines (Timoshenko, 1956). This is illustrated by the points along the line D-D with narrow spacing of the contour lines. In addition, at the corners of the rectangle , the spacing is large and the contour lines coincide with the surface of the membrane. In this case the slope of the surface of the membrane is zero, indicating that the shear stress is zero at the corners. (Timoshenko, 1956).

3.4 Boundary condition effects

3.4.1 Torsion machine grips--warping considerations

The torsion machine available for testing in this project was originally designed to accommodate circular members. Modifications were necessary to enable testing of rectangular members in torsion. Grip suggestions provided by ASTM (1996b) state that the grips to hold the rectangular member be a vise-like mechanism, and vise-like grips were used. Appendix A discusses details regarding these modifications.

Janowiak and Pellerin (1992) tested wood in torsion using small size specimens, 3/4 inch to 5/8 inch boards measuring 3.5 inches by 12 inches. Although these specimens were mainly tested for shear moduli values rather than shear strength values, the machine set up was similar to the machine set up used in the current study. Janowiak used vise grips to hold the specimen, but the setup appears to show that bolts connected the specimen to the grips. In this case, the grips restrained warping. Unrestrained warping affects the relationships between the applied torque and the shear modulus. Janowiak and Pellerin (1992) provide several references and discuss the method used to account for the grip end effects. However, for the current study wrapping was unrestrained because space was provided between the ends of the boards and the grips; in addition, the specimens were not bolted to the grips.

3.4.2 Torque loading conditions--Saint Venant principle

The torsion theory satisfies compatibility and equilibrium conditions. However, when applying torsion loads to a member the member ends show a complex stress distribution. The stress equation, Equation 3.6, represents the stress distribution a certain distance away from the ends of the member subjected to torsion loads (Boresi et al., 1993). This redistribution of stress from the end to a certain distance away from the end is referred to as Saint Venant's principle (Boresi and Chong, 1987). "Two statically equivalent force systems that act over a given small portion S on the surface of a body produce approximately the same stress and displacement at a point in the body sufficiently far removed from the region S over which the force systems act."

In other words, the torque applied to the ends of a member causes a nonuniform stress distribution along the length of the beam near the ends for a specific length distance from each end. This uniform stress, with respect to the length, becomes uniform after a particular distance away from the ends where the loads are applied. Therefore, for the torsion specimen the shear span is defined as the total specimen length minus the distance from each end. Although the equations used to calculate shear stress based on applied torque, Equation 3.9, are independent of the specimen length, the equations assume the shear stress is uniform along the length of the specimen. As a result, when testing specimens in torsion to determine the shear strength, the test specimens must have an adequate length distance to enable the shear stress to reach

uniformity along the length so that Equation 3.9 can be used to calculate shear strength.

At the start of this research, the distance from each end of non-uniform shear stress was unknown. A finite element model was used to investigate the distance where the shear stress becomes uniform along the length of the specimen for rectangular sections subjected to torsion. Chapter 5 discusses the results of the finite element modeling.

3.5 Shear strength failure modes

There are six possible modes of failure in shear for wood, shown in Figure 3.4. These six modes of failure can be arranged in to three categories: (1) shear parallel to the grain, (2) shear perpendicular to grain, and (3) rolling shear (Wangaard, 1981). Each mode has a given failure plane and a given sliding direction. The failure plane refers to the plane in which the shear failure occurs and is a result of the sliding direction. The sliding direction refers to the direction which the stress moves the wood fibers parallel or perpendicular to each other.

Failure modes 1a and 1b, Figure 3.4a, are shear failures parallel to the grain with sliding directions also parallel to the grain; this failure mode is known as *shear parallel to grain*. The failure plane differs between mode 1a, which fails in the radial-longitudinal plane (RL), and mode 1b, which fails in the tangential-

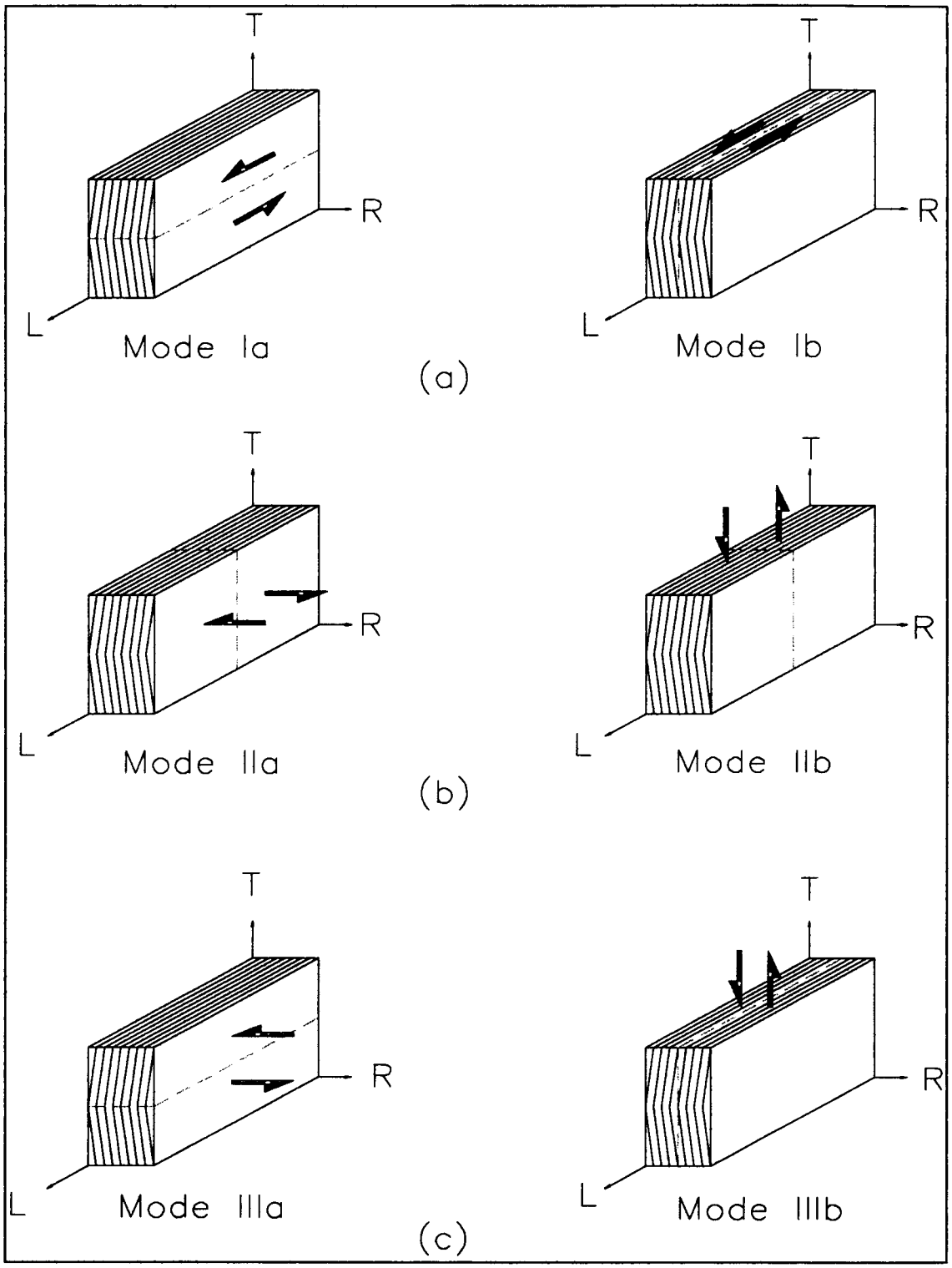

Figure 3.4: Shear failure modes (a) shear parallel to the grain, (b) shear perpendicular to the grain, (c) rolling shear (Wangaard, 1981)

longitudinal plane (TL). A wood specimen which fails according to this mode, should have a shear strength value near 1,450 psi (Wangaard, 1981).

For *shear perpendicular to grain*, failure modes IIa and IIb, Figure 3.4b, both have failure planes perpendicular to the grain and sliding directions perpendicular to the grain. The failure plane for both modes is the tangential-radial plane (TR). The difference between these two modes is the direction of the applied force. For mode IIa the force is perpendicular to the radial plane, and for mode IIb the force is perpendicular to the tangential plane. This shear strength, near 4,300 psi, is significantly stronger than the other two failures modes (Wangaard, 1981). This failure seldom occurs because the wood usually fails due to other stresses, particularly compression of the fibers, before it fails in shear perpendicular to grain (Wangaard, 1981).

The rolling shear failure modes IIIa and IIIb, Figure 3.4c, show a failure plane parallel to grain but a sliding direction perpendicular to grain. The rolling shear action is caused by the wood fibers rolling across one another; this occurs because the wood fibers are at right angles to the direction of the shear stress (Breyer, 1993; Silvester, 1967). Mode IIIa fails along the radial longitudinal plane (RL) and mode IIIb fails along the tangential-longitudinal plane (TL). When this failure occurs, it yields the smallest shear value of the three failure; the shear value for rolling shear is on the order of 500 to 700 psi (Wangaard, 1981). Although mode I and mode III involve the same failure planes, the low shear values for mode III are due to large distortions of cell cross sections since

the shearing action actually causes the cells to roll across each other (Tsumois, 1991). This type of shear failure is associated with deep, narrow, and solid timber beams and plywood and does not occur often (Silvester, 1967). One reason could be that for deep and narrow beams a given load yields a higher shear force to be distributed across a smaller shear area than a wider beam.

Previous research (Keenen et al., 1973) suggested that when determining shear strength values the test method should allow the shear failure plane to occur on the weakest plane for the specimen. A comparison of the failure modes for an ASTM shear block specimen, a bending specimen, and a torsion specimen demonstrate which failure mode is associated with each specimen type and if the failure mode is allowed to occur along the weakest plane.

3.5.1 ASTM D 143-94

When testing a small clear block according the current ASTM (1996a) standard, Figure 3.5a, the shear failure plane is forced in a particular direction. In the ASTM (1996a) case, the sliding direction is parallel to the grain, as well as the failure plane. The failure plane occurs in the RL direction for a grain angle of 0°, Figure 3.5a, or in the TL direction for a grain angle of 90°, Figure 3.5a. Therefore, this test corresponds to failure modes 1a and 1b of Figure 3.4. This test specimen was used in a recent study (Riyanto and Gupta, 1996) to determine the grain angle effect on shear strength; the results indicated that the ring angle does not affect the shear strength.

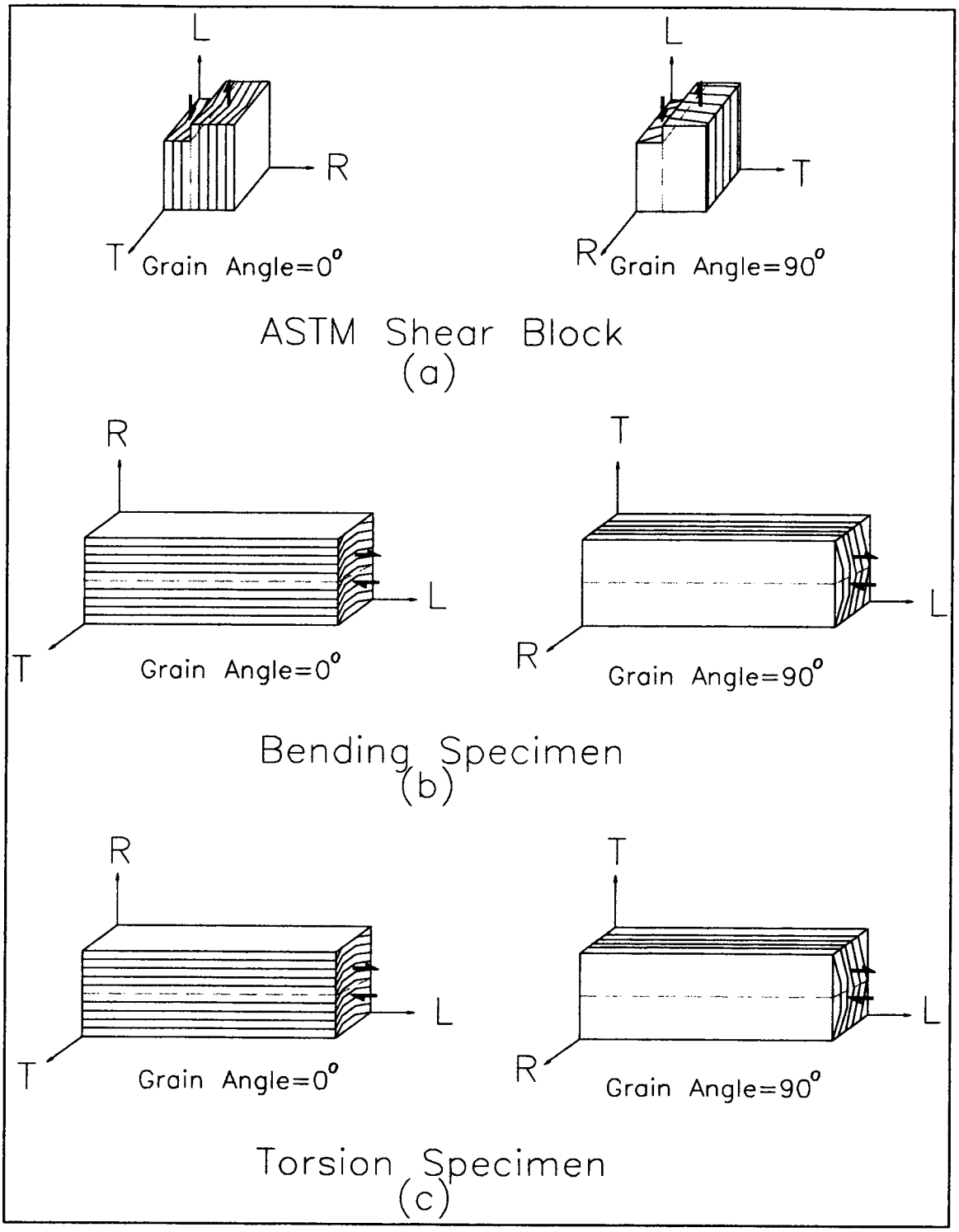

Figure 3.5: Comparison of common shear specimens (a) ASTM (1996) shear block, (b) bending specimen, and (c) torsion specimen

3.5.2 Structural size bending specimen

For a bending specimen, Figure 3.5b, the failure pane is not forced but occurs along the weakest plane, either RL, TL, or TR. Shear failure along the TR plane is approximately three to four times higher than RL and TL shear strengths. Consequently, if the beam is allowed to fail along the weakest plane, the specimen will fail either along the RL or TL planes. Thus, in bending, shear failure along the TR plane does not occur. This reasoning eliminates failure mode II, Figure 3.4. The loading setup does not allow for shear slipping as seen in failure mode III, Figure 3.4. Therefore, this test corresponds to failure mode Ia, Figure 3.4, for a grain angle of 90° and Ib, Figure 3.4, for a grain angle of 0°.

3.5.3 Structural size torsion specimen

The failure plane for a torsion specimen, Figure 3.5c, is not forced but occurs along the weakest plane, either RL, TL, or TR. Shear failure along the TR plane is approximately three to four times higher than RL and TL shear strength. As with the bending specimen, if the beam is allowed to fail along the weakest plane, the specimen will fail either along the RL or TL planes. Thus, in torsion, as well as in bending, shear along the TR plane does not occur. This reasoning eliminates failure mode II, Figure 3.4. The shear stress distribution, discussed in section 3.6.3, proves that torsion does not allow for rolling shear as shown in failure mode III. Therefore, this test corresponds to failure mode Ia,

Figure 3.4, for a grain angle of 90° and mode Ib, Figure 3.4, for a grain angle of 0°. The shear failure plane is parallel to the grain and the sliding direction is parallel to the grain; this is identical to the bending case described in section 3.5.2.

3.6 Comparison of stresses

As discussed previously, torsion loading theoretically induces pure shear stresses on a specimen subjected to torsion. Applying a torsion test to determine the pure shear strength for wood is reasonable since no other stresses interact with the shear stress that may alter the shear strength value. However, there is another concern that the shear stresses are different for an ASTM (1996a) block, a bending specimen, and a torsion specimen.

3.6.1 ASTM (1996a) shear block stress distribution

A primary concern with the ASTM (1996a) shear block is the stress concentration at the re-entrant corner of the specimen (Ylinen, 1963). This stress concentration is not representative of design conditions and adds to the uncertainty in the shear strength value obtained through this test. Because the ASTM block produces a significant stress concentration and does not allow for shear failure to occur along the weakest plane, the stress distribution will not be discussed further.

3.6.2 Bending specimen stress distribution

The shear failure mode can be explained by considering shear stresses in all directions in the bending specimen and analyzing various small elements within the beam. Figure 3.6 identifies small elements at various points in a simple beam subjected to downward loading, as in the case of the three-, four-, and five-point flexure tests studied to determine shear strength (Riyanto, 1996). Vectors shown indicate the direction and type of stress applied to the particular element.

Figure 3.6a shows shear stresses in the yz plane,τ_{yz}, the xz plane τ_{xz}, and the xy plane, τ_{xy}. However, static analysis of a bending specimen indicates that the loading conditions cause a shear stress only in the yz plane, τ_{yz}. As for the shear stress vectors shown on the rectangular schematic, τ_{xz} and τ_{xy} are equal to zero. As a result, τ_{xz} and τ_{xy} do not affect the sliding direction or the failure plane of the shear failure. The remaining shear stress caused by the applied bending load is τ_{yz}, which shears the specimen along the z-axis and acts parallel to the wood fibers. In addition, τ_{yz} results in a failure plane along the z-axis, parallel to the wood fibers. Therefore, this shear stress, τ_{yz}, causes a shear failure plane parallel to grain with a shearing direction parallel to grain also. This shear failure is identical to mode I, Figure 3.4.

Illustrated in Figure 3.6b is the shear stress distribution over the cross section of the beam, the xy plane. Along the x-axis, the shear stress is

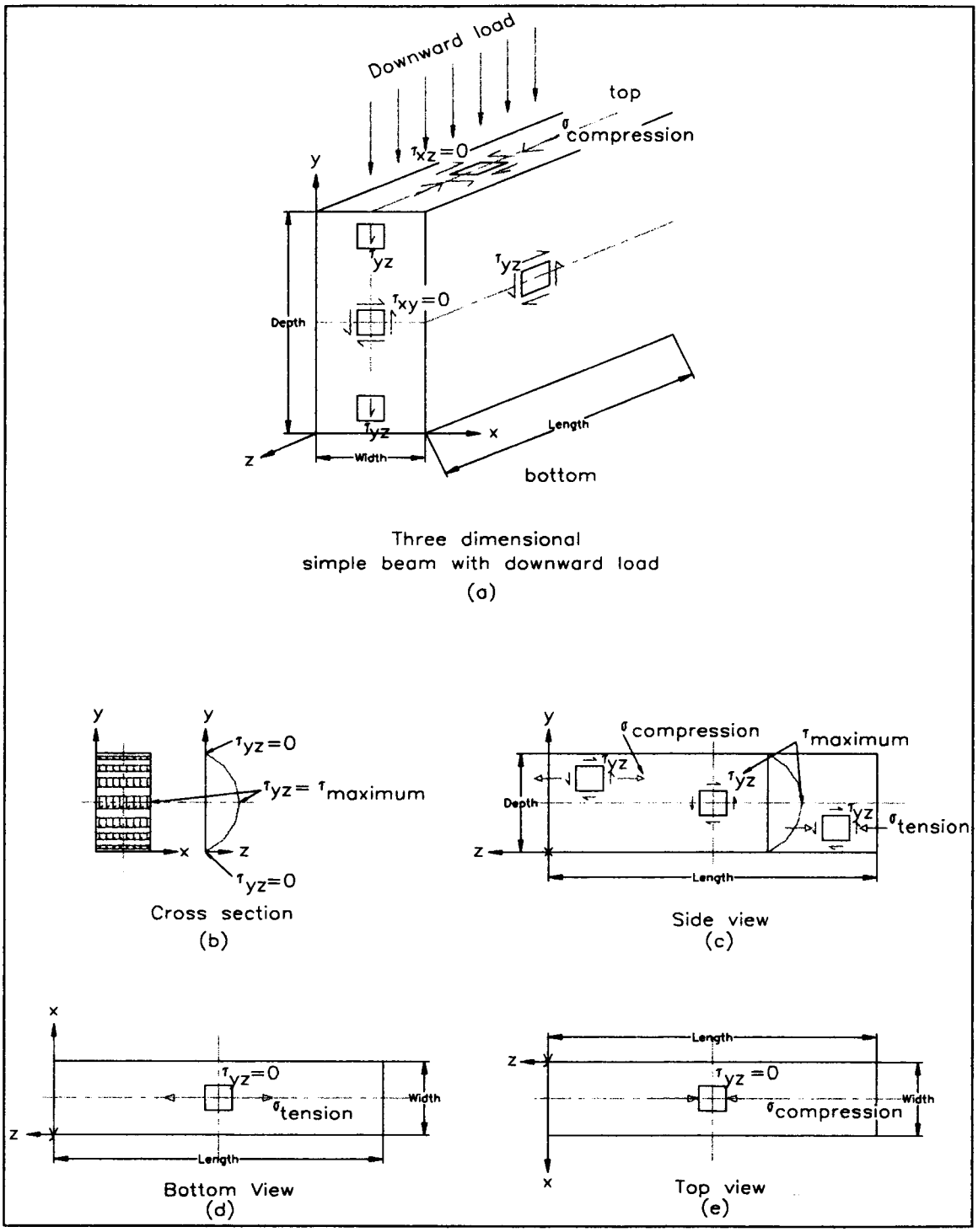

Figure 3.6: Bending specimen stress distribution (a) three dimensional view, (b) cross sectional view, (c) side view, (d) bottom view, (e) top view (Gere and Timoshenko, 1984)

distributed uniformly. This diagram shows that parabolic shear stress distribution occurs over the cross section with respect to the yz plane.

Viewing Figure 3.6a from the side in the yz plane, results in Figure 3.6c. The side view also shows that the shear stress is parabolic along the vertical, y, axis. This parabolic shear stress distribution has a maximum shear stress, τ_{yz}, at the neutral axis of the beam. For the structural lumber specimens tested, the material can be assumed to be symmetric about the center axis of the beam resulting in the neutral axis falling along the centerline of the beam. If an element above the neutral axis or below the neutral axis is analyzed the shear stress is not a maximum, and as a result there is an additional normal stress applied to the element. This normal stress is tensile for elements near the bottom of a bending specimen, and compressive for elements near the top of a bending specimen. The bottom element is viewed in the xz plane in Figure 3.6d; the shear stress is zero with a maximum tensile stress. In Figure 3.6e, the top element is shown; the shear stress is zero with a maximum compressive stress.

3.6.3 Torsion specimen stress distribution

The shear failure mode can be explained by considering shear stresses in all directions in the torsion specimen and analyzing various small elements within the beam. Figure 3.7 identifies small elements at various points in the beam subjected to a torque; vectors are shown which indicate the direction and type of stress applied to the particular element.

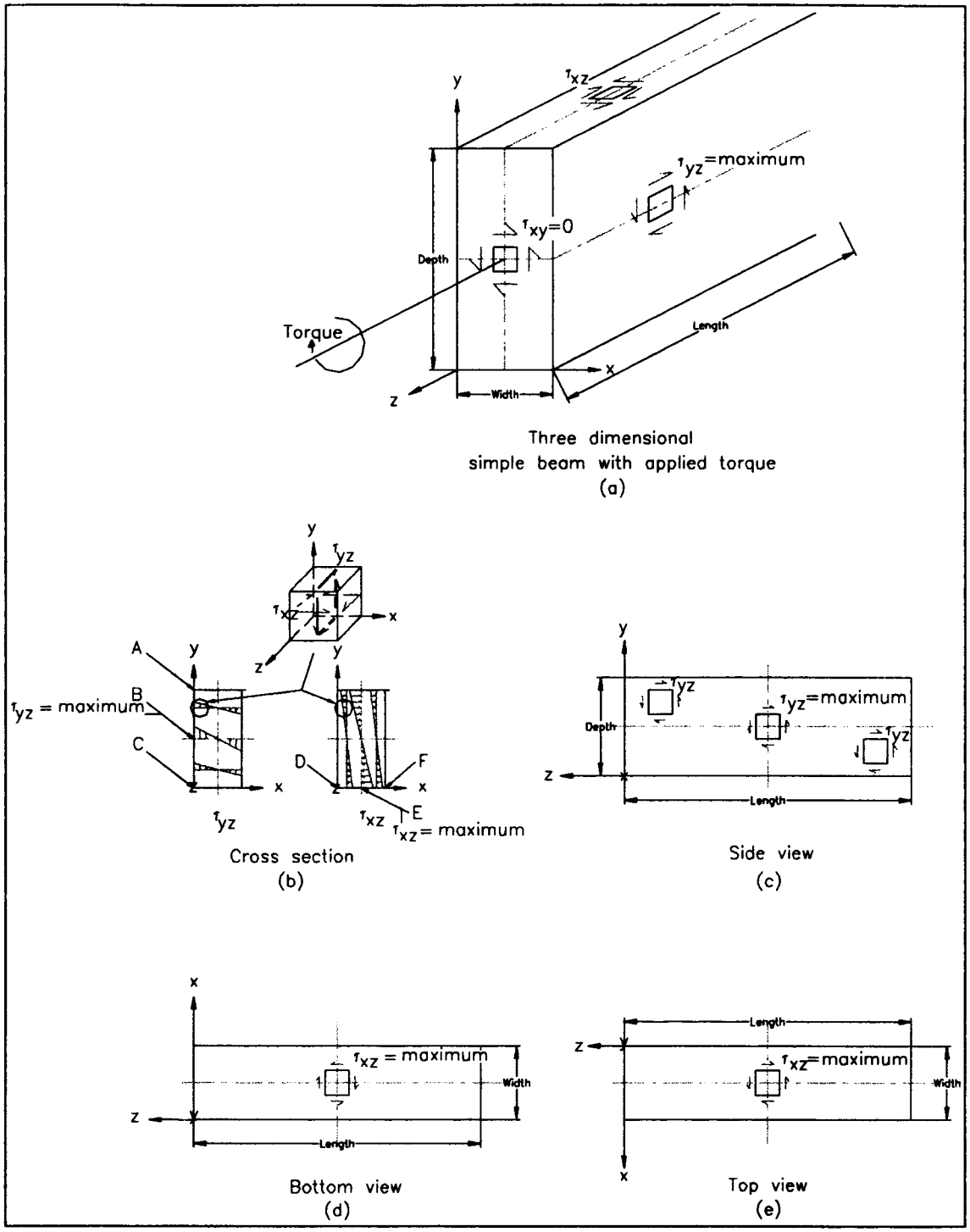

Figure 3.7: Torsion specimen stress distribution (a) three dimensional view, (b) cross sectional view, (c) side view, (d) bottom view, (e) top view (McGuire, 1968)

Figure 3.7a shows shear stresses in the yz plane,τ_{yz}, the xz plane τ_{xz}, and the xy plane, τ_{xy}. However, normal stresses are equal to zero and shear stress in the xy plane, τ_{xy}, equals zero (Boresi et al., 1993). As a result τ_{xy} does not affect the sliding direction or the failure plane of the shear failure. The remaining shear stresses caused by the applied torque are τ_{yz} and τ_{xz}. Either τ_{yz} and τ_{xz} could be the maximum shear stress experienced in the beam for orthotropic materials (Lekhnitskii, 1981). However, the torsion shear stress relationship recommended for use by the ASTM (1996b) standard was developed based on theory for isotropic materials. As a result, the maximum shear stress induced in the beam occurs at the middle point on the long side of the rectangle. This result has been confirmed (Lekhnitskii, 1981) for the species used in this study, Douglas-fir, using the orthotropic properties listed in Table 5.2 of Chapter 5, Finite Element Modeling. By analyzing a rectangular, homogeneous, orthotropic bar under torsion, the highest shear stress occurs at the middle point on the long side (Lekhnitskii, 1981).

Shown in Figure 3.7b is the shear stress distribution over the cross section of the beam, the xy plane. Along the x-axis, the shear stress is distributed linearly. As an element moves along the x-axis, τ_{yz} begins at a maximum positive value at one side of the x-axis, decreases to zero at the centerline, and continues to decrease to a maximum negative value on the opposite side of the x-axis. The shear stress values are symmetrical about the centerline; therefore, the maximum positive value is equal to the absolute value

of the maximum negative value. As an element moves along the y-axis, at point A τ_{yz}. begins at zero at one end of the y-axis, increases to a maximum shear value at the centerline at point B, and decreases to zero at the other end of the y-axis at point C. The shear stress values are symmetrical about the centerline.

In the case of the shear stress τ_{xz}, the relationships are similar. Moving along the x-axis, τ_{xz} begins at zero at one side of the x-axis at point D, increases to a maximum shear value at the centerline at point E, and decreases to zero at the opposite side of the x-axis at point F. The shear stress values are symmetrical about the centerline. Over the cross section along the y-axis the shear stress is distributed linearly. Moving along the y-axis, τ_{xz} begins at a maximum positive value at one end of the y-axis, decreases to zero at the centerline, and continues to decrease to a maximum negative value at the other end of the y-axis. The shear stress values are symmetrical about the centerline; therefore, the maximum positive value is equal to the absolute value of the maximum negative value.

In Figure 3.7b, the maximum shear stress, τ_{yz}, in a rectangular Douglas-fir beam, occurs at the center point on the long side of the rectangle, the y-axis. The maximum τ_{xz} value occurs at the center point on the short side of the rectangle, but this shear stress is smaller than τ_{yz}. The distributions indicate that the shear stresses, regardless of direction, are zero at the corners as suggested by the soap film analogy explained in section 3.3. The shear stress distribution is uniform along the length, the z-axis, except near the ends where the load is

applied (Saint Venant's principle discussed in section 3.4.2). This aspect is explored more closely in Chapter 5, Finite Element Modeling.

Viewing Figure 3.7a from the side in the yz plane results in Figure 3.7c. The side view shows that there is shear stress of some value at every point in the yz plane, and the shear stress distribution of the cross section is shown in Figure 3.7b. The shear stress values decrease as the small element moves away from the neutral axis of the beam toward the top or the bottom of the beam. For the structural lumber specimens, tested the material can be assumed to be symmetric about the center axis of the beam resulting in the neutral axis falling along the centerline of the beam. If an element above the neutral axis or below the neutral axis is analyzed the shear stress, τ_{yz}, is not a maximum, but no additional stress is applied to the element (McGuire, 1968). Both the bottom elements, Figure 3.7d, and the top element , Figure 3.7e, view the beam in the xz plane; the shear stress in this plane τ_{xz}, is at a maximum.

Assuming that all the shear stresses contribute to the failure of the specimen, the sliding direction and the failure plane are discussed by comparing the rectangular specimen with the typical grain pattern tested in this study, Figure 3.8a, to the failure modes shown previously in Figure 3.4.

Figure 3.8b shows τ_{xy} as this shear stress causes the wood specimen to slide perpendicular to the wood fibers; however, the failure plane, RL, is parallel to the wood fibers. Therefore, the shear in the xy direction, τ_{xz}, causes mode IIIa, rolling shear from Figure 3.4.

The shear stress, τ_{xz}. is shown in Figure 3.8c as this shear stress causes the wood specimen to slide parallel to the wood fibers, and the failure plane, TL, is also parallel to the wood fibers. Therefore, the shear in the xz direction, τ_{xz}, causes mode Ib, shear parallel to the grain, from Figure 3.4.

The maximum shear stress, τ_{yz}, is shown in Figure 3.8d as this shear stress causes the wood specimen to slide parallel to the wood fibers, and the failure plane, RL, is also parallel to the wood fibers. The shear in the yz direction causes mode Ia, shear parallel to the grain, from Figure 3.4. The location where τ_{yz} is a maximum τ_{xz} is zero; therefore a direct interaction of both shear stresses does not occur at the point of theoretical failure in the specimen. This theoretical point of failure occurs at the point of maximum shear stress, τ_{yz}, which is along the middle point of the long side of the rectangle. Other interactions between these two shear stresses, τ_{yz} and τ_{xz} are not known at this time. Additional research is necessary to determine if stress interaction from the shear stress τ_{xz} interferes with the shear failure due to τ_{yz}; however, theoretically, the shear stresses do not interact with each other, as shown in Figure 3.7.

Realistically, at the time of failure all three of these stresses do not occur simultaneously. This shear stress, τ_{xy}, equals zero, and as a result this shear stress is not present in torsion specimens (Boresi et al., 1993). Therefore, rolling shear cannot occur. Consequently shear failure either occurs along the centerline of the short side where τ_{xz} is a maximum, point E in Figure 3.7b, or shear failure occurs along the centerline of the long side where τ_{yz}, is a

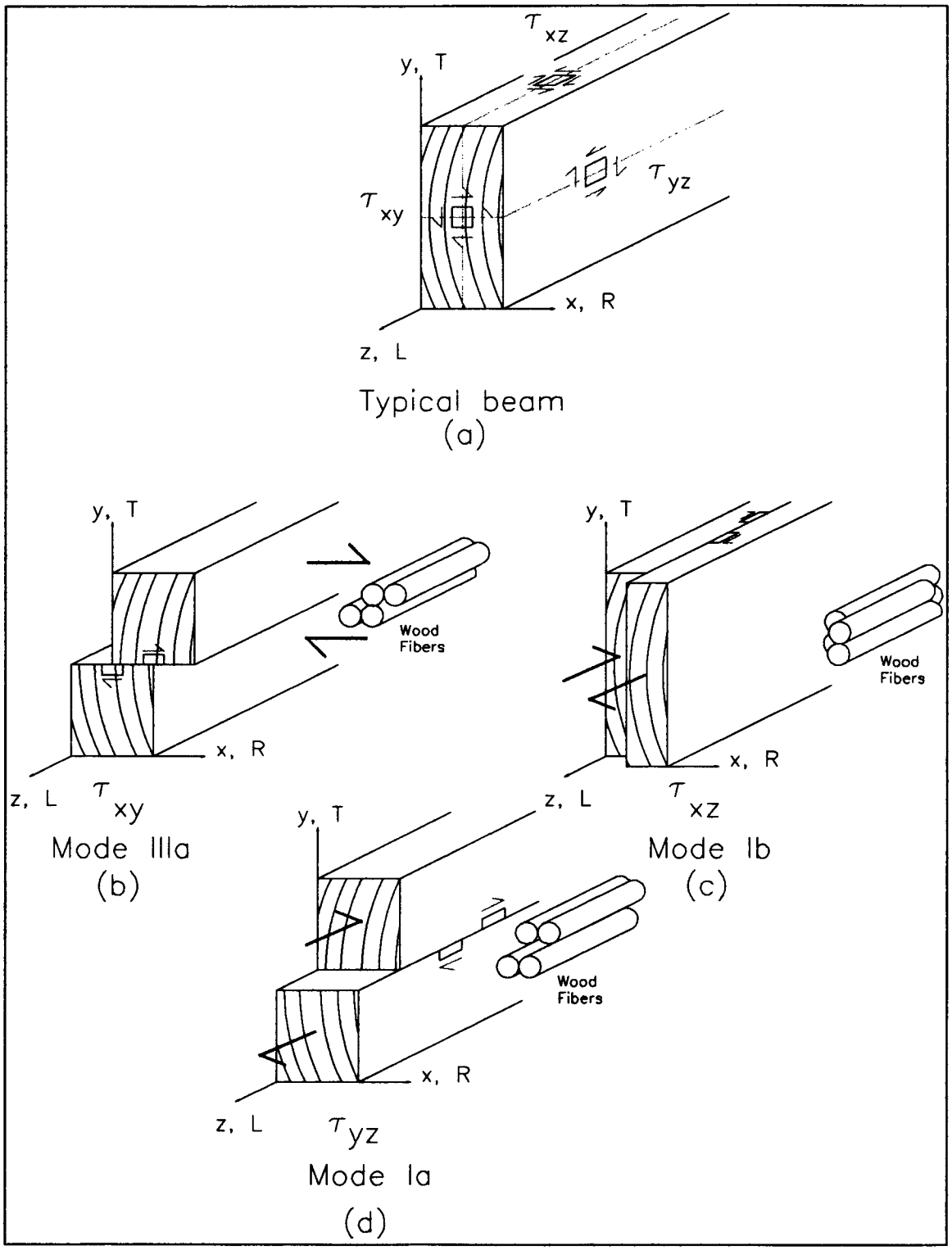

Figure 3.8: Comparison of failure modes to a torsion specimen (a) typical beam, (b) τ_{xy}, mode IIIa, (c) τ_{xz}, mode Ib, (d) τ_{yz}, mode Ia

maximum, point B in Figure 3.7b. The wood tested in this study initially failed at the middle point on the long side rather than the middle point of the short side, thus the wood possesses high enough shear strength to overcome the smaller shear stress, τ_{xz}. The highest shear stress, τ_{yz}, induced in the wood beam causes the shear failure. This stress is identical to the shear stress which occurs in beams subjected to bending loads.

The maximum shear stress at the middle of the long side is τ_{yz}. This maximum stress, τ_{yz}, is not at right angles to the wood fibers as in the case of the shear stress τ_{xy}, shown in Figure 3.8b. This maximum shear stress, τ_{yz}, is the same shear stress as produced in a bending specimen. However, instead of the shear stresses remaining uniform over the cross section with respect to the x-axis in Figure 3.6b for the bending case, the τ_{yz} shear stress of a torsion specimen, varies linearly such that at the center of the cross section the stress is zero. This maximum stress causes the same longitudinal shear failure in torsion specimens as in bending specimens. Although τ_{yz}, is the same in bending as it is in torsion, the distribution of τ_{yz} is different in bending compared to torsion, and torsion tests offer a state of pure shear and bending tests have compression perpendicular and parallel to the grain, tensile, and shear stresses.

4. Materials and Methods

Two studies were performed (1) the length effect study which varied the length of the torsion specimen and (2) the depth effect study which varied the depth of the torsion specimen. In addition, for each study small clear block specimens were tested according to ASTM (1996a) standards for comparison purposes.

4.1 Materials

4.1.1 Length Study

The ASTM (1996b) standard requires that the total length of the specimen should be at least eight times the larger cross sectional dimension. At the time of this writing, research supporting this length value has not been identified. Therefore, the purpose of this initial study was to validate the ASTM (1996b) recommendation that the total length of the specimen should be at least eight times the larger cross sectional dimension.

Fifty pieces of nominal 2x4 inch, 14 feet long, Douglas-fir (*Pseudotsuga menziesii*), MSR graded (1800F-1.6E) structural lumber were obtained from Frank Lumber Company, Mill City, Oregon. This lumber possessed typical natural characteristics for the grade of lumber chosen, such as knots and checks but no wane or splits.

After conditioning the specimens to 12% moisture content by placing the specimens in the standard conditioning room with 68% relative humidity and 73°F, ten of the 50 pieces with modulus of elasticity values close together were randomly sawn into the following smaller lengths for testing: a) 21.0" b) 28.5" c) 32.0" d) 35.5" e) 39.0" and f) ASTM (1996a) block. An example of a sawing pattern is illustrated in Figure 4.1. The length value included three parameters as shown in Figure 4.2, a shear span in the middle of the beam, a distance of two times the depth on both sides of the shear span to account for end effects on the shear stress distribution, and a distance of two inches at each end to account for the actual gripping distance necessary to securely hold the specimen in the torsion machine.

Table 4.1 shows the lengths tested for the length study and the sample size for each length. According to the ASTM (1996g) D2915-94 standard a sample size of 52 was calculated. This sample size assumed a coefficient of variation of 18% for shear strength as determined in a previous torsion study on Douglas-fir (*Pseudotsuga menziesii*) (Riyanto, 1996). This is the sample size sufficient for estimating the mean shear strength for Douglas-fir. Since this research objective was to determine a relationship between shear strength and size for Douglas-fir rather than determining the mean shear strength of Douglas-fir, ten pieces for each length size previously mentioned were tested. This provided a total of 50 data points to be used to determine if there was a correlation between specimen length and shear strength.

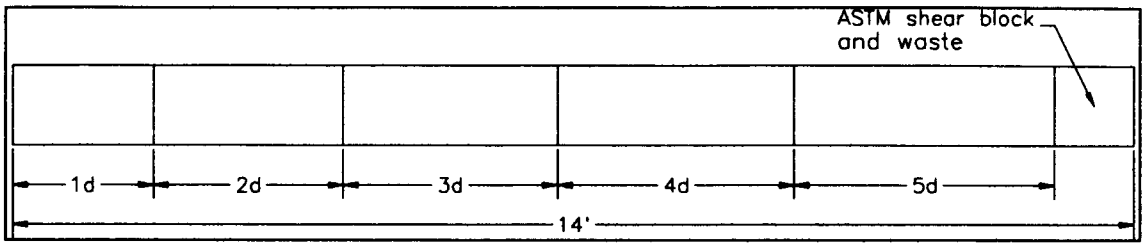

Figure 4.1: Typical sawing pattern for length study specimens

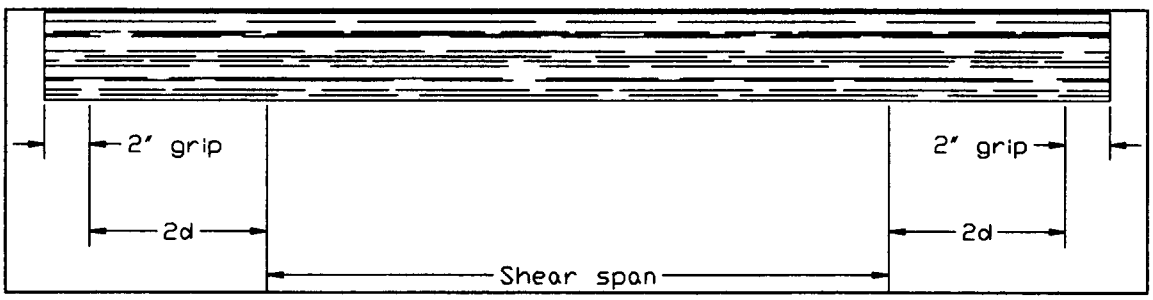

Figure 4.2: Length parameters for a torsion specimen

Table 4.1: Length study specimen length specifications

Nominal[1] Width x Depth (inches)	Sample size	Shear Span (Inches)	Total Length (inches)
2x4	10	3.5	21.0
2x4	10	7.0	28.5
2x4	10	10.5	32.0
2x4	10	14.0	35.5
2x4	10	17.5	39.0

[1] Actual width x depth dimensions were 1.5" x 3.5".

4.1.2 Depth Study

Similar to the length study, the depth was used to evaluate the torsion test as a method to determine shear strength. For the depth study, the objective was to determine if a relationship between the beam size and the shear strength existed. The following nominal beam sizes tested were 2x4, 2x6, 2x8, 2x10, and 2x12, based on the common sizes used in wood structures (AFPA, 1991).

Approximately ten boards, ten feet long, for each depth size of Douglas-fir visually graded, structural select #2 or better lumber were obtained from the Philomath Forest Products Lumber Company, Philomath, Oregon. To decrease variability in the results, boards were selected based on modulus of elasticity values close to each other; each board's modulus of elasticity was determined via the E-computer Metriguard 340. The lumber had typical defects for the grade of lumber chosen, such as knots and checks, but wane and splits were avoided as much as possible. At the time of selection, the lumber was not kiln dried and had an average moisture content of 30%. Each ten foot piece was sawn into two five foot specimens and placed in the kiln to dry according to Table 4.2.

Table 4.2: Kiln schedule for lumber used in depth study

Stage	Hours (approximate Days)	Dry Bulb (°F)	Wet Bulb (°F)
1	49 hrs (2 Days)	142	130
2	23 hrs (1 Day)	152	137
3	64 hrs (2.67 Days)	138	131

Stages 1 and 2, in Table 4.2, reduced the initial average moisture content of 30% to approximately 15%. These moisture contents were determined on various specimens at the end of stage 2 with a resistance moisture content meter (Delmhorst Instrument Co., model J-3, serial number 10266) and confirmed with a capacitance moisture content meter (Wagner Electronics Products, model L601-3). The final stage, in Table 4.2, allowed the wood to come to equilibrium at 15% in the kiln before removing the wood to place it in the standard conditioning room at 73°F and 68% relative humidity. At the end of stage 3, the wood was placed in the standard conditioning room to allow the moisture content to equilibrate to 12%.

After conditioning, the five foot long specimens were cut into the appropriate lengths as determined through the length effect study. The results for the length study are given in Chapter 6, Experimental Results, Analysis, and Discussion. For 2x4 specimens, one to two samples were cut from each five foot piece; whereas for the 2x6 through 2x12 specimens, one sample was cut from each five foot piece. Therefore, since the boards were initially ten feet long, three to four 2x4 specimens were sawn from one ten foot long board and one to two 2x6 through 2x12 specimens were sawn from one ten foot long board. The lengths for each specimen varied according to the results gained from the length study, as shown in Table 4.3. The total length was based on the eight times the depth recommendation from ASTM (1996b). Due to machine limitations the lengths for specimen sizes 2x8 and larger were limited to 55 inches. The

sample size for each depth was ten for the same reason as stated in the length study section 4.1.1.

Table 4.3: Depth study specimen length specifications

Nominal Width x Depth (inches)	Actual Width x Depth (inches)	Sample size	8 times depth (inches)	Actual Length (inches)
2x4	1.5x3.5	10	28	28
2x6	1.5x5.5	10	44	44
2x8	1.5x7.25	10	58	55
2x10	1.5x9.25	10	74	55
2x12	1.5x11.25	10	90	55

4.1.3 ASTM shear block

The ASTM (1996a) shear block test standard was followed for ASTM specimens tested in the length study and the depth study. The ASTM specimens were used to compare the ASTM shear block-based strength with the torsion-based shear strength from the length study and the depth study.

This standard (ASTM, 1996a) was followed using the block dimensions shown in Figure 4.3 to determine the

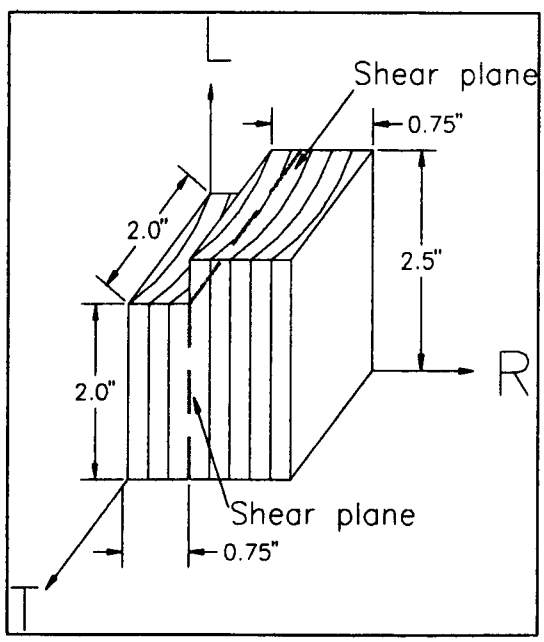

Figure 4.3: ASTM shear block dimensions used for the length and the depth study

shear strength value from the small clear blocks. The overall dimensions differed from the standard because the beams tested were actually 1.5 inches wide and sawing the specimens to allow shear strength along the longitudinal plane fixed either the width dimension in the radial direction or the width dimension in the tangential direction to equal 1.5 inches. Although one dimension differed from the standard, the shear area along the length, either in the radial-longitudinal direction or the transverse-longitudinal direction remained nominally two inches by two inches, as required by the standard (ASTM, 1996a).

For the length study, there were ten long boards resulting in ten small clear shear blocks. For the depth study, there were 50 long boards resulting in 50 small clear blocks. For the ASTM specimens from the depth study, one specimen was disqualified because it did not fail along the shear plane, and two other specimens were disqualified because clear wood was not available to allow for a shear block test. Consequently, only 47 ASTM (1996a) shear blocks were tested.

4.2 Methods

4.2.1 Testing Machines

4.2.1.1 Torsion Machine

Each torsion specimen was tested similarly to determine the maximum torque at failure using a Tinus Olsen Torsion machine (Figure 4.4), SN 2800

with a balance arm beam that displays the applied torque; this arm beam was patented in 1891. A schematic diagram of the machine is shown in Figure 4.5. Appendix A details the machine alterations necessary to computerize the recording mechanism.

The vise-like grips, as suggested by ASTM (1996b), were designed to securely clench a rectangular specimen into the machine. These grips allow the specimen to rotate about its longitudinal axis while subjected to the torsion load. The setup did not allow for longitudinal movement of either grips during twisting. Allowing longitudinal movement of grips was suggested by Hancox (1972) to avoid tensile stress build up in the specimen as it is twisting. As compensation, a gap of nearly 1/8 inch between the grip end and the specimen end was provided for unrestrained warping to occur. In a different study (Janowiak, and Pellerin, 1992), which used torsion equipment similar to the equipment used for the current study, longitudinal movement was not allowed, but an experimental correction procedure based on theoretical concepts as developed by Nederveen and Tilstra (1971) to account for restrained warping was used. Because wood is much stronger in shear parallel to the grain than in tension, observed failures in the specimen would have been tensile failures if the tensile force was significant. All observed specimen failures were shear and did not indicate tensile stresses.

The torque was applied to the specimen by a motor that was attached to the rotating head. The head on the opposite end of the specimen remained fixed and transferred the torque to the load cell. The computer then recorded

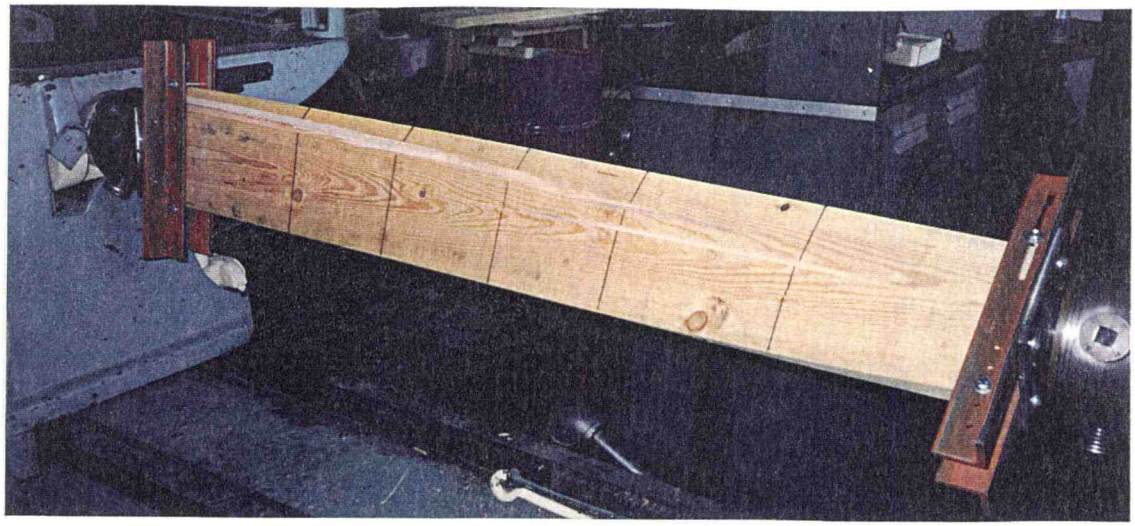

Figure 4.4: Torsion machine with secured specimen used in testing the shear strength of structural lumber

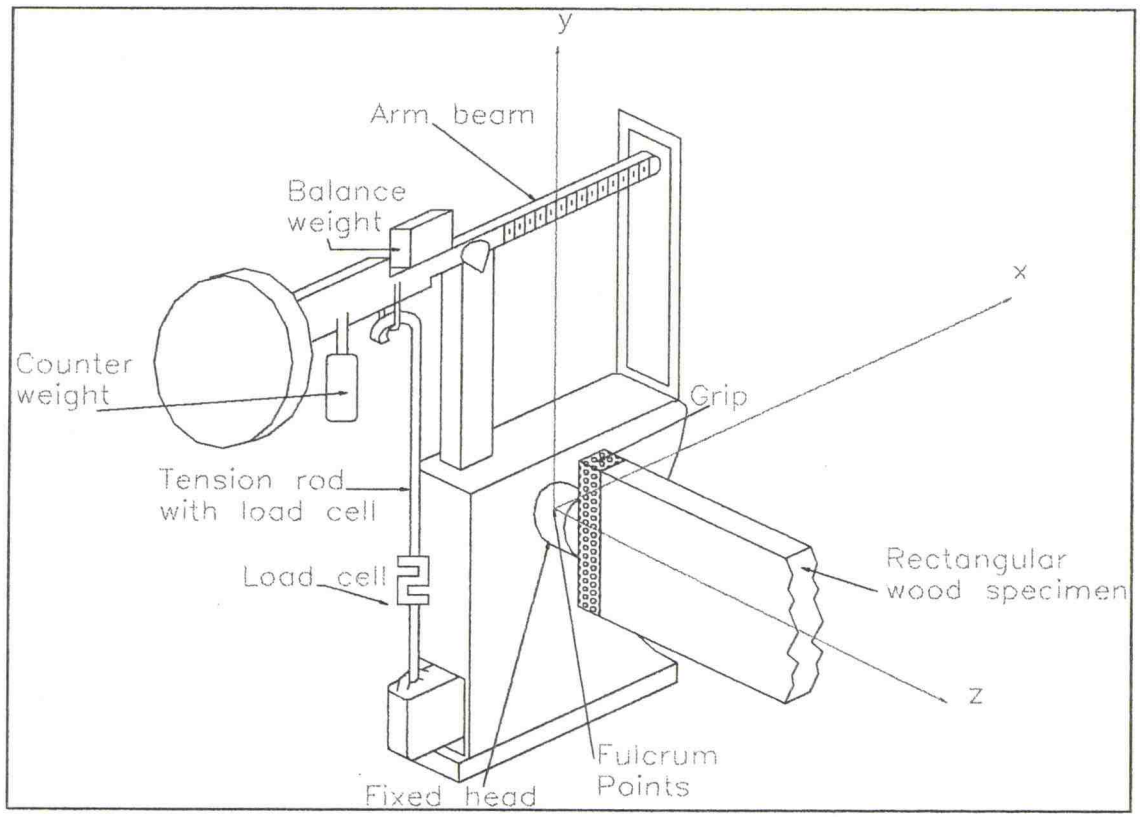

Figure 4.5: Schematic of the torsion machine used in testing the shear strength of structural lumber

the voltages read by the load cell. Appendix A explains the operation of the torsion machine. In order for the electronic apparatus to provide useful torque and rotation values, calibrations were necessary, and appendix B describes the calibration procedures and results.

The torque was applied to the specimen at the lowest speed capable by the motor; however, due to the variability of wood, the actual torque speed application varied among specimens. The 2x4 specimens averaged 0.24 degrees per inch per minute and this value decreased to an average of 0.12 degrees per inch per minute for the 2x8 and larger specimens. As suggested by ASTM (1996b), for the determination of torque-twist data for a torsion specimen, the speed of testing should be 0.223 degrees per inch per minute, or in the range of 0.115 degrees per inch per minute to 0.344 degrees per inch per minute. The speeds for the specimens in the depth study met the criteria suggested by the ASTM (1996b) standard. However, for the length study, the speed of testing was affected by the length of the specimen (2-sided p-value =0.000), the shortest length, 21.5 inches, was the only specimen group out of the length study and the depth study combined which the average speed did not meet the ASTM (1996b) suggestion; the speed for this group was higher than the suggested ASTM (1996b) standard by approximately 10%. Although the applied speed rate is affected by the specimen length, the speed is not affected by the specimen depth (2-sided p-value = 0.681; considering 2x8, 2x10, and 2x12 specimens in the linear regression). The motor was able to move at a

slower speed due to the load applied on the machine from the longer specimens compared to the shorter specimens. As for the determination of shear strength the torque should be applied at a constant rate of twist to cause failures in 10 minutes or in the range of 5 to 20 minutes. Although the average of the 2x4 specimens failed in 4.4 minutes, the larger specimens failed between 6 and 9 minutes. Because most of the specimens' loading rates and failure times were within the ASTM accepted range, modification of the motor to produced longer failure times to failure was not economically and practically justified.

4.2.1.2 ASTM Shear Tool

The current standard is detailed in ASTM D 143-94 (ASTM, 1996a) and a photograph of the shear tool used is shown in Figure 4.6.

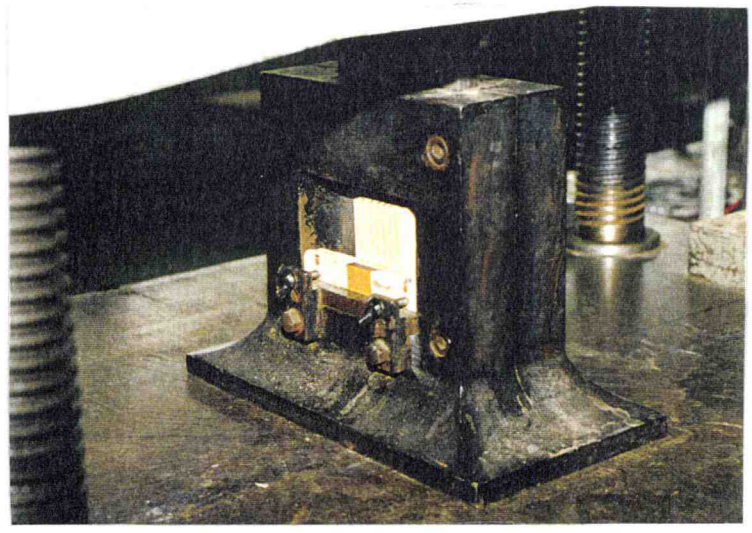

Figure 4.6: Shear tool used to perform ASTM D 143 shear test on the small clear shear blocks

4.2.2 Measurements

Measurements recorded for each specimen in the length study and the depth study included modulus of elasticity (± 0.01 x10^6psi), length (± 1/16 inch), width (± 0.001 inch), depth (± 0.001 inch), weight (± 0.001 lbs), moisture content

(± 0.1%), specific gravity (± 0.01), maximum torque (± 1 lb-in), rotation angle (± 1.0 degree), time to failure (± .1 minute), rate of loading (± .1 lb-in/sec), and number of growth rings per inch (± 0.5 ring).

For the beams, the specific gravity can vary significantly along the length of the beam (Panshin and de Zeeuw, 1980). Consequently, for the length study and depth study torsion beams, the specific gravity samples were taken as close to the shear failure as possible. The same samples used for the specific gravity test were used for the moisture content prior to the specific gravity test.

For the ASTM shear block, measurements included, length (± 0.0001 inch) and width (± 0.0001 inch) of the shear plane, moisture content (± 0.1%), specific gravity (± 0.01), and maximum load at failure (± 10 lbs).

Two properties were determined for each 14 foot long board used for the length study, (1) the modulus of elasticity and (2) the initial moisture content. The modulus of elasticity was determined using the E-computer (model 340 manufactured by Metriguard) before the lumber was sawn into the test size specimens. Also, before the lumber was sawn, a capacitance moisture meter (Wagner Electronic Products, model L601-3) was used to determine the initial moisture content of the long board. At the time of selection, the lumber had an average moisture content of 10%-15%. These pieces were placed in a standard conditioning room at 73°F and 68% relative humidity to bring the specimens to an equilibrium moisture content of 12%.

The depth study specimens were tested nondestructively to determine the modulus of elasticity. Two different methods were used to determine the modulus of elasticity. The first method was applied to the 2x8, 2x10, and 2x12 specimens; this method is known as the mechanical method. The 2x4 and 2x6 specimens were not long enough to fit into the apparatus used for the mechanical method; therefore a second method was applied to these specimens, the manual method. The mechanical method used a static bending proof tester model 440 manufactured by Metriguard. The specimen was set on two roller supports and the midspan deflection was read after a load was applied at the midspan of the beam. The manual method is similar to the mechanical method in that the midspan deflection was read after a load was applied at the midspan. However, in the manual case, the load was applied manually using calibrated weights rather than by a calibrated machine. Using the deflection and corresponding load values, the modulus of elasticity was determined based on the usual strengths of materials equation for bending deflection of a simple span.

Additional properties were determined for all torsion specimens in the length and depth study, after the longer boards were sawn into the test sizes specified previously. Before the torsion testing, the length, width, depth, weight, and the number of rings per inch were recorded for each test piece. The width and the depth were each measured in three places, and the average values for both properties were reported. During testing, physical properties were recorded on a specimen sketch, which included knots, piths, checks, splits (if any), growth

ring orientation, and failure cracks. After these specimens were tested in the torsion machine, additional properties were determined from each test piece. These properties included moisture content and specific gravity. The moisture content was determined in accordance with the ASTM D4442-92, method A (ASTM, 1996h). The same specimen used for the moisture content calculation was then used for the specific gravity determination in accordance with the ASTM D2395-93, method B (ASTM, 1996f). In addition to documenting the failure crack and physical properties, the depth specimens were photographed after testing.

4.2.3 Calculations

The torque values recorded from the torsion machine at failure and the recorded cross sectional dimensions are the main parameters used to calculate the maximum shear stress for the specimen. Additional torsion factors, based on the depth to width ratio of the cross section, are also necessary in the shear stress equations.

The shear stress equations, Equation 4.1 and Equation 4.2, were detailed in Chapter three, Torsion Theory (Trayer and March, 1929). The maximum shear stress at the middle point of the long side, τ_l, is a function of the applied torque, T; beam depth, 2h; beam width, 2b; and geometric factors, μ and γ, as defined in Table 4.4 (Trayer and March, 1929). The maximum shear stress at the middle point of the short side, τ_s, is a function of the applied torque, T; beam

width, 2b; and geometric factors, μ and γ_1, as defined in Table 4.3 (Trayer and March, 1929).

$$\tau_l = \frac{\gamma T}{\mu h b^2} \tag{4.1}$$

$$\tau_s = \frac{\gamma_1 T}{\mu b^3} \tag{4.2}$$

Table 4.4: Factors for calculating shear stress of rectangular beams[1]

Specimen Size	Ratio of Sides	μ	γ	γ_1
2x4	2.26	3.8893	1.9153	0.6431
2x6	3.59	4.397	1.9882	0.4155
2x8	4.8	4.6661	1.9973	0.3118
2x10	6.09	4.7803	1.9998	0.2485
2x12	7.43	4.879	2.0000	0.2015

[1] Trayer and March, 1929

For the ASTM (1996a) shear blocks the ASTM (1996a) standard was followed, and the shear stress was calculated using the required load at failure and the cross sectional area of the shearing plane as given by Equation 4.3 (ASTM, 1996h) where τ=shear stress, P=the load applied to the specimen at

failure, and A=the product of the width and height of the shear plane, shown in Figure 4.3.

$$\tau = \frac{P}{A} \tag{4.3}$$

5. Finite Element Modeling

The finite element model provided an improved understanding for a torsion specimen regarding (1) the stress distribution, (2) the shear span and (3) the failure mode, defined in Figure 3.4.

5.1 Geometric development of finite element model

The finite element model was developed using the educational version of a commercially available finite element modeling program, ANSYS® (Swanson, 1992). Using the SOLID45 element (3-D, 8 nodes), the rectangular beam was modeled with the coordinate definition as shown in Figure 5.1. Each node had six degrees of freedom, allowing translations and rotations in the x, y, and z directions.

Two rectangular beams were analyzed, a 2x4 (1.5 inches by 3.5 inches) and a 2x12 (1.5 inches by 11.25 inches). Due to the limitation, of 16,000 nodes for the educational version of ANSYS® available for this study, the 2x4 mesh differed slightly from the 2x12 mesh. For both meshes, the

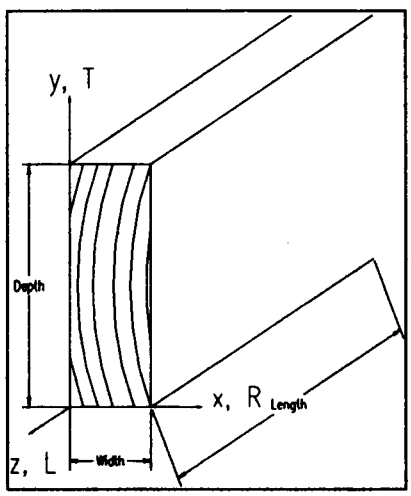

Figure 5.1: Typical beam modeled and tested

applied load and the constrained node patterns were similar. Since length was thought to be a factor affecting shear strength, two lengths for each depth were analyzed: 28 inches and 43 inches for the 2x4 beam and 55 inches and 90 inches for the 2x12 beam.

5.1.1 Mesh size

A convergence study, detailed in section 5.2.1, was performed to determine the optimum geometric design of the finite element model for the 2x4 and the 2x12 beam. Meshes resulting from this convergence study are summarized in Table 5.1 for the purpose of discussing the geometric development of the finite element model.

Table 5.1: Mesh specifications

Mesh Property	Beam Size			
	2x4	**2x4**	**2x12**	**2x12**
Dimensions	1.5"x3.5"x28"	1.5"x3.5"x43"	1.5"x11.25"x55"	1.5"x11.25"x90"
Element length[1]	1.00"	1.00"	1.00"	1.00"
Ratio[2]	1/4	1/4	1/4	1/4
Divisions for x-axis	16	16	12	12
Divisions for y-axis	20	20	12	12
Nodes	10,353	15,708	9,464	15,379

[1] Along length of beam, z axis in Figure 5.1.

[2] Ratio of outside element depth to middle element depth and ratio of outside element width to middle element width, where outside element is any element bordering the outside surface of the beam.

Table 5.1 outlines the final mesh specifications and Figure 5.2 and Figure 5.3 show the final cross sectional mesh used for a 2x12 and a 2x4, respectively. Both the 28 inch long 2x4 and the 43 inch long 2x4 had a mesh ratio of outside edge element to middle inside element of 1/4 with 16 elements along the x-axis and 20 elements along the y-axis. For the 55 inch 2x12 the mesh ratio was the same as for the 2x4, 1/4, but with only 12 elements in the x direction and 12 elements in the y direction. Due to the length increase from the 43 inch 2x4 to the 55 inch 2x12, the number of elements in the x direction was modified from 16 elements and the y direction was modified from 20 elements, as used for the 2x4, to 12 elements in the x and y directions for the 2x12 model to avoid exceeding the node limit.

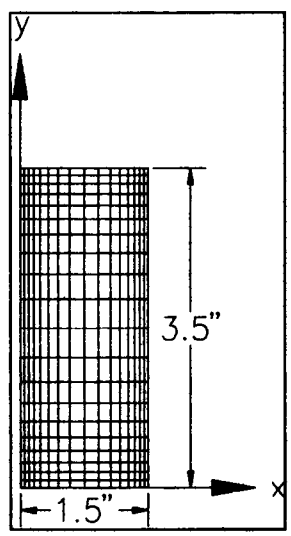

Figure 5.3: Cross sectional mesh for 2x4

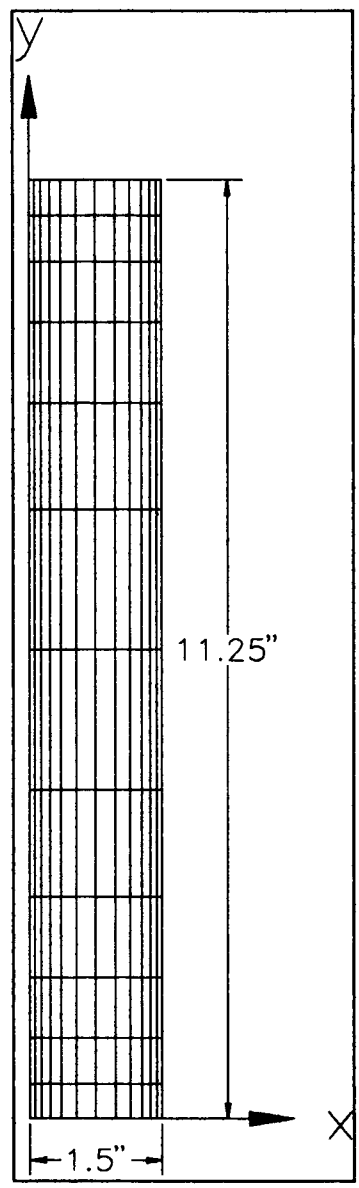

Figure 5.2: Cross sectional mesh for 2x12

5.1.2 Boundary conditions

On the opposite end of the beam from the applied load, the nodes are constrained for a distance of two inches along the length, in the z direction, and over the entire depth, in the y direction, on each side of the beam. Figure 5.4 shows the location of the constrained nodes and the location of the applied pressure.

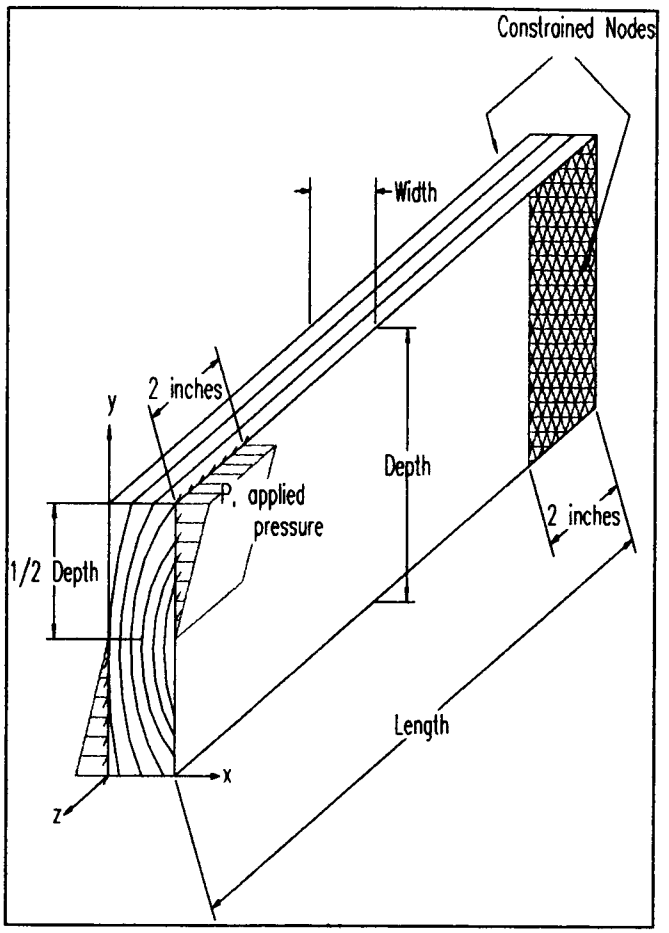

Figure 5.4: Applied pressure, representing the applied torque, and constrained nodes

The finite element model best represented the laboratory torsion specimen by leaving the nodes on the beam face end, the top, and the bottom unrestrained. Since warping was unrestrained in the laboratory experiments, as discussed in chapter 4, Materials and Methods, the model must also reflect unrestrained conditions. In addition, the nodes were constrained in all directions to provide model stability.

5.1.3 Applied loads

Since a torque could not be directly applied to the end of the beam, the method used to simulate torque in ANSYS® (Swanson, 1992) was to apply loads to one end of the rectangular beam as a force couple. Figure 5.4 illustrates the loading applied to the rectangular beam. In the laboratory, the load consistently impacted the corners on the opposite sides of the cross section of the rectangle more than the center of the cross section of the rectangle. To account for more bearing on the corners compared to the center, a triangular load distribution was used rather than a uniform load distribution. One half of the couple was distributed over the lower half depth, and the other half was distributed over the upper half depth on the opposite side of the beam. The applied pressure values were based on experimental results; the torque applied to the model was within the linear region of the load-time plot observed in the laboratory for a typical beam. For the 2x4 beams the torque was 2,000 inch-pounds, and for the 2x12 beams the torque was 6,000 inch-pounds. These torque values for the 2x4 and 2x12 beams translated into equivalent pressures of 490 pounds per square inch and 27.1 pounds per square inch, respectively, for the maximum triangular pressure, P, shown in Figure 5.4. Equation 5.1 was used to convert the torque into a triangular force couple, based on statics, where P= maximum pressure,

T= applied torque, d=depth of rectangular beam, and z= distance along z-axis over which the triangular load is distributed.

$$P = 6\frac{T}{d^2 z} \tag{5.1}$$

Although the torque was an applied couple rather than an applied rotation, the loaded end of the model represents the experimental set up more closely than the constrained end of the model because the constrained end of the model was restrained in the z direction, where the laboratory specimens were allowed to move along the z direction. As a result, the constrained end of the finite element model may affect the shear stress distribution for longer distances toward the center point of the modeled beam.

5.1.4 Properties

During the initial finite element analysis, isotropic properties were used to represent the wood material. An isotropic material assumption eliminated any influences orthotropic properties may have had on the development of the model. Once the finite element model yielded results that compared favorably to theoretical calculations using an isotropic material assumption, orthotropic properties were introduced into the model. Table 5.2 and Table 5.3 list the isotropic properties and the orthotropic properties, respectively, used in the model.

Table 5.2: Isotropic properties representing wood material

Modulus of Elasticity (psi)	Shear Modulus (psi)	Poisson's Ratio
$E=1.6X10^6$	$G=1.0X10^5$	PR=0.4

Table 5.3: Orthotropic properties representing wood material

Modulus of Elasticity (psi)	Shear Modulus (psi)	Poisson's Ratio
$E_X=0.1424X10^6$	$G_{YZ}=0.1077X10^6$	$PR_{YZ}=0.0169632$
$E_Y=0.0912X10^6$	$G_{XY}=0.01234X10^6$	$PR_{XY}=0.4320416$
$E_Z=2.141X10^6$	$G_{XZ}=0.1160X10^6$	$PR_{XZ}=0.0216448$

[1] Orthotropic properties of wood were taken from Bodig and Jayne, 1982

5.2 Results

5.2.1 Convergence study for the mesh study

A convergence study was performed to optimize the mesh size. Various analyses were performed and the results were compared with theoretical calculations. Results compared with theory included the maximum shear stress value, the location of the maximum shear stress in the cross section, and the shear stress at the corners of the cross section. The convergence study was performed using isotropic wood properties for a 28 inch long, 2x4 beam so that comparisons could be made between the finite element model and theory. The

model geometry that compared favorably with theory was used as the model geometry with orthotropic properties.

Figure 5.5 shows the plot of four different mesh sizes, listed in Table 5.4, used in the convergence study. The difference between mesh a and mesh b is the length of the element. Figure 5.5 shows that these two meshes are similar in their accuracy of the shear stress, τ_{yz}. Also, mesh c and d differ only in the length of the element, plotting these mesh results on Figure 5.5 indicate that the two meshes are similar in their accuracy of the shear stress, τ_{yz}. Therefore decreasing the length of each element along the z axis did not alter the location of the maximum shear stress and showed a negligible increase in the maximum shear stress value.

Table 5.4: Meshes examined for the convergence study.

	Mesh			
	a	**b**	**c**	**d**
Width, x	0.5	0.5	0.25	0.25
Depth, y	0.5	0.5	0.25	0.25
Length, z	1.0	0.5	0.5	0.25

However, meshes a and b differ from meshes c and d in width and depth dimensions. By increasing the cross sectional dimensions of the element, Figure 5.5 shows an improvement in the accuracy of the maximum shear stress

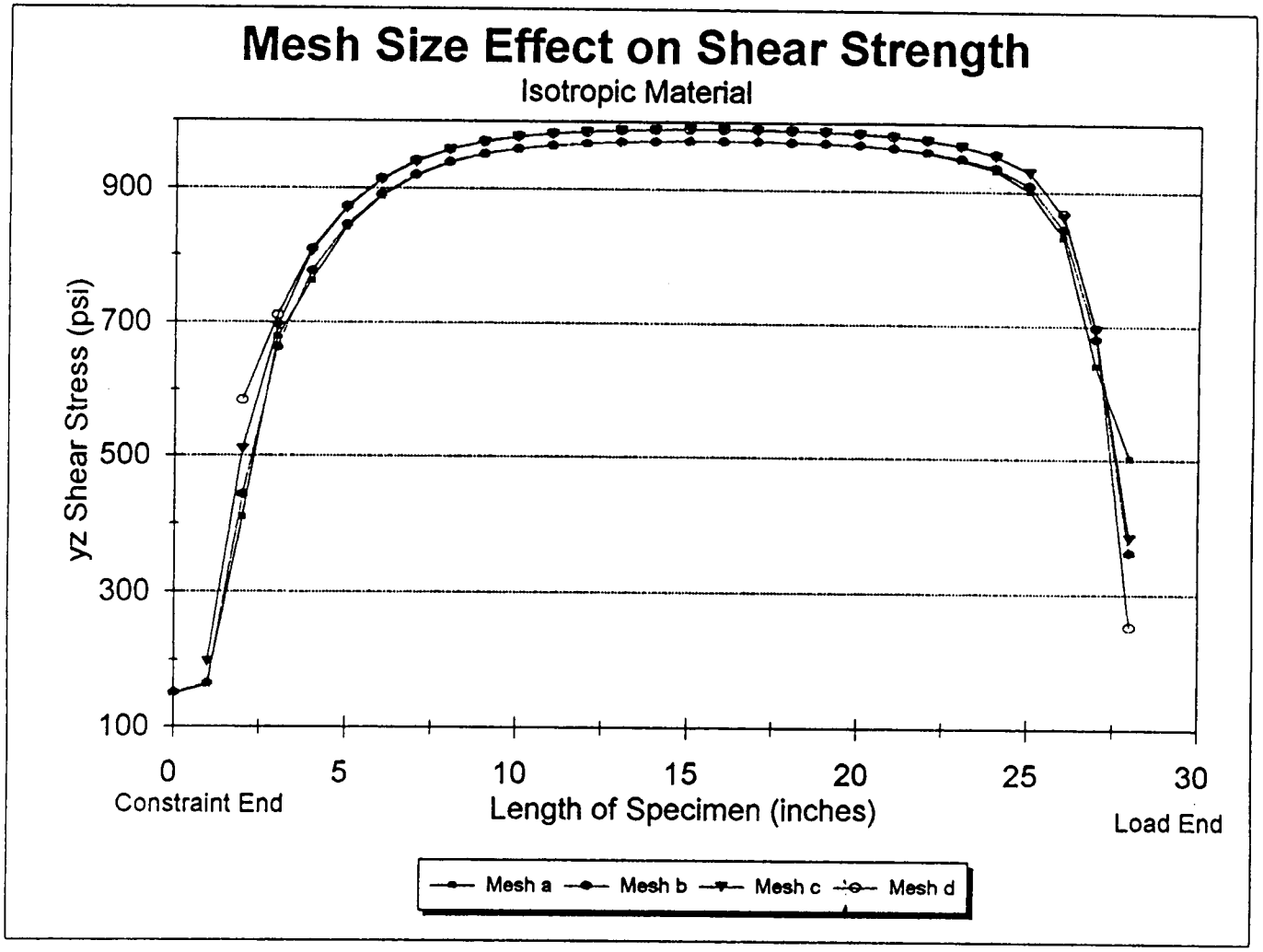

Figure 5.5: Mesh size effect on shear strength for a 2x4 finite element model with 2,000 in-lb torque

value. Both a and b meshes are 3.2% lower than the theoretical calculated τ_{yz} of 1000 psi, based on equation 3.9 (Trayer and March, 1929), but mesh c and d are only 1.5% lower than theoretical calculated τ_{yz} of 1000 psi, based on equation 3.9 (Trayer and March, 1929).

Figure 5.6 shows the effect of length on the shear stress, τ_{yz} by comparing a 28 inch long 2x4 beam to a 55 inch long 2x4 beam. Although the magnitude and the location of the maximum shear stress did not change when the overall length of the specimen was altered, the specimen length increase allows a longer shear span to establish a uniform shear stress, which will be detailed in section 5.2.3.

The mesh ratio, which varied the element size by using smaller elements along the edges and larger elements in the middle of the cross section, allowed for more elements to define the cross section, and as a result improved the accuracy of the corner shear stress value. Although changing the mesh ratio caused a negligible effect on the maximum shear stress value, the mesh ratio had a substantial effect on the shear stress at the corners. The corner shear stress, which should theoretically be equal to zero, decreased by 116% from 302 psi for the model with a constant element size to 140 psi for the model with a variable element size.

5.2.2 Stress distribution

Observing the stress distribution assisted in determining the shear span, the sliding direction, and the failure direction for a torsion specimen. Figure 5.7 and Figure 5.8 present the distribution of the shear stress which initiates failure, τ_{yz}. Viewing the top of the beam in Figure 5.7, τ_{yz} is in the color range of 114.2 psi to -114.2 pounds per square inch. However, on the side of the beam in Figure 5.8, τ_{yz} varies in color and thus varies in shear stress values. On the side of the beam, the shear stress reaches a large value near the center of the long side and near the center of the beam length corresponding to the color range of 799.5 to 1028 pounds per square inch.

Outside of the shear span, which will be determined in section 5.2.3, the stress distribution is not predicted by theory. This occurs near the constrained end and near the loaded end where the color varies significantly. Especially at the loaded end of the beam, there is compression perpendicular to the grain of the wood due to the grips that are required to hold the specimen in the machine and apply the torque to the beam. As a result, normal stresses in several directions as well as shear stresses in several directions occur at the ends of the beam.

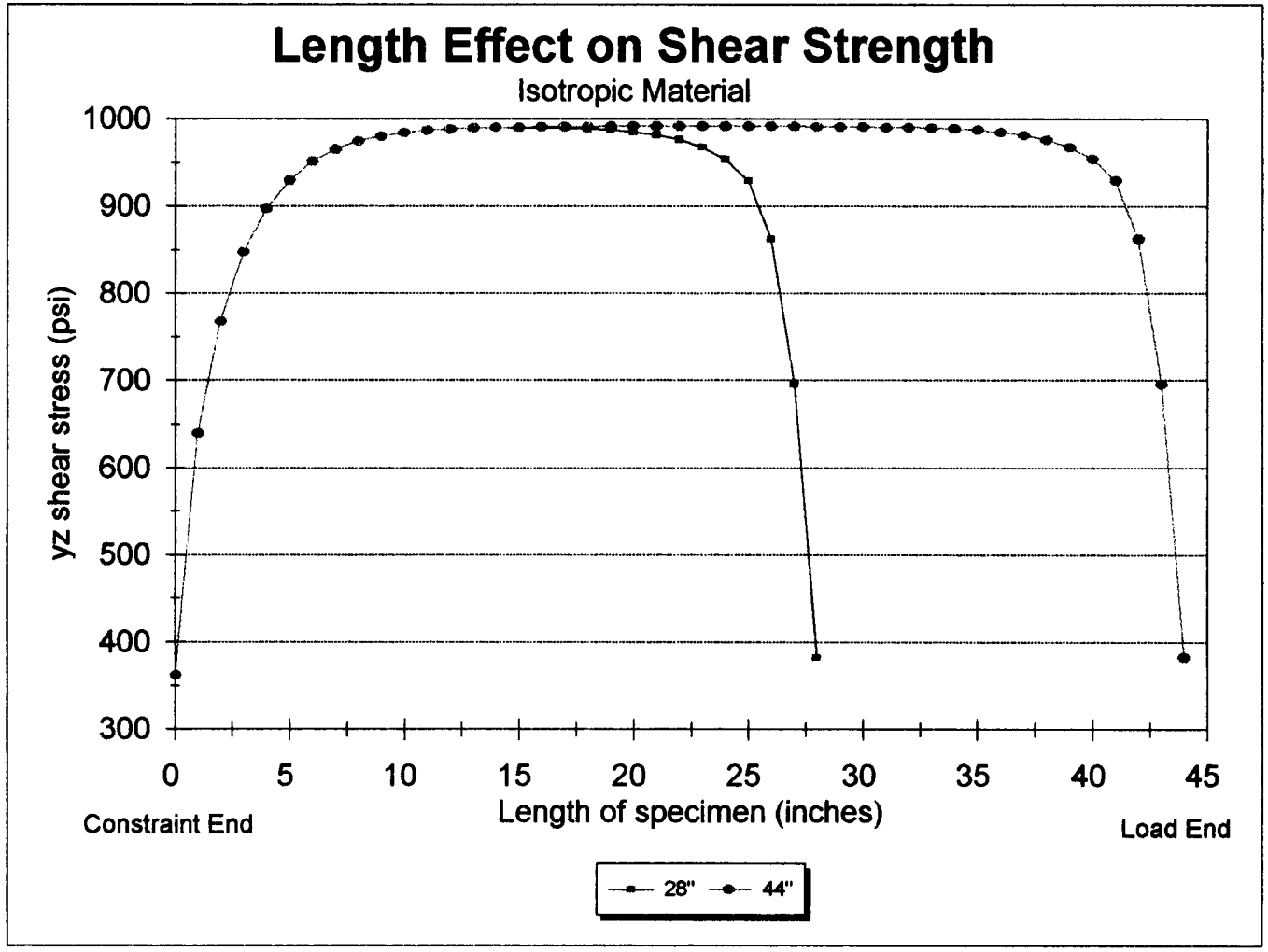

Figure 5.6: Beam length effect on shear strength for a 2x4 finite element model with 2,000 in-lb torque

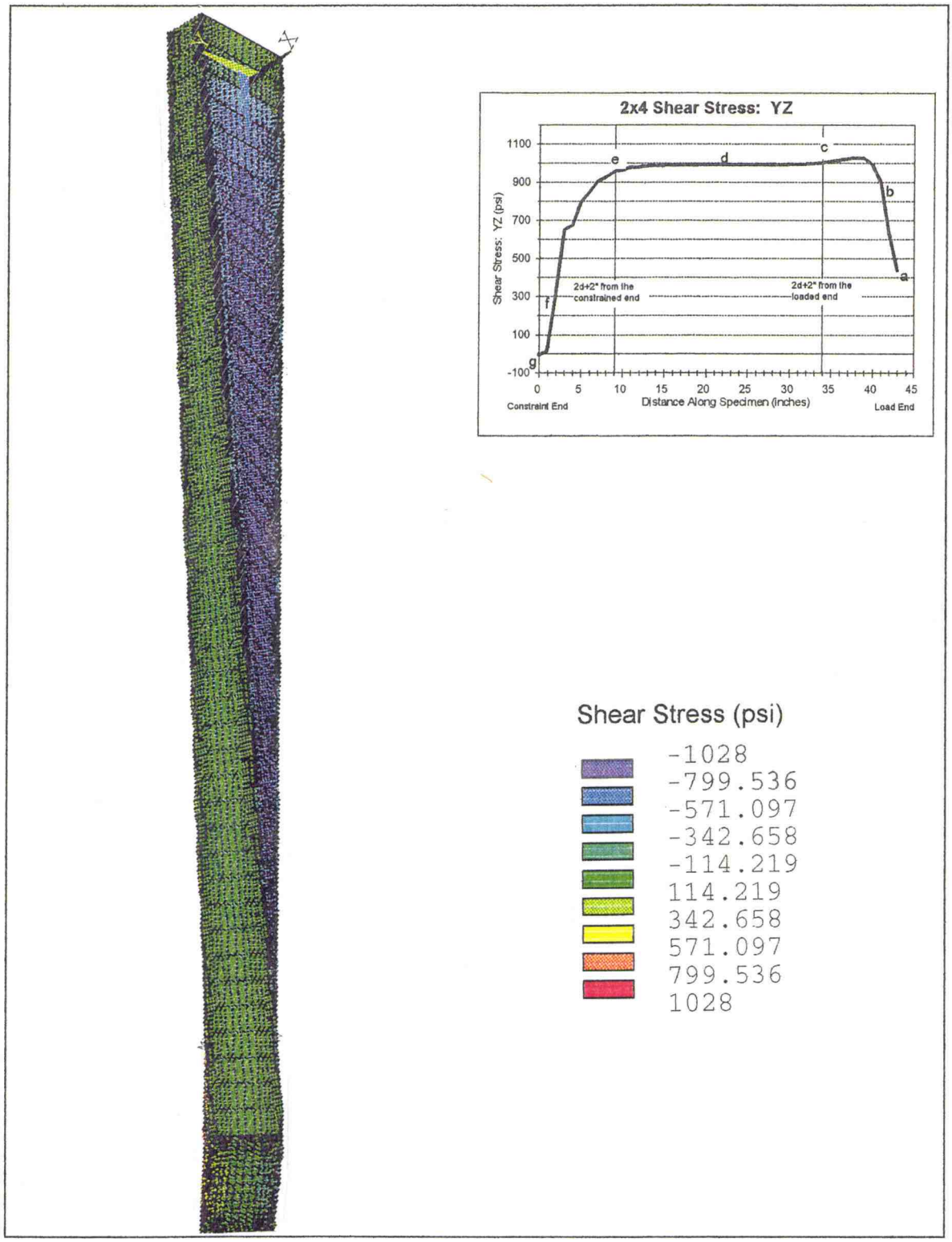

Figure 5.7: Top view of 2x4--τ_{yz} distribution for a 43" long beam with a 2,000 in-lbs. applied torque

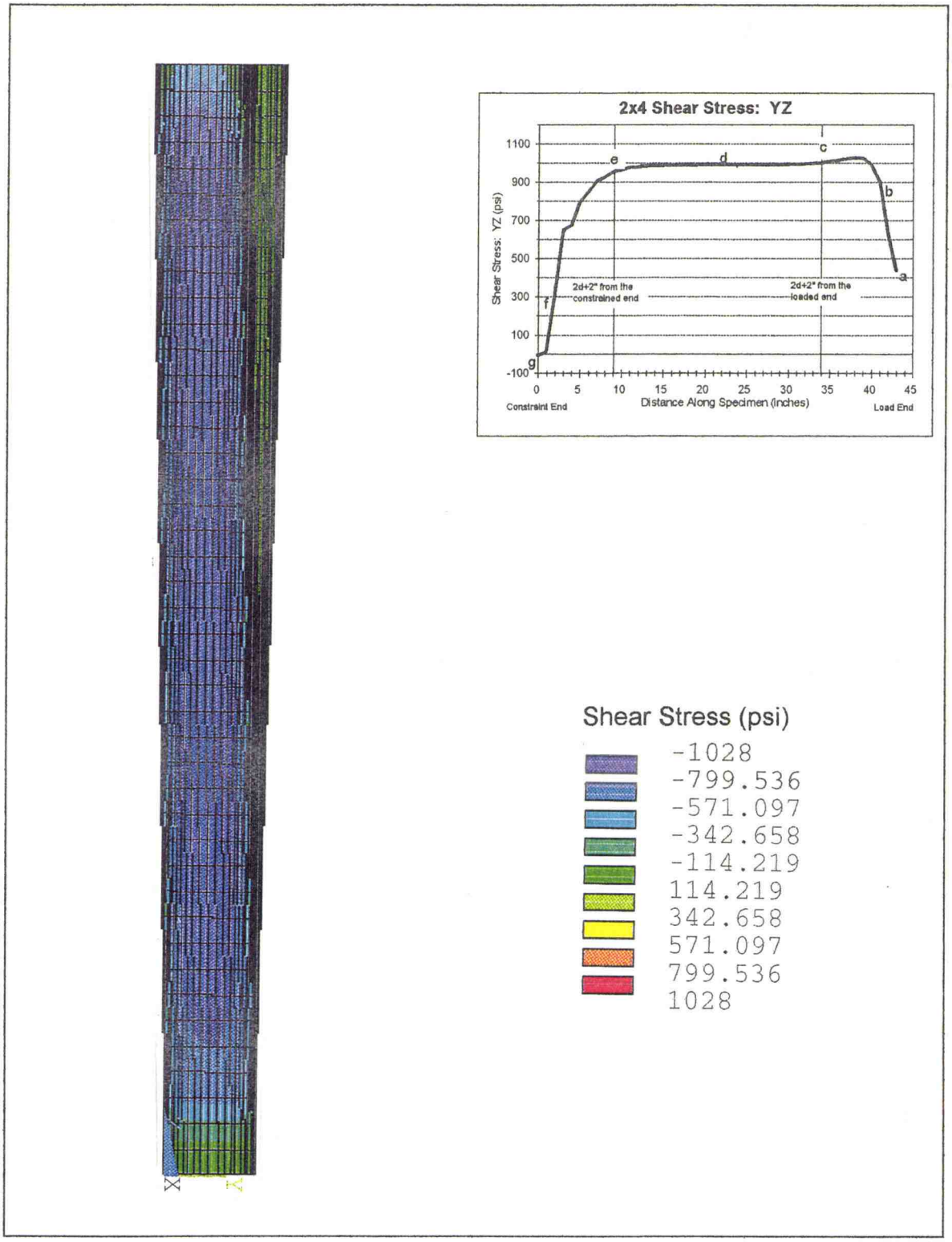

Figure 5.8: Side view of 2x4--τ_{yz} distribution for a 43" long beam with a 2,000 in-lbs. applied torque

Figure 5.9 and Table 5.5 together identify stresses and values obtained from the finite element model for particular points in a 2x4 beam. The identification code used for the points of interest are abbreviations that represent the loaded end (LE), loaded grip section (LG), middle section (M), constrained end (CE), constrained grip section (CG), middle point of short side (S), middle point of long side (L), and center point of cross section (C). The finite element results, as displayed in Table 5.5, indicate that within the shear span, from the loaded grip section to the constrained grip section, only one shear stress occurs in the beam and normal stresses do not occur.

The model presents a case which is substantially different from theory. This occurs at the point along the center of the cross section at the loaded end, LEC, for τ_{xy}. Theoretically all τ_{xy} values should be zero, at LEC point τ_{xy} equals 282 psi. The loading conditions, a triangular distributed load at this end, may be causing an initially large τ_{xy} value. Moving along the length of the beam, τ_{xy} decreases dramatically such that within the shear span τ_{xy} is zero or within 10% of zero; this compares favorably with theory. Since theory only applies within the shear span, where all stresses should be uniform, the large τ_{xy} values outside the shear span are of little concern.

Theoretically τ_{xy} equals zero everywhere on a rectangular beam subject to torsion. Although the model shows a value for τ_{xy} =-2 psi at the center point of the cross section for the loaded grip end (LGC) and τ_{xy} =-9 psi at the center point of the cross section at the constrained grip end (CGC), these values are

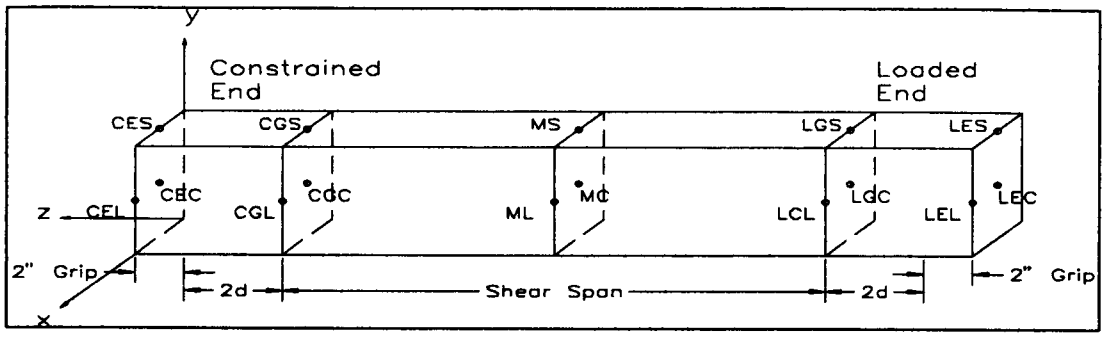

Figure 5.9: Schematic of 2x4 with points of interest for the finite element results presented in Table 5.5

Table 5.5: Finite element results[1], from 2x4 with a 2,000 in-lb. applied torque

Point on Figure 5.9	τ_{yz} (psi)	τ_{xz} (psi)	τ_{xy} (psi)	σ_x (psi)	σ_y (psi)	σ_z (psi)
Short side:						
CES	0	-49	2	0	0	0
CGS	0	780	0	0	0	0
MS	0	781	0	0	0	0
LGS	0	780	0	0	0	0
LES	0	133	20	-260	0	14
Long side:						
CEL	-7	0	-13	0	0	0
CGL	955	0	0	0	0	0
ML	989	0	0	0	0	0
LGL	1002	0	0	0	0	0
LEL	437	2	-25	0	-25	1
Center:						
CEC	0	0	-11	0	0	0
CGC	0	0	-9	0	0	0
MC	0	0	0	0	0	0
LGC	0	0	-2	0	0	0
LEC	0	0	282	19	-9	3

[1] For practical purposes when comparing the shear stresses, any stress that was less than 1.0 psi was considered negligible and reported as zero.

negligible compared to the other shear stresses observed, τ_{yz} =1002 psi, 989 psi, and 955 psi; and τ_{xz}=780 psi, 781 psi, and 780 psi. Within the shear span, the finite element model results predicted theoretical results reasonable well: (1) all shear stresses are nearly zero at the cross sectional center line along the z axis of the rectangular specimen, (2) one shear stress occurs at the point of failure, τ_{yz}=987 psi (average of 26 points within the shear span and coefficient of variation of 0.96%), at the middle point of the long side, (3) the shear stress τ_{xy} is zero for all practical purposes (and can be considered negligible) throughout the shear span. Therefore, the stress at the middle point of the long side, τ_{yz}, is taken as the shear strength of Douglas fir lumber which is always higher than the stress at the middle point of the short side, τ_{xz} (Lekhnitskii, 1981)

Stress distribution plots for τ_{yz} are illustrated in Figure 5.10. The graph presented in each figure shows the τ_{yz} plot along the length of the beam for the point on the middle of the long side for a 2x4 beam 43 inches long with a 2,000 inch-pound applied torque. Viewing the cross section of the beam from the loaded end for the 43 inch beam, Figure 5.10a shows that the shear stress is small in the center and at the corners. Although near the middle of the long sides the shear stress is a small value, it is increasing. The stress τ_{yz} continues to increase along the length of the beam, as shown in Figure 5.10b, the cross section at the end of the grips for the 43 inch beam, 41 inches from the constrained end. In this figure, the stress distribution shows small values at the corners and in the center and increasing values from the cross section center to the middle point of the long side. The region of large shear stress at the middle

section of the long side increases in size as one moves along the beam, from Figure 5.10b, 41 inches from the constrained end, to Figure 5.10c, 34 inches from the constrained end. At the beginning of the shear span, Figure 5.10c, shows a cross section nearly identical to Figure 5.10b, but the region of large shear stress has increased in size.

At the beginning of the shear span, in Figure 5.10c, the shear stress has almost reached uniformity within the cross section and nearly matches the theoretical stress of 1,000 psi for a rectangular specimen under torsion, based on equation 3.9 (Trayer and March, 1929). Figure 5.10d illustrates a cross section at the middle of the beam where length equals 21.5 inches. Again this section, which is in the middle of the shear span, is almost identical to the section shown at the beginning of the shear span, Figure 5.10c.

Due to the method of applying the torsion loads on the finite element model, the stresses on cross sections at the loaded end may differ slightly from those for the cross sections at the constrained end. Figure 5.10e displays the location 9 inches from the constrained end where the stresses do not appear to have changed from those at the cross section at the middle of the shear span. However, 2 inches from the constrained end in Figure 5.10f, the shear stress at the middle point of the long side decreases dramatically and the stress approaches zero. Finally, the shear stress reaches zero in the cross section at the constrained end, Figure 5.10g.

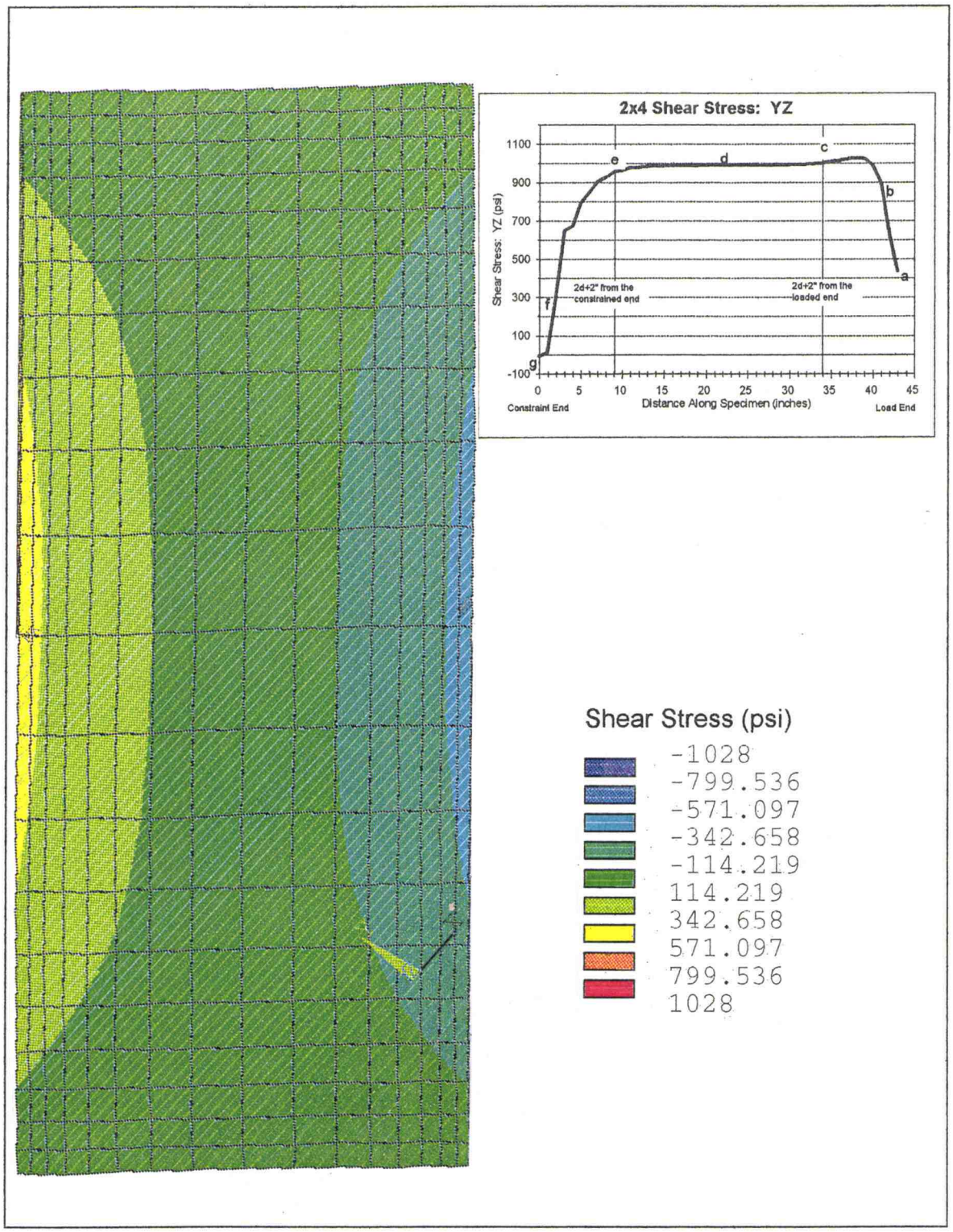

Figure 5.10: Finite element τ_{yz} shear stress plots (a) τ_{yz} over the cross section at the loaded beam end for 2x4 beam length of 43 inches and applied torque of 2,000 in-lbs.

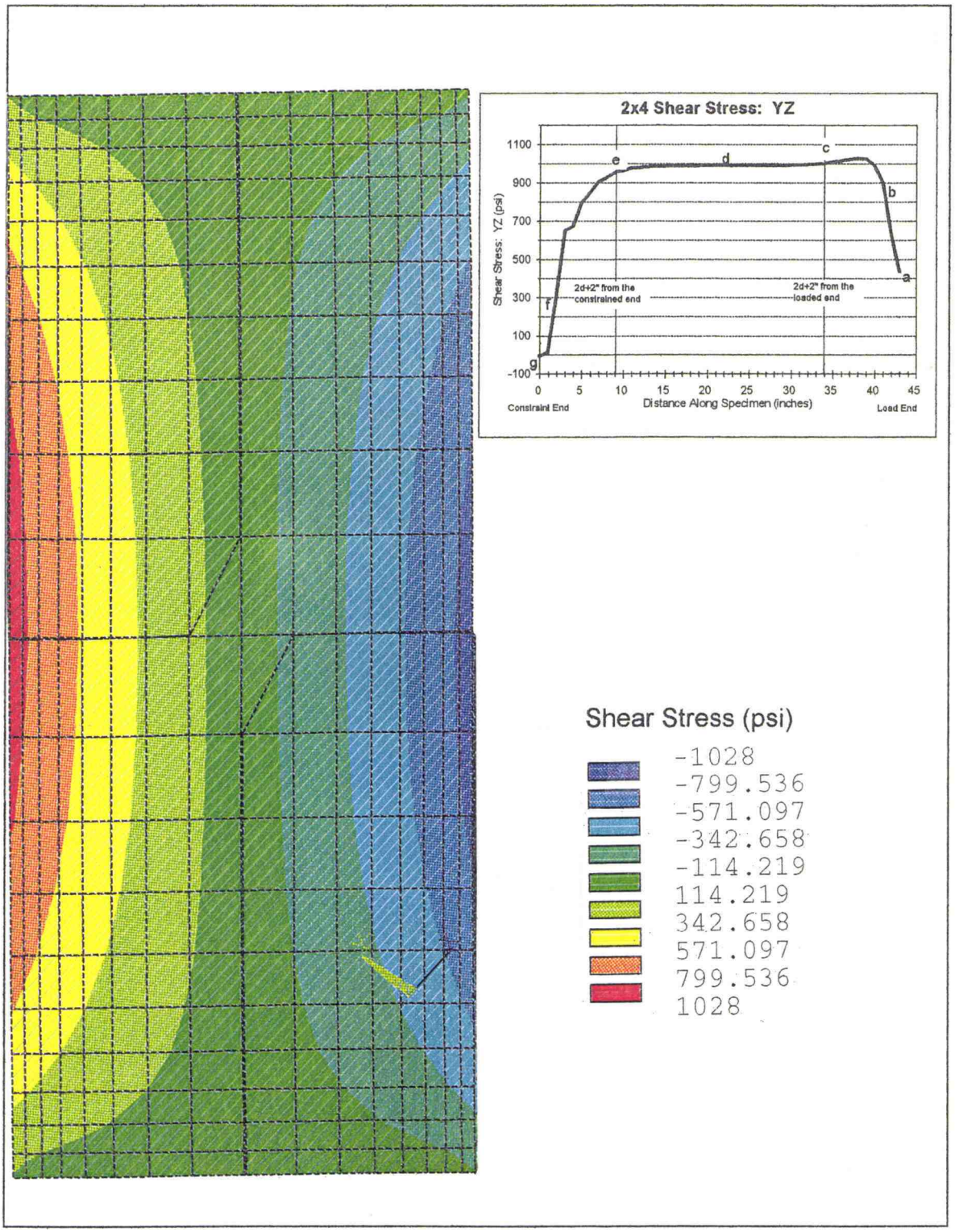

Figure 5.10: Finite element τ_{yz} shear stress plots (b) τ_{yz} over the cross section at the edge of the grips; 41 inches from the constrained end for 2x4 beam length of 43 inches and applied torque of 2,000 in-lbs.

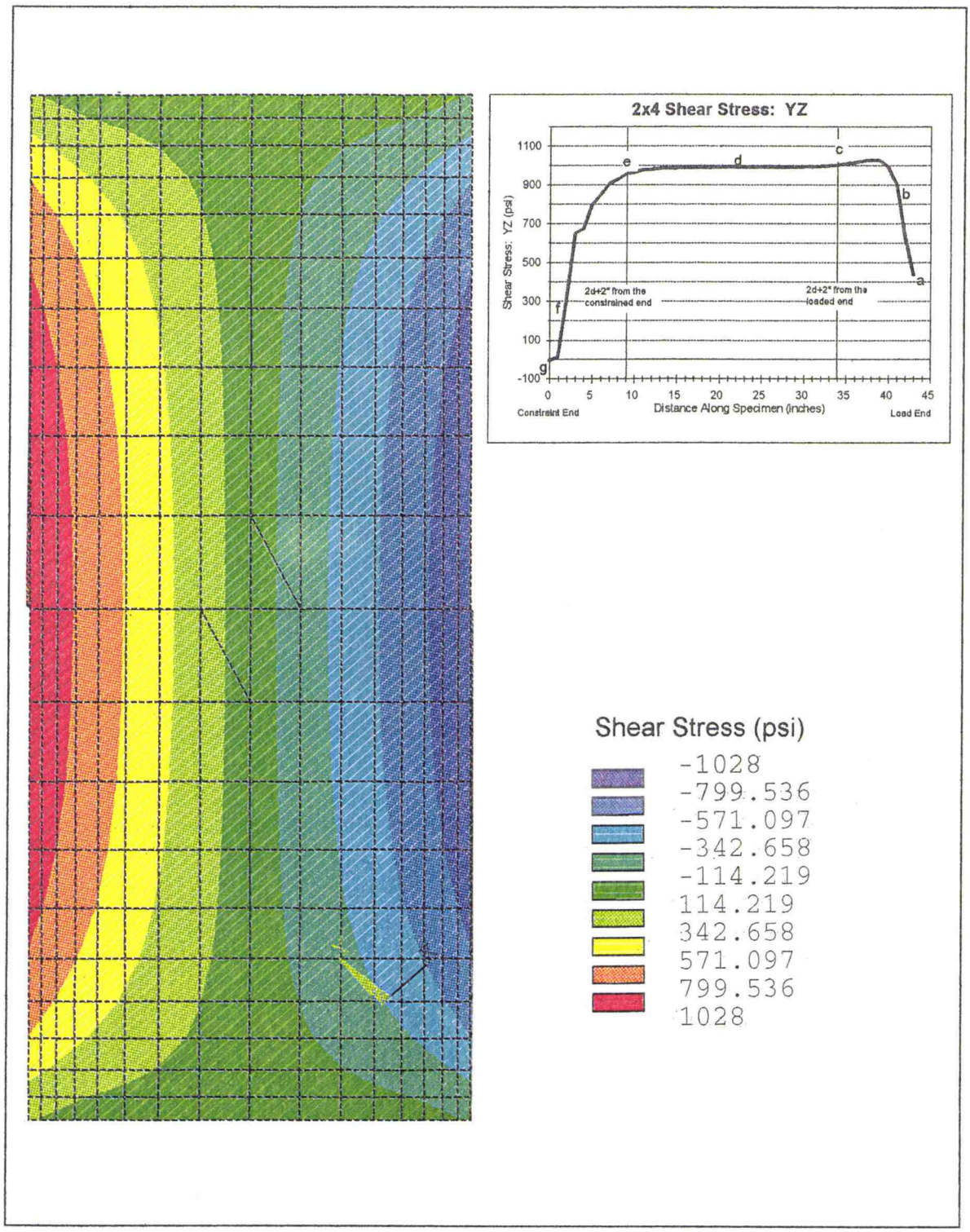

Figure 5.10: Finite element τ_{yz} shear stress plots (c) τ_{yz} over the cross section at the beginning of the shear span; 34 inches from the constrained end for 2x4 beam length of 43 inches and applied torque of 2,000 in-lbs.

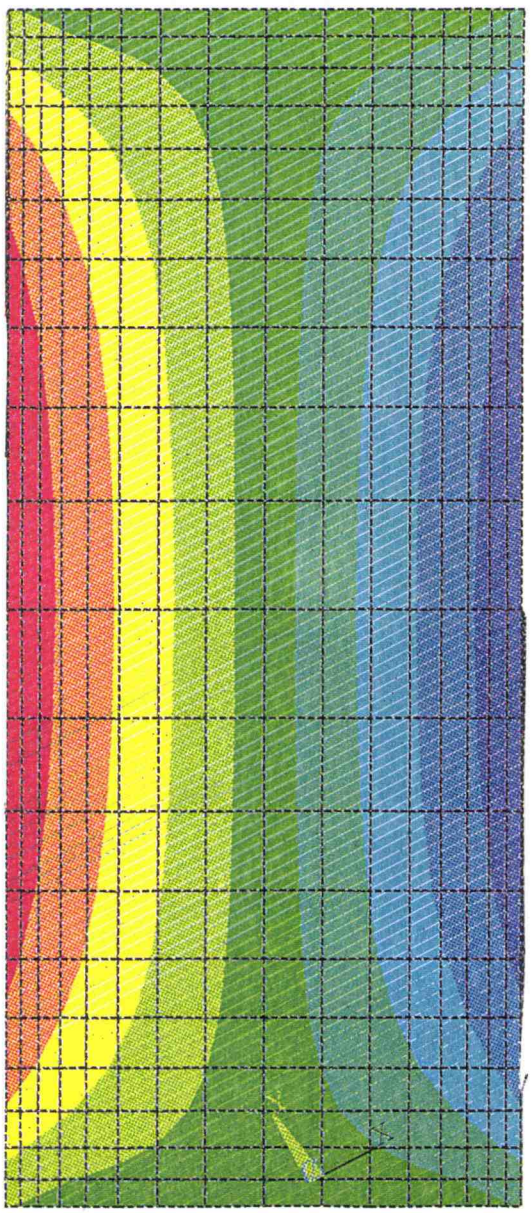

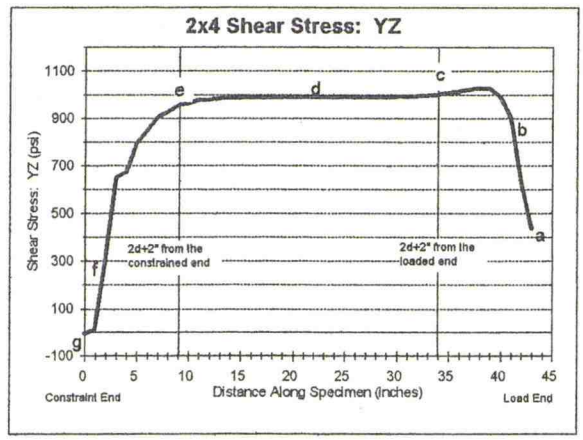

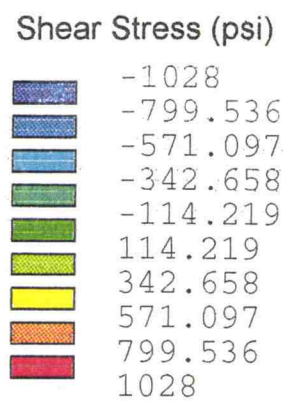

Figure 5.10: Finite element τ_{yz} shear stress plots (d) τ_{yz} over the cross section at the middle of beam; 21.5 inches from the constrained end for 2x4 beam length of 43 inches and applied torque of 2,000 in-lbs.

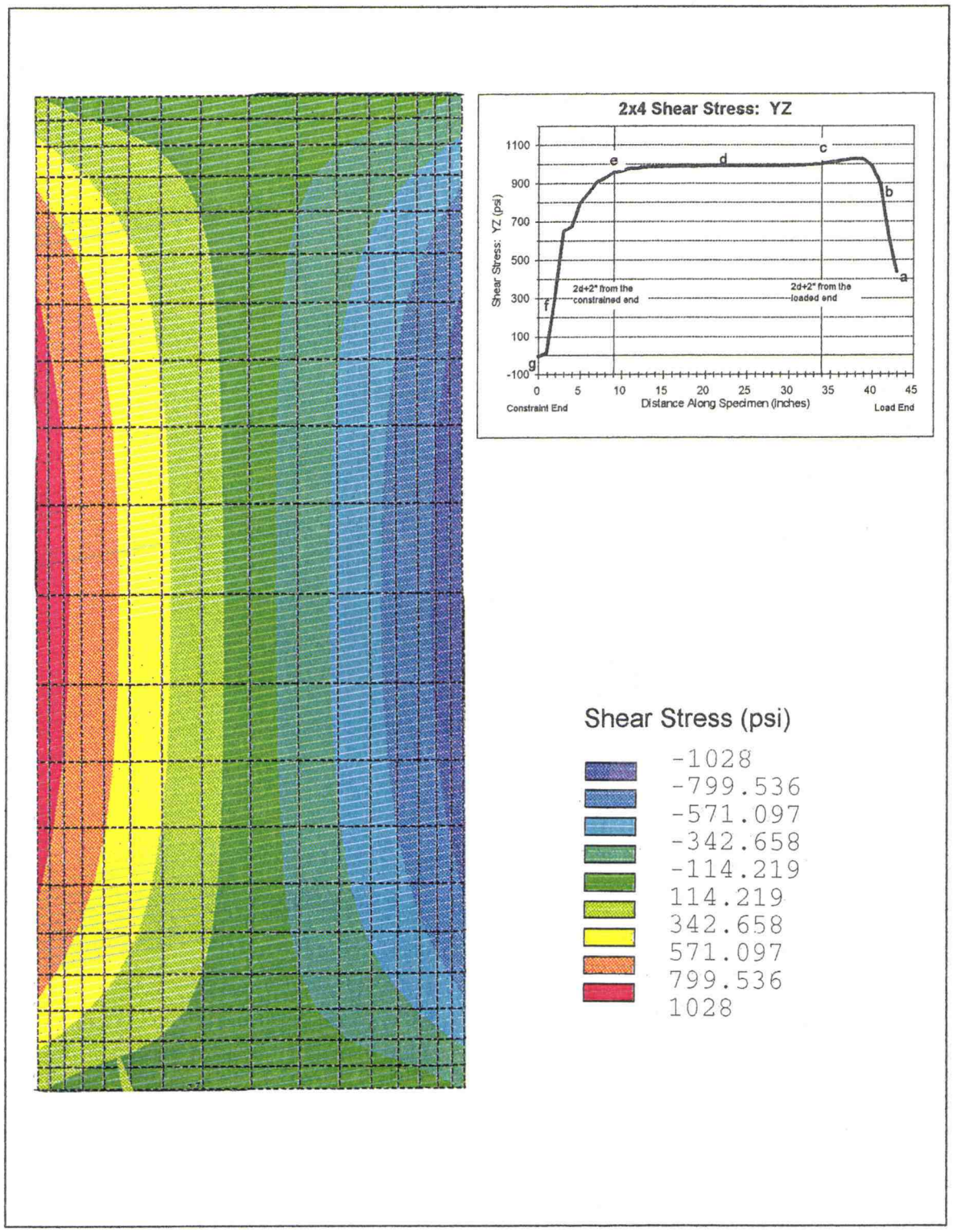

Figure 5.10: Finite element τ_{yz} shear stress plots (e) τ_{yz} over the cross section at the end of the shear span; 9 inches from the constrained end for 2x4 beam length of 43 inches and applied torque of 2,000 in-lbs.

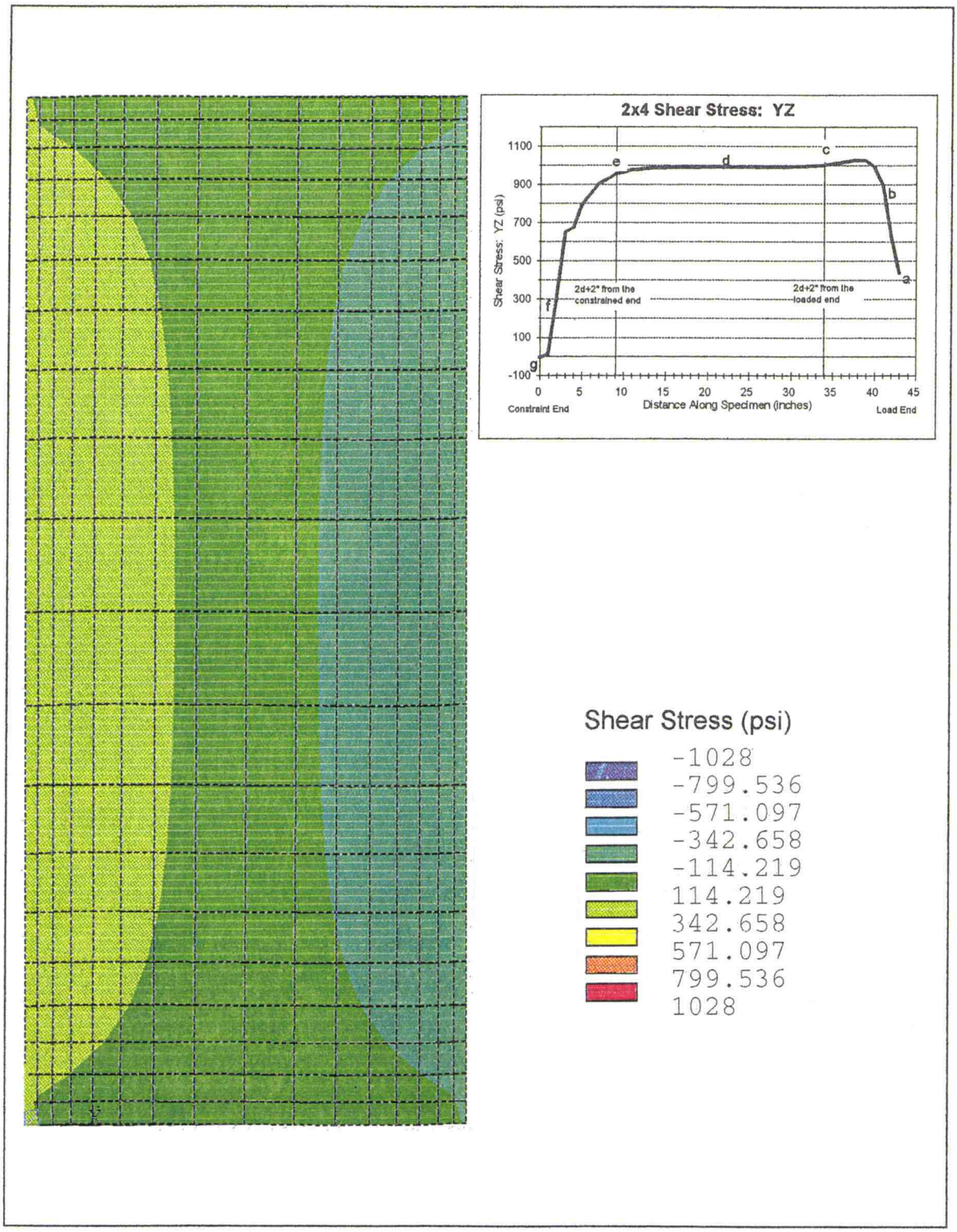

Figure 5.10: Finite element τ_{yz} shear stress plots (f) τ_{yz} over the cross section at the edge of the grips; 2 inches from the constrained end for 2x4 beam length of 43 inches and applied torque of 2,000 in-lbs.

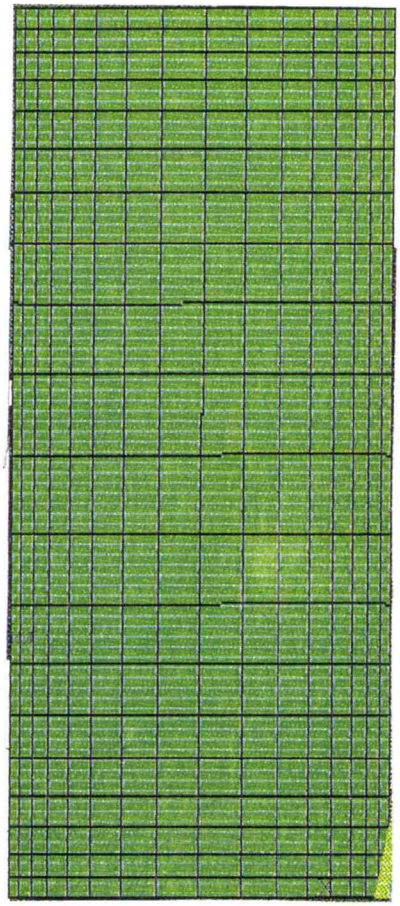

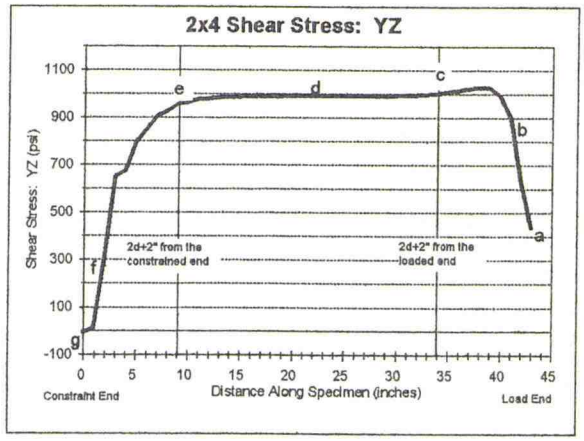

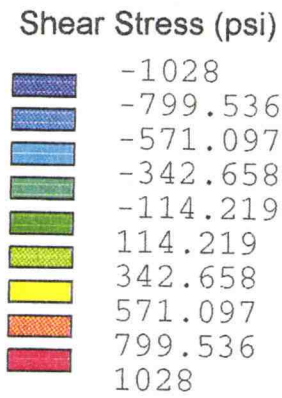

Figure 5.10: Finite element τ_{yz} shear stress plots (g) τ_{yz} over the cross section at the constrained end for 2x4 beam length of 43 inches and applied torque of 2,000 in-lbs.

This stress distribution, shown throughout the cross sections in Figure 5.10, is re-emphasized in the finite element values listed in Table 5.4. The shear stress, τ_{yz}, starts small, 439 psi, at the loaded end, increases along the length, within the shear span, to larger values, 1002 psi, 989 psi, and 955 psi, and decreases to a value near zero, -7 psi, at the constrained end.

Based on theory, equation 3.9, for a rectangular 2x4 beam subjected to the a torque of 2,000 inch-pounds, the shear stress, τ_{yz}, is 1,000 psi. The finite element model predicted the shear stress to be 987 psi (average of 26 data points along the shear span, with a coefficient of variation of 0.96%); resulting in an error of only 1.3%.

In addition, these sequential illustrations of stress plots reveal that within the shear span of 9 inches, which is two times the depth plus the grip distance, the variation in the primary shear stress, τ_{yz}, that causes failure is small and is approaching uniformity.

5.2.3 Shear span

The method of applying torque alters the distribution of shear stresses near the ends of the beam. The details of Saint Venant's Principle were presented in chapter three, Torsion Theory; however a summary of the principle is repeated here for convenience (Boresi & Chong, 1987); "Two statically equivalent force systems that act over a given small portion S on the surface of a body produce approximately the same stress and displacement at a point in the

body sufficiently far removed from the region S over which the force systems act."

According to Saint Venant's principle, theory should represent the shear stress distribution of a laboratory specimen at a distance "sufficiently far removed" from the loaded end. Also, at this distance, the laboratory specimen and finite element model will achieve relatively uniform shear stress along the shear span. Adequate shear span lengths allow for the development of uniform shear stress over the portion of the beam length. Sufficient shear span lengths are important because the theory, used to develop the torque-shear stress relationships assumes a uniform shear stress over the length of the beam.

As mentioned in chapter three, Torsion Theory, literature was not identified to support the ASTM (1996b) recommendation of the total length of a torsion specimen to be at least eight times the depth of the specimen. Therefore, in addition to the length study, the finite element model was used to investigate the minimum length of a torsion specimen.

Theory showed that the maximum shear stress experienced in an isotropic, rectangular beam occurs at the middle point of the long side (Boresi et al., 1993), point A on Figure 5.11 and Figure 5.12. This has also been shown to be true for Douglas-fir rectangular lumber via orthotropic calculations (Lekhnitskii, 1981) and finite element modeling stress plots, Figure 5.10.

The shear span length is determined using the shear stress τ_{yz} since this stress causes the failure of the wood. Shear stress, τ_{yz}, values were recorded at

the middle point of the long side of the cross section for every inch along the beam length, Figure 5.13. The shear stress plots, τ_{yz}, visually appeared to be uniform at the center of the beam, as seen in Figure 5.13 for a 43 inch long 2x4. In addition, Saint Venant's principle, as explained in Chapter 3, Torsion Theory, indicates that uniform shear stress occurs a particular distance away from each end (Boresi and Chong, 1987) implying that the uniform shear stress should occur near the center of the beam. Therefore, the shear stress, τ_{yz}, value at the center of the beam was used to compare to the other shear stress, τ_{yz}, values along the length.

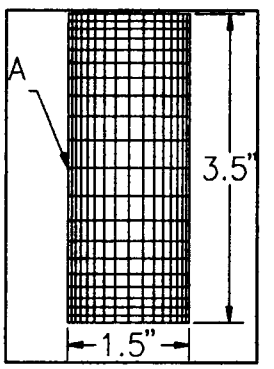

Figure 5.12: Maximum shear stress location for 2x4--Cross sectional view

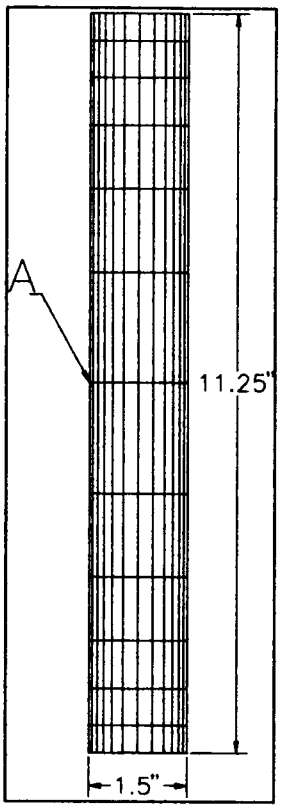

Figure 5.11: Maximum shear stress location for 2x12--Cross sectional view

Shear stress, τ_{yz}, values were considered to be uniform along the length extending toward the loaded end side until reaching a shear stress value greater than 1% of the center shear stress value.

Due to the asymmetry of the τ_{yz} distribution within the beam recognized near the ends caused by the method of applying the torque, the method of applying the constraints, and the orthotropic properties (Figure 5.13), one end of

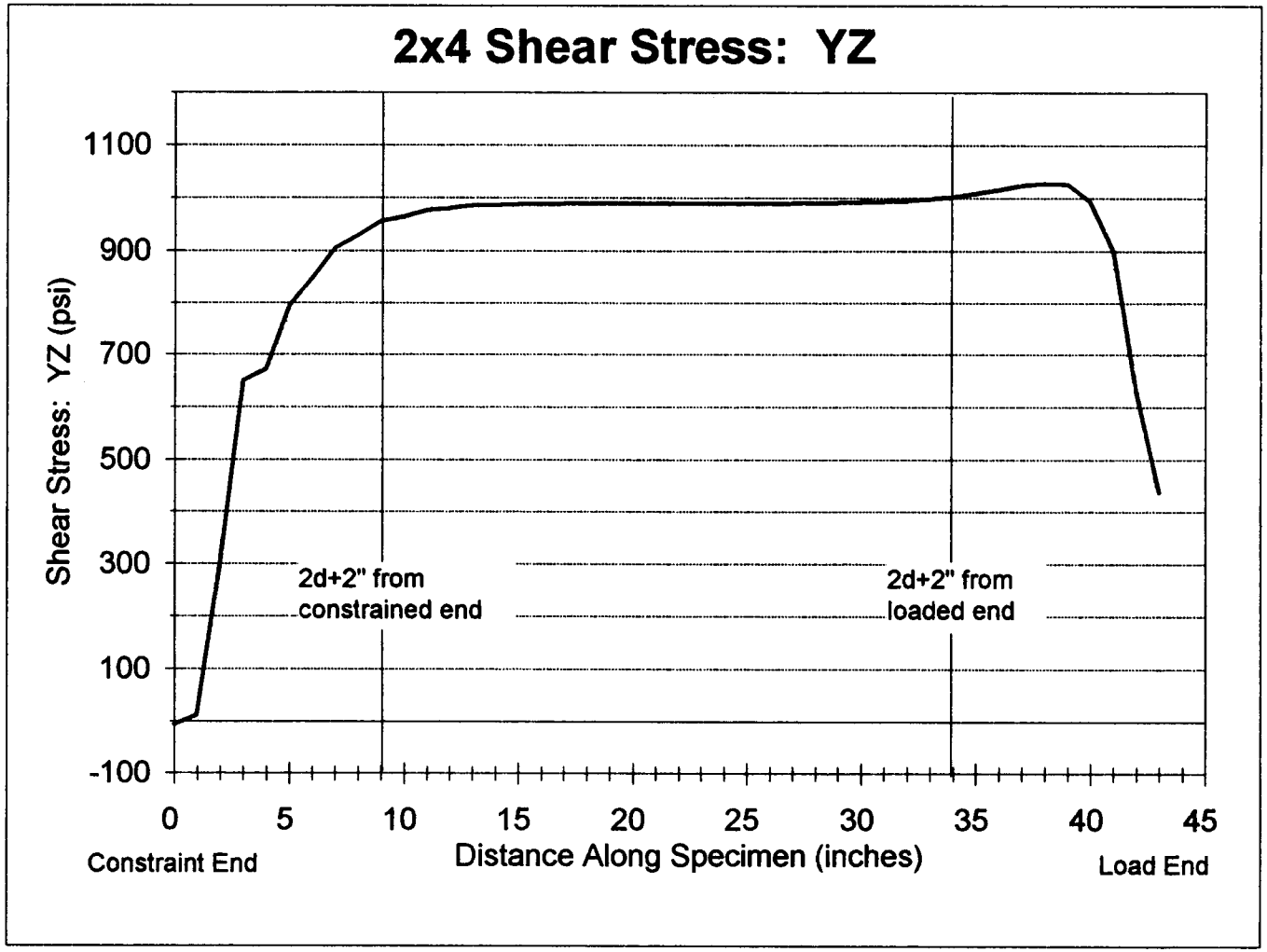

Figure 5.13: Shear stress, τ_{yz}, for a 43 inch long 2x4 finite element model with 2,000 in-lb torque

the beam was chosen to determine the excess distance to subtract from each side to yield the shear span in the center of the beam. For the laboratory specimen, it had identical grips on both ends of the specimen. Thus, the shear stress distribution along the length of the laboratory specimen would be expected to be symmetrical, unlike the finite element model (Figure 5.13). In addition, the constrained end of the finite element model was restrained in the z direction, whereas the laboratory specimen was allowed to move along the z direction. As a result, the constrained end of the model may be causing the low shear stress values for a longer distances along the length toward the center point of the modeled beam (Figure 5.13). Therefore, the loaded end of the model was recognized as the end which represents the laboratory specimen more closely and was used to determine the excess distance.

The asymmetrical nature of the finite element model is clear through the shear stress, τ_{yz}, distribution in Figure 5.13. Near the constraint end an abrupt change in shear stress with respect to length is apparent as a small "kink" in the distribution plot. This change occurs after the nodes are released from horizontal, vertical, and longitudinal restraint and is attributed to the model design of the constrained nodes. These shear stress distributions may confirm Saint Venant's principal that as long as the beam length allows for a shear span long enough to reach a uniform shear stress, the end constraints and loading conditions do not affect the shear stress value within the shear span where the stress is uniform. The large increase near the loaded end and the abrupt

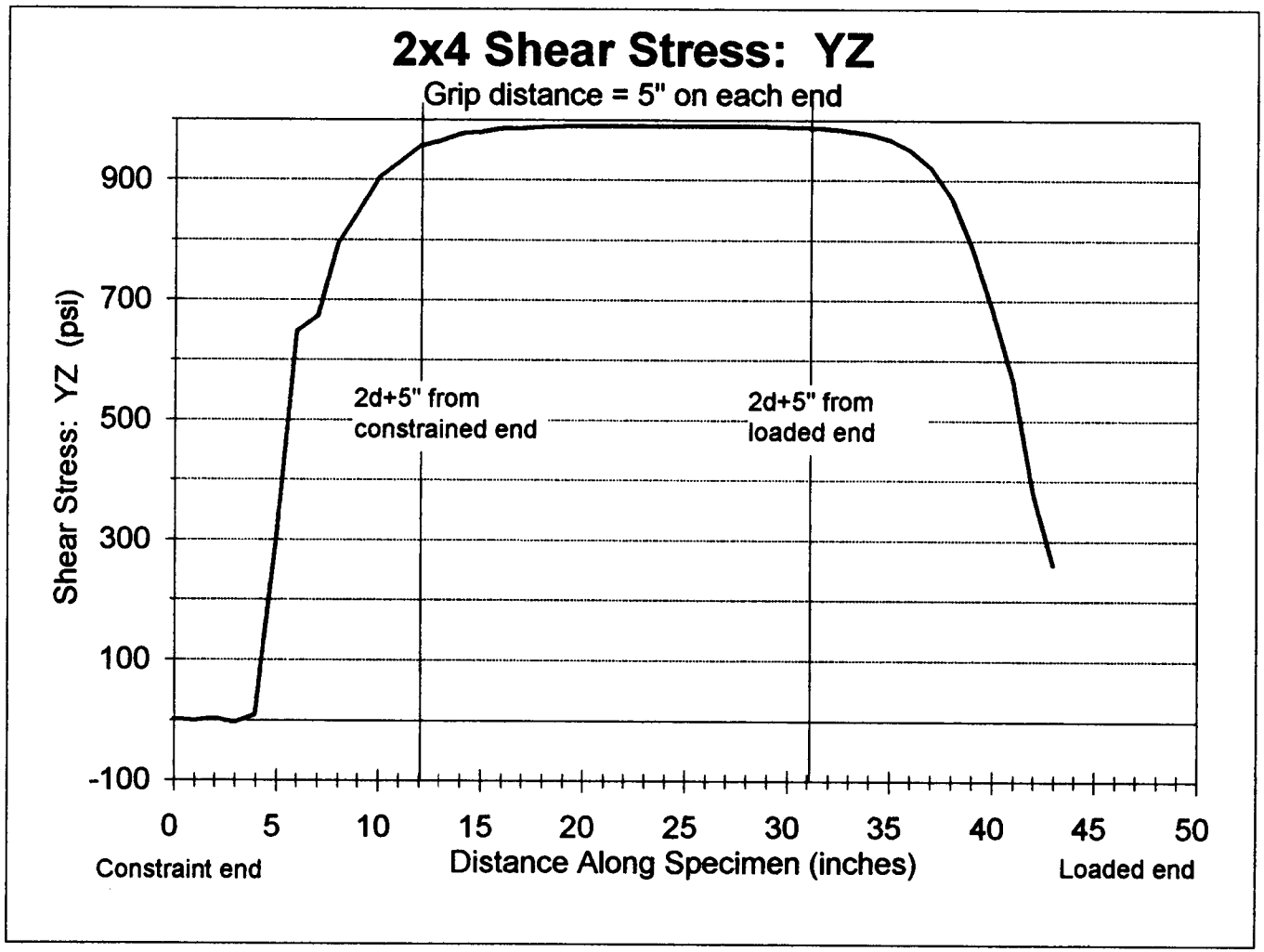

Figure 5.14: Shear stress, τ_{yz}, for a 43 inch long 2x4 finite element model with 2,000 in-lb torque and 5 inch grips

change in shear stress at the constrained end are results of the effect of orthotropic properties and the application of the constraints and loads on the model of the torsion specimen and are not affected by refining the mesh.

As observed in the laboratory, the initial shear failure did not have a preference of initiating near either the loaded end or the fixed end of the torsion machine; this also implies that the shear stress distribution, for either τ_{yz} or τ_{xz}, is symmetrical with respect to the length of a torsion specimen in the laboratory.

This shear span criteria indicated that a distance subtracted from each side of the beam of twice the depth of the specimen plus the grip distance provides a uniform shear span.

To understand the effect of the grips on the shear span, a finite element model was analyzed that had 5 inch grips on each end. The plot of τ_{yz} for this model is shown as Figure 5.14. Using the shear span criteria explained previously, uniform shear stress, τ_{yz} is reached at two times the depth plus five inches from each end. This confirms that the total grip distance must be subtracted from each end in addition to twice the depth to obtain the shear span. Figure 5.14 not only identifies the location of uniform shear stress, but also shows a more symmetrical shear stress distribution when comparing the constrained ends with the loaded ends of Figure 5.13 and Figure 5.14.

Based on the shear stress plots for the 2x4 and the 2x12 specimens, the shear span of a torsion specimen tested for shear strength is summarized in

equation 5.2, where S= shear span, L= total length of the specimen, d= depth of specimen, and g= distance compressed by the grips.

$$S = L - 2(2d + g) \tag{5.2}$$

5.2.4 Sliding direction and failure plane

As described in chapter three, Torsion Theory, there are six types of shear failures, shown in Figure 3.4. To show that the finite element model provides additional support to the theoretical calculations, numerical values of the three shear stress components that occur in torsion specimens were examined via the finite element model. This supported the theoretical results that the shear failure mode for a rectangular wood specimen slides parallel to the grain and fails parallel to the grain,.

The sliding direction and failure plane are discussed using the rectangle specimen with the typical grain pattern tested in this study, as shown in Figure 5.15. As described in section 3.6.3, the shear stress, τ_{xy} causes rolling shear (Figure 3.4), and τ_{xy} is theoretically always zero for torsion specimens. Table 5.5 confirms that τ_{xy} is almost zero, and for practical purposes τ_{xy} may be considered

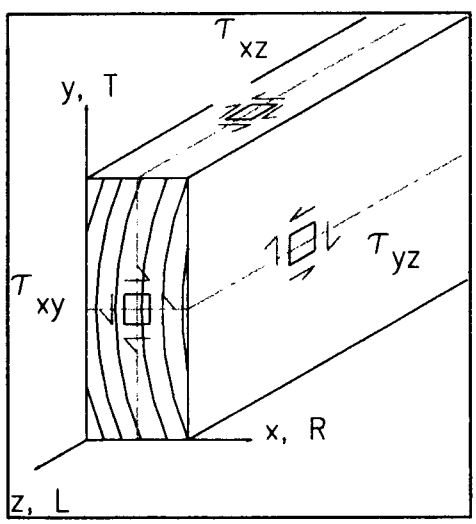

Figure 5.15: Typical rectangular specimen tested in laboratory for this study

negligible. The shear stress, τ_{xz}, causes shear parallel to the grain for a grain angle of 0°(Figure 3.4), as discussed in section 3.6.3. The shear stress, τ_{yz}, also causes shear parallel to the grain (Figure 3.4), but with a grain angle of 90°, details are presented in section 3.6.3.

Therefore, there are two shear stresses which act parallel to the grain and cause failures parallel to the grain, τ_{yz} and τ_{xz}. Torsion theory shows that for an orthotropic rectangular torsion specimen, either τ_{yz} or τ_{xz} could be the largest shear stress. The stress τ_{yz}, which occurs at the middle point on the long side of the rectangle, is the largest shear stress as confirmed using orthotropic properties for Douglas-fir and isotropic properties for isotropic materials (Boresi et al., 1993; Lekhnitskii, 1981). As a result, the failure occurs along the middle line of the long side as shown as point A in Figure 5.11 and Figure 5.12. Table 5.5 confirms that τ_{yz} is larger than τ_{xz} for the orthotropic Douglas-fir lumber beam examined using the finite element model. In addition, the failure observed in the experimental studies occurred along the middle line of the long side of the rectangular specimen.

6. Experimental Results, Analysis, and Discussion

The experimental data obtained from the length effect on shear strength and the depth effect on shear strength are presented, analyzed, and discussed with the primary objective to evaluate the potential use of the torsion test as a method to determine the shear strength of full-size structural lumber. As part of the primary goal, secondary objectives are discussed (1) length effects on shear strength, (2) depth effects on shear strength, (3) differences between the ASTM (1996a) clear block shear strength and the torsion test shear strength, and (4) experimental differences between the bending tests and the torsion test.

6.1 Selection of Materials

The boards obtained from the lumber mills were selected to reduce the modulus of elasticity variability and to avoid split boards. Even though research has shown that shear strength is not related to the modulus of elasticity (Riyanto, 1996; Riyanto and Gupta, 1996), an attempt was made to reduce the variability of the modulus of elasticity. In addition, split beams were avoided to eliminate any potential effects on shear strength; additional research is necessary to assess the effect splits have on shear strength using the torsion test method.

As indicated in chapter 4, Materials and Methods, sample sizes for each beam length for the length study and each beam depth for the depth study were

smaller than recommended by ASTM (1996g) to yield an accurate mean shear strength for the particular beam size. However, observations of the relationships between the length and shear strength and between the depth and shear strength were the focus of this study. Therefore, the objective of this study is to evaluate the potential use of the torsion test as a method to determine the shear strength of full-size structural lumber rather than determining the mean shear strength value of full-size structural lumber.

Because the selection of boards was not random due to the avoidance of a large modulus of elasticity variability and split beams, this research is an observational study, as opposed to a randomized study. Consequently, the inferences and conclusions from this study will only be applicable to this study's sample. However, the recommendations from this research will help in deciding whether or not to pursue the torsion test using a much larger set of random samples to determine an actual mean value for shear strength of structural lumber via the torsion test which could be used in designs.

6.2 Length study

The length effect study on the shear strength was performed to (1) determine if length affects shear strength and (2) confirm the ASTM (1996b) recommendation for the minimum total length of eight times the depth for a torsion specimen or establish and support a new recommendation for the minimum total length requirement.

6.2.1 Statistical analysis

The statistical summary for each length parameter tested, Table 6.1, shows the sample sizes, means, and coefficients of variation for the moisture content, specific gravity, and shear strength. The data collected for the evaluation of the length effect on shear strength, for the 2x4 beams tested, is presented in Appendix D.

Table 6.1: Summary statistics for the length study[1]

Shear Span[2] (d=3.5 inches)	Total Beam Length (inches)	Sample Size	Moisture Content (%)		Specific Gravity		Shear Strength[3] (psi)	
			Mean	COV (%)	Mean	COV (%)	Mean	COV (%)
1d	21.0	10	12.4	7.8	0.49	7.1	1484	19.0
2d	28.5	10	12.5	8.1	0.49	5.0	1534	13.5
3d	32.0	10	12.3	8.1	0.49	5.9	1519	12.5
4d	35.5	10	12.3	8.9	0.49	6.7	1511	17.4
5d	39.0	10	12.5	7.2	0.52	6.9	1581	17.9
ASTM[4]	---	10	12.3	8.4	0.48	6.3	1202	10.9

[1] Appendix D contains complete length study data.

[2] All specimens were nominally 2x4 beams.

[3] Individual shear strength values adjusted to 12% moisture content, (ASTM, 1996h) then averaged.

[4] One board yielded one ASTM block and one specimen for each length parameter.

To determine if there were differences in mean shear strength values among the different lengths tested in the length study, an analysis of variance (ANOVA) was performed. Since the F-test does not indicate which lengths differ in the mean shear strength values, a regression analysis was performed If the

linear regression proved to be significant, the relationship between beam length and shear strength would indicate a minimum length requirement for torsion specimens.

Several factors present during the development of the ANOVA and multiple regression models related to the specimens or the testing method: rings per inch, specific gravity, time to failure, strain rate, modulus of elasticity, and rotation. These scatter plots helped identify if certain factors were related to one another by visual identification, but a linear regressions were not performed. Possible related factors include:

- Specific gravity vs. rings per inch (Figure 6.1)
- Specific gravity vs. failure time (Figure 6.2)
- Specific gravity vs. applied strain rate (Figure 6.3)
- Applied strain rate vs. failure time (Figure 6.4)
- Applied strain rate vs. rotation (Figure 6.5)
- Modulus of elasticity vs. failure time (Figure 6.6)
- Modulus of elasticity vs. rotation (Figure 6.7)
- Rotation vs. failure time (Figure 6.8)

Some of these scatter plots were expected to show a relationship and other scatter plots were not expected to show a relationship. Strain rate, a measure of degrees per inch of specimen per time, versus failure time; strain rate versus rotation; and rotation versus failure time are all measurements of the

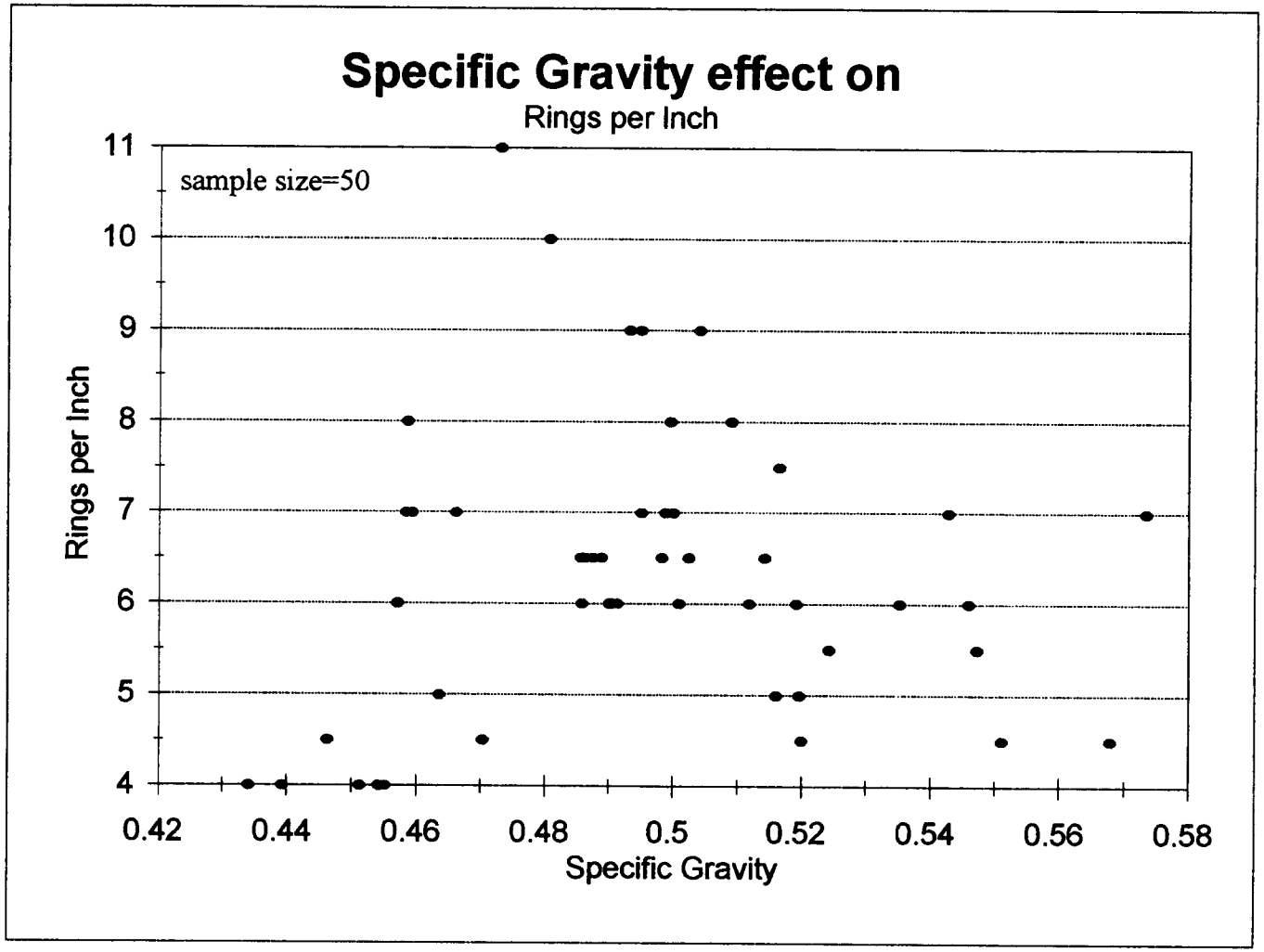

Figure 6.1: Scatter plot of specific gravity vs. rings per inch for the length study

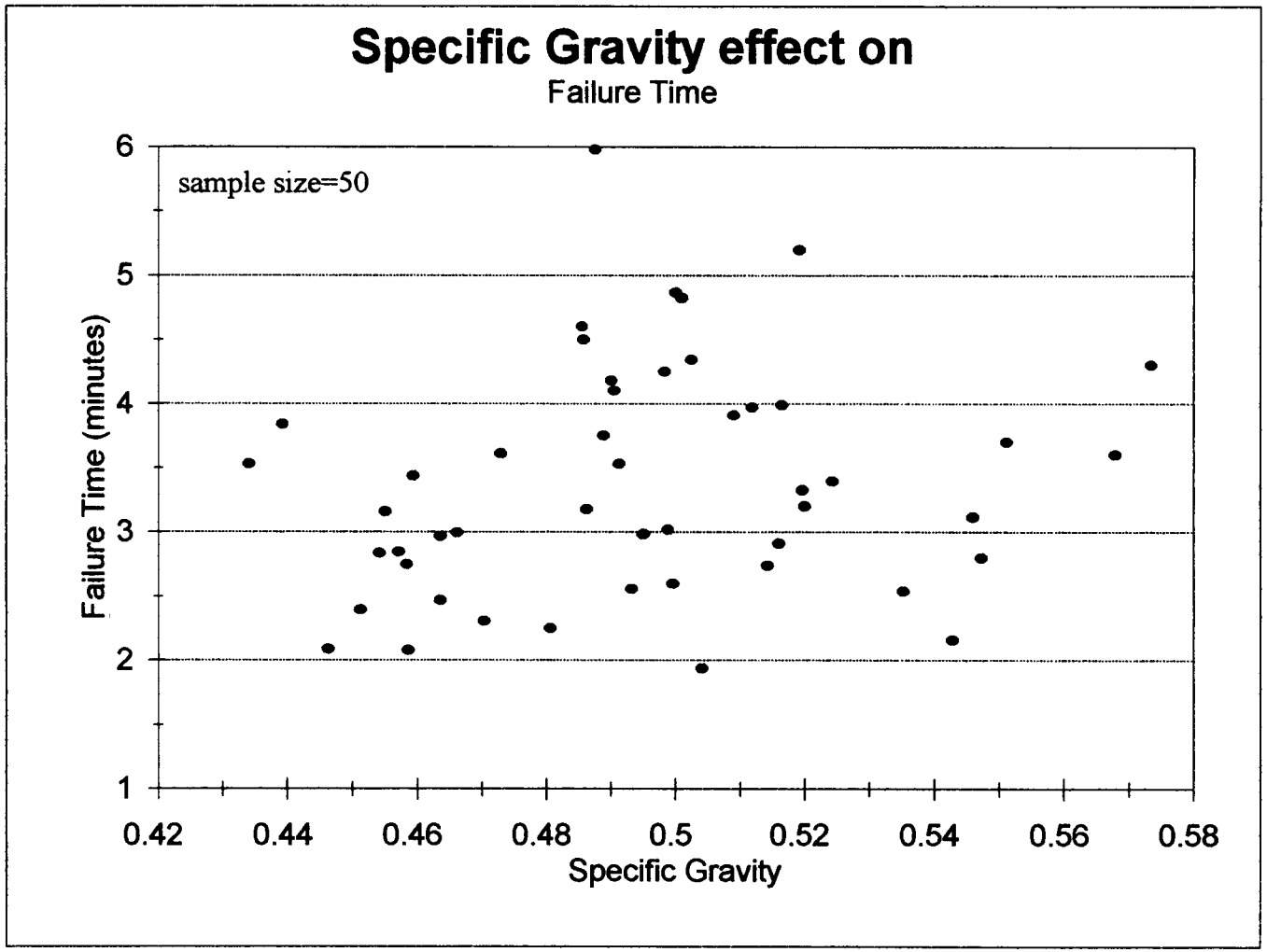

Figure 6.2: Scatter plot of specific gravity vs. failure time for the length study

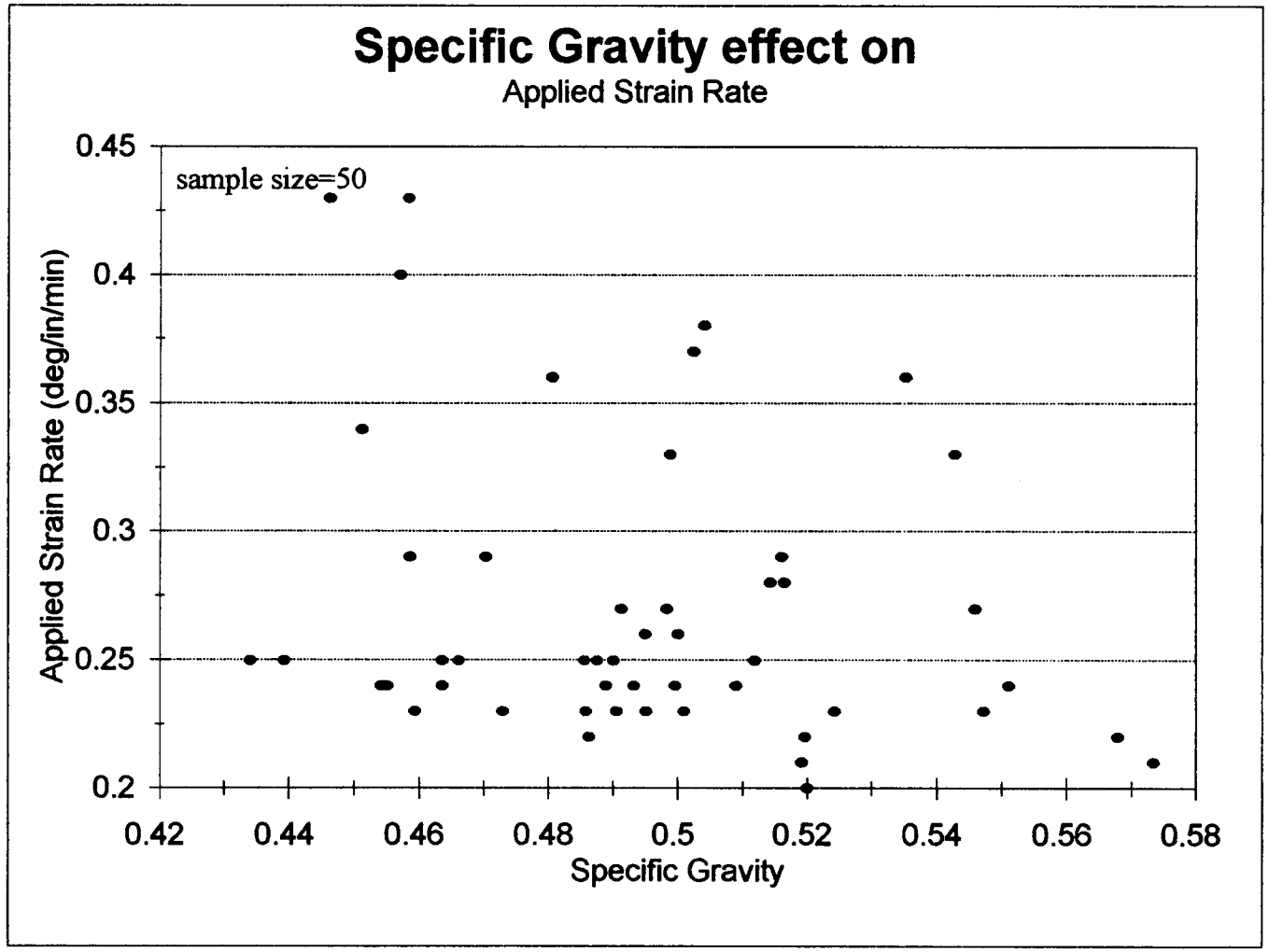

Figure 6.3: Scatter plot of specific gravity vs. applied strain rate for the length study

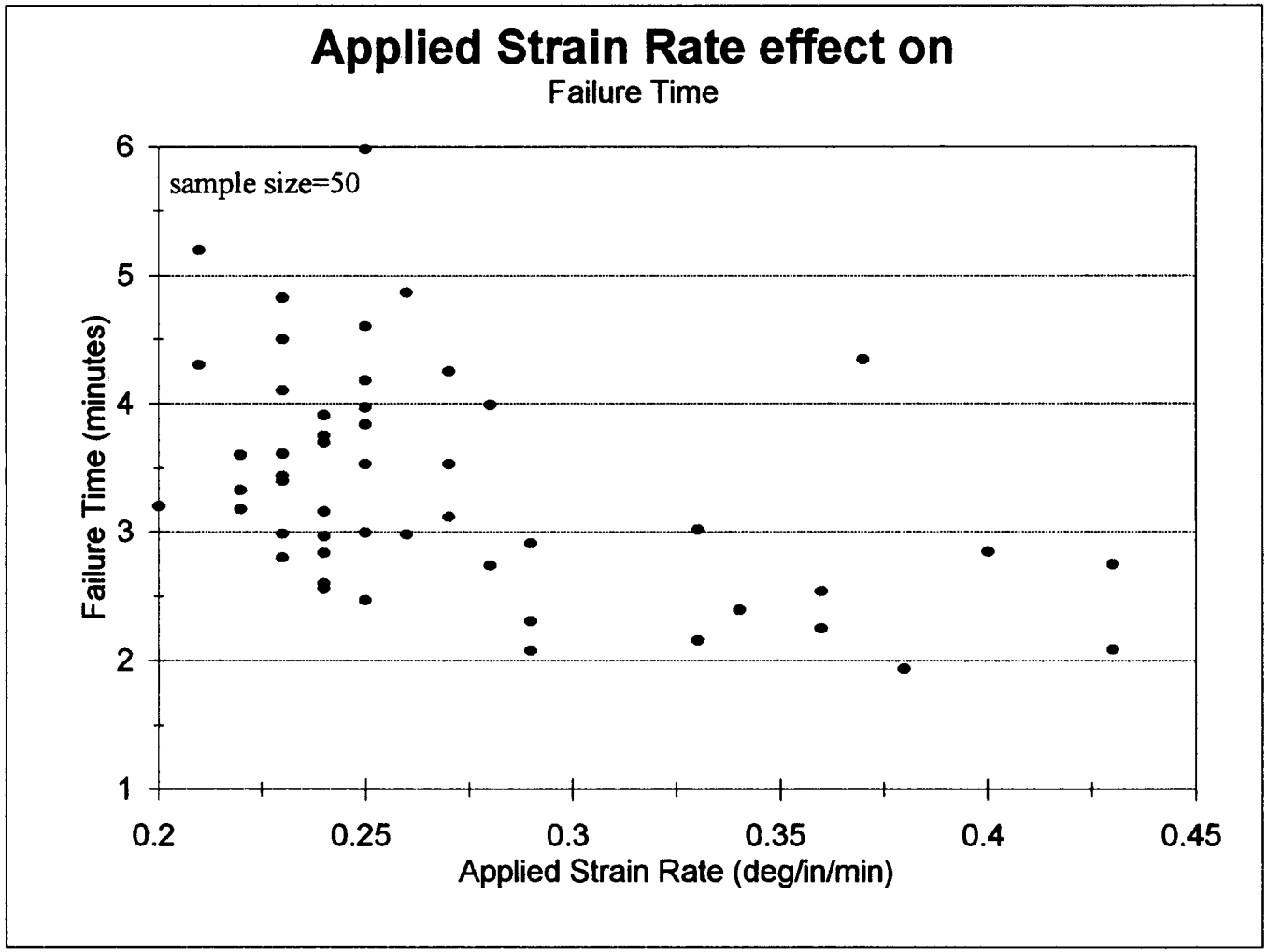

Figure 6.4: Scatter plot of applied strain rate vs. failure time for the length study

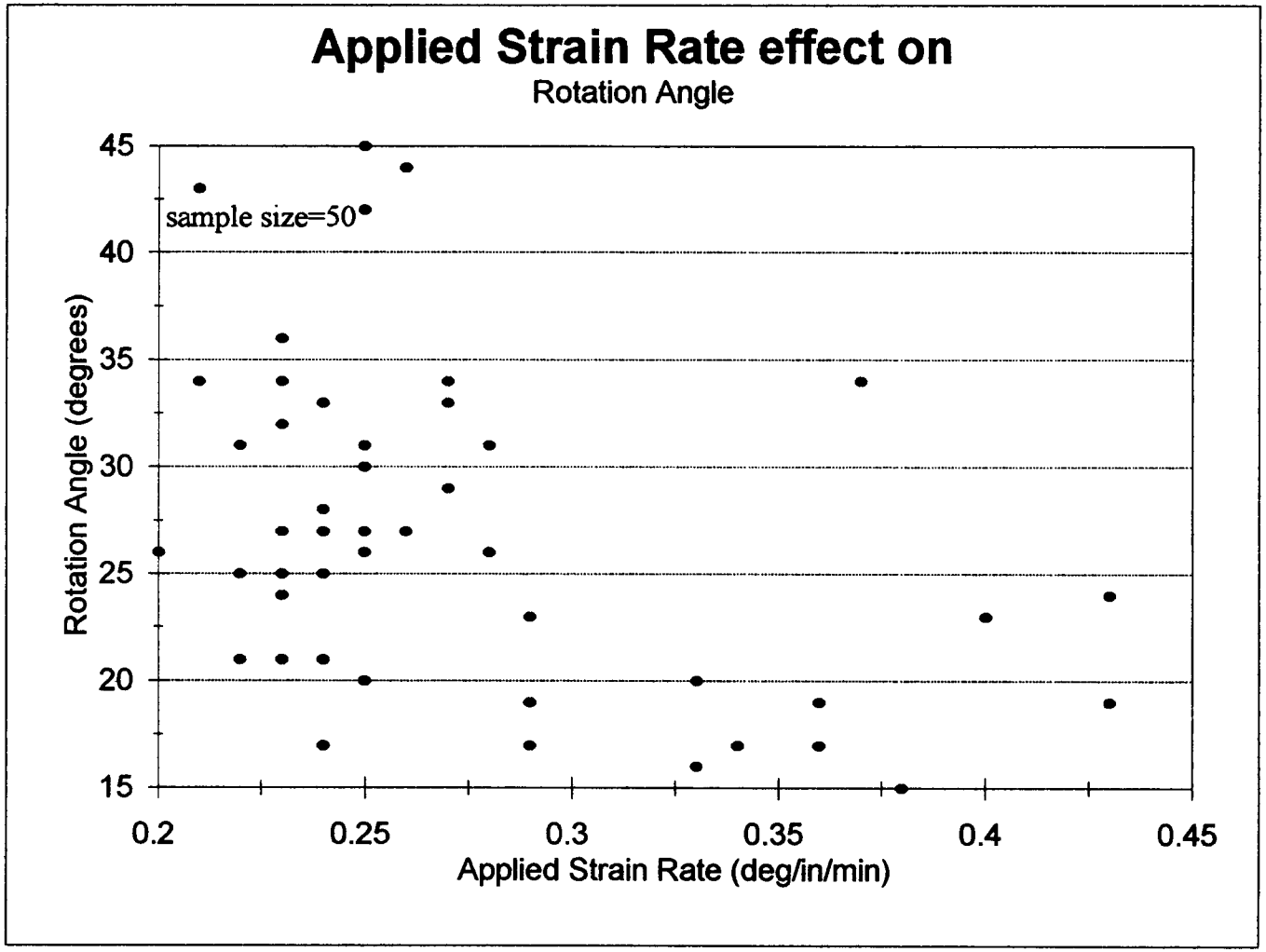

Figure 6.5: Scatter plot of applied strain rate vs. rotation angle for the length study

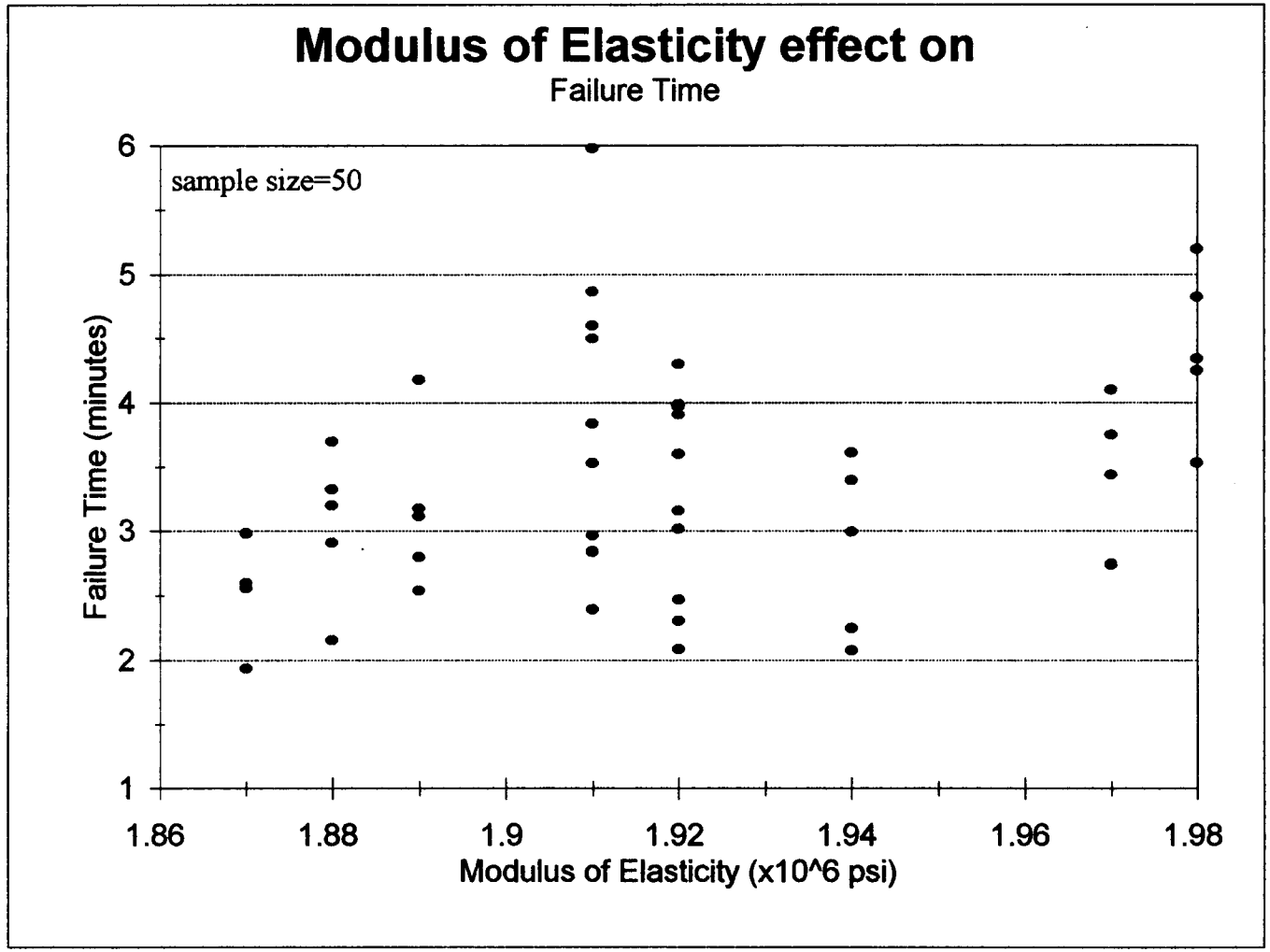

Figure 6.6: Scatter plot of modulus of elasticity vs. failure time for the length study

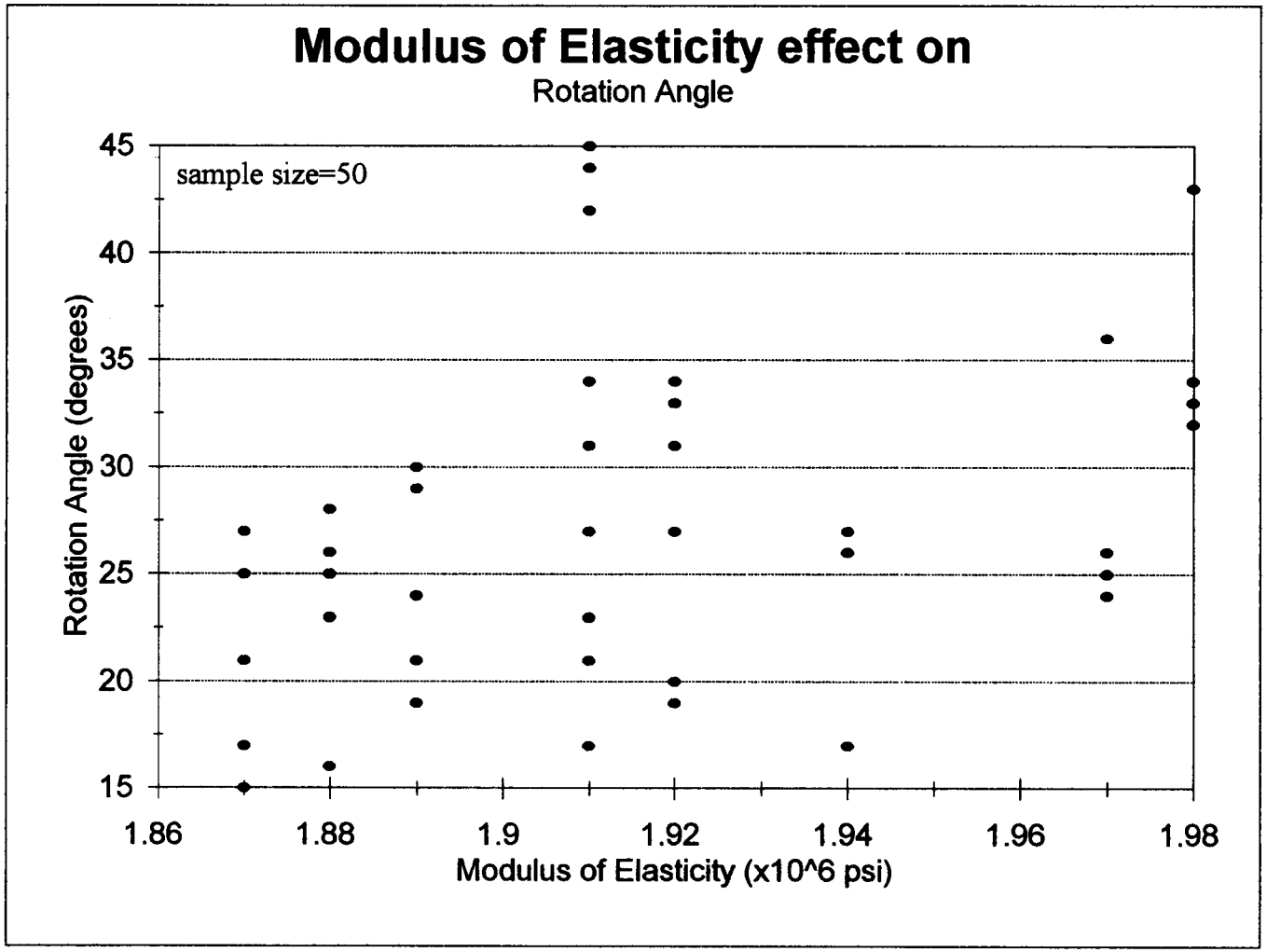

Figure 6.7: Scatter plot of modulus of elasticity vs. rotation angle for the length study

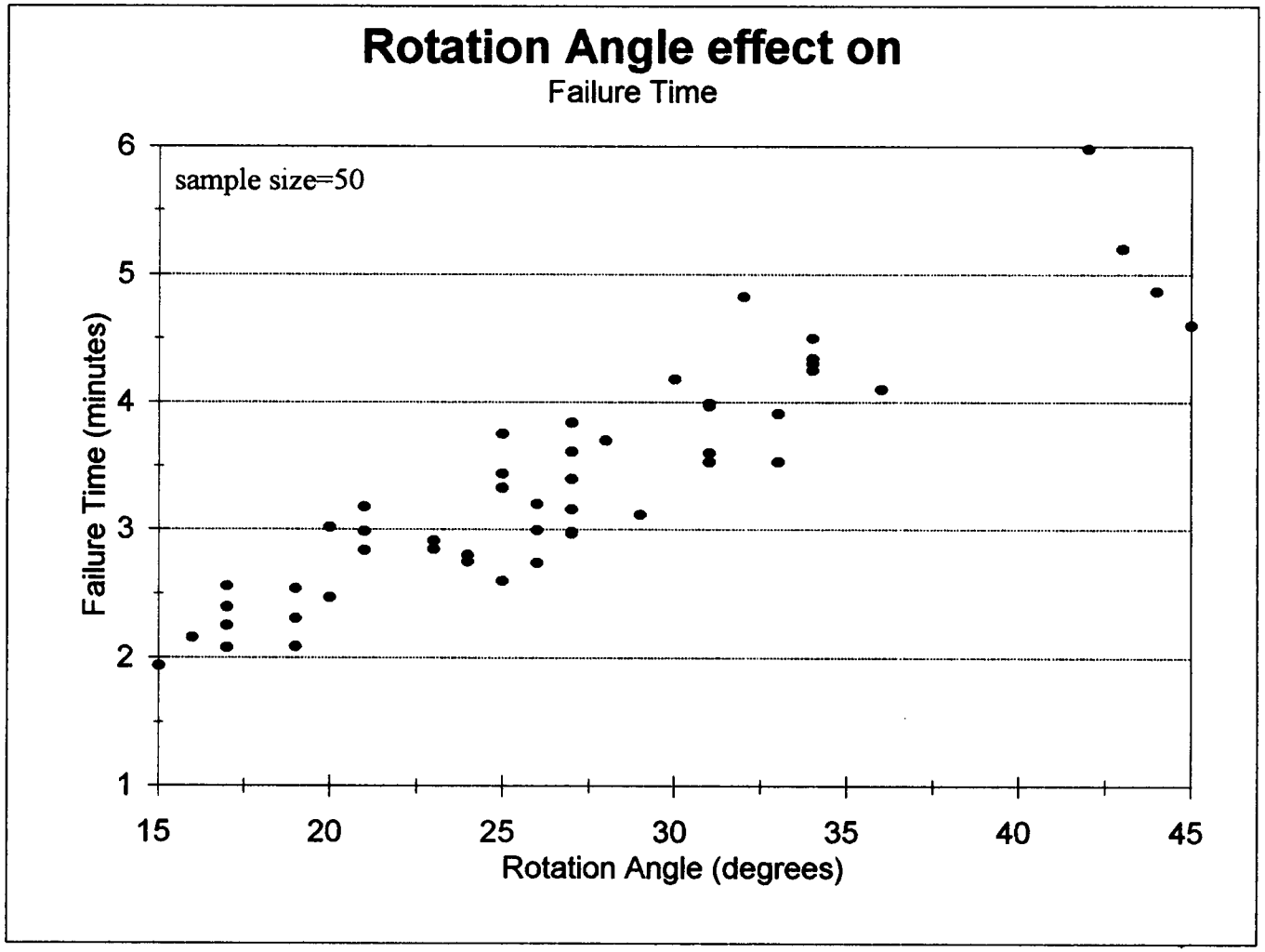

Figure 6.8: Scatter plot of rotation angle vs. failure time for the length study

motor used to apply the torque. As a result, these relationships were expected but may or may not be directly related to wood properties. The relationships, specific gravity versus failure time, specific gravity versus strain rate, modulus of elasticity versus failure time, and modulus of elasticity versus rotation were plotted to clarify if the failure time and applied torque rate were functions of the wood. Initially, these four relationships were not expected but did show a possible effect due to the wood properties. The primary relationship expected from the scatter plots is the effect from the number of rings per inch on specific gravity. Specific gravity has been shown to increase due to an increase in latewood (Panshin and de Zeeuw, 1980); therefore, as the number of rings per inch increase the amount of latewood may also increase, causing an increase in specific gravity. This was observed, to a small degree, in the scatter plot, Figure 6.1. The variability observed in these scatter plots and other plots throughout the experimental studies were expected due to the variability observed in wood (Tsoumis, 1991).

Because the scatter plots of specific gravity showed relationships with rings per inch (Figure 6.1), failure time (Figure 6.2), and applied torque rate (Figure 6.3), specific gravity was selected as a covariate in the multiple regression model. The modulus of elasticity was also incorporated into the multiple regression model since it showed a possible effect on rotation.

Summarized in Table 6.2 is the relationships considered for the length study, their corresponding R^2 value, their 2-sided p-value, and brief comments

regarding the significance of the relationship. A detailed explanation of each relationship follows in Table 6.2.

Table 6.2: Observed relationships in the length study

Relationship Observed[1]	R^2	2-sided p-value
$\tau = 3680(SG) - 298$ Strong evidence that specific gravity affects shear strength	0.26	0.0002 (SG)
$\tau = -2.47(SPAN) + 3790(SG) - 327$ Strong evidence that specific gravity affects shear strength; but no evidence that shear span affects shear strength	0.26	0.6972 (SPAN) 0.0003 (SG)
$\tau = 547(MOE) - 2.76(SPAN) + 3680(SG) - 1500$ No evidence that MOE affects shear strength	0.26	0.5270 (MOE)

[1] τ=shear strength (psi), SG=specific gravity, MOE=modulus of elasticity ($x10^6$ psi) SPAN=shear span (inches) as defined in section 5.2.3.

The specific gravity versus shear strength scatter plot, Figure 6.9, indicated that shear strength is dependent upon specific gravity. In recent studies (Asselin et al., 1996; Rammer et al., 1996), shear strength was adjusted for specific gravity. The adjustments made in these studies are not recognized in ASTM standards; consequently direct specific gravity adjustments were not made to the shear strength values obtained for this current study. However, due to the strong effect on shear strength from specific gravity (2 sided p-value=0.0002), Figure 6.9, specific gravity must be accounted for, in some manner, when analyzing effects on shear strength. The linear relationship,

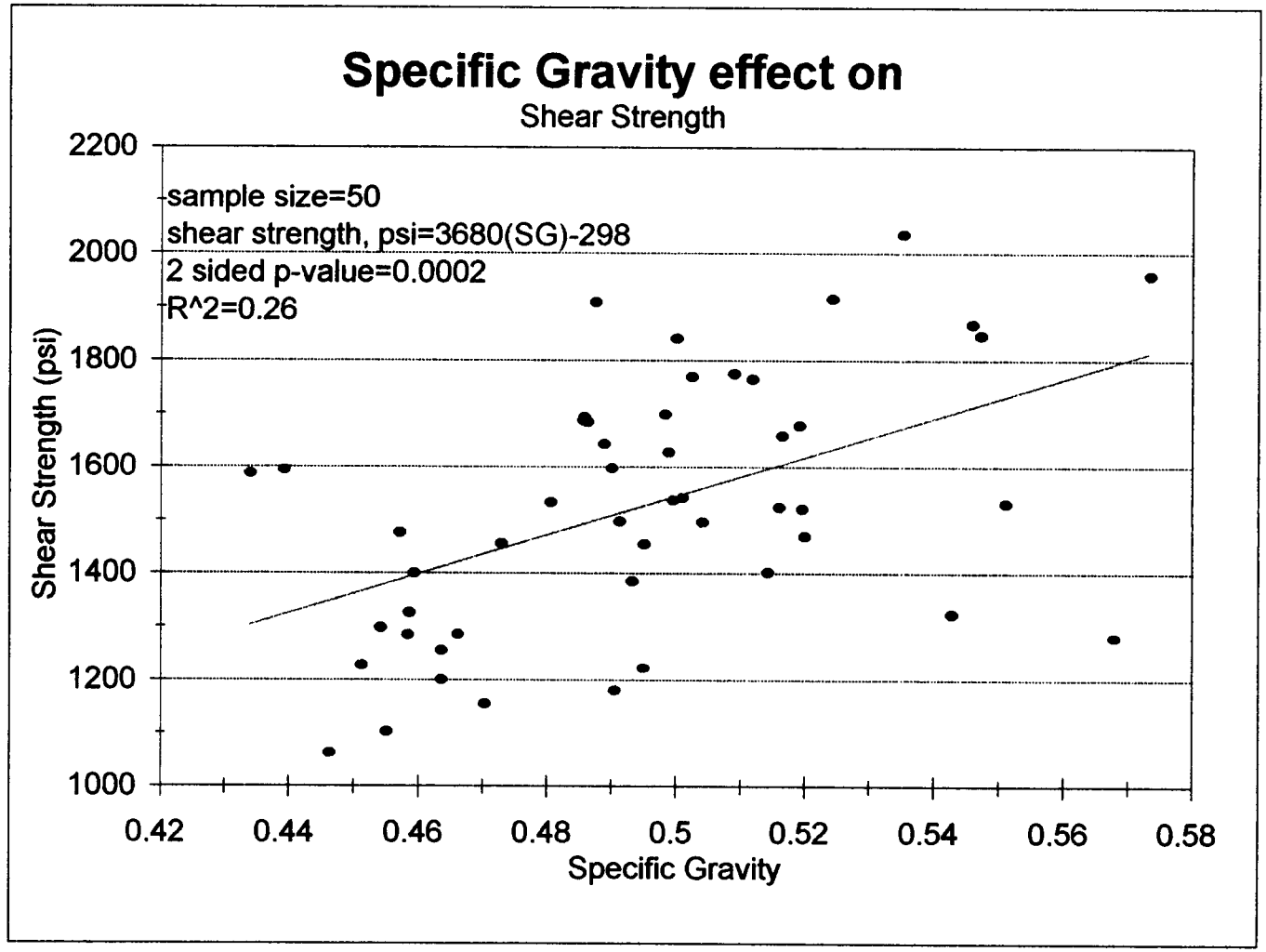

Figure 6.9: Specific gravity effect on shear strength for the length study

Equation 6.1, which accounts for 26% of the variability (R^2=0.26), indicates that as the specific gravity increases, the shear strength also increases, where τ=shear strength (psi) and SG= specific gravity.

$$\tau = 3680(SG) - 298 \qquad (6.1)$$

The increase in shear strength with an increase in specific gravity was expected. Specific gravity, a measure of density, measures the amount of wood material; higher amounts of wood material cause an increase in strength (Tsoumis, 1991). Other research (Riyanto, 1996; Riyanto and Gupta, 1996) also showed that the shear strength for the torsion test and the ASTM (1996a) shear block test both had good relationships with specific gravity (R^2=31%, torsion tests and R^2=43%, ASTM (1996a) shear block tests). Rammer et al. (1996) also showed a strong relationship between the specific gravity and the ASTM (1996a) shear blocks (R^2=0.49). However, for the bending tests, Riyanto (1996) observed a poor relationship between specific gravity and shear strength (R^2=8%-9%). Because the bending tests show that shear strength is not affected by the specific gravity, bending tests may yield apparent shear strength values that are not representative of the material tested.

Since the shear strength values were not directly adjusted for specific gravity, specific gravity was entered into the multiple regression model in addition to the beam size parameter. The only size parameter for the regression

model in the length study was the shear span because the depth and width of the beam remained constant throughout the study.

The multiple regression model developed included shear strength as the response variable and the shear span and specific gravity as the explanatory variables. As indicated through the ANOVA test, there is convincing evidence that shear strength is associated with either the shear span or the specific gravity (2-sided p-value=0.0009, extra sum of squares F-test). The multiple regression analysis revealed that there is strong evidence that specific gravity effects shear strength even after accounting for the shear span (2 sided p-value=0.0003, t-test). However, there is no evidence that shear strength is affected by shear span after accounting for specific gravity (2-sided p-value=0.6972, t-test), implying that the shear span parameter can be removed from the linear regression model.

The shear strength did not show a relationship with modulus of elasticity even after accounting for shear span and specific gravity (2 sided p-value=0.5270, t-test). Consequently the modulus of elasticity was removed from the multiple regression model, and the model consisted of shear strength as the response variable and shear span and specific gravity as the final covariates. This lack of a significant relationship between modulus of elasticity and shear strength was also shown previously (Riyanto, 1996).

Due to the absence of a shear strength dependence on the shear span, all samples were combined to form one group. Table 6.3 presents the summary statistics for the entire length study sample group. The length study, for 2x4

beams, showed an average shear strength of 1,526 psi with a coefficient of variation of 15.7% after adjusting the shear strength values to 12% moisture content.

Table 6.3: Summary statistics for all length study specimens

Test	Sample Size	Moisture Content (%)		Specific Gravity		Shear Strength[2] (psi)	
		Mean	COV (%)	Mean	COV (%)	Mean	COV (%)
Torsion[1]	50	12.4	7.7	0.49	6.6	1,526	15.7
ASTM	10	12.3	8.4	0.48	6.3	1,202	10.9

[1] All specimens nominally 2x4 beams.

[2] Individual shear strength values adjusted to 12% moisture content, then averaged.

6.2.2 ASTM study

As stated previously in chapter 4, Materials and Methods, one board was sawn into six pieces, five of the pieces corresponded to the lengths tested and the remaining piece provided an ASTM (1996a) shear block. As a result, ten ASTM (1996a) shear blocks were tested for a shear strength comparison with the torsion method. Because the ASTM (1996a) shear block is independent of the size of the beam from which the block was sawn, all ten specimens could be combined to form one sample group.

Table 6.3 lists the summary statistics for the ASTM (1996a) shear blocks tested. The average shear strength for the ASTM (1996a) shear blocks is 1,202 psi, with a coefficient of variation of 10.9%, after adjusting to 12% moisture content.

The average torsion-based shear strength from the length study is 35% higher than the published ASTM (1996a) shear block average shear strength value of 1,130 psi (coefficient of variation of 14%) for dry coastal Douglas-fir species (Wood Handbook, 1987), and the torsion-based shear strength is 21% higher than the corresponding ASTM (1996a) shear blocks. For the ASTM (1996a) shear blocks, the current study observed a 6.4% higher shear strength than the published value and a 3.1% lower coefficient of variation than the published value of 14%. The difference between the published average specific gravity value of 0.45 and the current study average specific gravity value of 0.48 may be the reason for the differences in the published shear strength values.

6.2.3 Discussion

The large increase in the observed shear strength over the ASTM (1996a) shear strength, as observed in the current study, has also been seen in previous torsion tests (Riyanto and Gupta, 1997). Riyanto and Gupta (1997) tested 76 nominal 2x4 Douglas-fir beams which yielded an average shear strength value of 1,834 psi with a coefficient of variation of 18%, which is 62.3% higher than the published shear strength value. Although these torsion test results are higher

(20.2%) than the current study's average shear strength, the previous study did have a larger sample size (34%) and Riyanto's (1996) shear strength values were based on a different measuring arrangement detailed below. Nevertheless, the higher observed shear strengths obtained in the torsion test of the current research and previous research (Riyanto, 1996), which tested full-size lumber with natural characteristics, implies that the small clear block specimen may be underestimating the shear strength of full-size lumber.

The smaller coefficient of variation for the current research (15.7%) may be explained by the electronic recording system designed for this study, which was not available to Riyanto (1996). Riyanto (1996) used the manual method and read the final torque reading at failure from the arm beam of the torsion machine. The arm beam is connected to a series of lever arms and fulcrum points which transfers the applied torque from the specimen to the balance beam. This beam must be continuously and manually balanced as the torque is applied to the specimen. At the point of specimen failure, the lever arms and fulcrum points discontinue to transfer torque to the balance beam and the beam drops. For an isotropic material with little material variability, unlike wood, the failure point is clear and the beam drops abruptly. However for wood, which has significant material variability, the failure is less defined and the beam does not always abruptly drop to indicate the failure. As a result, human error is introduced into interpreting the point of failure, in addition to balancing the beam. This human error is reduced with the use of electronic recording mechanism, as

detailed in Appendix A. The electronic voltage recordings were calibrated to torque values using an isotropic material to avoid material variability when balancing the beam. The calibration, as detailed in Appendix B, was performed before the testing and after the testing was completed; both calibrations showed similar results. Through the electronic recording system, consistency increased in interpreting applied torque values and failure points. Although possible electronic noise may also affect torque recordings, this is negligible compared to the possible human errors discussed previously.

Small scale torsion specimens with circular cross sections in the shear span and square cross sections at the gripped ends were tested by Mack in 1940. Among various other species, Mack (1940) tested Douglas-fir (*Pseudotsuga taxifolia* synonymous with *Pseudotsuga menziesii*) of various diameters sizes, 1/2", 3/4", 1", and 1 1/2". The lengths of these specimens ranged from two times the diameter to twelve times the diameter. The result, within the range of sizes tested, indicated that length did not effect the shear strength (Mack, 1940). Since these specimens did not reveal a length effect, all specimens were combined into one group with an average shear strength of 1,716 psi and a coefficient of variation of 3.8% (Mack, 1940). Because these specimens were small torsion samples, the wood did not possess significant defects. As expected, the small samples tested in torsion possessed higher shear strength values than the large scale torsion specimens tested in the current study due to the few natural wood characteristics in the small torsion specimens. In addition to Mack's (1940) research, the finite element model from

shear strength, as discussed in section 5.2.1. Based on the length study and confirmed by previous studies and the finite element model, the length of a torsion specimen showed no effect on the shear strength for 2x4 specimen lengths of 21.0 inches, 28.5 inches, 32.0 inches, 35.5 inches, 39.0 inches. Therefore, the recommended ASTM (1996b) minimum total length of eight times the depth of the specimen was followed for the specimens tested in the depth study.

6.3 Depth study

For the specimens tested in the depth study the lengths are presented in Table 6.4. Due to the length restriction of the torsion machine available for this study, the longest length possible for a torsion specimen was 55 inches. For the 2x4 through the 2x6 specimens, the total length met the ASTM (1996b) requirement of eight times the depth. However, for the 2x8, 2x10 and 2x12 specimens, the machine length restriction reduced the length to 55 inches. Because length was shown not to affect the shear strength of 2x4 beams through the experiment and the finite element model, the main concern is that the specimen should have a long enough shear span so that the shear stress can reach uniformity. The shear span varied from approximately three times the depth for the 2x4, 2x6, and 2x8, to one and one-half times the depth for the 2x10 and one-half times the depth for the 2x12. In the finite element study, a plot of shear stress with respect to length of the beam for a 2x12 confirmed that the

shear stress with respect to length of the beam for a 2x12 confirmed that the shear span of one-half times the depth was adequate for allowing uniform shear stress to develop within the beam.

Table 6.4: Length specifications for depth study

Nominal Width x Depth (inches)	Actual Width x Depth (inches)	ASTM Requirement 8 times depth (inches)	Actual Length[1] (inches)	Shear Span[2] (inches)
2x4	1.5x3.5	28	28	2.86d (10 inches)
2x6	1.5x5.5	44	44	3.27d (18 inches)
2x8	1.5x7.25	58	55	3.03d (22 inches)
2x10	1.5x9.25	74	55	1.51d (14 inches)
2x12	1.5x11.25	90	55	0.53d (6 inches)

[1] 2x8, 2x10, and 2x12 specimens were restricted to 55 inches long due to machine limitations.
[2] Where d is the actual depth of the specimen.

The statistical summary for each depth tested, Table 6.5, shows the sample sizes, means, and coefficients of variation for the moisture content, specific gravity, and shear strength. The data collected for the evaluation of the depth effect on shear strength is presented in Appendix E.

Table 6.5: Summary statistics for the depth study[1]

Nominal Size (inches)	Sample Size	Moisture Content (%)		Specific Gravity		Shear Strength[2] (psi)	
		Mean	COV (%)	Mean	COV (%)	Mean	COV (%)
2x4	10	13.1	7.2	0.50	11.0	1440	9.3
2x6	10	13.5	5.2	0.52	7.6	1528	16.3
2x8	10	13.0	3.1	0.52	6.2	1507	18.0
2x10	10	13.2	1.6	0.55	9.5	1335	10.5
2x12	10	13.0	3.4	0.52	7.0	1346	6.84
ASTM[3, 4]	47	12.5	3.6	0.51	8.9	1287	12.8

[1] Appendix E contains complete length study data.

[2] Individual shear strength values adjusted to 12% moisture content (ASTM, 1996h), then averaged.

[3] One ASTM block was tested for each specimen

[4] One ASTM block did not fail along the shear plane and two specimens did not have enough clear wood to allow for one ASTM block

6.3.1 Statistical analysis

To determine if there were differences in shear strengths for the different depths tested in the depth study, an analysis of variance (ANOVA) test was performed. The ANOVA F-test revealed Since the F-test from the ANOVA does not indicate which depths differ from each other with respect to shear strength or the relationship between depth and shear strength, a multiple linear regression analysis was also performed to determine the linear relationship between depth and shear strength. If the linear regression proved to be significant, the equation would relate the shear strength to the beam depth. Other relationships which incorporated curvature or logarithmic scales into the analysis were also considered if various scatter plots identified other possible relationships.

Several factors present during the development of the ANOVA test and multiple regression models related to the specimens or the testing method, as shown in Appendix E: rings per inch, specific gravity, time to failure, torque rate, modulus of elasticity, and rotation. Scatter plots of these variables helped to identify if certain factors were related to one another by visual identification, but a linear regression was not performed. Possible related factors include:

- Specific gravity vs. rings per inch (Figure 6.10)
- Specific gravity vs. failure time (Figure 6.11)
- Specific gravity vs. applied torque rate (Figure 6.12)
- Applied torque rate vs. failure time (Figure 6.13)
- Applied torque rate vs. rotation (Figure 6.14)
- Modulus of elasticity vs. failure time (Figure 6.15)
- Modulus of elasticity vs. rotation (Figure 6.16)
- Rotation vs. failure time (Figure 6.17)

Some of these relationships were expected while others were not expected but checked as part of good statistical practice. A brief explanation for the relationships expected and those not expected was provided in the length study analysis, section 6.2.1, and also applies for the depth study.

Because the scatter plots of specific gravity showed relationships with rings per inch (Figure 6.1), failure time (Figure 6.2), and applied torque rate (Figure 6.3), specific gravity was selected as a covariate in the multiple regression model. The modulus of elasticity was also incorporated into the multiple regression model since it showed a possible effect on rotation.

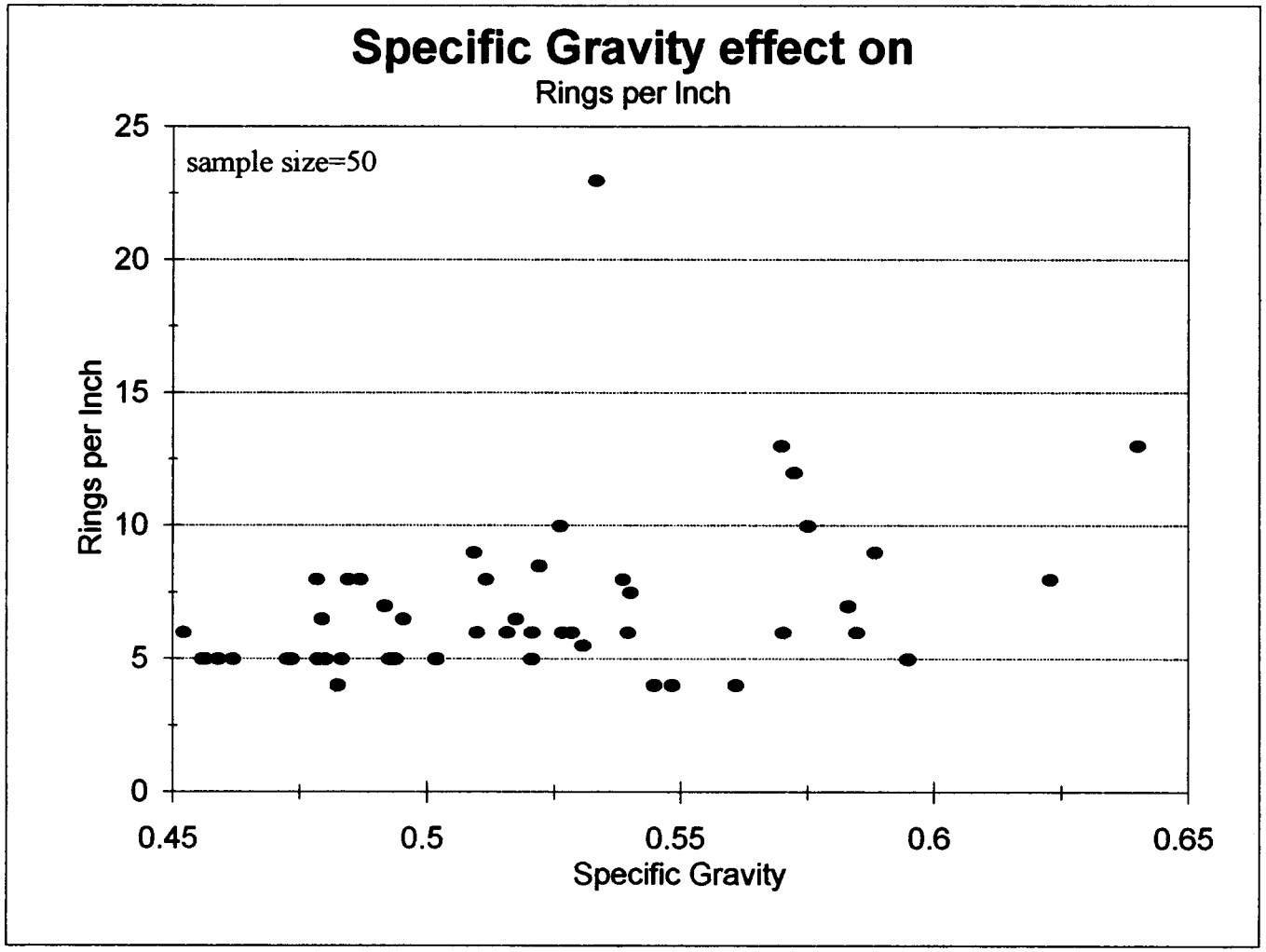

Figure 6.10: Scatter plot of specific gravity vs. rings per inch for the depth study

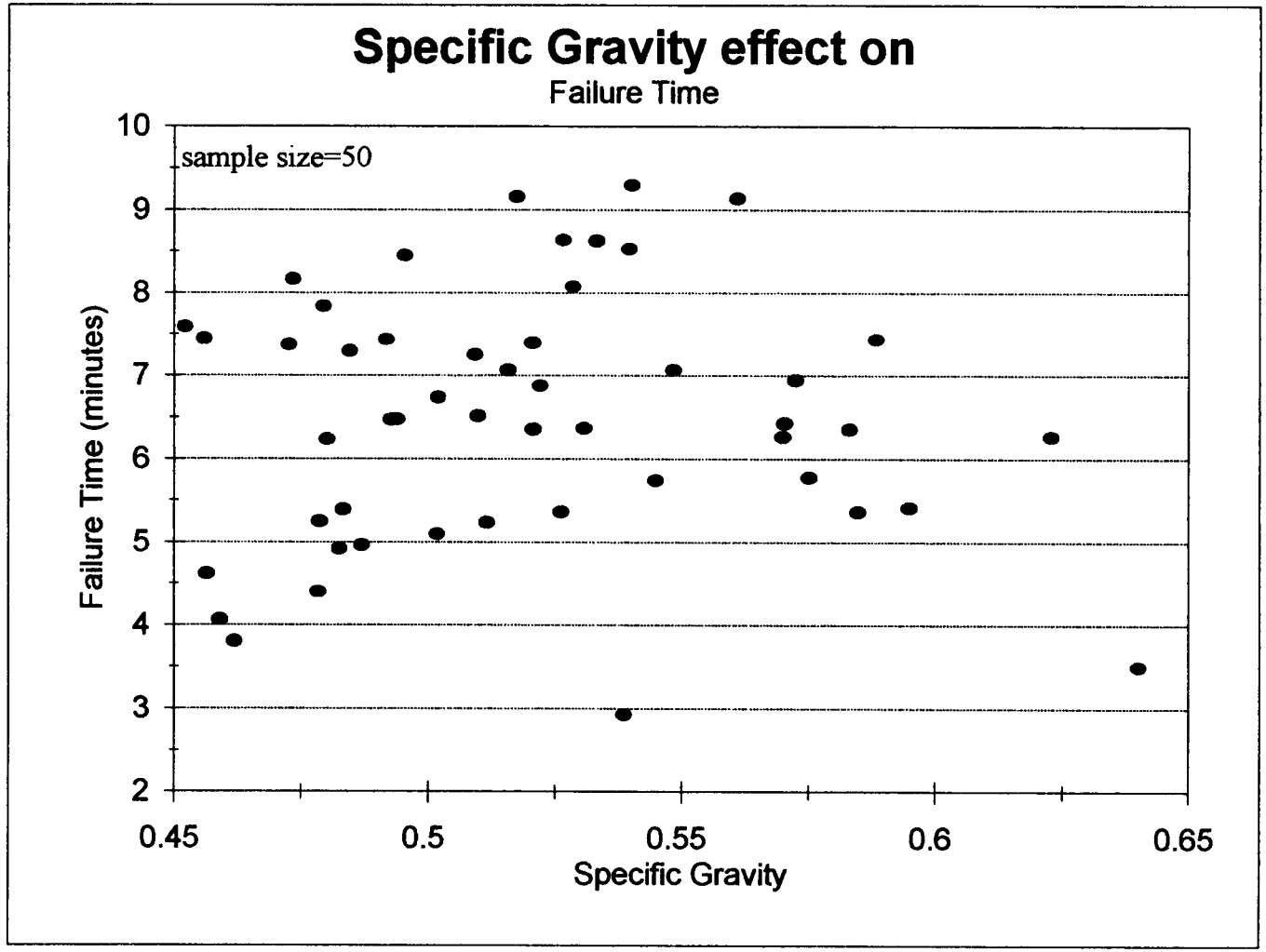

Figure 6.11: Scatter plot of specific gravity vs. failure time for the depth study

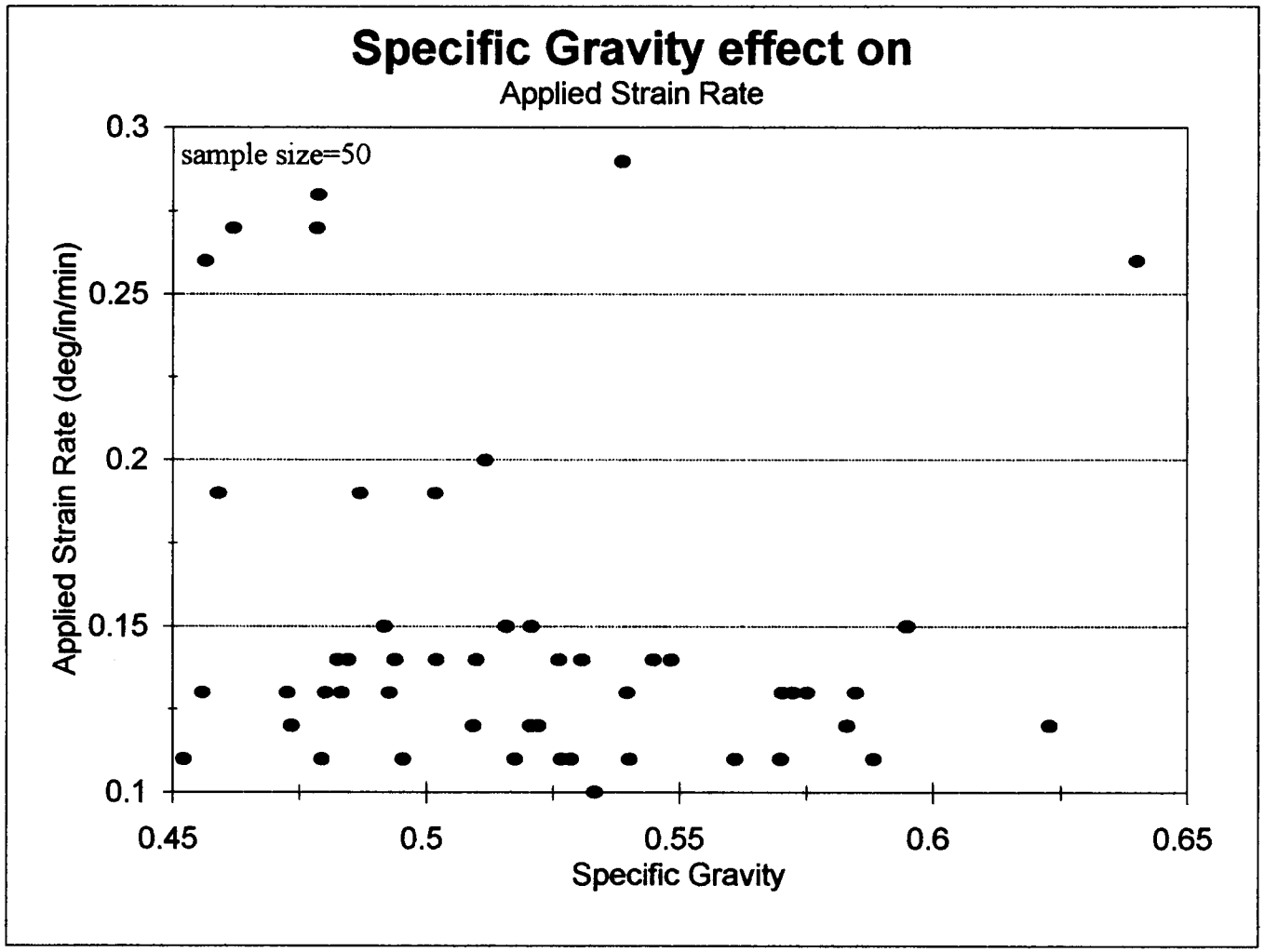

Figure 6.12: Scatter plot of specific gravity vs. applied strain rate for the depth study

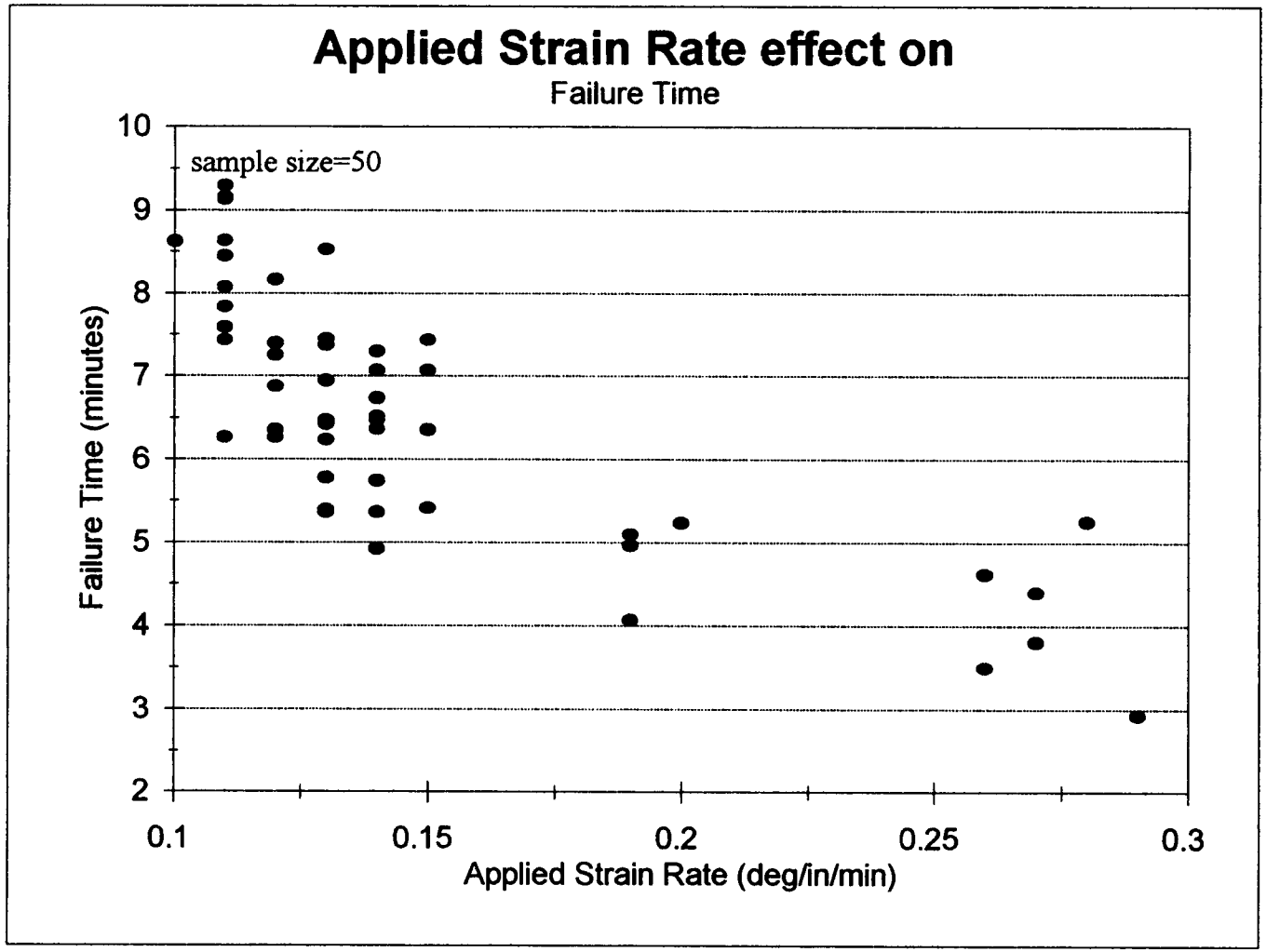

Figure 6.13: Scatter plot of applied strain rate vs. failure time for the depth study

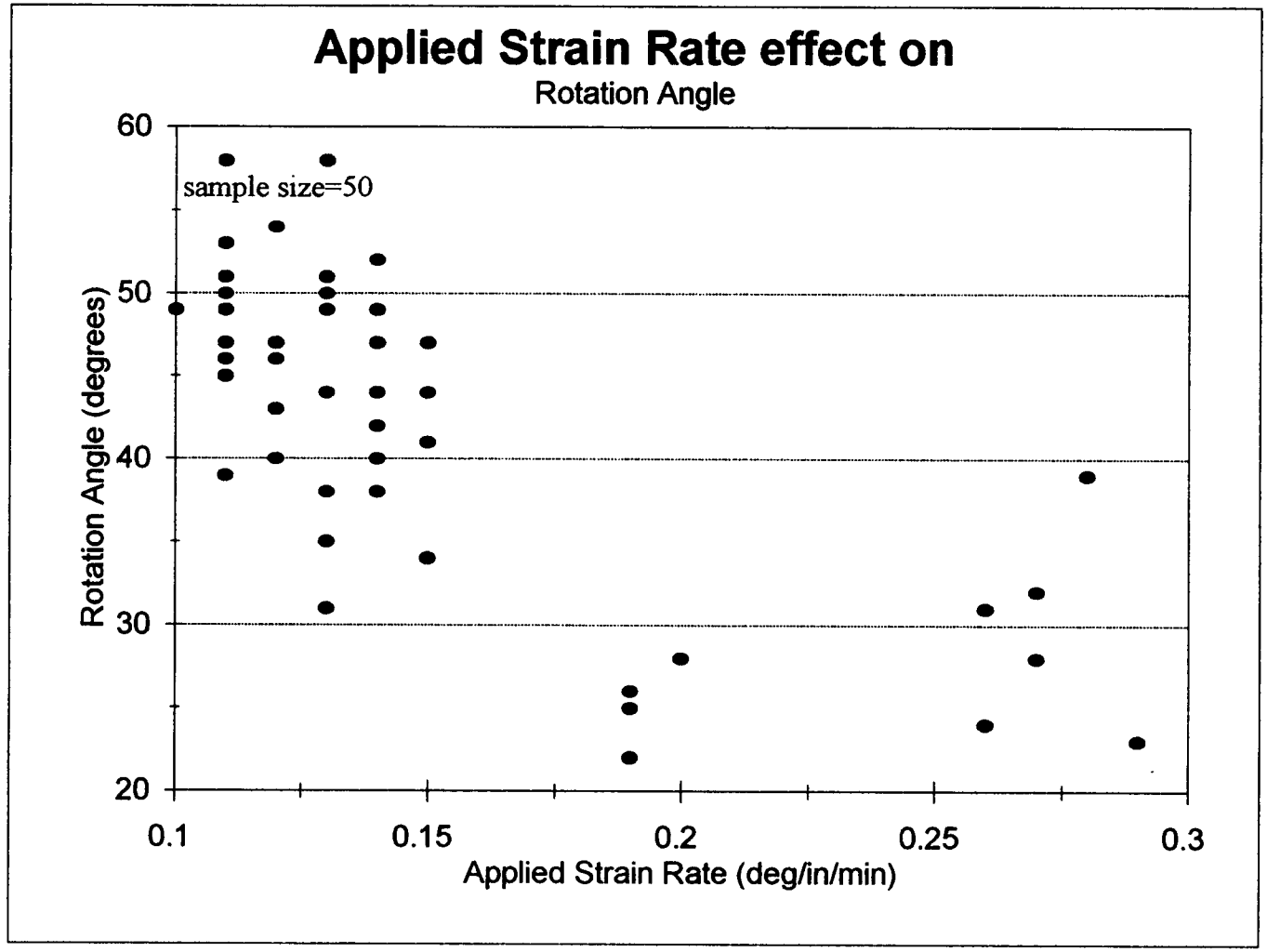

Figure 6.14: Scatter plot of applied strain rate vs. rotation angle for the depth study

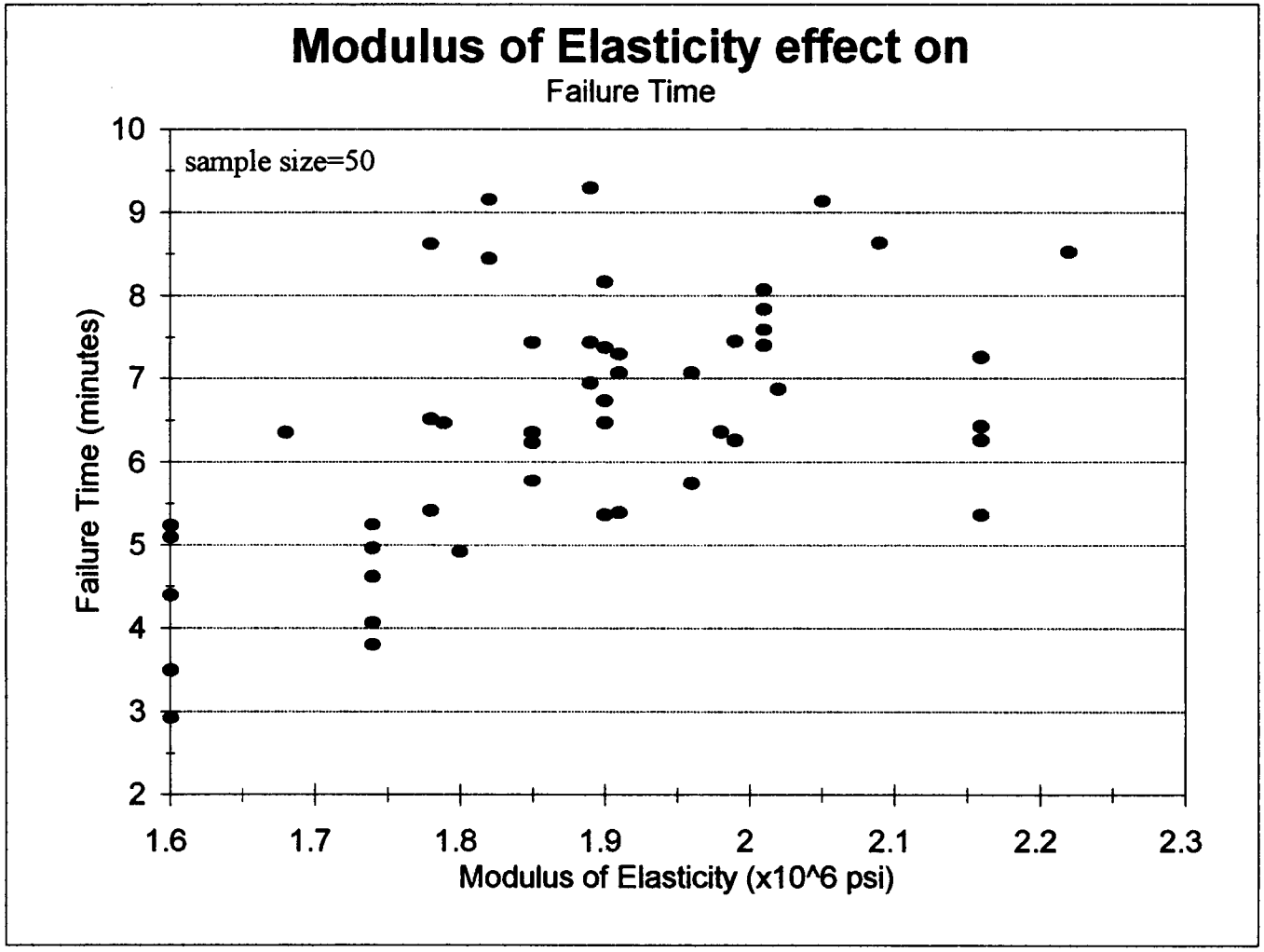

Figure 6.15: Scatter plot of modulus of elasticity vs. failure time for the depth study

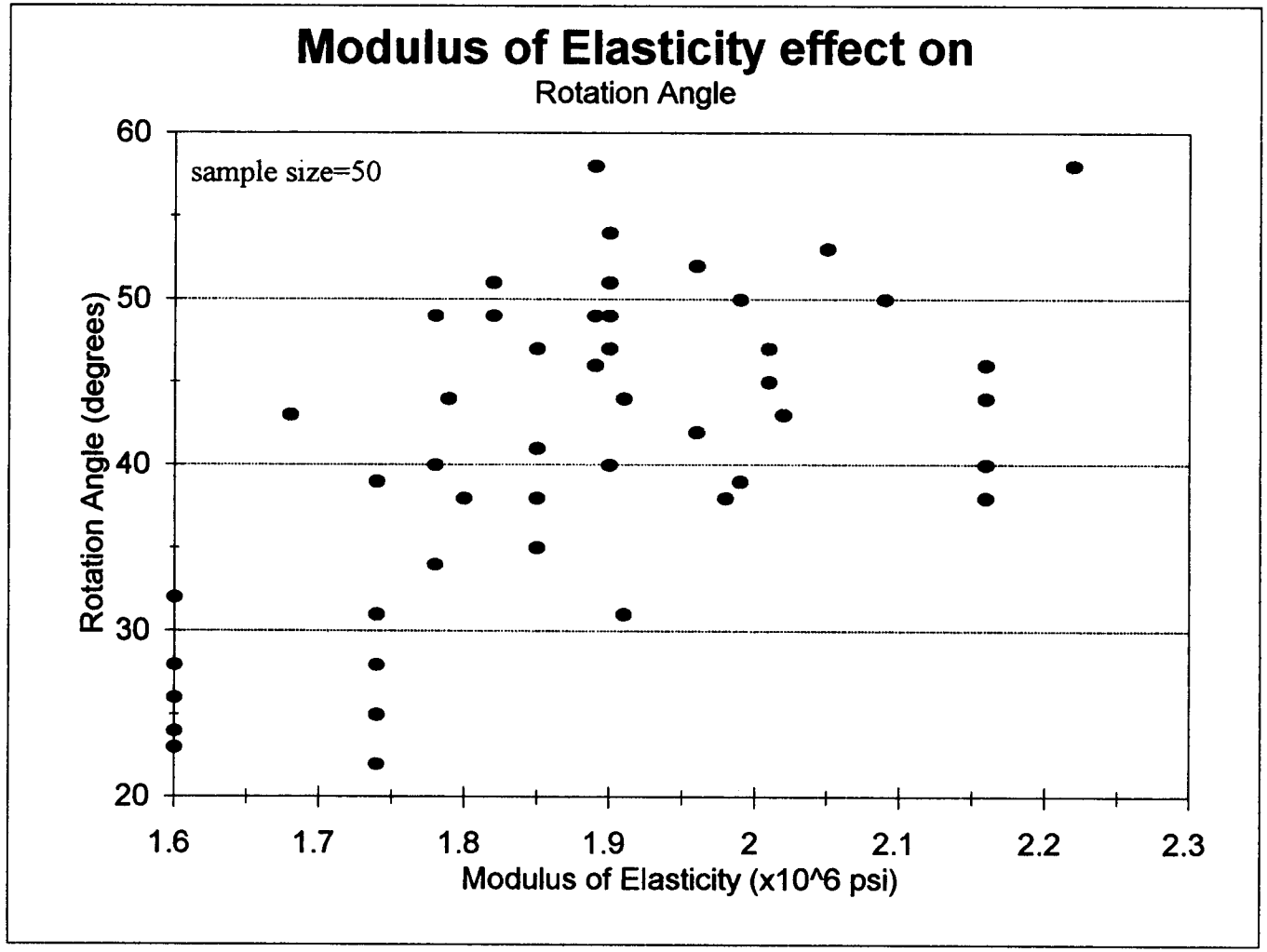

Figure 6.16: Scatter plot of modulus of elasticity vs. rotation angle for the depth study

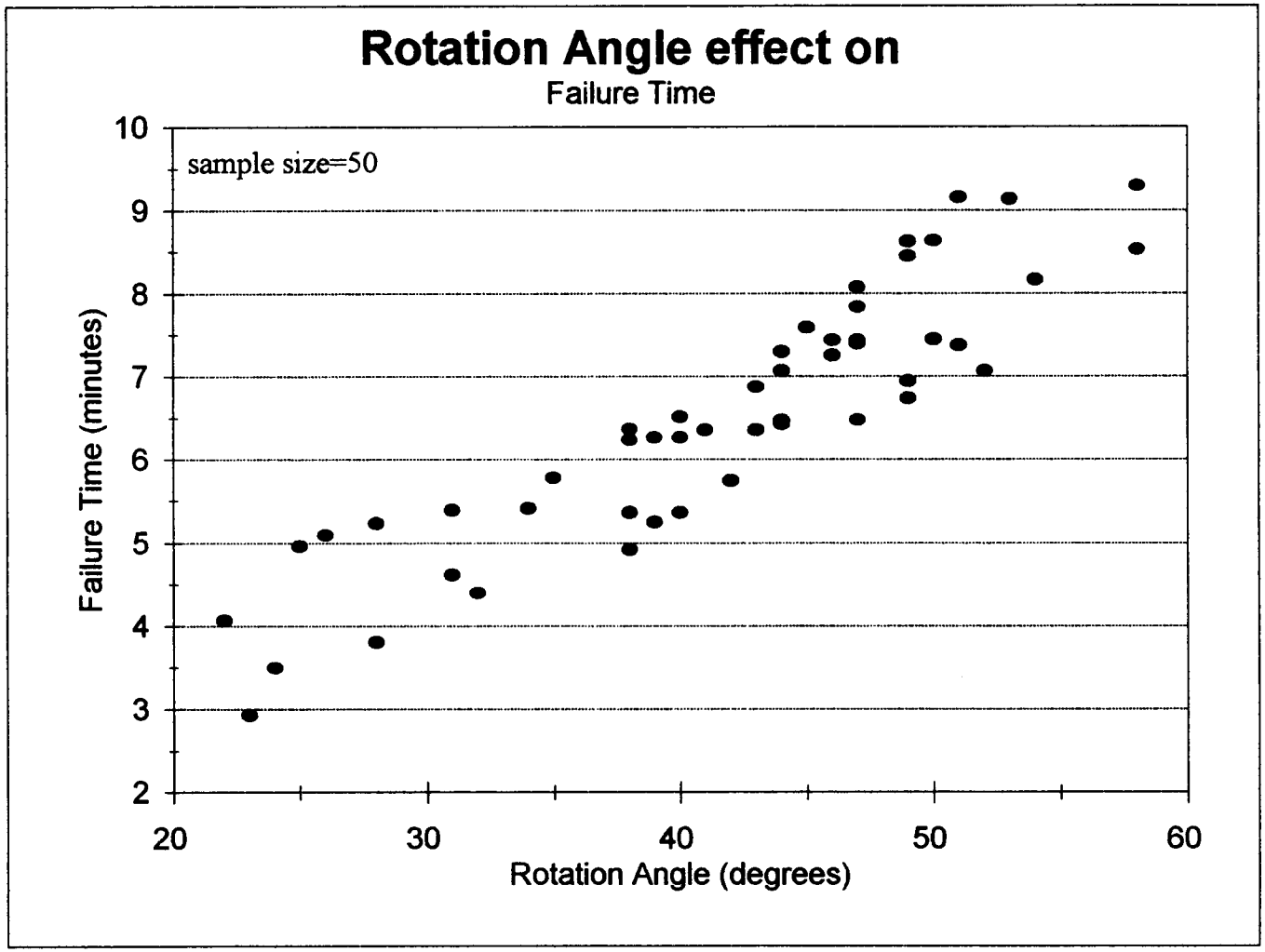

Figure 6.17: Scatter plot of rotation angle vs. failure time for the depth study

Occasionally more than one specimen came from the same board. Statistically, samples of wood from the same board would be expected to yield similar shear strength values. By including more than one specimen from the same board, the results could be misleading since the data would indicate that all specimens are independent from one another. In order to determine if independence was a problem among specimens from the same board, an ANOVA was performed twice: (1) excluding specific gravity as a covariate and (2) including specific gravity as a covariate.

The ANOVA F-test which excluded specific gravity indicated that there was suggestive but inconclusive evidence that specimens from the same board yielded more similar shear strength values than the non-related specimens (2 sided p-value=0.0445, extra sum of squares F-test). However, after including specific gravity into the model, the F-test from the ANOVA indicated that there was no evidence that specimens from the same board yield more similar shear strength values than the non-related specimens (2 sided p-value>0.1, extra sum of squares F-test). In the case with specific gravity as a covariate all specimens may be considered independent regardless of whether or not they came from the same board.

Summarized in Table 6.6 are the linear relationships considered, their corresponding R^2 values, 2-sided p-values, and brief comments regarding the significance of the relationship. Explanations for each relationship follow in Table 6.6

Table 6.6: Observed relationships in depth study[1]

Relationship Observed	R^2	2-sided p-value
$\tau = 1380(SG) + 716$ Moderate evidence that specific gravity affects shear strength	0.096	0.0290 (SG)
$\tau = 8.91(SPAN) - 12.8(d) - 184(MOE) + 1580(SG) + 920$ No evidence that modulus of elasticity affects shear strength	0.25	0.4379 (MOE)
$\tau = 0.073(A_{Beam}) + 1360(SG) + 716$ No evidence that beam area affects shear strength	0.096	0.9104 (A_{Beam})
$\tau = 6.77(SPAN) - 20.4(d) + 1570(SG) + 668$ Strong evidence that specific gravity affects shear strength; suggestive but inconclusive evidence that depth affects shear strength; and no evidence that shear span affects shear strength.	0.24	0.0103 (SG) 0.0478 (d) 0.1696 (SPAN)

[1] τ=shear strength (psi), SG=specific gravity, MOE=modulus of elasticity (x10^6 psi) SPAN=shear span (inches) as defined in section 5.2.3, and A_{Beam}=product of the depth and the shear span (inches^2).

Although the linear relationship between specific gravity and shear strength is poor for the depth study data (R^2=0.096), there is moderate evidence that specific gravity affects shear strength as shown in Equation 6.2 and Figure 6.18, where τ=shear strength (psi) and SG=specific gravity (2 sided p-value=0.0290, t-test). Because of the moderate evidence that indicated an effect on shear strength by specific gravity, and the evidence from the length study that indicated that specific gravity strongly affected shear strength, specific gravity was retained in the ANOVA model. In addition, the effect of specific gravity on

strength is known to be significant (Tsoumis, 1991), as was discussed previously in the length study.

$$\tau = 1380(SG) + 716 \tag{6.2}$$

Specific gravity must also be accounted for when analyzing for depth effects on shear strength. As a result, specific gravity and beam size were included in the multiple regression model as explanatory variables. Since the shear span varied among sizes, two beam size parameters were used in the multiple regression model, shear span and depth. Another factor considered in a preliminary multiple regression analysis was the modulus of elasticity. The modulus of elasticity did not show any evidence of an effect on shear strength (2 sided p-value=0.4379, t-test) even after accounting for specific gravity, depth, and shear span; thus, it was removed from the final multiple regression model. This confirmed the lack of a linear relationship between the modulus of elasticity and shear strength found in the length study and previous research (Riyanto, 1996).

The multiple regression model was used again with specific gravity and a modified size parameter, the product of the shear span and depth to yield the beam area (note that beam area does not equal the shear area which is the product of the shear span and the width of the beam). The F-test from the ANOVA indicated that there was suggestive but inconclusive evidence that shear strength was related to the beam area or specific gravity (2 sided p-

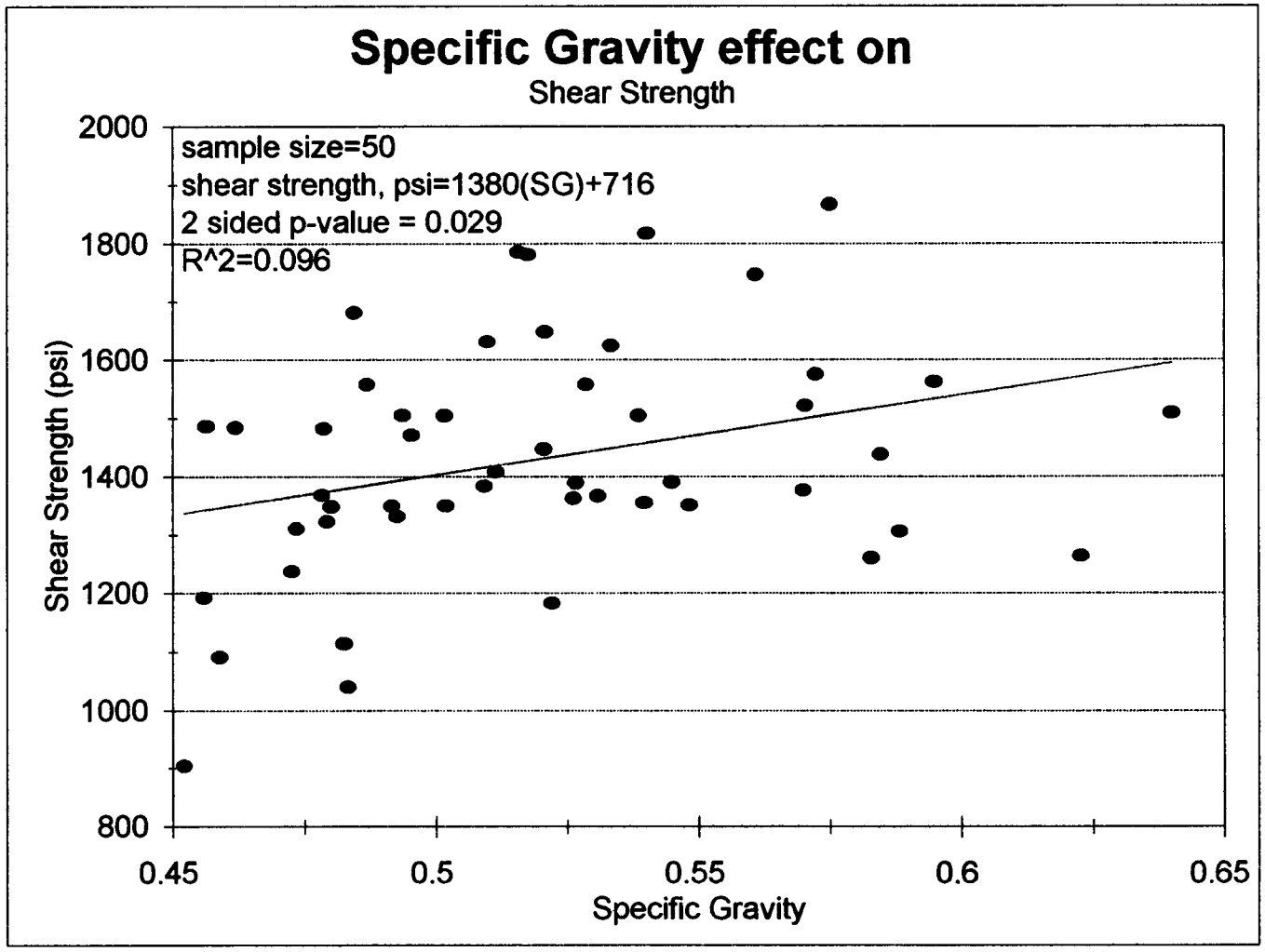

Figure 6.18: Specific gravity effect on shear strength for the depth study

value=0.0939, extra sum of squares F-test). From the multiple regression analysis, there was moderate evidence that specific gravity affected shear strength after the beam area was taken into account (2 sided p-value=0.0361, t-test). However, there was no evidence that the beam area was related to shear strength after considering specific gravity (2 sided p-value=0.9104, t-test). In addition, the linear relationship obtained with these variables was poor (R^2=0.096).

The final multiple linear regression model developed included shear strength as the response variable and the shear span, depth, and specific gravity as the covariate explanatory variables. The ANOVA, using these covariates, indicated convincing evidence that shear strength is associated with either shear span, depth, or specific gravity (2 sided p-value=0.0052; extra sum of squares F-test). To determine how the covariates affect the shear strength, a multiple regression was performed. The regression analysis yielded strong evidence that specific gravity affected shear strength after accounting for shear span and depth (2 sided p-value=0.0103, t-test), similar to the length study. There was no evidence that shear strength was affected by shear span after accounting for depth or specific gravity (2-sided p-value=0.1696, t-test). In addition, there was only suggestive but inconclusive evidence that shear strength was dependent on depth after accounting for shear span and specific gravity (2-sided p-value=0.0478, t-test); the multiple regression indicated that the relationship between shear strength, shear span, depth, and specific gravity

was weak (R^2=0.24) in Equation 6.3, where τ=shear strength, l=shear span, d=depth, and SG=specific gravity.

$$\tau = 668 + 6.77(l) - 20.4(d) + 1570(SG) \quad (6.3)$$

After considering the linear effect specific gravity, beam area, depth, and shear span had on shear strength, additional non-linear relationships, as shown in Table 6.7, were analyzed. These non-linear relationships were investigated based on previous research (Rammer et al., 1996) results which tested for shear strength via the five point bending method. Rammer et al. (1996) observed that the similar forms of the equations shown in Table 6.7, without the specific gravity component, demonstrated significant evidence of an effect of size on shear strength as determined by the bending method. However, for this study of shear strength using the torsion method, these equations proved to be weak relationships (with R^2 values ranging from 9.6% to 22.3%), but showed moderate evidence of a depth effect on shear strength--especially after accounting for specific gravity.

Table 6.7: Non-linear relationships reflecting the size effect on shear strength

Relationship[1]	Independent Variable	R^2	2-sided p-value
$\tau = 618 + 32.7(d) - 3.92(d)^2 + 1560(SG)$	depth[2]	0.2230	0.6010
$\tau = 683 - 4.88(A) + 0.265(A)^2 + 1370(SG)$	shear area[3]	0.1770	0.8077
$\tau = 790 - 2.30(V) + 0.008(V)^2 + 1490(SG)$	volume[4]	0.1173	0.3134
$\tau = 843 - 148\ln(d) + 1670(SG)$	depth	0.1867	0.0262
$\tau = 412 + 117\ln(A) + 1290(SG)$	shear area	0.1631	0.0573
$\tau = 736 - 5.76\ln(V) + 1390(SG)$	volume	0.0957	0.9140
$\tau = 842e^{(1.24(SG) - 0.017(d))}$	depth	0.2082	0.0171
$\tau = 774e^{(1.00(SG) + 0.004(A))}$	shear area	0.1559	0.0993
$\tau = 825e^{(1.05(SG) - 4.80x10\text{^}-5(V))}$	volume	0.1056	0.8756
$\tau = \frac{2760}{d^{0.108}}(SG)^{0.704}$	depth	0.2101	0.0229
$\tau = 1670A^{0.068}(SG)^{0.555}$	shear area	0.1614	0.1221
$\tau = \frac{2290}{V^{0.016}}(SG)^{0.608}$	volume	0.1207	0.6671

[1] τ is the shear strength (psi)

[2] Depth, d, is the actual beam depth (inches)

[3] Shear area, A, is the product of shear span and actual beam width (inches^2)

[4] Volume, V, is the product of shear area and the actual beam depth (inches^3)

Because the statistical analysis did not yield convincing evidence that the shear strength was dependent upon the beam size, specifically depth, the data were combined into one group of 50 specimens; Table 6.8 shows the summary statistics for all specimens combined into one group.

Table 6.8: Summary statistics for all depth study specimens

Beam Size	Sample Size	Moisture Content (%)		Specific Gravity		Shear Strength[2] (psi)	
		Mean	COV (%)	Mean	COV (%)	Mean	COV (%)
Torsion	50	13.2	4.6	0.52	8.6	1,431	14.0
ASTM[3, 4]	47	12.5	3.6	0.51	8.9	1,287	12.8

[1] Total includes all 2x4, 2x6, 2x8, 2x10, and 2x12 specimens in one group

[2] Individual shear strength adjusted to 12% moisture content (ASTM, 1996h), then averaged

[3] One ASTM block was tested for each specimen

[4] One ASTM block did not fail along the shear plane and two specimens did not have enough clear wood to allow for one ASTM (1996a) shear block

6.3.2 ASTM (1996a) study

One ASTM (1996a) shear block specimen, which was tested according to the ASTM (1996a) standards, corresponded to each full-size structural lumber specimen tested in torsion. A comparison between the torsion-based shear strength and the ASTM-based (1996a) shear strength was made to determine the relationship between the two methods. All ASTM (1996a) specimens were combined into one group because a simple linear regression reported inconclusive evidence that the depth of the specimen affected the ASTM-based shear strength (2 sided p-value=0.056), and that previous research also did not indicate a size affect on the ASTM based shear strength of a beam (Rammer et al., 1996).

Summarized in Table 6.9 are the relationships considered for the ASTM (1996a) study using the ASTM (1996a) shear block data from the depth study.

The R^2 values, 2-sided p-values, and brief comments regarding the significance of the relationships are detailed in the table. Explanations for each relationship follows in Table 6.9

Table 6.9: Observed relationships for ASTM shear blocks from the depth study

Relationship Observed	R^2	2-sided p-value
$\tau = 914 + 0.403(\tau_{ASTM})$ Moderate evidence that the ASTM-based shear strength is related to the torsion-based shear strength	0.104	0.0272 (τ_{ASTM})
$\tau = 52.8\tau_{ASTM}^{0.42} A^{0.086}$ Moderate to convincing evidence that ASTM-based shear strength is related to torsion-based shear strength	0.193	0.012 (τ_{ASTM}) 0.059(A)
$\tau = 38.2\frac{\tau_{ASTM}^{0.541}}{d^{0.132}}$ Convincing evidence that ASTM-based shear strength is related to torsion-based shear strength; moderate evidence that depth is related to torsion-based shear strength	0.24	0.002 (τ_{ASTM}) 0.012 (d)

[1] τ is the torsion-based shear strength (psi), τ_{ASTM} is the ASTM-based (1996a) shear strength (psi), d is the depth (inches)

A simple linear regression was performed to determine whether the ASTM-based (1996a) shear strength method was related to the torsion-based shear strength method tested in this study. This regression model used the shear strength obtained via the depth study torsion tests as the response

variable, and the shear strength obtained via the ASTM method as the explanatory variable. In this case the specific gravity was not incorporated into the model, because there was no evidence which indicated that the specific gravity obtained from the torsion specimens differed from the specific gravity obtained with the ASTM (1996a) specimens (2 sided p-value=0.142, t-test).

The simple linear regression, Figure 6.19, indicates that there is convincing to moderate evidence that the ASTM-based (1996a) shear strength is related to the torsion-based shear strength (2 sided p-value=0.0272), but the linear relationship, Equation 6.4, is poor and only accounts for 10% of the variability (R^2=0.104). Equation 6.4 relates $\tau_{torsion}$ = shear strength (psi), obtained via the torsion method to τ_{ASTM} = shear strength (psi), obtained via the ASTM (1996a) method.

$$\tau_{Torsion} = 914 + 0.403(\tau_{ASTM}) \qquad (6.4)$$

Riyanto (1996) showed that there was convincing evidence (2 sided p-value=0.00) that the ASTM-based (1996a) shear strength is linearly related to the torsion-based shear strength, Equation 6.5 (R^2=0.25). However, Riyanto's (1996) relationship accounts for 15% more data variability than Equation 6.4. The low percentage of data variability accounted in the current study, Equation 6.4, may be due to the smaller sample size used to develop the equation.

$$\tau_{Torsion} = 602 + 0.719\tau_{ASTM} \qquad (6.5)$$

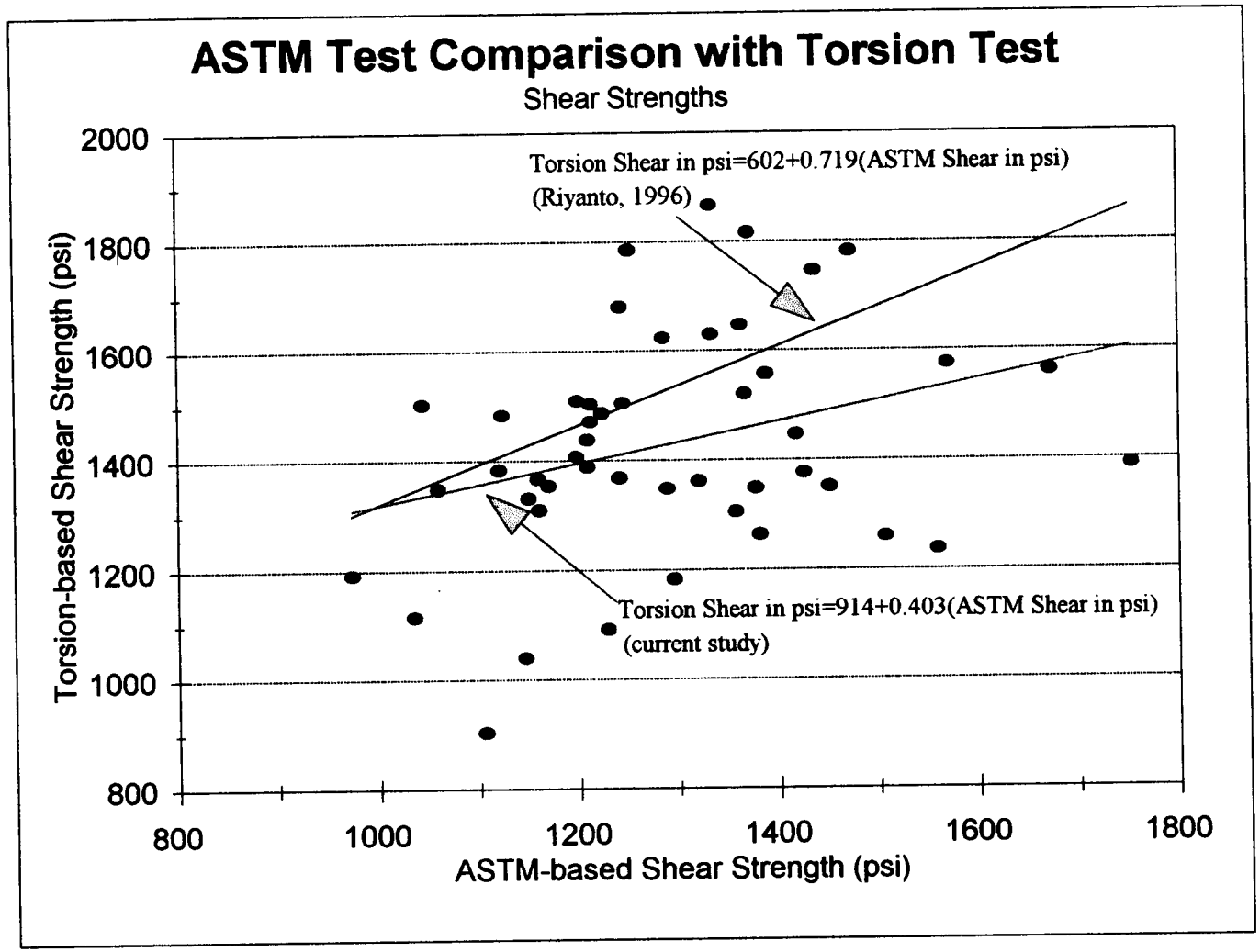

Figure 6.19: Comparison of Torsion-based shear strength with ASTM (1996a)-based shear strength

Another expression examined through a multiple regression analysis incorporated the torsion-based, the ASTM-based (1996a) shear strengths as well as the shear area of the torsion specimen. This power equation, Equation 6.6 (R^2=0.193), fits the data better than the linear relationship, provides moderate to convincing evidence that the shear strength obtained by the ASTM (1996a) method is related to the shear strength obtained by the torsion method (2 sided p-value=0.012, t-test), and provides inconclusive evidence that shear area affects the shear strength (2-sided p-value=0.059). For Equation 6.6, $\tau_{Torsion}$ (psi) torsion-based shear strength, A=shear area (inches^2) of beam, τ_{ASTM}, (psi) ASTM-based shear strength.

$$\tau_{Torsion} = 52.8\tau_{ASTM}^{0.42} A^{0.086} \qquad (6.6)$$

Rammer et al. (1996) used shear data from bending tests combined with shear data from ASTM (1996a) shear block tests that revealed that ASTM (1996a) shear block values could be adjusted to the shear strength based on bending tests, $\tau_{bending}$ (psi), through Equation 6.7, where τ_{ASTM} (psi) is ASTM-based (1996a) shear strength, A is the shear area (inches^2), and C_f is the shear block stress concentration factor of 2.0. Equation 6.6, is substantially different from the literature reported power equation, Equation 6.7 (Rammer et al., 1996). The primary reason these two equations differ may be due to the method of testing the large scale beams. The torsion method was used for Equation 6.6 and provided different results from the five point bending method that was used

for Equation 6.7 (Rammer et al., 1996). Because of this difference in shear strength values obtained by the two testing methods, the difference between the two relationships is not surprising.

$$\tau_{bending} = \frac{1.3 C_f \tau_{ASTM}}{A^{1/5}} \tag{6.7}$$

A different relationship was considered, Equation 6.8, by replacing the shear area covariate with depth, d (inches). Equation 6.8 provides convincing evidence that the ASTM-based shear strength is related to the torsion-based shear strength (2-sided p-value=0.002, t-test) and moderate to convincing evidence that the torsion-based shear strength is related to the beam depth (2-sided p-value=0.012). However, Equation 6.8 only accounts for 24% of the data variability (R^2=0.24). In other words, 76% of the data is not explained by Equation 6.8, which may result in large prediction errors if Equation 6.8 is used to predict the torsion-based shear strength based on a given ASTM-based (1996a) shear strength. In Equation 6.8, τ_{ASTM} (psi), is related to the shear strength obtained by the torsion method, $\tau_{torsion}$ (psi), (2 sided p-value=0.30).

$$\tau_{torsion} = 38.2 \frac{\tau_{ASTM}^{0.541}}{d^{0.132}} \tag{6.8}$$

Figure 6.20 shows the effect of Equation 6.4, Equation 6.6 and Equation 6.8 when used to predict torsion-based shear strengths with ASTM-based (1996a) shear strengths. Although Equation 6.8 is better than the other two

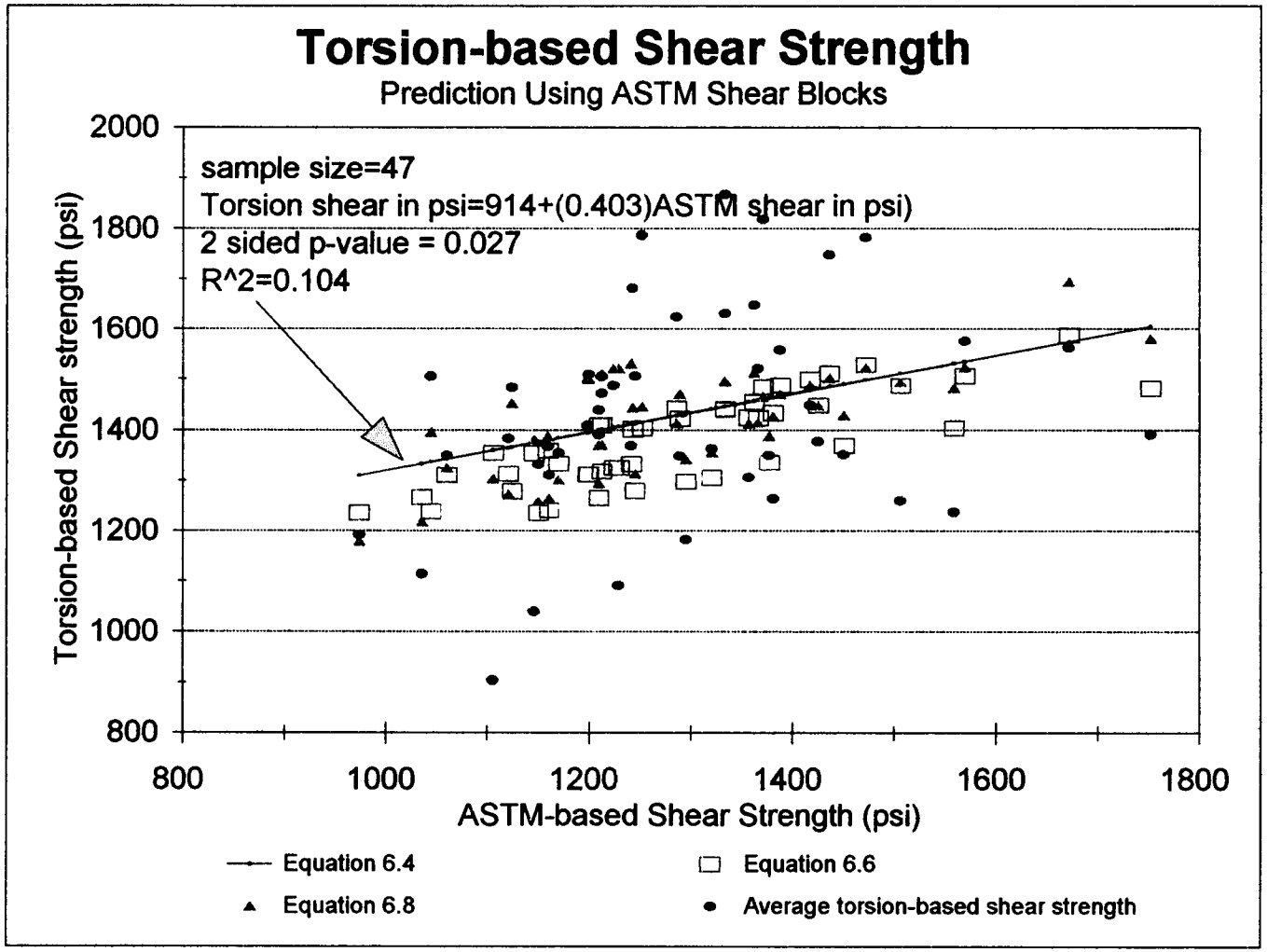

Figure 6.20: Torsion-based shear strength prediction using ASTM (1996a)-based shear strength

equations, none of the equations adequately predict the torsion-based shear strength using the ASTM-based (1996a) shear strength. Consequently none of the relationships are recommended for use in modifying ASTM-based (1996a) shear strengths to torsion-based shear strengths due to the lack of a strong relationship that represents the data.

6.3.3 Discussion

The average shear strength for the depth study, 1,431 psi, is 27% higher than the published ASTM shear block average shear strength value, 1,130 psi (coefficient of variation of 14%) for dry coastal Douglas-fir species (Wood Handbook, 1987). This large increase in shear strength was not only observed in the current length study, but also for Riyanto's (1996) torsion study. As observed by Riyanto and Gupta (1997) 76 nominal 2x4 Douglas-fir beams yielded an average shear strength value of 1,834 psi with a coefficient of variation of 18%. Although these torsion test shear strengths are higher (28.2%) than the current study's average shear strength, the previous study did have a larger (34%) sample size and Riyanto did not reflect the torsion machine calibration in the shear strength values. As mentioned in section 6.2.3 and Appendix A and Appendix B, the differences in shear strength and the smaller coefficient of variation for the current research may be explained by the electronic recording system designed for this study.

Various equations were examined to determine a relationship between beam size and shear strength determined by the torsion method, Table 6.7 and Equation 6.3. Based on the statistical analysis, one equation from Table 6.7, repeated here as Equation 6.9, accounts for the most data variability (R^2=0.2082) and indicates moderate evidence that the torsion-based shear strength is dependent upon the depth of the beam (2-sided p-value=0.0171, t-test). This result contradicts previous research studies that showed a convincing effect on shear strength due to depth, shear area, and/or shear volume (Asselin et al., 1996; Rammer et al., 1996; Sanders, 1996; Rammer and Soltis, 1994). Equation 6.9 represents the effect of depth, d (inches) on the torsion-based shear strength, τ (psi), and specific gravity, SG.

$$\tau = 842e^{(1.24(SG)-0.017(d))} \tag{6.9}$$

Rammer et al. (1996) indicated that for solid sawn Douglas fir beams, the shear strength, adjusted for 0.24% moisture content and 0.45 specific gravity, depended on the size of the beam, Equation 6.10. In Equation 6.10, τ is the shear strength based on the bending test method (psi) and A is the shear area of the beam (inches^2). A similar relationship was observed in glue laminated beams as well as for solid sawn beams (Rammer and Soltis, 1994). In both cases, solid sawn lumber and glue laminated beams, the specimens were tested via the five point bending method. A relationship of the form similar to Equation 6.10 was not observed with the current torsion test study.

$$\tau = \frac{3{,}070}{A^{0.25}} \qquad (6.10)$$

Adjusted for 24% moisture content
Adjusted for 0.45 specific gravity

A significant difference between the earlier studies and the current study is the method of testing for shear strength of the beams. In the bending test, there occurs additional stresses in the shear span, for example, compression parallel to the grain, compression perpendicular to the grain, tension parallel to the grain, and shear parallel to the grain stress. The interaction between these stresses and shear strength may cause an indirect size effect on the shear strength of the beams. However, in the torsion test, interactions between other stresses in the shear span do not occur since the only stress experienced in the specimen is the shear stress. Because bending strength, compression parallel to the grain strength and tension parallel to the grain strength are wood material properties which are affected by the size of the beam (AFPA, 1991), their corresponding stress may interact with the shear parallel to the grain stress to show a size dependence on shear strength.

The interactions between the compression parallel to grain, tension parallel to grain, and shear stress for bending specimens have not been studied extensively to determine if the size relationship with shear strength is based on these stress interactions. Compression perpendicular to the grain stress has been studied, and the observations reveal a linear relationship: as the compression perpendicular to the grain stress increases, the shear stress also increases at the failure point in the wood (Mandery, 1969). Riyanto (1996)

observed that for the five point bending test the highest compression perpendicular to the grain stress occurs in the same location within the beam as the high shear stresses, suggesting the five point bending test may not be an appropriate method to determine the shear strength of wood. The stress interactions in a three- and five- point bending specimen have been observed indirectly through a finite element model of these bending specimens developed by Cofer et al. (1997). The finite element model of a clear beam did not reproduce convincing evidence that there is a size effect on shear strength, which may suggest that the increased frequency and increased severity of natural characteristics in larger beams may influence a size effect on shear strength (Cofer et al., 1997). Because the torsion test, which eliminates compressive, tensile, and shear stress interactions, does not show a convincing size effect on shear strength, stress interactions in bending specimens tested for shear strength as well as the frequency of the natural characteristics of wood, should be considered before proposing a size relationship for design.

6.4 Discussion of ASTM, torsion, and bending shear strength tests

Several studies have focused on bending methods to determine the shear strength of beams (Riyanto, 1996; Sanders, 1996; Rammer et al, 1996; Rammer and Soltis, 1994). Table 6.10 outlines the number of shear failures per sample size, the average shear strength, and the coefficient of variation for three point and the five point bending tests for 2x4 beams and the corresponding ASTM

(1996a) shear block tests (Riyanto, 1996; Sanders, 1996). For comparison with previous bending test results, Table 6.11 summarizes the torsion test shear strength results from the length study, the depth study, and their corresponding ASTM (1996a) shear block test results.

Table 6.10: Comparison of 2x4 bending tests from previous research[1] with ASTM values in parenthesis

Researcher	Three point bending test			Five point bending test		
	Sample Size[2]	Average Shear Strength (psi)	COV (%)	Sample Size[2]	Average Shear Strength (psi)	COV (%)
Riyanto[3]	43/76	1315 (1151)	16 (15)	37/76	1608 (1151)	18 (15)
Sanders[4]	22/60	1216 (1011)	26 (12.1)	21/60	1582 (1306)	24 (12.6)

[1] Shear strength based on dry samples near 12% moisture content

[2] Sample size given as the number of shear failures out of the total number of specimens tested

[3] Riyanto, 1996

[4] Sanders, 1996

Table 6.11: Summary of torsion test shear strength results

Study	Sample Size	Average Shear Strength[1] (psi)	COV (%)
Length	50	1,526	15.7
ASTM	10	1,202	10.9
Depth	50	1,431	14.0
ASTM	47	1,287	12.8

[1] Individual shear strengths adjusted to 12% moisture content (ASTM, 1996h) then averaged

Lower shear strength values were not only observed for the ASTM blocks in the length study of the current torsion test, but also in the three- and five-point bending studies performed previously (Riyanto, 1996; Sanders, 1996). ASTM-based shear strengths were generally lower than the torsion test (27% for the length study and 12% for the depth study), the three point bending test (14% for Riyanto in 1996 and 20% for Sanders in 1996), and the five point bending test (40% for Riyanto in 1996 and 21% for Sanders in 1996). As previously stated in the length study, this result implies that the ASTM (1996a) shear block method may be underestimating the shear capacity of full-size lumber.

The coefficient of variation for shear strength from the five point bending test is significantly higher than that from the torsion test and slightly higher for the three point bending test shear strength than for that from the torsion test. This smaller coefficient of variation for the torsion test shear strength indicates that the test may provide better consistency than either bending methods. In addition, torsion tests result in 100% shear failures as opposed to 37% to 57% for the three point and 35% to 49% for the five point bending test.

Not only do the ASTM-based (1996a) shear strength differ from the full-size lumber tests, but each of the full-size lumber tests differ from themselves. When comparing the shear strength results from the testing of full-size beams, the three point bending method has a lower shear strength value than the torsion test (16% to 25%) and the five point bending method has a higher shear

strength value than the torsion test (5% to 4%). Cofer et al. (1997) also found in the finite element study, the three point bending method consistently reported lower shear strength values than the five point bending method. He noticed that Tsai-Hill failure criterion indicated that the three point test is more likely to fail in tension than in shear. As a result, those specimens which do fail I shear, which are the only beams used to determine the shear strength, may be reporting the lower shear strength values for the shear strength distribution corresponding the wood species tested (Cofer et al., 1997). Consequently, with the three point test, a representative sample of specimens and their corresponding shear strength values are not achievable. The torsion test may offer a more representative sample of specimens and corresponding shear strengths since 100% of the samples fail in shear (Riyanto, 1996). With large variability in shear strength values between different shear tests, establishing a standard shear test method for full-size lumber is important.

Although Cofer et al. (1997) indicates that the five point bending method is more likely to fail in shear, Riyanto (1996) showed that even the five point test method only allows for 49% of shear failures. Again, since not all samples fail in shear, the shear strength results may not be a good representation of the shear strength.

Another disadvantage for the bending tests, which have low percentages of shear failures, is that an initially randomized sample does not remain random. The random sample decreases in sample size because the samples considered in determining the shear strength are those samples which only failed in shear.

In addition, an initially randomized sample group looses its power of being randomly selected because the samples used to measure shear strength were samples based on a selection criteria, in this case the criteria is the shear failure mode: all samples used to determine the shear strength were required to fail in shear. Previous research (Riyanto, 1996) and the current research has shown that the torsion test method offers 100% shear failures. Therefore, a randomized sample group is not reduced based on a selection criteria.

6.5 Shear failures

The shear failures were as expected for all the tests, the length study, the depth study, and the ASTM shear block study. The tested shear strength was the shear strength parallel to the grain, as described in Chapter 3, Torsion Theory. In general, the shear failures occurred parallel to the grain. However, the grain angle may not necessarily have been parallel to the longitudinal axis of the specimen. In rare occasions, the shear failure drifted off the travel path parallel to the grain angle; in these cases, knots were associated as the point of path change. Since a natural defect appeared to be the cause of the path change and the failure still represented a shear failure, the specimens were not tossed from the sample group.

Figure 6.21 identifies major parts of the torque-time graph and corresponding photographs of the failed specimen. Figure 6.21a and Figure 6.21b show the torque increasing; for Figure 6.21a, the specimen does not

appear to show any failure, but for Figure 6.21b the specimen begins to show a slight crack around the knots. A major shear failure crack is not noticed until Figure 6.21c where the graph also shows a peak in the applied torque. Points c and d occur quickly resulting in difficulty in distinguishing the exact failure time. Figure 6.21c and d also demonstrate that at the point of failure, the shear crack is not large and still occurs within the elastic region of the load application. Figure 6.21e through Figure 6.21g illustrate the shear crack expanding as the torque stabilizes between 6,000 and 7,000 inch-pounds. Complete failure of the wood specimen is seen in Figure 6.21h and Figure 6.21i as the torque application is continued. The final stages are Figure 6.21j and Figure 6.21k, which illustrate the longitudinal and cross sectional shear cracks after the specimen has been removed from the torsion machine.

Other typical failures are illustrated in Figure 6.22 through Figure 6.26, which show the torque verses time graph and the corresponding specimen identifying the failure crack. As observed in the length and depth study, a longitudinal crack began at the middle point of the long side, near the center of the span, of the specimen. The crack propagated along the length, toward the ends of the specimen, and through the cross section perpendicular to the growth rings, Figure 6.24. In some cases the crack traveled along the growth rings in portions of the cross, as shown in Figure 6.23. In this case, the failure was along the earlywood-latewood boundary. As the shear crack approached a knot, in Figure 6.23, the crack traveled around the knot and often stopped on the other

side of the knot, indicating that knots may provide some resistance to shear failures.

An anatomical study of shear failures in wood was not performed as part of this research, but is recommended in future research of the shear strength of wood. However, some microscopic characteristics of the shear failure can be speculated. The observed failures in the cross section, Figure 6.21k, Figure 6.23, Figure 6.24, and Figure 6.25 show the shear failure traveling in the radial direction. The shear failure parallel to the grain may be causing separation of wood planes parallel to on another as a result of a discontinuity in the wood material between the longitudinal tracheids and the ray cells. In addition, the transverse cells may also provide some resistance to the shear failure since the transverse cells are located perpendicular to the shear failures.

The chemical components of the cells may also affect the shear strength. Tension wood, which contains less lignin than normal wood has less shear strength than normal wood (as summarized in Panshin and de Zeeuw, 1980). Because the lignin works as a mortar for the cellulose chains, perhaps lignin provides some resistance to the sliding of wood fibers, as observed in shear failures. Correlating the amount of lignin to shear strength may provided insights on the chemistry composition effects on shear strength.

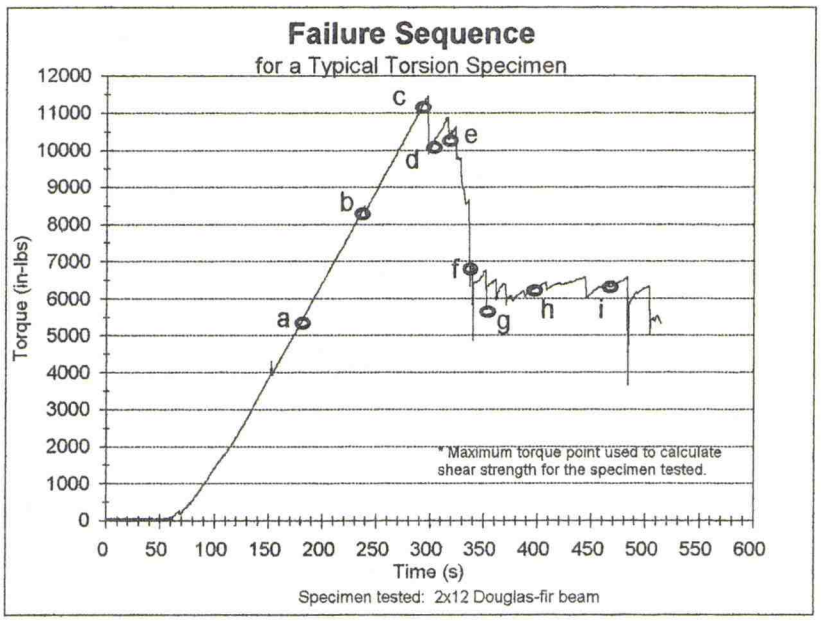

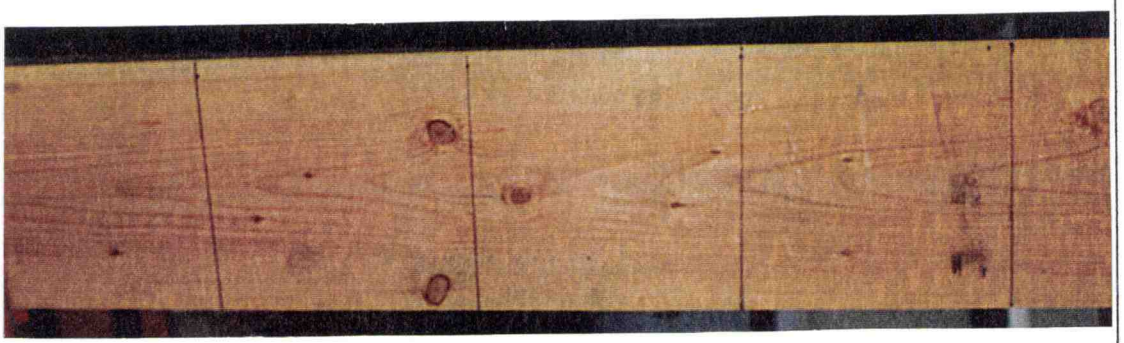

Figure 6.21: Typical shear failure observed in structural lumber tested in torsion. (a) Torque increasing and no sign of failure

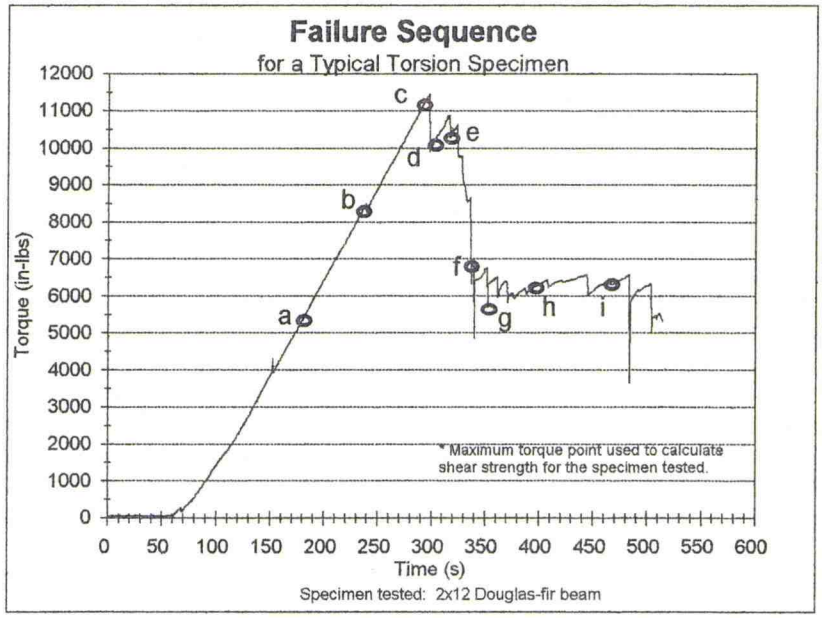

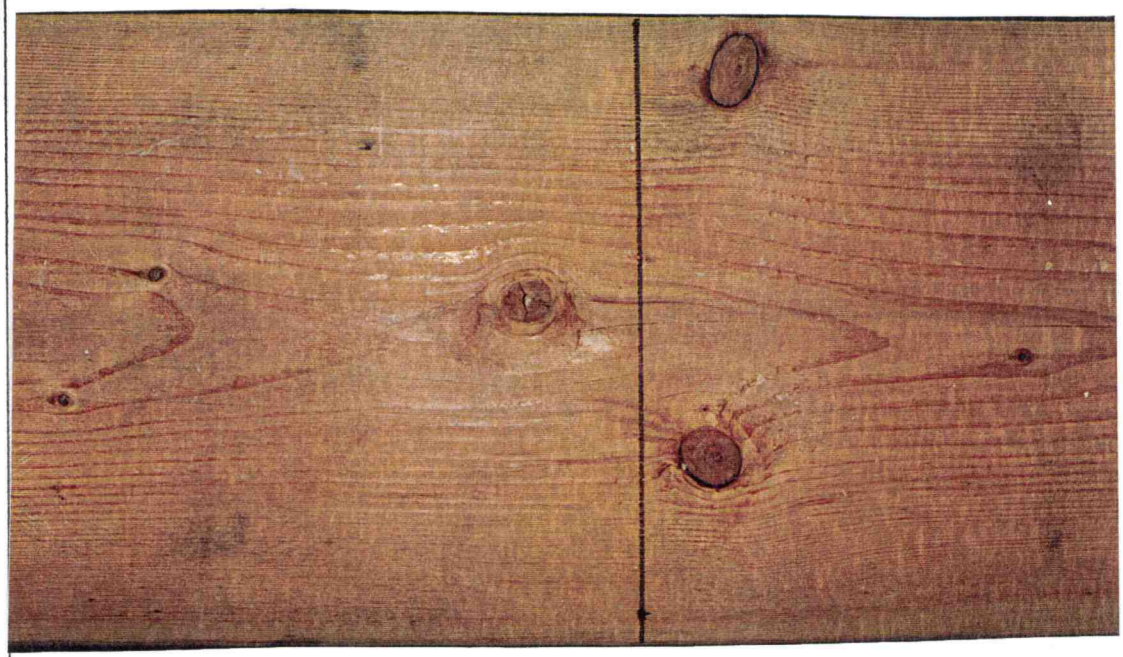

Figure 6.21: Typical shear failure observed in structural lumber tested in torsion. (b) Torque increasing and no sign of failure

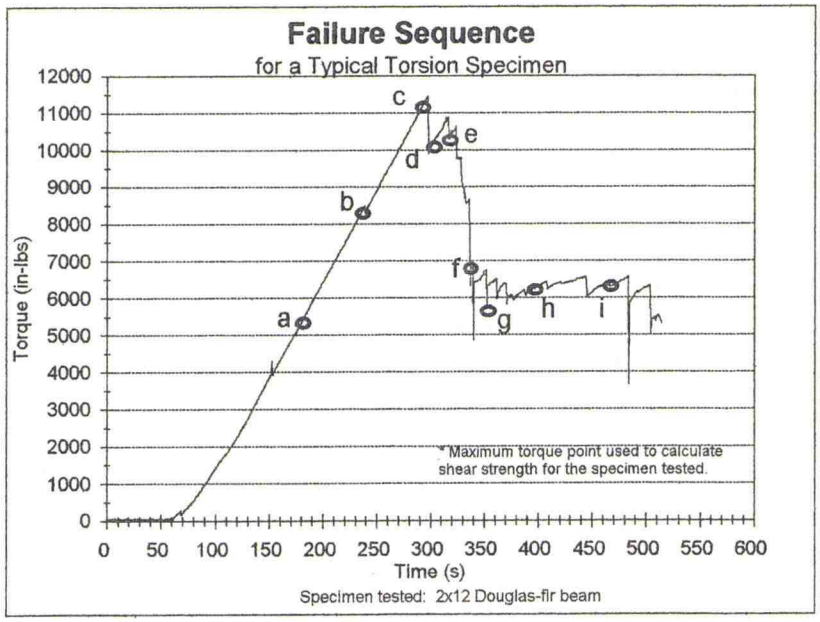

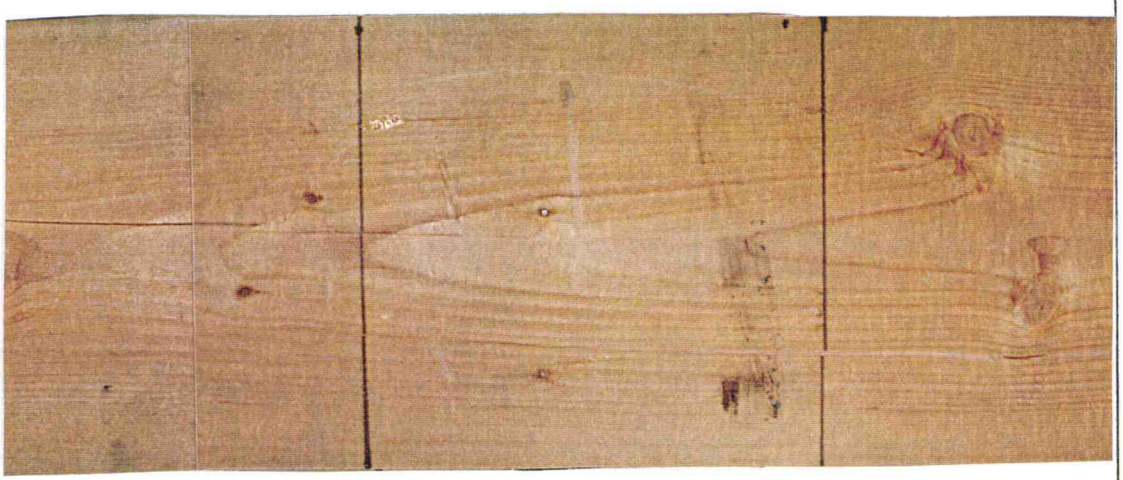

(c) and (d)

Figure 6.21: Typical shear failure observed in structural lumber tested in torsion. (c) Near maximum applied torque, specimen showing significant shear failure (d) Past maximum applied torque, difficult to distinguish on the specimen between the maximum torque point and a point directly after the maximum failure point

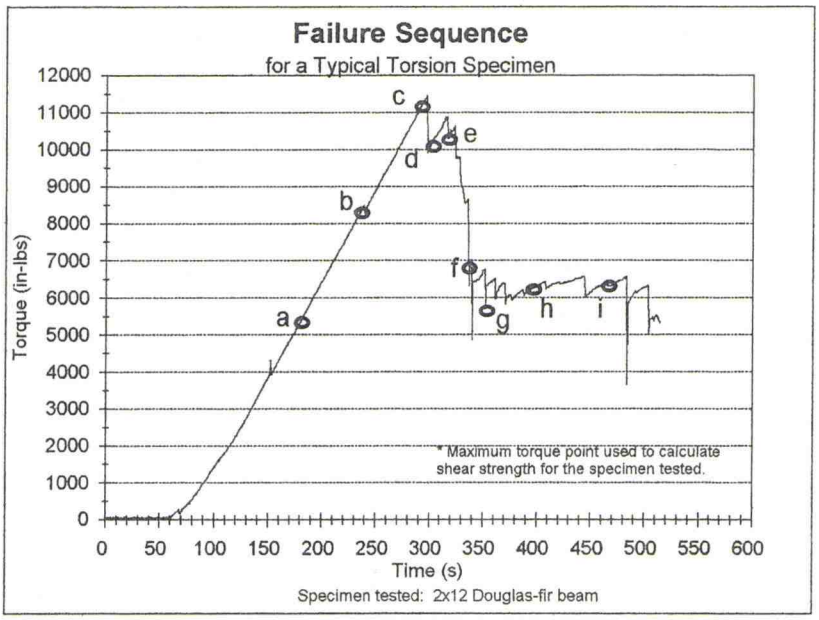

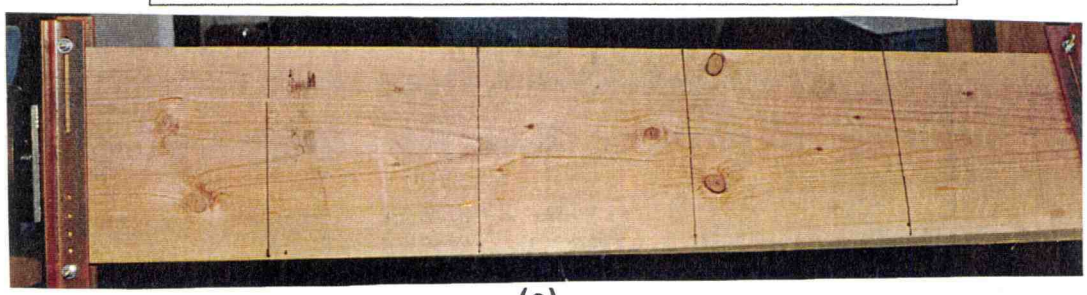

(e)

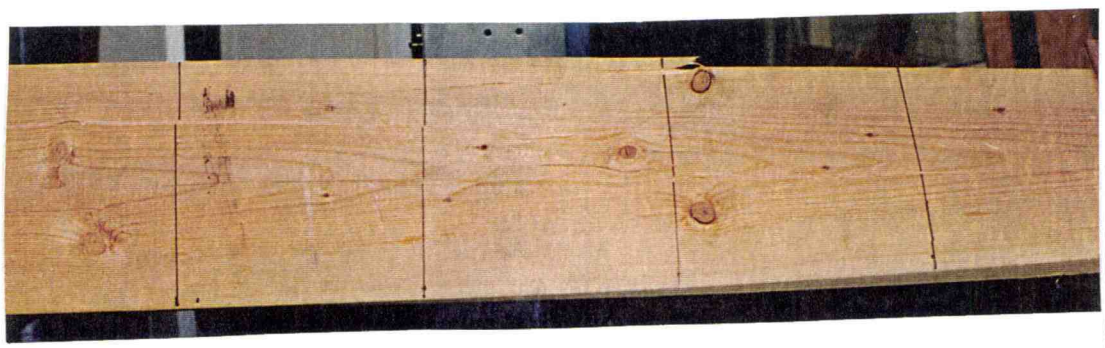

(f)

Figure 6.21: Typical shear failure observed in structural lumber tested in torsion. (e) and (f) Torque stabilizes between 6,000 in-lbs. and 7,000 in-lbs., and shear crack expanding

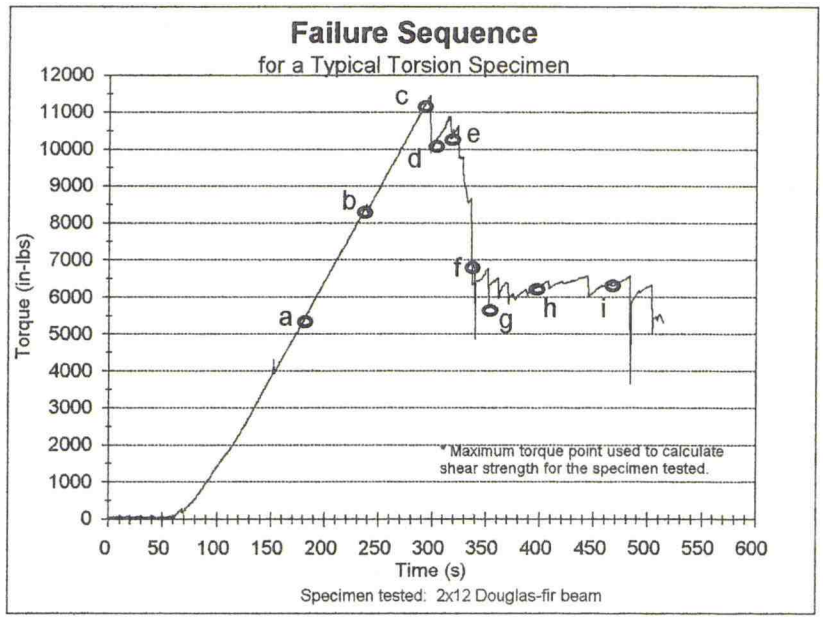

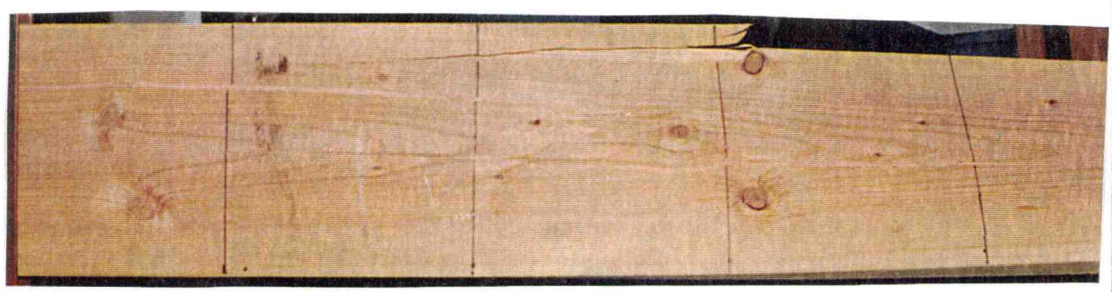

Figure 6.21: Typical shear failure observed in structural lumber tested in torsion. (g) Torque stabilizes between 6,000 in-lbs. and 7,000 in-lbs., and shear crack expanding

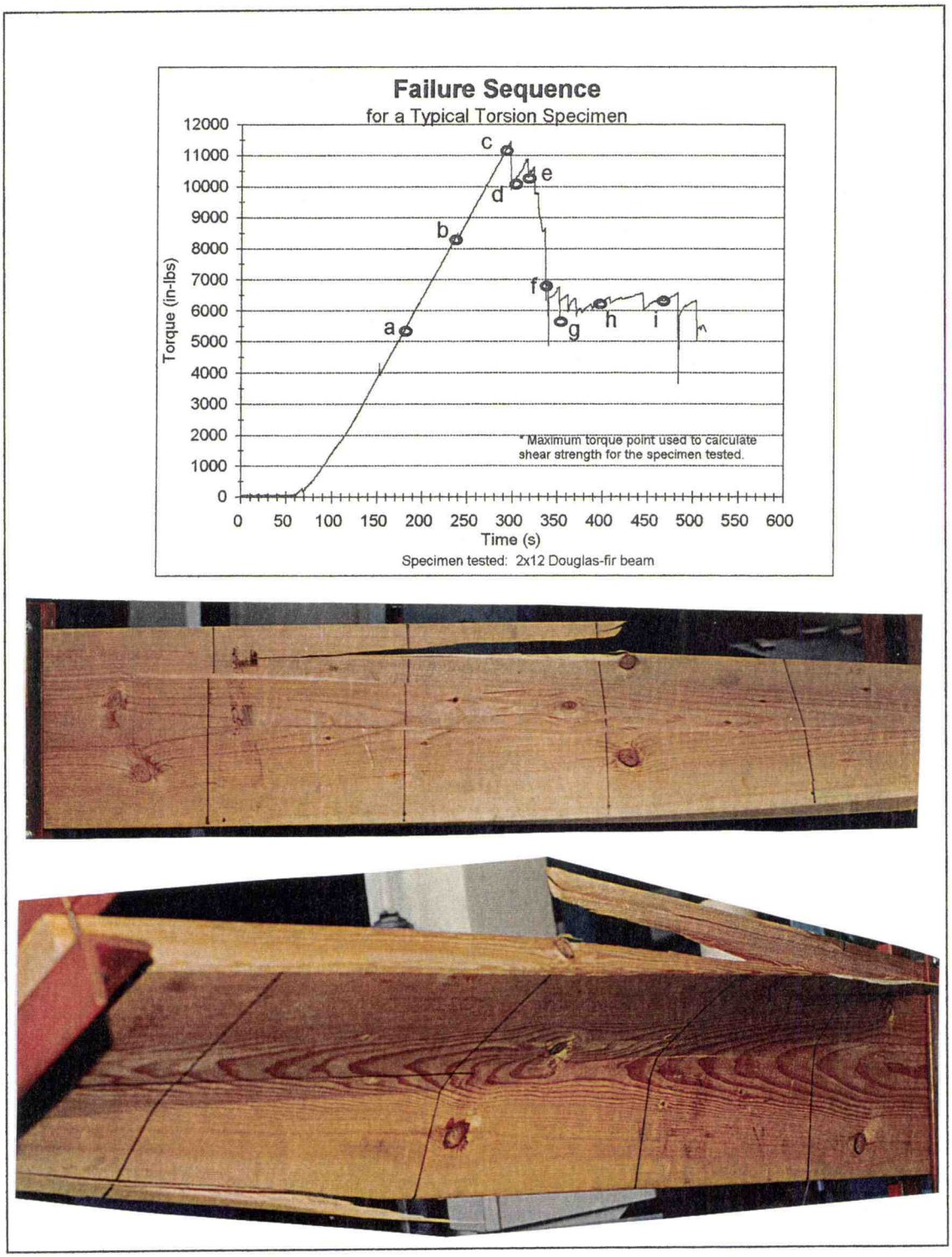

Figure 6.21: Typical shear failure observed in structural lumber tested in torsion. (h) Torque application continued and specimen is reaching complete failure

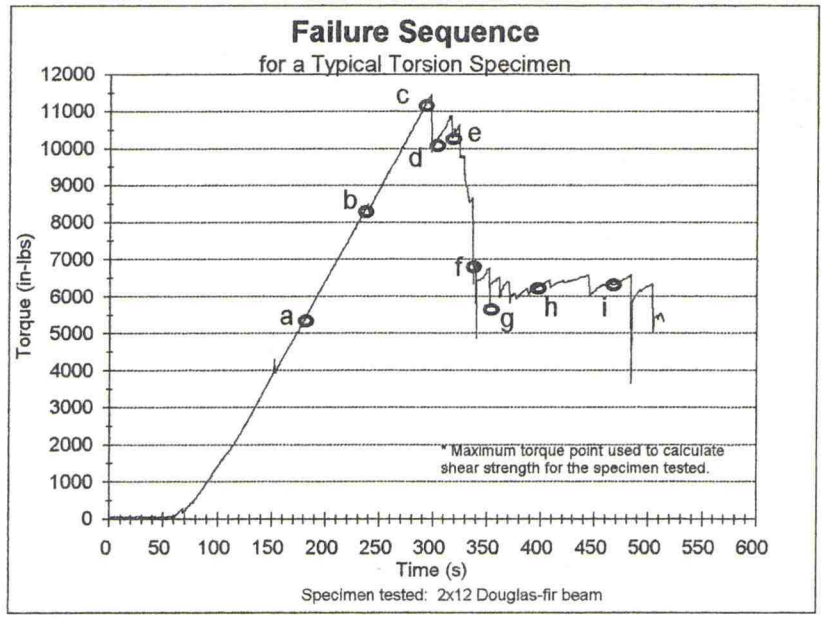

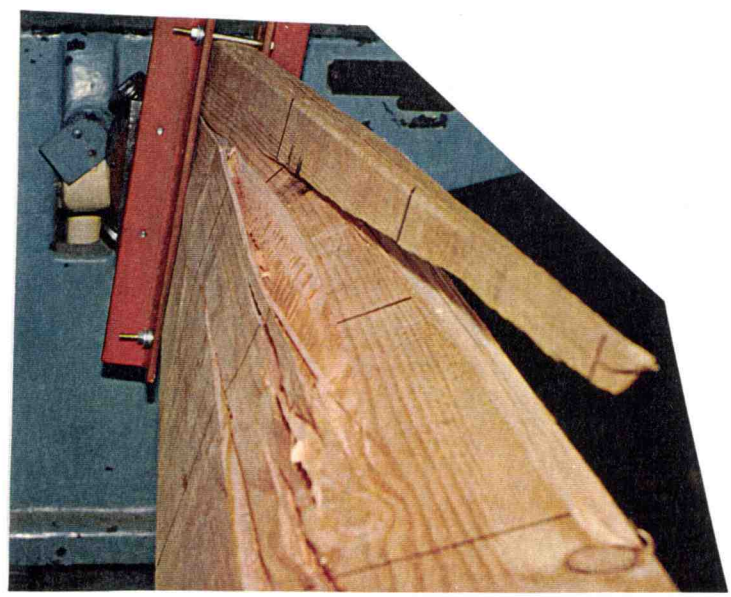

Figure 6.21: Typical shear failure observed in structural lumber tested in torsion. (i) Torque application continued and specimen is reaching complete failure

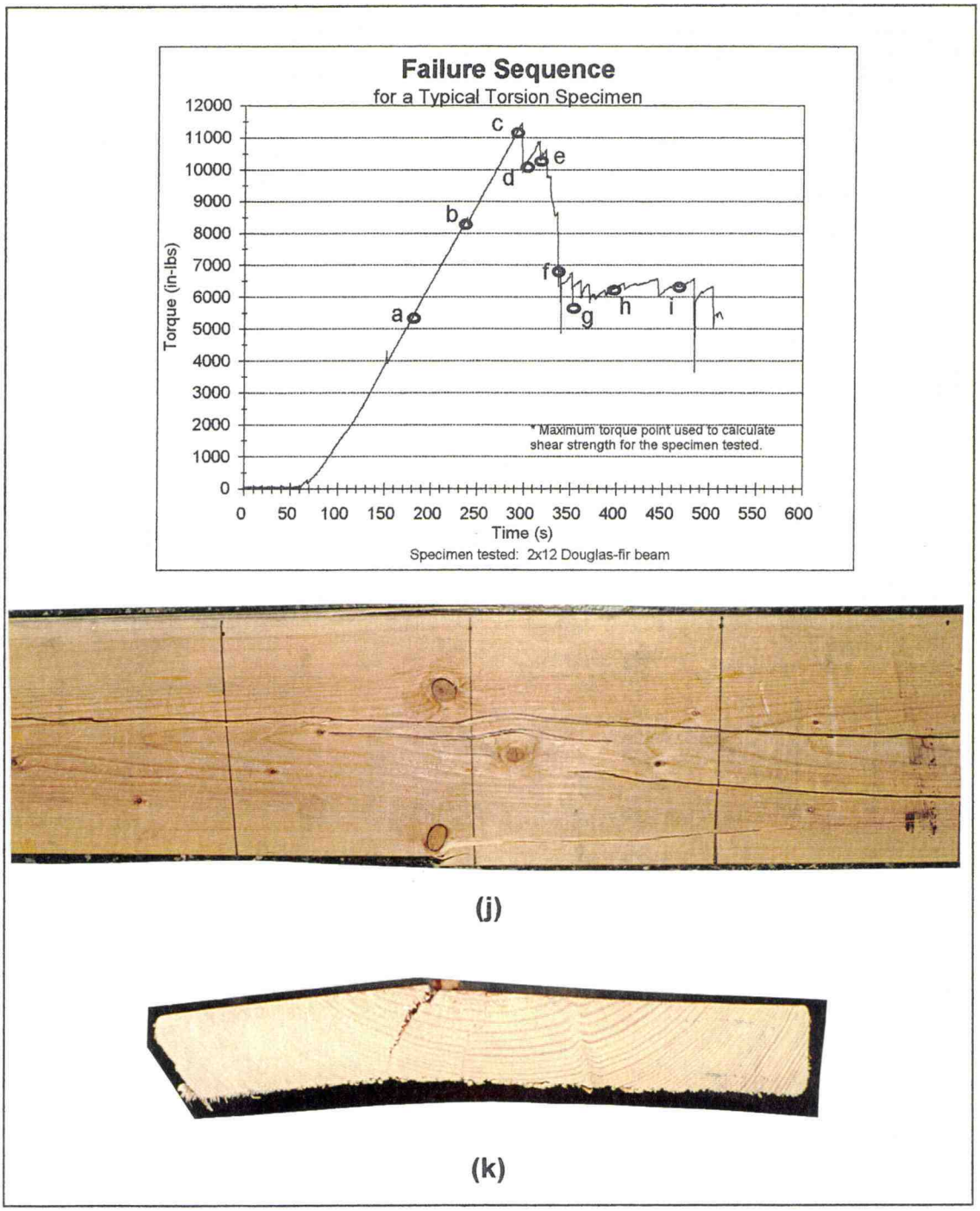

Figure 6.21: Typical shear failure observed in structural lumber tested in torsion. After specimen is removed from the torsion machine the shear failure is noticeable. (j) Longitudinal shear failure (k) cross sectional shear failure

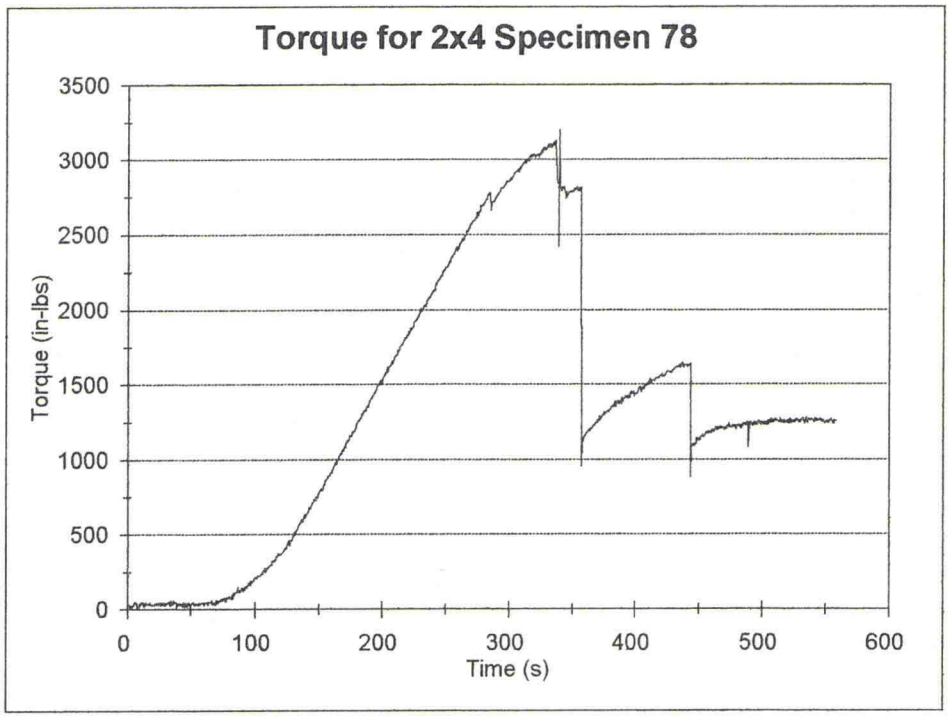

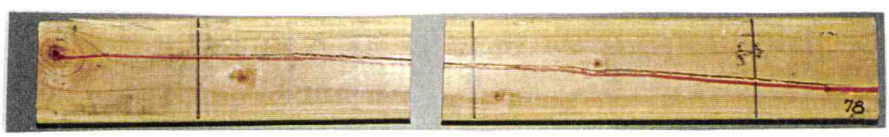

Figure 6.22: Typical shear failure observed for a 2x4

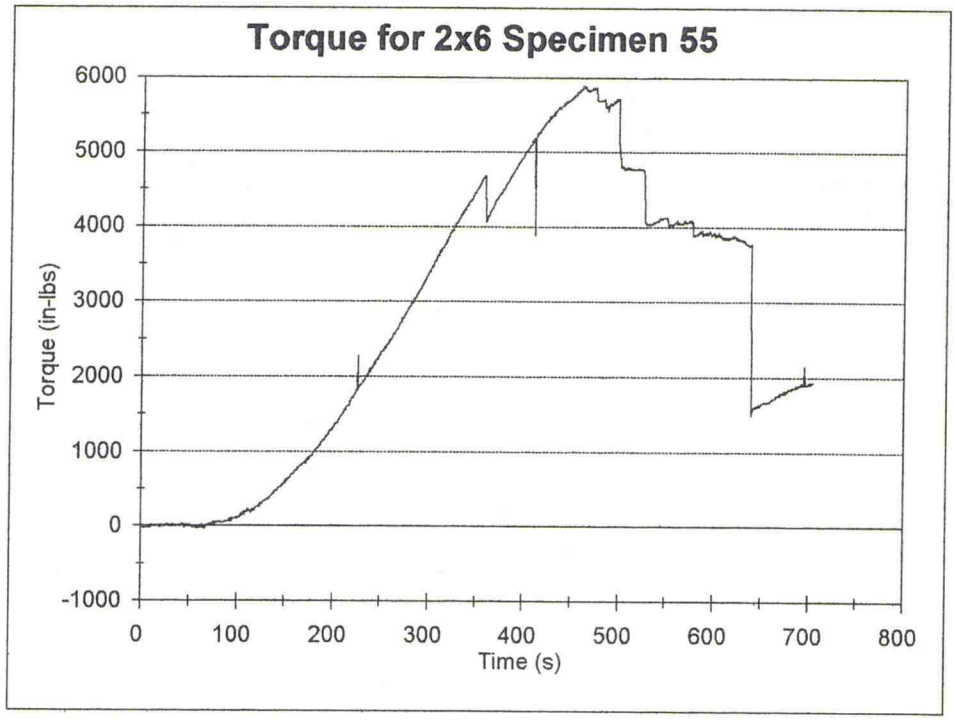

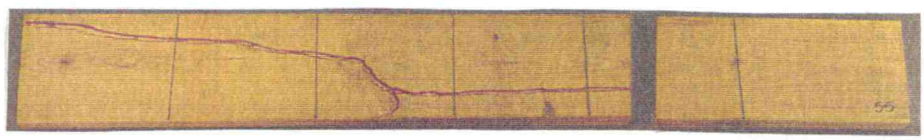

Figure 6.23: Typical shear failure observed for a 2x6

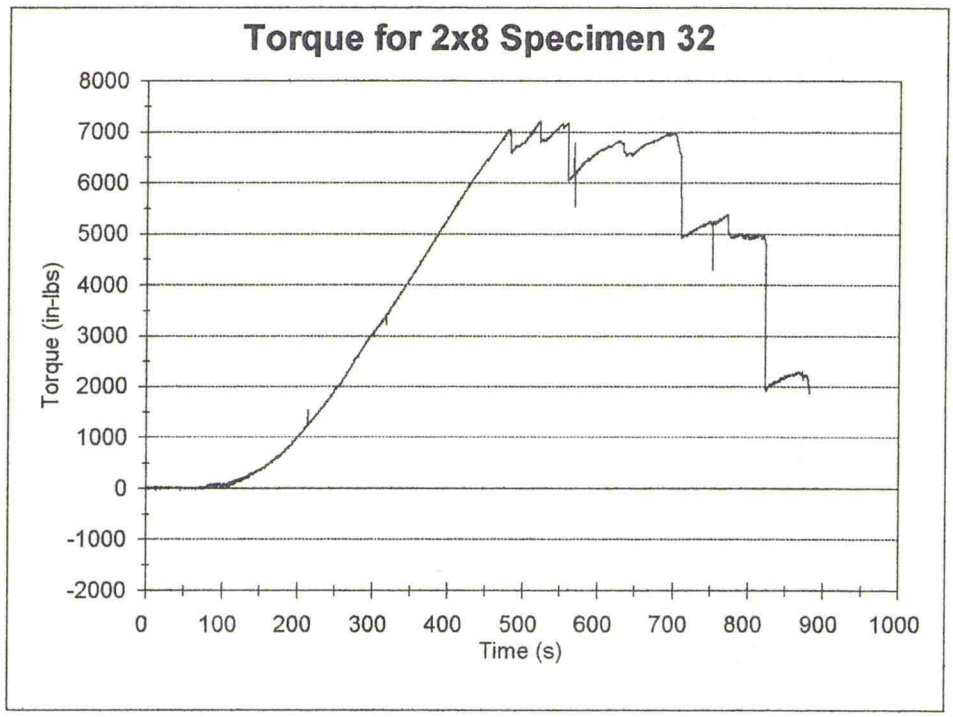

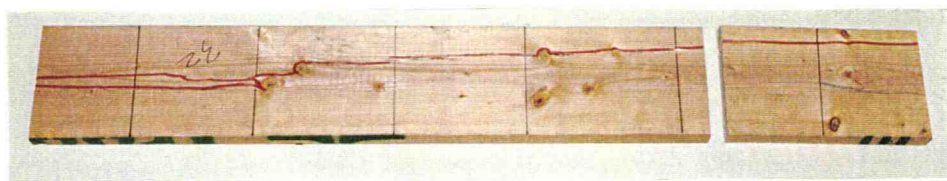

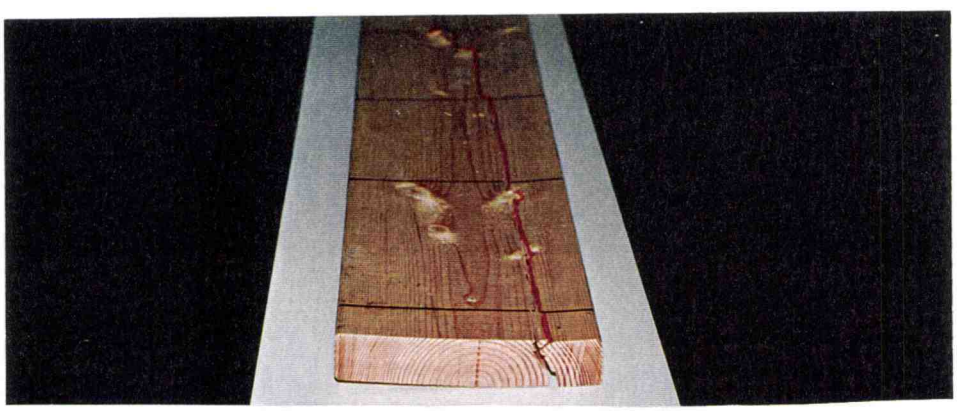

Figure 6.24: Typical shear failure observed for a 2x8

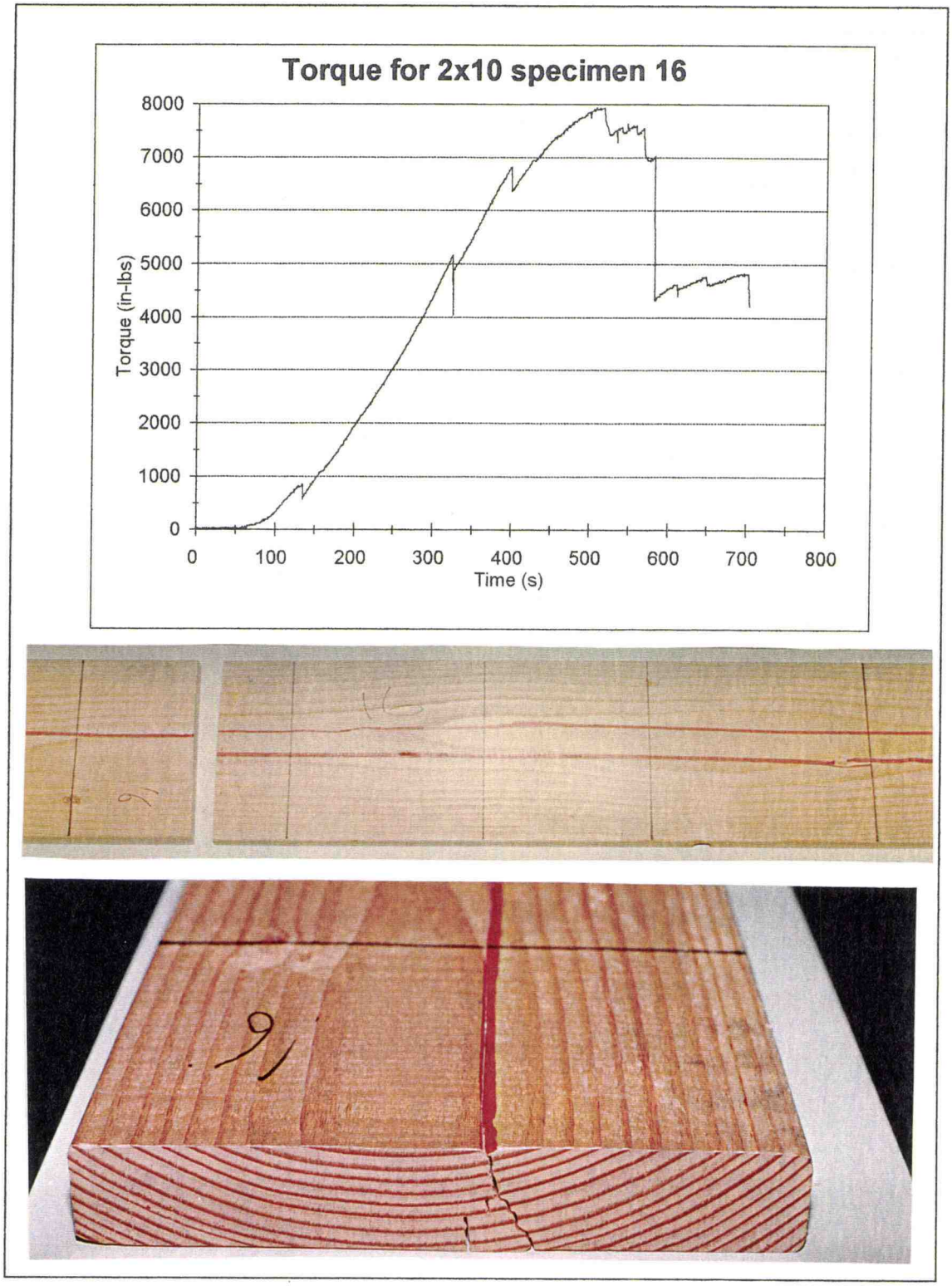

Figure 6.25: Typical shear failure observed for a 2x10

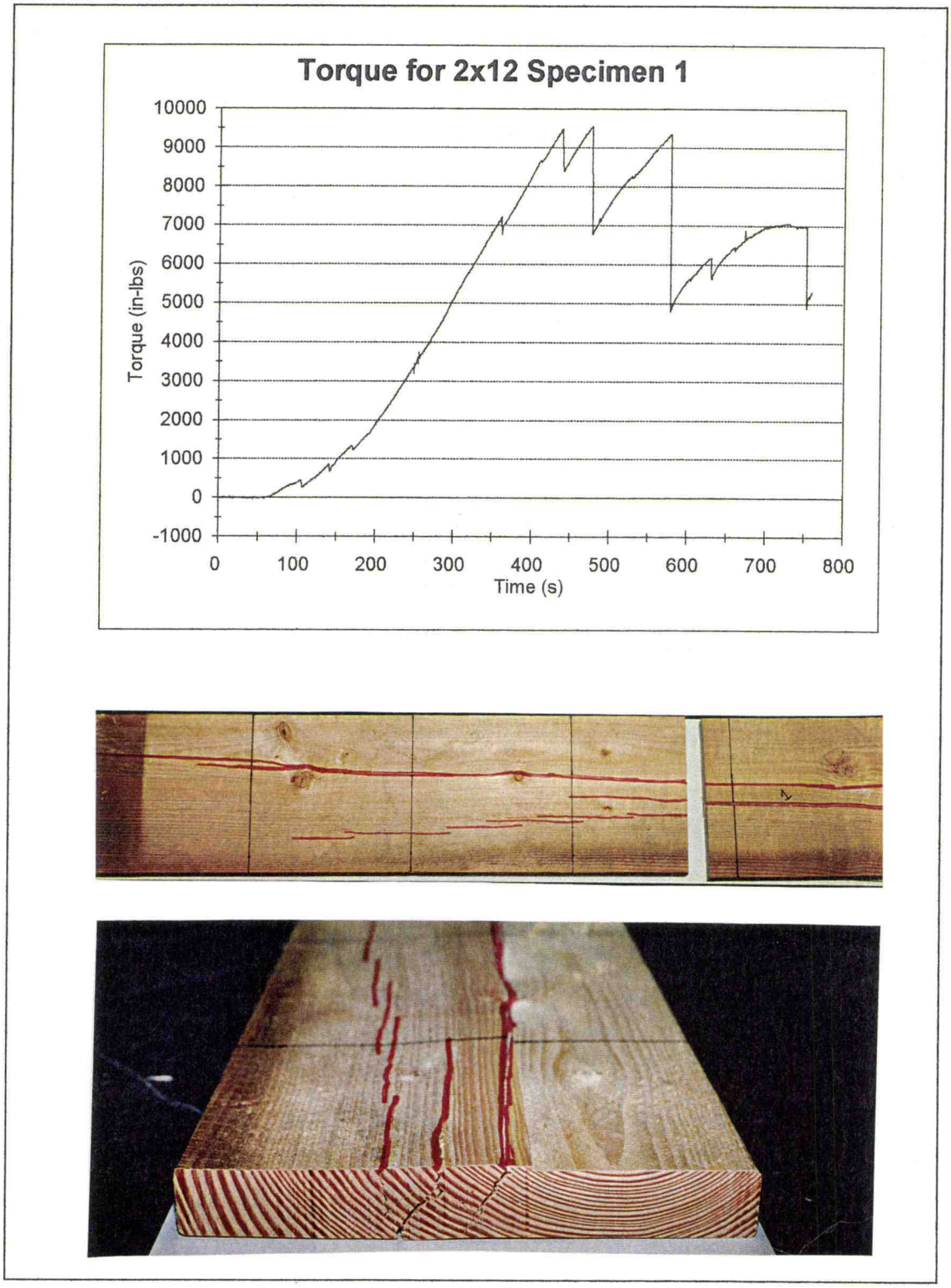

Figure 6.26: Typical shear failure observed for a 2x12

7. Conclusions and Recommendations

As a result of this study on the shear strength of full-size structural lumber using the torsion test, the following conclusions have been recorded and the following recommendations are suggested.

7.1 Conclusions

1. Based on the results of this study, which also verified that the torsion test yields 100% shear failures and subjects the specimen to a state of pure shear stress, the torsion test is the best practical method to determine the pure shear strength of full-size structural lumber.

2. Because the torsion test method directly measures the torsional strength of wood, this test is an excellent method to determine the torsional strength of wood.

3. The shear stress that causes shear failures in structural lumber subjected to torsion is identical to the shear stress that causes shear failures in structural lumber subjected to bending loads: The shear sliding direction is parallel to the grain and the shear failure plane is parallel to the grain.

4. The finite element model revealed that the shear span, which possesses uniform shear stress, occurs at a distance away from each end of the beam that is equal to two times the depth plus the grip distance.

5. Both the length study and the depth study indicated a significant linear relationship between shear strength and specific gravity, but no evidence of a relationship between shear strength and modulus of elasticity.

6. The length study did not reveal any evidence that the shear span of the torsion specimen affects the maximum shear strength for 2x4 beams even after accounting for specific gravity.

7. The ASTM D 198-94 standard recommendation for the minimum total length, for a torsion test, of at least eight times the depth is a general suggestion which should provide uniform shear stress within the shear span.

8. There is suggestive but inconclusive evidence that shear strength is linearly dependent on depth after accounting for shear span and specific gravity.

9. There is moderate evidence that shear strength is non-linearly dependent on shear area or volume after accounting for specific gravity.

10. There is no evidence that shear strength is related to depth, volume, or shear area through power or logarithmic relationships.

11. There is convincing evidence that the shear strength obtained with the torsion method is linearly related to the shear strength obtained with the standard ASTM D 143 method even after accounting for specific gravity. However, the relationship comparing the torsion-based shear strength with the ASTM-based shear strength accounts for less than 25% of the data variability.

7.2 Recommendations

1. The torsion test is recommended as the method to determine the torsional strength of wood for the design of members subject to direct torsion.

2. Additional research should be conducted to determine the effect of compressive stress perpendicular to the grain, compressive stress parallel to the grain, tensile stress, and shear stress interactions of specimens subjected to bending loads.

3. The torsion test method provides the same shear stress failure as observed in bending specimens and pure shear stress in the torsion specimen. In addition, the torsion test yields 100% shear failures as initial failures, and this

test can be used to test full-size lumber specimens, similar to those used in design, with natural characteristics, unlike the ASTM (1996a) shear block. Therefore the torsion test method should be considered as a standard to measure shear strength of structural lumber.

4. Additional testing of 2x4, 2x6, 2x8, 2x10, and 2x12 beams should be performed to establish a database of samples tested via the torsion method for shear strength and to determine mean torsional strength values and mean shear strength values for the wood species tested.

5. As a part of the database testing, strain measurements should be taken for several torsion specimens to compare experimental strain values with strains calculated from the finite element model developed in this study. Using the modulus of elasticity value obtained in the laboratory for the specimens, strains measurements can be converted to stresses and compared to the calculated stresses from the finite element model.

6. Anatomical investigations of the failed specimen should be performed to understand shear failure at a microscopic level.

References

Adams, D. and E. Lewis. 1995. Experimental Study of Three- and Four-Point Shear Test Specimens. Journal of Composites Technology and Research. (17)4: 341-349.

AFPA. 1991. ANSI/NFPA NDS-1991 National Design Specification for Wood Construction. American Forest and Paper Association, Washington, DC.

American Institute of Steel Construction (AISC). 1994. Load & Resistance Factor Design: Manual of Steel Construction. Second Edition. AISC.

American Iron and Steel Institute (AISI). 1969. Steel Research for construction: Strength of Plate Girders with Longitudinal Stiffeners. Lehigh University. Bulletin No. 16. April: 62-84. New York, NY.

American Society for Testing and Materials. 1996(a). Standard Methods of Testing Small Clear Specimens of Timber ASTM D 143-94. Volume 04.10 Wood. West Conshohocken, PA.

American Society for Testing and Materials. 1996(b). Standard Methods of Static Test of Lumber in Structural Size ASTM D 198-94. Volume 04.10 Wood. West Conshohocken, PA.

American Society for Testing and Materials. 1996(c). Standard Practice for Establishing Structural Grades and Related Allowable Properties for Visually Graded Lumber ASTM D 245-93. Volume 04.10 Wood. West Conshohocken, PA.

American Society for Testing and Materials. 1996(d). Standard Test Method for Shear Strength of Plastics by Punch Tool ASTM D 732-93. Volume 8.01 Plastics. West Conshohocken, PA.

American Society for Testing and Materials. 1996(e). Standard Practice for Establishing Allowable Properties for Visually-Graded Dimension Lumber from In-Grade Test of Full-Size Specimens. ASTM D 1990-95. Volume 04.10 Wood. West Conshohocken, PA.

American Society for Testing and Materials. 1996(f). Standard Test Methods for Specific Gravity of Wood and Wood Based Materials. ASTM D 2395-93. Volume 04.10 Wood. West Conshohocken, PA.

American Society for Testing and Materials. 1996(g). Standard Practice for Evaluating Allowable Properties for Grades of Structural Lumber ASTM D 2915-94. Volume 04.10 Wood. West Conshohocken, PA.

American Society for Testing and Materials. 1996(h). Standard Test Methods for Direct Moisture Content Measurement of Wood and Wood-Base Materials ASTM D 4442-92. Volume 04.10 Wood. West Conshohocken, PA.

American Society for Testing and Materials. 1996(i). Standard Test Method for Apparent Horizontal Shear Strength of Pultruded Reinforced Plastic Rods By the Short-Beam Method ASTM D 4475-85. Volume 8.03 Plastics. West Conshohocken, PA.

American Society for Testing and Materials. 1958. Test for Shear Strength of Plastics ASTM D 732-46. Part 9. Philadelphia, PA.

Arcan, M. 1984. The Iosipescu Shear Test as Applied to Composite Materials. Experimental Mechanics. March: 66.

Asselin, S., D. McLean, and D., Rammer. 1995. Effects of Member Size on the Shear Strength of Sawn Lumber Beams. Draft paper received from the authors.

Bakhsh, A., F. Wafa, and A. Akhtaruzzaman. 1990. Torsional Behavior of Plain High Strength Concrete Beams. ACI Structural Journal. September/October: 583-588.

Bodig, J. and B. Jayne. 1982. Mechanics of Wood and Wood Composites. Malabar, Florida: Krieger Publishing Company.

Bohannan, B. 1966. Effect of Size on Bending Strength of Wood Members. USDA Forest Service Research Paper. FPL-56. Forest Products Laboratory, Madison, WI.

Boresi, A., and K. Chong. 1987. Elasticity in Engineering Mechanics. New York: Elsevier.

Boresi, A., R. Schmidt, and O. Sidebottom. 1993. Advanced Mechanics of Materials. Fifth Edition. New York: John Wiley & Sons Inc.

Breyer, D. 1993. Design of Wood Structures. Third edition. New York: McGraw-Hill, Inc.

Cofer, W., F. Proctor, Jr., and D. McLean. 1997. Prediction of the Shear Strength of Wood Beams Using Finite Element Analysis. Mechanics of Cellulosic Materials. ASME 1997. New York, NY.

Elgaaly, M., R. Hamilton, A. Seshadri. 1996. Shear Strength of Beams with Corrugated Webs. Journal of Structural Engineering. April: 390-398.

Elzanaty, A., A. Nilson, and F. Slate. 1986. Shear Capacity of Prestressed Concrete Beams using High Strength Concrete. ACI Structural Journal. May-June: 359-361.

Ethington, R., W. Galligan, and H. Monteray. 1979. Evolution of Allowable Stresses in Shear for Lumber. FPL-23. US Department of Agriculture, Forest Service, Forest Products Laboratory, Madison, WI.

Foschi, R and J. Barrett. 1975. Longitudinal Shear Strength of Douglas-fir. Canadian Journal of Civil Engineering. Vol. 3: 198-208.

Gaylord, E. Jr., C. Gaylord, and J. Stallmeyer. 1992. Design of Steel Structures. Third Edition. New York: McGraw-Hill, Inc.

Gere, J., and S. Timoshekno. 1984. Mechanics of Materials. Third Edition. Boston, Massachusetts: PWS Publishing Company.

Gipple, K. and D. Hoyns. 1994. Measurement of the Out-of-plane Shear Response of Thick Section Composite Materials using the V-Notched Beam Specimen. Journal of Composite Materials. (28)6: 543-572.

Goldenberg, N., M. Arcan, and E. Nicolau. 1959. On the Most Suitable Specimen Shape for Testing Shear Strength of Plastics. International Symposium on Plastics Testing and Standardization, ASTM STP 247. American Society of Testing and Materials. Philadelphia, PA.

Green, D, B. Shelley, and H. Vokey. 1989. In-Grade Testing of Structural Lumber Proceedings 47363. Forest Products Research Society, Madison, WI.

Hancox, N. 1972. The Use of a Torsion Machine to Measure the Shear Strength and Modulus of Unidirectional Carbon Fibre Reinforced Plastics. Journal of Material Science. (7)7: 1030-1036.

Hilbrand, H. 1964. Comparison of Block Shear Methods for Determining Shearing Strength of Solid Wood. FPL-030. US Department of Agriculture, Forest Service, Forest Products Laboratory, Madison, WI.

Horiguchi, T., N. Saeki., and Y. Fujita. 1988. Evaluation of Pullout Test for Estimating Shear, Flexural, and Compressive Strength of Fiber Reinforced Silica Fume Concrete. ACI Materials Journal. March-April: 126-132.

Janowiak, J. and R. Pellerin. 1992. Shear Moduli Determination Using Torsional Stiffness Measurements. Wood and Fiber Science. 24(4): 392-400.

Keenan, F. 1974. Shear Strength of Wood Beams. Forest Products Journal. 24(9): 63-70.

Keenan, F. and K. Selby. 1973. The Shear Strength of Douglas-fir Glued-Laminated Timber Beams. Publication No. 73-01. Department of Civil Engineering, University of Toronto. Toronto, Ontario.

Lee, S. and M. Munro. 1986. Evaluation of In-plane Shear Test Methods for Advanced Composites Materials by the Decision Analysis Technique. Composites. (17)1: 13-22.

Lekhnitskii, S. G. 1981. Theory of Elasticity of an Anisotropic Body. Moscow, USSR: MIR Publishers.

Liu, J. 1984. New Shear Strength Test for Solid Wood. Wood and Fiber Science. (16)4: 567-574.

Liu, J. and L. Floeter. 1984. Shear Strength in Principal Plane of Wood. Journal of Engineering Mechanics. (110)6: 930-936.

Longworth, J., 1977. Longitudinal Shear Strength of Timber Beams. Forest Products Journal. 27(9):19-23.

Lyse, I. and B. Johnston. 1936. Structural Beams in Torsion. Transactions of the American Society of Civil Engineers. No 101 Part 2. Vol. 62. Philadelphia, PA.

Mack, J. 1940. A Study of the Torsion Test. Progress Report No. 1. Effect of Size of Specimen. SUB-PROJECT T.M. 22/4. CSIRO, Melbourne, New South Wales, Australia.

MacLeod, I., and A. Houmsi. 1994. Shear Strength of Haunched Beams Without Shear Reinforcement. ACI Structural Journal. January/February: 79-89.

Mandery, W. 1969. Relationship Between Perpendicular Compressive Stress and Shear Strength of Wood. Wood Science 1(3): 177-182.

McGuire, W., 1968. Steel Structures. Prentice-Hall, Inc., Englewood Cliffs, New Jersey.

Morton, J. H. Ho, M. Tsai, and G. Farley. 1992. An Evaluation of the Iosipescu Specimen for Composite Materials Shear Property Measurement. Journal of Composite Materials. (26)5: 708-749.

Nederveen, C. and L. Tilstra. 1971. Clamping Corrections for Torsional Stiffness of Prismatic Bars. Journal of Applied Physics, Series D. 4(11): 1661-1667.

Norris, C.B. 1957. Comparison of Standard Block-Shear Test to the Panel Shear Test. Forest Products Journal. 7(9): 299-301.

Novak, R. 1969. Fracture in Graphite Filament Reinforced Epoxy Loaded in Shear. Composite Materials: Testing and Design, ASTM STP 460. American Society of Testing and Materials, Philadelphia. pp. 540-549.

Odom, E., D. Blackketter, and B. Suratno. 1994. Experimental and Analytical Investigation of the Modified Wyoming Shear-test Fixture. Experimental Mechanics. March: 10-15.

Panshin, A., and C. de Zeeuw. 1980. Textbook of Wood Technology. Fourth Edition. New York: McGraw-Hill, Inc.

Pindera, M. 1989. Shear Testing of Fiber Reinforced Metal Matrix Composites. Metal Matrix Composites: Testing, Analysis, and Failure Modes ASTM STP 1032. American Society for Testing and Materials, Philadelphia, PA.

Pindera, M., P. Ifju, and D. Post. 1990. Iosipescu Shear Characterization of Polymeric and Metal Matrix Composites. Experimental Mechanics. March: 101-108.

Radcliffe, B. and S. Suddarth. 1955. The Notched Beam Shear Test for Wood. Forest Products Journal. April: 131-135.

Rajagopalan, K. and P. Ferguson. 1968. Exploratory Shear Tests Emphasizing Percentage of Longitudinal Steel. ACI Journal. August: 634-638.

Rammer, D. and L, Soltis. 1994. Experimental Shear Strength of Glued Laminated Beams. FPL-RP-527. US Department of Agriculture, Forest Service, Forest Products Laboratory. Madison, WI.

Rammer, D., L. Soltis, and P. Lebow. 1996. Experimental Shear Strength of Unchecked Solid Sawn Douglas-fir. FPL-RP-553. US Department of Agriculture, Forest Service, Forest Products Laboratory. Madison, WI.

Rebeiz, K.S., S.P. Serhal, and D.W. Fowler. 1993. Shear Behavior of Steel Reinforced Polymer Concrete Using Recycled Plastic, ACI Structural Journal, 90:675-682.

Rebeiz, K.S., S.P. Serhal, and D.W. Fowler. 1995. Shear Strength of Reinforced Polyester Concrete Using Recycled PET, Journal of Structural Engineering. 121:1370-1375.

Riyanto, D. 1996. Comparative Test Methods for Evaluating Shear Strength of Structural Lumber. MS Thesis. Department of Forest Products, Oregon State University. Corvallis, Oregon.

Riyanto, D. and R. Gupta. 1997. A Comparison of Test Methods for Evaluating Shear Strength of Structural Lumber. Forest Products Journal (In Press).

Riyanto, D. and R. Gupta. 1996. Effect of Ring Angle on Shear Strength Parallel to the Grain of Wood. Forest Products Journal. 46(7/8): 87-92.

Roberts, T., A. Davies, R. Bennett. 1995. Fatigue Shear Strength of Slender Web Plates. Journal of Structural Engineering. 121(10): 1396-1401.

Salandra, M. and S. Ahmad. 1989. Shear capacity of Reinforced Lightweight High Strength Concrete Beams. ACI Structural Journal. 86(6): 697-704.

Sanders, C. 1996. The Effects of Testing Conditions on the Measured Shear Strength of Wood Beams. MS Thesis. Department of Civil and Environmental Engineering, Washington State University. Pullman, Washington.

Sharma, K. 1986. Shear Strength of Steel Fiber Reinforced Concrete Beams. ACI Structural Journal. July/August: 624-627.

Siao, W. 1995. Deep Beams Revisited. ACI Structural Journal. January-February: 95-102.

Silvester, D. 1967. Timber--Its Mechanical Properties and Factors Affecting Its Structural use. Oxford, New York: Pergamon Press.

Swanson Analysis Systems, Inc. 1992. ANSYS User's Manual for Revision 5.0. Version 5.3. Houston, PA.

Timoshenko, S. 1956. Strength of Materials, Parts I and II, 3rd ed., Princeton, New Jersey: D. Van Nostrand Co., Inc.

Trayer, G. and H. March. 1929. The Torsion of Members Having Sections Common in Aircraft Construction. National Advisory Committee for Aeronautics Report No. 334.

Tsai, C. and I. Daniel. 1989. Determination of In-plane and Out-of-plane Shear Moduli of Composite Materials. Experimental Mechanics. September: 295-299.

Tsoumis, G. 1991. Science and Technology of Wood: Structure, Properties, and Utilization. New York: Van Nostrand Reinhold.

Ugural, A., S. Fenster. 1995. Advanced Strength and Applied Elasticity. Third Edition. New Jersey: Prentice Hall.

Walrath, D and D. Adams. 1983. The Iosipescu Shear Test as Applied to Composite materials. Experimental Mechanics. March: 105-110.

Wangaard, F.F. 1981. Wood: Its Structure & Properties. Clark C. Heritage Memorial Series on Wood. Volume 1. Forest Products Laboratory. Madison, WI.

Whitney, J. and C. Browning. 1985. On Short-Beam Shear Tests for Composite Materials. Experimental Mechanics. September: 294-300.

Wood Handbook: Wood as an Engineering Material. 1987. Agriculture Handbook 72. USDA, Washington, D.C.

Yen, S., J. Craddock and K. Teh. 1988. Evaluation of a Modified Arcan Fixture for the In-plane Shear Test of Materials. Experimental Techniques. December: 22-25.

Ylinen, A. 1963. A Comparative Study of Different Types of Shear Test of Wood. Fifth Conference on Wood Technology. US Forest Products Laboratory. Madison, WI. The State Institute for Technical Research. Helsinki, Finland.

Yoshihara, H. and M. Ohta. 1997. Analysis of Shear Stress/Shear Strain Relationships in Wood Obtained by Torsion Tests. Mokuzai Gakkaishi. 43(6): 457-463.

Yoshihara, H. and M. Ohta. 1996. Analysis of the Yield Behavior of Wood Under Combined Shear Stresses in Torsion Tests. Mokuzai Gakkaishi. 42(6): 541-545.

Yoshihara, H. and M. Ohta. 1995a. Determination of the Shear Stress-Shear Strain Relationship of Wood by Torsion Tests. Mokuzai Gakkaishi. 41(11): 988-993.

Yoshihara, H. and M. Ohta. 1995b. Shear Stress-Shear Strain Relationship of Wood in the Plastic Region. Mokuzai Gakkaishi. 41(6): 529-536.

Yoshihara, H. and M. Ohta. 1993. Measurement of the Shear Moduli of Wood by the Torsion of a Rectangular Bar. Mokuzai Gakkaishi. 39(9): 993-997.

Youngquist, W. and E. Kuenzi. 1961. Shear and Torsion Testing of Wood, Plywood, and Sandwich Constructions At the US Forest Products Laboratory. Symposium on Shear and Torsion Testing ASTM STP 289. American Society of Testing and Materials. Philadelphia, PA.

Yuliang, X., S. Ahmad, T. Yu, S. Hino, and W. Chung. 1994. Shear Ductiity of Reinforced Concrete Beams of Normal and High Strength Concrete. ACI Structural Journal. March/April: 140-149.

Zielinski, Z. and M. Rigotti. 1995. Tests on Shear Capacity of Reinforced Concrete, Journal of Structural Engineering. 121:1660-1666

Appendices

Appendix A
Experimental Set Up

A.1 Historical Operation

The torsion machine used to apply the torque to the specimens was a Tinius Olsen torsion machine SN 2800 with a balance arm beam, patented in January 27, 1891 (Figure A-1). This machine was refurbished in 1988 when a motor was installed. The torque is applied to the rotating head via the motor which has a speed dial that can be controlled by the operator. The specimen is secured between the rotating grip and the fixed grip. The fixed grip transfers the torque, applied by the rotating head, to the fulcrum points on the inside of the machine. These fulcrum points allow torque transfer from the fixed head to the tension rod via a series of lever arms and fulcrum points. The tension in the rod pulls the arm beam out of balance, and as a result the weight on the arm beam must be moved across the beam until the it balances. At this point, when the beam is balanced, the torque value read from the arm beam is the amount of torque applied to the specimen secured in the grips.

A.1.1 Original Procedure for Torque Testing

Originally, the machine was designed for circular cross sections. As the torque is applied to the specimen, the arm beam should be continuously

balanced by the operator so that the torque value at failure can be determined accurately. Failure is defined when the arm beam drops abruptly. The

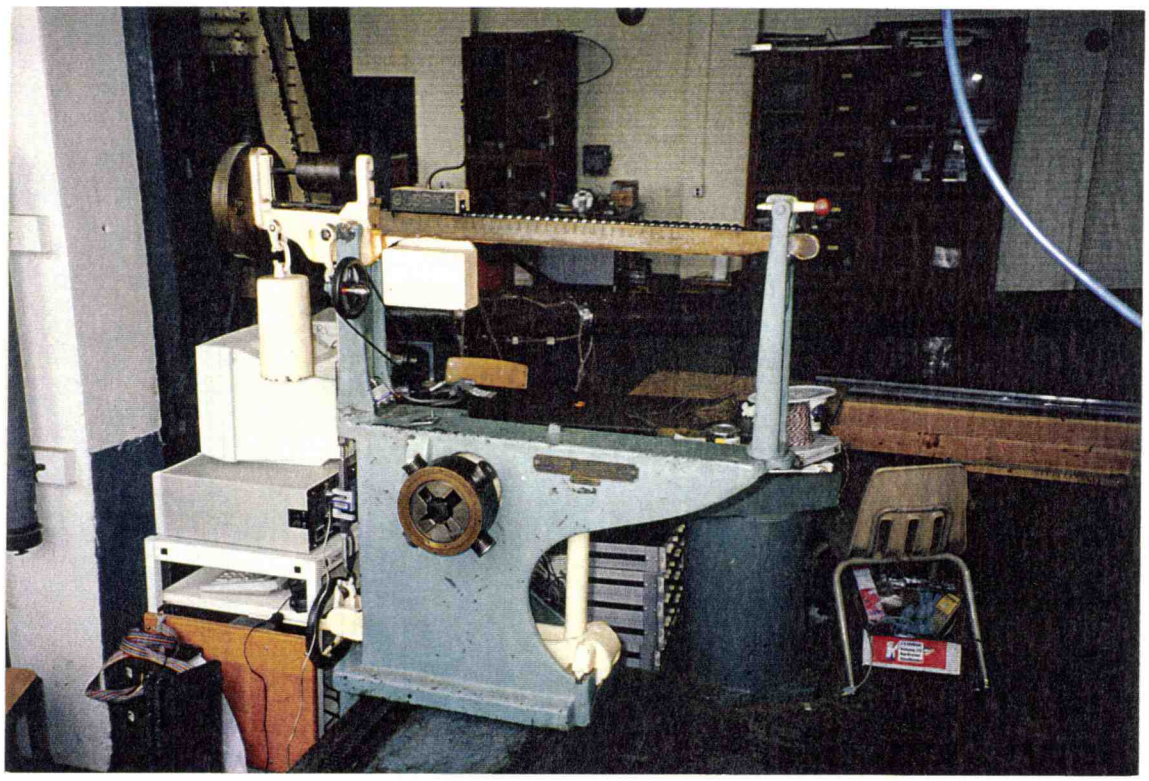

Figure A.1: Torsion machine used in the shear strength testing of structural lumber; the fixed grip and the balance arm beam is shown above

abruptness of the arm beam drop indicates that the specimen is not continuing to transfer as much torque as it previously had transferred to the tension rod. At failure, the torque reading is the ultimate torsional strength of the specimen.

A.2 Modifications

For the purposes of this study, this machine needed to be modified to allow torsion testing of rectangular wood specimens. The tension rod, the rotating head, and the grips required modifications. Based on a pilot study, the variability of the wood posed a challenge when determining failure. Abrupt dropping of the arm beam seldom occurred; for wood the torque transferred to the tension rod tapered off more slowly. Upgrading the machine to electronically record the response of the specimen in terms of the torque applied and the rotation would provide more information. For example, plots of time versus torque and plots of torque verses rotation could be obtained. Torsion failure was less difficult to establish after examining these plots.

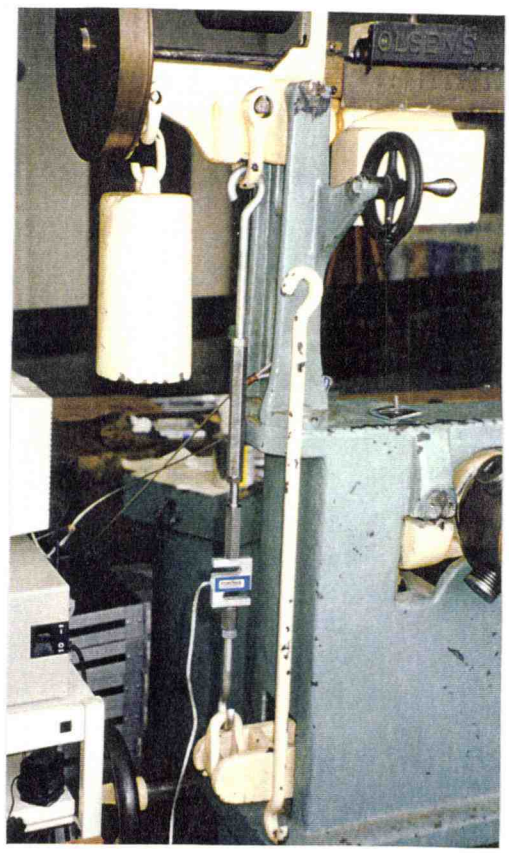

Figure A.2: Original tension rod next to the new tension rod with load cell

A.2.1 Torque Measurement Modifications

The original solid steel tension rod was removed and replaced with a new steel tension rod that has a load cell in the middle (Figure A-2). This load cell tension rod performs the same function as the original tension rod that came with the Tinius Olsen torsion machine. The Interface© load cell, model SSM-AJ-250, SN C93961, used has a 250 pound capacity.

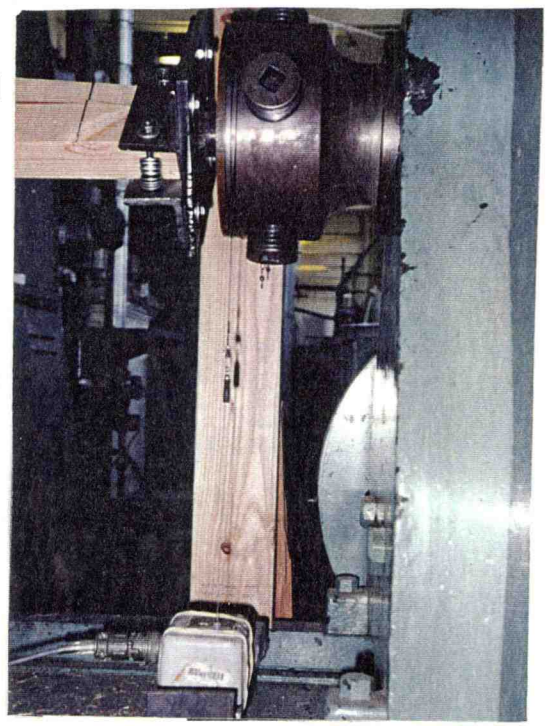

Figure A.3: String potentiometer used to record the rotation angle

A.2.2 Angular Displacement Modifications

On the rotating head, a Celesco string potentiometer model PT101-0010-111-1110, SN A5601 with sensitivity of 94.38 mv/V/in was used to record the rotation of the specimen. The string potentiometer wire was wrapped around the rotating head of the torsion machine

Figure A.4: Grips used with the torsion machine

two and a half times. The wire then hung down where it connected to the string potentiometer (Figure A-3).

A.2.3 Grip Modification

The original grips on the torsion machine allowed for testing of circular specimens. Figure A.4 illustrates the new grips which accomodated rectangular specimens; the new grips were placed into the original grips of the torsion machine. A solid steel circular bar was welded to the center of a 1/4 inch thick steel plate, and two 5/8 inch thick steel angles were connected to the steel plate using bolts, as seen in Figure A-4. These angles provided the vise-like grip necessary to apply torque loading to the rectangular wood specimens while still allowing for unrestrained torsion in the specimens. These grips meet the ASTM (1996b) requirements for torsion testing of structural size lumber.

A.3 Data Acquisition System

Figure A-5 illustrates the interaction between the new tension rod, the string potentiometer, the vise grips, the transducer, and the computer. Figure A-6 represents a schematic of the data acquisition system. The string potentiometer and the load cell were connected into a Statham Universal Transducer Readout model SC1001. The transducer sends the voltage signals to the data acquisition card in the 286 computer where the voltages are recorded. The data acquisition software was Labtech Notebook Version 5.1.3, SN 16433.

Figure A.5: Interaction of new tension rod, string potentiometer, transducer, and computer

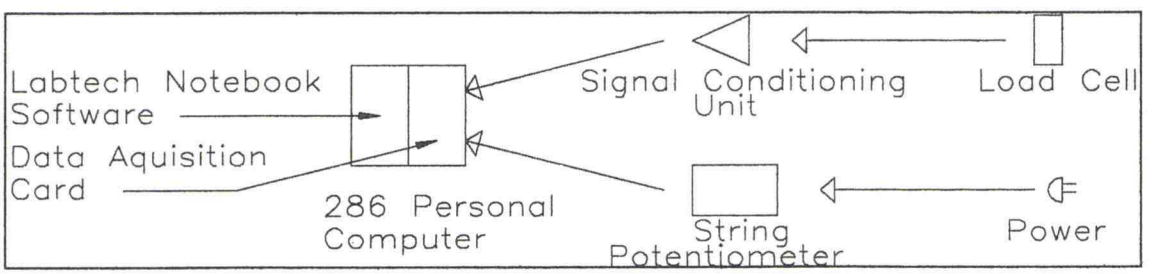

Figure A.6: Schematic of data acquisition system

A.3.1 Data Acquisition Procedure

1. Torque is applied to the specimen by turning the motor on.
2. Angular displacement is read by the rotating head which pulls the wire from the string potentiometer around the rotating head causing a signal to pass through the transducer and a voltage to be recorded via the computer software.
3. Specimen transfers this torque to the fixed head which causes the load cell, due to the increase in tension in the tension rod, to send a signal to the transducer and a voltage to be recorded via the computer software.

Appendix B describes the calibration procedures and results necessary to provide useful torque and rotation values from the electronic equipment.

Appendix B
Equipment Calibration

B.1 Equipment Calibration

In order for the electronic apparatus to provide useful torque and rotation values, calibrations were necessary. The load cell voltage was calibrated to the torsion machine torque readings and the string potentiometer voltage was calibrated to the torsion machine rotational readings. The torsion machine itself was calibrated after all modifications, the grip modification, the tension rod modification, and the rotation angle measurement modification, were complete.

B.1.1 Load Cell

Since the torsion machine was specifically designed for circular sections, a solid steel bar was used to calibrate the load cell to the torque readings on the balance beam of the machine. This steel bar was secured in the grips (Figure B-1). Since the motor was off, no torque was applied to the steel rod, and the arm beam was balanced at zero torque. The load cell voltages were read from a voltmeter. First, a voltage was recorded at zero torque. Next, the motor was allowed to run for approximately 10 seconds and then turned off. At this point, the voltage value was read from the voltmeter, and the arm beam was balanced. After balancing the arm beam, the torque value was read from the torsion

machine. This procedure was repeated numerous times. As a result of the repeated readings, a linear relationship between load cell voltages and torque values was established.

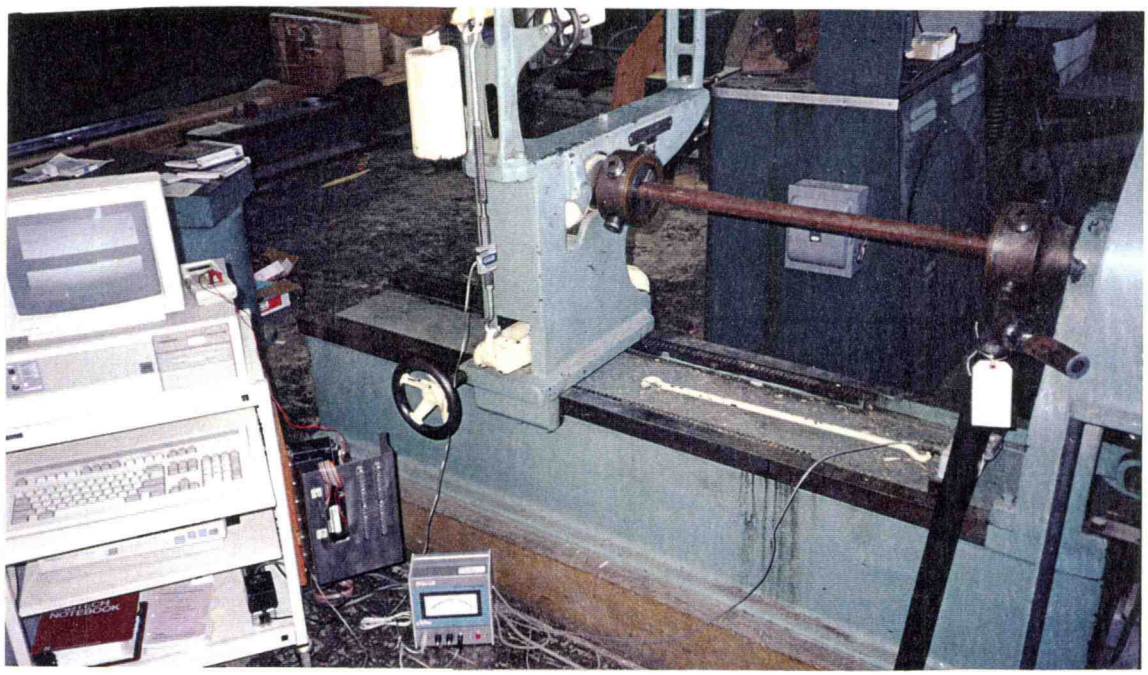

Figure B.1: Load cell calibration with isotropic steel bar secured in torsion machine grips

A relationship was determined before and after the depth study as well as before and after the length study. The calibration equations remained strongly linear, as shown in Figure B.2; however the slope value used in the data reduction varied slightly. For the length effect on torsion study the slope relationship between the torque readings and the load cell voltage was 2480 in-lbs/V. The calibration of the load cell for the depth study showed identical

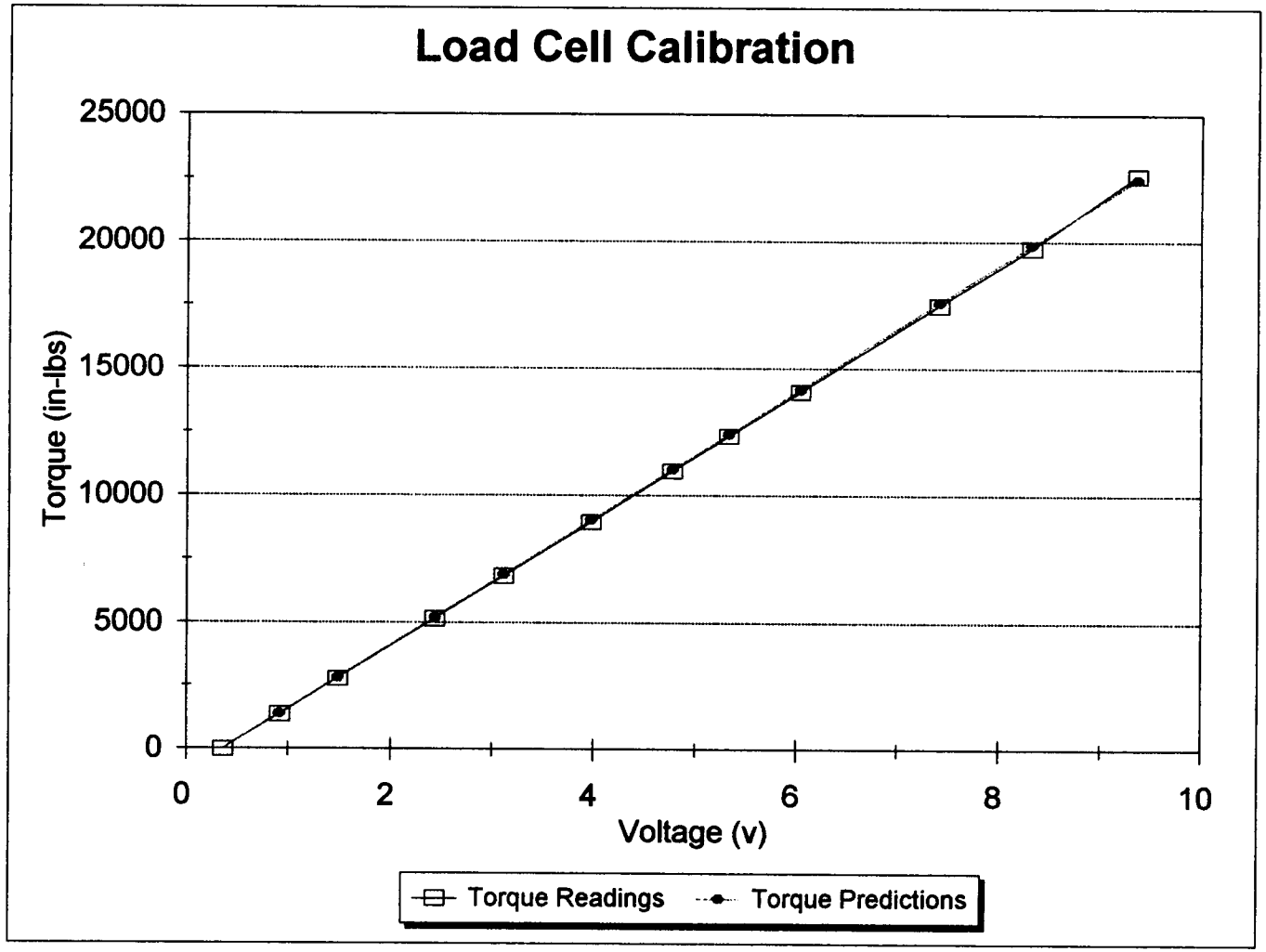

Figure B.2: Load cell calibration relationship

results. The intercept, based on a zero torque reading at the known zero voltage reading for that particular specimen of the linear calibration equation, was calculated for each specimen

B.1.2 String Potentiometer

The voltages read from the string potentiometer via the transducer must be calibrated by correlating the voltage readings from the potentiometer to the rotation readings from the torsion machine.

The string potentiometer was calibrated without connection to the torsion machine. The wire was pulled out of the string potentiometer a known distance, using a ruler, and the voltage was recorded from the voltmeter. This procedure was repeated several times to determine a linear relationship between the wire displacement from the string potentiometer and the corresponding voltage.

This relationship of inches of displacement versus voltage was then converted to degrees of rotation versus voltage. The conversion was based on the 3.5 inch radius of the circular torsion head to which the string potentiometer wire was connected. The slope of the plot of degrees versus voltage used in this study was 69.3 degrees/V. The intercept of this calibration equation was calculated for each specimen. The intercept was based on the condition that at zero torque there is zero degrees of rotation. A known zero voltage reading was recorded for each specimen.

B.1.3 Torsion Machine

A recent calibration date for the Tinius Olsen machine was not available. Based on conversations with Oregon State University professors, the latest calibration for this machine is believed to be the machine's manufacture date. The machine was purchased in 1911 by the Oregon Agricultural College, which has evolved in to the current Oregon State University. In a personal communication with Fred Beam with Cal-Cert Calibration company, he indicated that the Tinius Olsen machine is most likely as accurate as the day it was manufactured. Due to the exorbitant cost of calibrating and certifying the machine, another method using lead weights and a lever arm was employed. Since the calibration was not performed with certified weights, this calibration result cannot be certified. However, this procedure is suitable to check the accuracy of the machine, which was necessary especially due to the electronic modifications.

The calibration procedure was performed with the original rod in place and again with the load cell rod in place. Since the load cell rod was used for this research, the following discussion presents the calibration results of the Tinius Olsen machine with the load cell rod as the tension rod.

Figure B-3 is a schematic of the calibration set up using the load cell tension rod rather than the original tension rod in the Tinius Olsen torsion machine, and Figure B-4 is a photograph of the torsion machine calibration. The calibration rod, of circular cross section, is placed into the torsion machine grips.

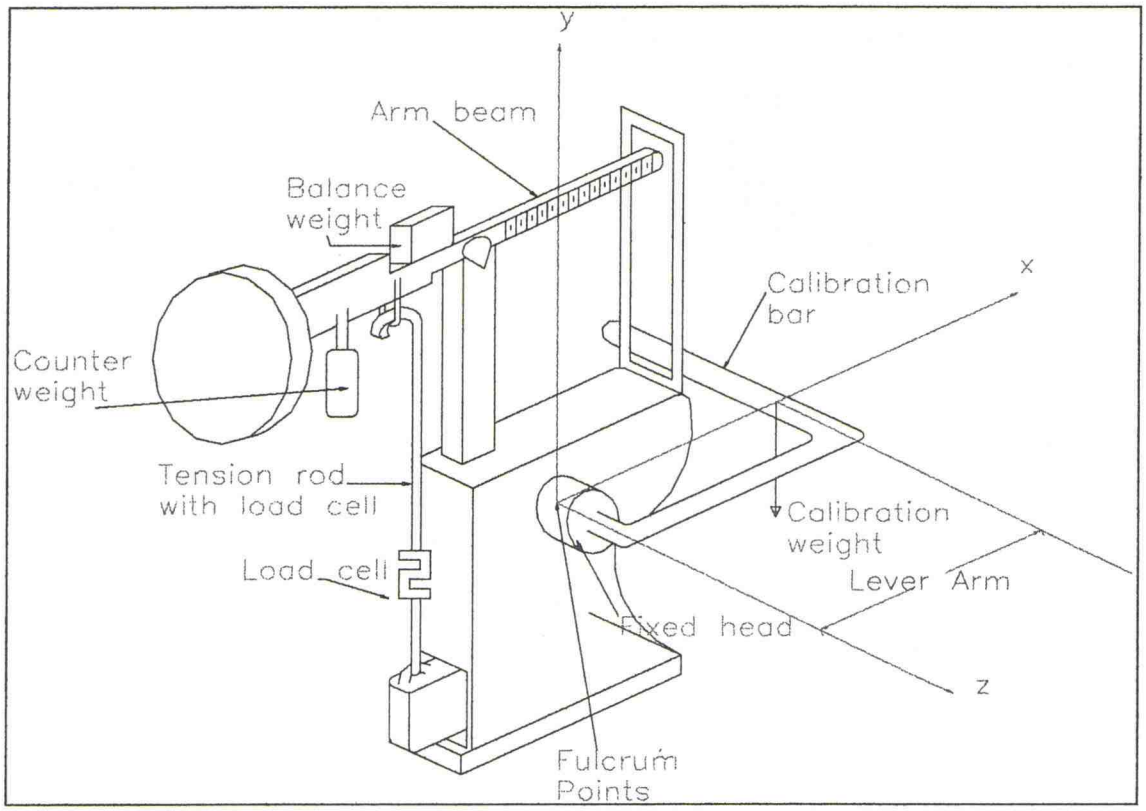

Figure B.3: Schematic of calibration set up of the torsion machine

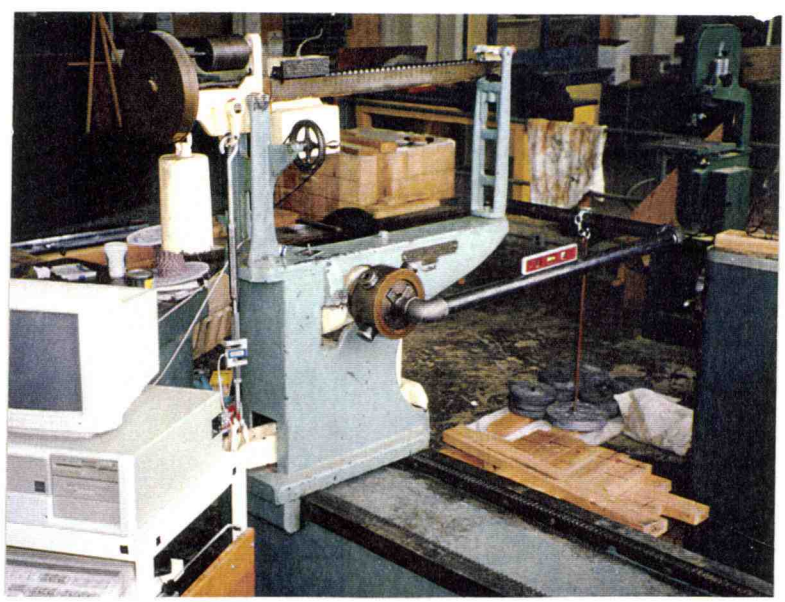

Figure B.4: Calibration set up for torsion machine

The rod remains in the x-z plane during the calibration; in other words the rod does not deflect along the y-axis. To avoid a moment about the x-axis, the calibration weight is applied along the z-axis at a distance of zero and along the x-axis at a lever arm distance, L. The origin of the axes is chosen such that it corresponds to the fulcrum points inside the torsion machine. The fulcrum points at the origin are the main mechanisms which transfer the torque to the tension rod as a tension force. As described in Appendix A, the torque transfer occurs from the fixed head to the tension rod via a series of lever arms and fulcrum points. The moment applied to the machine via the calibration weights (W) is referred to as the applied torque, $T_{applied}$; this torque value is determined by Equation B.1, obtained from statics where L is the lever arm distance as shown in Figure B.3 and W is the applied weight. This applied torque value should match with the torque value read from the arm beam of the machine. Several applied torque values were calculated and recorded with the corresponding torque reading values read from the arm beam of the machine. If the torsion machine is calibrated correctly, the applied torque values should fall on the same line as the torque reading values.

$$T_{applied} = L(W) \tag{B.1}$$

Figure B.5 displays the relationship between the applied weight, the applied torque, and the torque reading. The torque reading values are approximately 7% higher than the applied torque.

This calibration procedure was performed initially on September 12, 1996 prior to the depth study, and again on December 20, 1996 after the length study. The September calibration results were very similar to the December calibration results. Therefore, the following formula, Equation B.2, should be used to translate the torque values read from the machine ($T_{machine}$) to the actual torque values applied to the specimen, T_{actual}. It is imperative that this calibration rod be level since a deflection along the y-axis would change the lever arm used in Equation B.1. A level rod allows for the determination of the lever arm with less error than for a deflected rod.

$$T_{actual} = T_{machine}(0.929) \qquad \text{(B.2)}$$

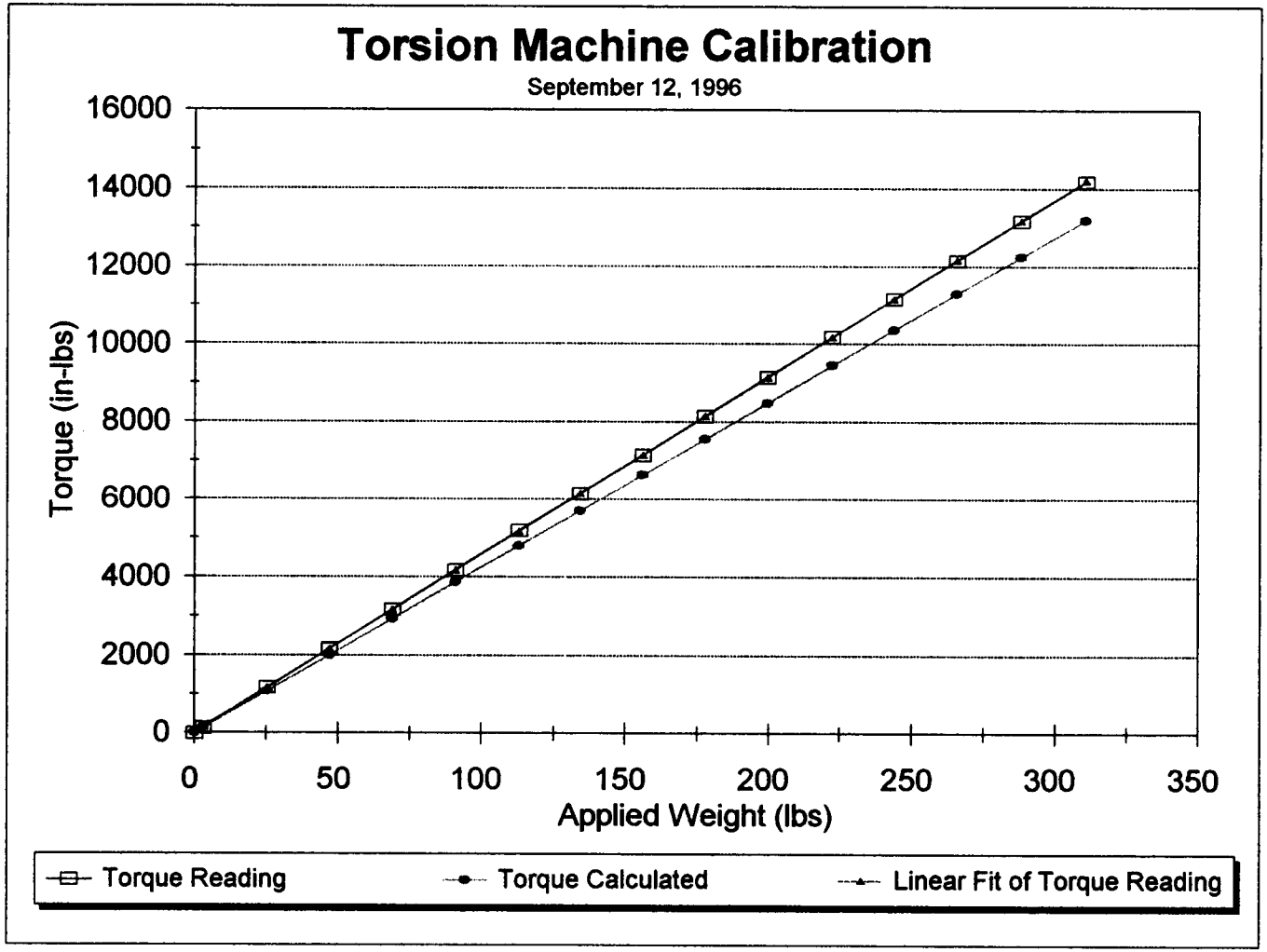

Figure B.5: Torsion machine calibration relationship

Appendix C
Data Reduction

C.1 Testing Procedure

Using the software, Labtech Notebook version 5.1.3, serial number 16422, with the ADAC data acquisition card, the voltage readings from the load cell and the string pot were recorded by the computer. The following outline presents the procedure used to collect the torque, rotation, and time data necessary for this research.

Testing Procedure

1. Zero balance beam of torsion machine by moving the counter weight, shown in Figure B.3. Make sure that the balance beam moves freely if touched, but if balanced the beam returns to the balanced position easily.
2. Recall data acquisition setup file: ZEROSPEC
3. The setup file, ZEROSPEC, will record data for 3 minutes at 5 hertz. This is the zero reading for the specimen. This data will determine the zero voltage from the load cell used for zero torque and the zero voltage from the string pot used for zero rotation. The data is saved as the file zs@_&.prn[1] .
4. Choose specimen to test.

---

[1] In the file name: @ = date (mmdd), & = number (this allows only ten specimens to be tested per day without overwriting the previously saved files #0-9). File name change must be made if more than ten specimens are to be tested in one day.

5. Recall data acquisition setup file: SPECIMEN
6. Place specimen in grips and tighten. Be sure to allow for unrestrained warping; thus do not over tighten the grips.
7. Begin collecting data with the computer before turning on the motor.
8. After a minute, turn on the motor and collect data for 14 additional minutes at 2 hertz. For this research, the motor should be set at the lowest speed to ensure that the specimen failure time will be between five and twenty minutes. The data will be saved as SIZE@_&.prn.[1] Do not attempt to balance the arm balance while administering the test.
9. Stop collecting data.
10. Reverse the motor to return the grips back to the initial position.
11. Remove the specimen.
12. Repeat steps 1-11 for the next 9 specimens. Note: Step 1 may not need to be repeated. If the balance beam freely floats to the balanced position then do not change the position of the counter weight from its initial position established in Step 1.

---

[1] In the file name: SIZE=the appropriate size value the operator must type in the file name in the file line of Labtech command windows (2x4, 2x6, 2x8, 2x10, or 2x12), @ = date (mmdd), & = number (this allows only ten specimens to be tested per day without overwriting the previously saved files #0-9). File name change must be made if more than ten specimens are to be tested in one day.

C.2 Data Reduction

After collecting the necessary data using the procedure outlined above, the data must be reduced to convert the voltage data collected to the corresponding torque and rotation values. The calibration results are used to reduce the collected voltage data. The following is the procedure used to reduce the data for this research.

Data Reduction

1. Average the zero torque voltages from the setup file ZEROSPEC. This average value is the voltage which will correspond to zero torque on the specimen.
2. Use the average zero voltage from step 1 to determine the y-intercept of the load cell calibration equation obtained from Appendix B, Calibration. The slope of this equation never changes but the y-intercept changes as the zero voltage for torque changes with each specimen.
3. Convert "torque" voltages to actual torque values with the load cell calibration equation.
4. Repeat steps 1 and 2 using the string pot calibration equation obtained from Appendix B, Calibration.
5. Convert "rotation" voltages to actual degrees of rotation with the string pot calibration equation obtained from Appendix B, Calibration.
6. Record the maximum positive torque value.

7. The time difference from zero torque to the maximum positive torque value indicates the time to failure. Use the zero torque value obtained after turning on the motor.
8. The rotation rate can also be determined during the time to failure span, assuming the rate is linear the rate equals the change in degrees divided by the change in time.

Typical plots after data reduction, for the Douglas-fir specimens tested in this study, are shown in Figure C.1, for a torque-time relationship, and Figure C.2, for a torque-rotation relationship.

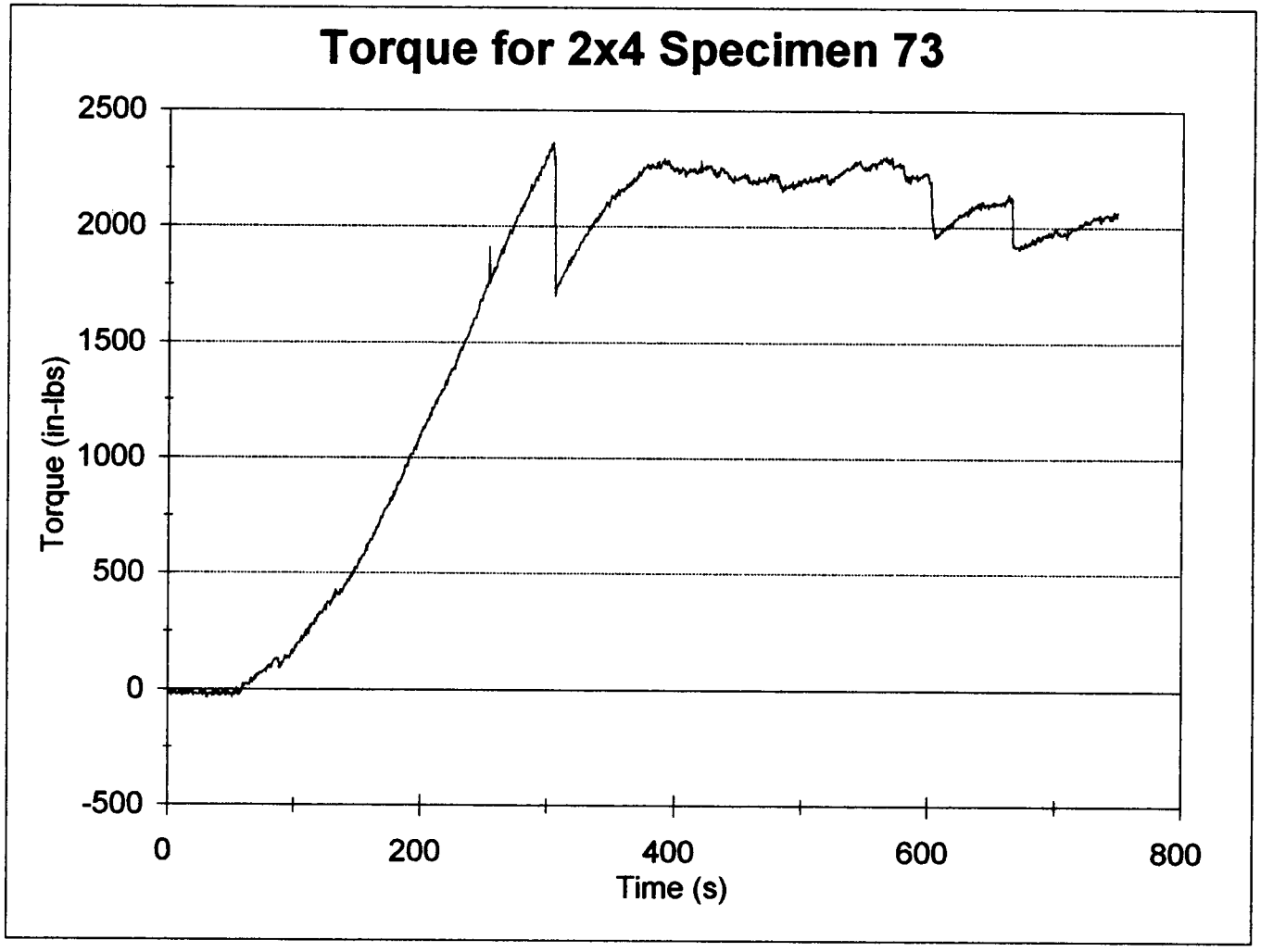

Figure C.1: Typical torque-time relationship after data reduction

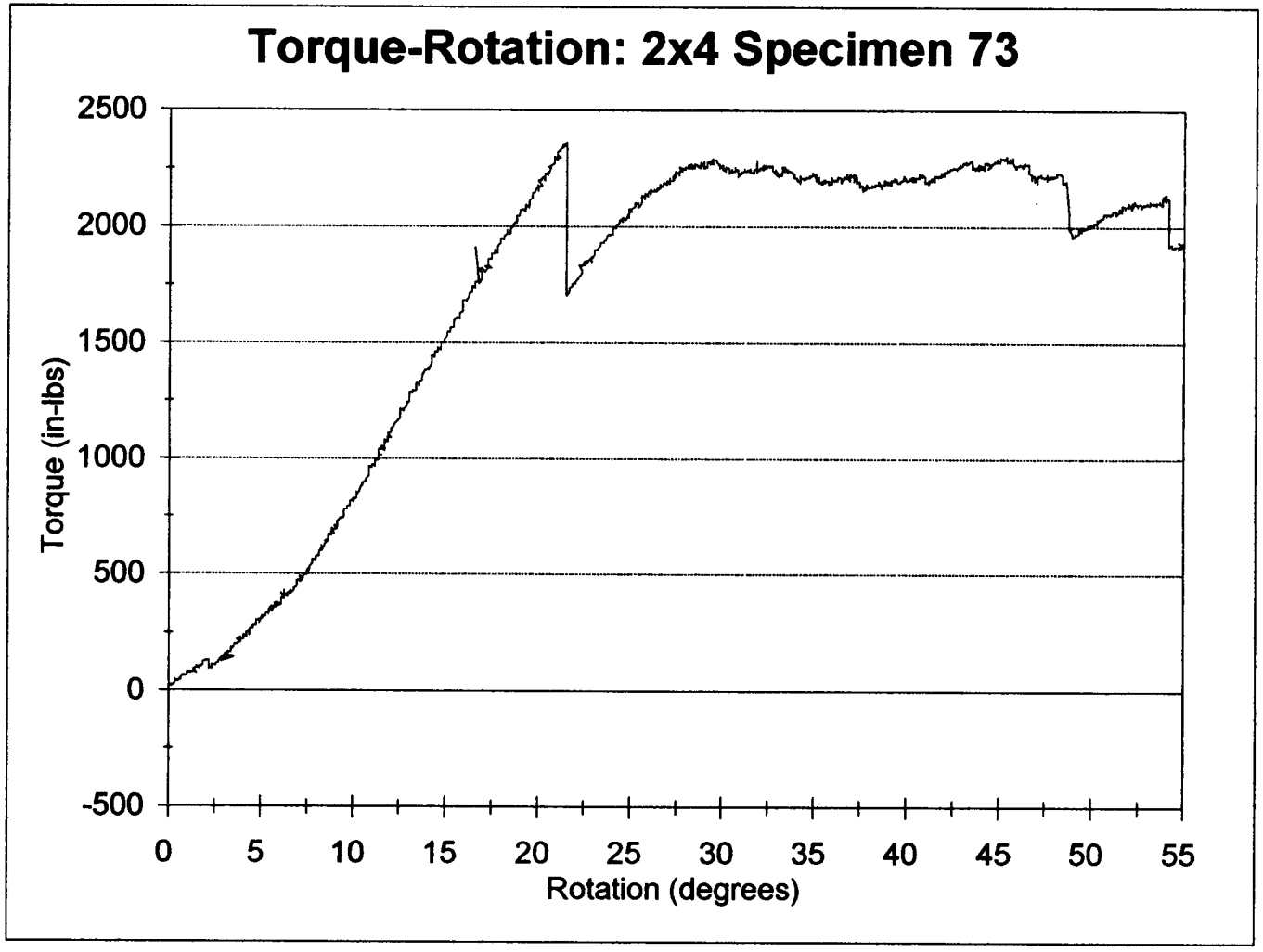

Figure C.2: Typical torque-rotation relationship after data reduction

Appendix D
Length Study Data

D.1 Identification code for the length study data

- MOE= the modulus of elasticity.
- Ratio= the ratio of beam depth to width. This ratio is used to determine the geometric factors in the Torsion equations, Equation 3.9.
- MC= the moisture content of the specimen at testing.
- SG= the specific gravity of the specimen.
- Calibrated Max Torque= the applied torque as calibrated according to Appendix B.
- Rotation angle= the amount of rotation of the specimen.
- Time to failure= length of time until initial shear failure occurred.
- Rate= the applied strain rate to the specimen.
- Gamma= γ, a geometric factor used in the torsion equations, Equation 3.9.
- Mu=μ, a geometric factor used in the torsion equations, Equation 3.9.
- SS or Shear stress= the shear stress as calculated using the calculated maximum torque and Equation 3.9.
- Adjusted SS for 12%= the shear stress adjusted to the standard moisture content of 12% according to ASTM D 1990-95 (ASTM 1996e).
- Gamma 1= γ_1, a geometric factor used in the torsion equations, Equation 3.9.

Length Effect on Torsion Specimens

Specimen No.		MOE	Specimen Size/Weight: Length	Width	Depth	Weight	MC	SG	Torsion Results: Max Torque	Calibrated Torque	Rotation Angle	Time to failure	Rate
		(X 10^6 psi)	(in)	(in)	(in)	(lbs)	(%)	---	(in-lb)	(in-lb)	(degrees)	(min)	(deg/in/min)
25	1d	1.92	21.5	1.510	3.510	1.946	11.0	0.45	2360	2192	19	2.1	0.43
13	1d	1.97	21.5	1.498	3.491	2.046	13.0	0.46	2707	2514	24	2.8	0.43
5	1d	1.92	21.5	1.500	3.498	2.232	12.8	0.50	3457	3211	20	3.0	0.33
42	1d	1.91	21.5	1.500	3.505	1.922	11.7	0.45	2659	2470	17	2.4	0.34
7	1d	1.94	21.5	1.503	3.505	2.088	11.7	0.48	3331	3094	17	2.3	0.36
26	1d	1.89	21.5	1.504	3.500	2.390	11.6	0.54	4429	4114	19	2.5	0.36
29	1d	1.88	21.5	1.501	3.499	2.342	13.1	0.54	2807	2607	16	2.2	0.33
17	1d	1.98	21.5	1.495	3.488	2.102	13.7	0.50	3677	3415	34	4.3	0.37
47	1d	1.91	21.5	1.488	3.478	2.000	13.8	0.46	3023	2808	23	2.9	0.4
28	1d	1.87	21.5	1.497	3.500	2.216	12.0	0.50	3207	2979	15	1.9	0.38
Avg:		1.92		1.50	3.50	2.13	12.44	0.49	3165.70	2940.38	20.40	2.6	0.37
COV (%):		1.88		0.39	0.26	7.57	7.76	7.10	18.94	18.94	27.36	26.3	9.96

Specimen No.		Rings per Inch	Shear Stress--SS-- (Middle Point of Long Side): Gamma	Mu	SS	Adjusted SS for 12%	Shear Stress--SS-- (Middle Point of Short Side): Gamma 1	Mu	SS	Adjusted SS for 12%
					(psi)	(psi)			(psi)	(psi)
25	1d	4.5	1.9153	3.8893	1079	1063	0.6431	3.8893	842	830
13	1d	7	1.9153	3.8893	1265	1285	0.6431	3.8893	990	1006
5	1d	7	1.9153	3.8893	1608	1628	0.6431	3.8893	1259	1274
42	1d	4	1.9153	3.8893	1234	1228	0.6431	3.8893	968	964
7	1d	10	1.9153	3.8893	1541	1533	0.6431	3.8893	1207	1201
26	1d	6	1.9153	3.8893	2047	2037	0.6431	3.8893	1600	1591
29	1d	7	1.9153	3.8893	1303	1324	0.6431	3.8893	1020	1036
17	1d	6.5	1.9153	3.8893	1727	1770	0.6431	3.8893	1353	1387
47	1d	6	1.9153	3.8893	1437	1476	0.6431	3.8893	1128	1159
28	1d	9	1.9153	3.8893	1496	1496	0.6431	3.8893	1174	1174
Avg:		6.70			1473.61	1483.99			1154.05	1162.18
COV (%):		27.07			18.97	19.04			18.93	19.00

Length Effect on Torsion Specimens

Specimen No.		MOE	Specimen Size/Weight: Length	Width	Depth	Weight	MC	SG	Torsion Results: Max Torque	Calibrated Torque	Rotation Angle	Time to failure	Rate
		(X 10^6 psi)	(in)	(in)	(in)	(lbs)	(%)	---	(in-lb)	(in-lb)	(degrees)	(min)	(deg/in/min)
5	2d	1.92	25.0	1.492	3.494	2.596	13.3	0.52	3461	3215	31	4.0	0.28
29	2d	1.88	25.0	1.487	3.489	2.686	13.2	0.52	3155	2930	23	2.9	0.29
7	2d	1.94	25.0	1.502	3.505	2.356	11.7	0.46	2880	2675	17	2.1	0.29
25	2d	1.92	25.0	1.503	3.511	2.392	11.1	0.47	2539	2358	19	2.3	0.29
17	2d	1.98	25.0	1.494	3.485	2.530	13.6	0.50	3200	2972	32	4.8	0.23
13	2d	1.97	25.0	1.493	3.488	2.522	13.2	0.49	3427	3183	25	3.8	0.24
28	2d	1.87	25.0	1.498	3.506	2.510	11.9	0.49	2981	2769	17	2.6	0.24
47	2d	1.91	25.0	1.492	3.469	2.438	13.9	0.49	3914	3635	42	6.0	0.25
42	2d	1.91	25.0	1.499	3.506	2.214	11.5	0.44	3456	3210	27	3.8	0.25
26	2d	1.89	25.0	1.502	3.505	2.544	11.9	0.49	3459	3213	30	4.2	0.25
Avg:		1.92		1.50	3.50	2.48	12.53	0.49	3247.20	3016.08	26.30	3.6	0.26
COV (%):		1.88		0.37	0.38	5.39	8.09	5.00	11.83	11.83	29.83	33.3	9.11

Specimen No.		Rings per Inch	Shear Stress--SS-- (Middle Point of Long Side): Gamma	Mu	SS	Adjusted SS for 12%	Shear Stress--SS-- (Middle Point of Short Side): Gamma 1	Mu	SS	Adjusted SS for 12%
					(psi)	(psi)			(psi)	(psi)
5	2d	7.5	1.9153	3.8893	1629	1660	0.6431	3.8893	1281	1305
29	2d	5	1.9153	3.8893	1497	1524	0.6431	3.8893	1180	1201
7	2d	8	1.9153	3.8893	1332	1326	0.6431	3.8893	1044	1039
25	2d	4.5	1.9153	3.8893	1171	1155	0.6431	3.8893	918	906
17	2d	6	1.9153	3.8893	1505	1541	0.6431	3.8893	1178	1207
13	2d	6.5	1.9153	3.8893	1614	1643	0.6431	3.8893	1266	1289
28	2d	9	1.9153	3.8893	1387	1386	0.6431	3.8893	1090	1089
47	2d	6.5	1.9153	3.8893	1854	1909	0.6431	3.8893	1447	1490
42	2d	4	1.9153	3.8893	1606	1594	0.6431	3.8893	1262	1252
26	2d	6	1.9153	3.8893	1600	1597	0.6431	3.8893	1253	1251
Avg:		6.30			1519.53	1533.67			1192.01	1203.09
COV (%):		24.87			12.44	13.48			12.34	13.38

Length Effect on Torsion Specimens

Specimen No.		MOE	Specimen Size/Weight: Length	Width	Depth	Weight	MC	SG	Torsion Results: Max Torque	Calibrated Torque	Rotation Angle	Time to failure	Rate
		(X 10^6 psi)	(in)	(in)	(in)	(lbs)	(%)	---	(in-lb)	(in-lb)	(degrees)	(min)	(deg/in/min)
17	3d	1.98	28.5	1.498	3.495	2.846	13.5	0.50	3558	3305	34	4.3	0.27
26	3d	1.89	28.5	1.501	3.504	2.810	11.6	0.49	3657	3397	21	3.2	0.22
28	3d	1.87	28.5	1.501	3.508	2.814	11.5	0.50	3161	2936	21	3.0	0.23
13	3d	1.97	28.5	1.502	3.495	2.570	12.5	0.46	2991	2778	25	3.4	0.23
7	3d	1.94	28.5	1.505	3.515	2.758	11.3	0.47	3199	2971	27	3.6	0.23
47	3d	1.91	28.5	1.484	3.472	2.632	14.1	0.49	3429	3185	34	4.5	0.23
42	3d	1.91	28.5	1.496	3.507	2.576	11.9	0.45	2791	2592	21	2.8	0.24
29	3d	1.88	28.5	1.494	3.491	2.988	13.0	0.55	3210	2982	28	3.7	0.24
5	3d	1.92	28.5	1.500	3.504	2.930	12.1	0.51	3798	3528	31	4.0	0.25
25	3d	1.92	28.5	1.504	3.509	2.720	11.1	0.46	2639	2451	20	2.5	0.25
Avg:		1.92		1.50	3.50	2.76	12.27	0.49	3243.30	3012.46	26.20	3.5	0.24
COV (%):		1.88		0.41	0.35	5.14	8.10	5.91	11.52	11.52	20.89	18.3	6.06

Specimen No.		Rings per Inch	Shear Stress--SS-- (Middle Point of Long Side): Gamma	Mu	SS	Adjusted SS for 12%	Shear Stress--SS-- (Middle Point of Short Side): Gamma 1	Mu	SS	Adjusted SS for 12%
					(psi)	(psi)			(psi)	(psi)
17	3d	6.5	1.9153	3.8893	1661	1699	0.6431	3.8893	1301	1331
26	3d	6.5	1.9153	3.8893	1695	1685	0.6431	3.8893	1329	1321
28	3d	7	1.9153	3.8893	1464	1455	0.6431	3.8893	1150	1142
13	3d	7	1.9153	3.8893	1389	1400	0.6431	3.8893	1085	1094
7	3d	11	1.9153	3.8893	1471	1456	0.6431	3.8893	1153	1142
47	3d	6	1.9153	3.8893	1641	1694	0.6431	3.8893	1289	1331
42	3d	4	1.9153	3.8893	1301	1299	0.6431	3.8893	1024	1022
29	3d	4.5	1.9153	3.8893	1508	1531	0.6431	3.8893	1183	1201
5	3d	6	1.9153	3.8893	1763	1765	0.6431	3.8893	1384	1385
25	3d	5	1.9153	3.8893	1217	1201	0.6431	3.8893	953	941
Avg:		6.35			1510.91	1518.40			1185.09	1190.97
COV (%):		30.39			11.81	12.47			11.82	12.48

Length Effect on Torsion Specimens

Specimen No.		MOE	Specimen Size/Weight: Length	Width	Depth	Weight	MC	SG	Torsion Results: Max Torque	Calibrated Torque	Rotation Angle	Time to failure	Rate
		(X 10^6 psi)	(in)	(in)	(in)	(lbs)	(%)	---	(in-lb)	(in-lb)	(degrees)	(min)	(deg/in/min)
29	4d	1.88	32.0	1.486	3.494	3.376	13.2	0.52	3151	2927	25	3.3	0.22
5	4d	1.92	32.0	1.496	3.489	3.344	12.9	0.51	3737	3471	33	3.9	0.24
25	4d	1.92	32.0	1.499	3.504	3.030	10.9	0.46	2412	2240	27	3.2	0.24
7	4d	1.94	32.0	1.498	3.502	3.044	11.6	0.47	2781	2583	26	3.0	0.25
47	4d	1.91	32.0	1.492	3.464	3.064	13.7	0.50	3780	3511	44	4.9	0.26
42	4d	1.91	32.0	1.494	3.501	2.730	11.2	0.43	3431	3187	31	3.5	0.25
28	4d	1.87	32.0	1.494	3.501	3.246	11.5	0.50	2630	2443	27	3.0	0.26
17	4d	1.98	32.0	1.489	3.481	3.170	13.5	0.49	3088	2868	33	3.5	0.27
26	4d	1.89	32.0	1.496	3.499	3.528	11.6	0.55	4020	3734	29	3.1	0.27
13	4d	1.97	32.0	1.489	3.474	3.238	13.4	0.51	2891	2685	26	2.7	0.28
Avg:		1.92		1.49	3.49	3.18	12.35	0.49	3192.10	2964.90	30.10	3.4	0.25
COV (%):		1.88		0.29	0.39	7.05	8.78	6.73	16.78	16.78	18.89	17.9	6.99

Specimen No.		Rings per Inch	Shear Stress--SS-- (Middle Point of Long Side): Gamma	Mu	SS	Adjusted SS for 12%	Shear Stress--SS-- (Middle Point of Short Side): Gamma 1	Mu	SS	Adjusted SS for 12%
					(psi)	(psi)			(psi)	(psi)
29	4d	5	1.9153	3.8893	1494	1521	0.6431	3.8893	1179	1201
5	4d	8	1.9153	3.8893	1752	1775	0.6431	3.8893	1372	1390
25	4d	4	1.9153	3.8893	1121	1103	0.6431	3.8893	880	866
7	4d	7	1.9153	3.8893	1295	1286	0.6431	3.8893	1016	1009
47	4d	7	1.9153	3.8893	1794	1841	0.6431	3.8893	1399	1436
42	4d	4	1.9153	3.8893	1607	1588	0.6431	3.8893	1265	1249
28	4d	9	1.9153	3.8893	1232	1223	0.6431	3.8893	969	962
17	4d	6	1.9153	3.8893	1464	1497	0.6431	3.8893	1149	1175
26	4d	6	1.9153	3.8893	1879	1868	0.6431	3.8893	1476	1467
13	4d	6.5	1.9153	3.8893	1374	1403	0.6431	3.8893	1077	1099
Avg:		6.25			1501.18	1510.55			1178.27	1185.60
COV (%):		25.92			16.92	17.43			16.81	17.31

Length Effect on Torsion Specimens

Specimen No.		MOE	Specimen Size/Weight: Length	Width	Depth	Weight	MC	SG	Torsion Results: Max Torque	Calibrated Torque	Rotation Angle	Time to failure	Rate
		(X 10^6 psi)	(in)	(in)	(in)	(lbs)	(%)	---	(in-lb)	(in-lb)	(degrees)	(min)	(deg/in/min)
28	5d	1.87	35.5	1.498	3.502	3.592	11.8	0.50	3313	3077	25	2.6	0.25
42	5d	1.91	35.5	1.499	3.506	3.330	12.1	0.46	2695	2503	27	3.0	0.25
47	5d	1.91	35.5	1.497	3.476	3.402	14.1	0.49	3485	3237	45	4.6	0.25
13	5d	1.97	35.5	1.500	3.493	3.444	13.2	0.49	2492	2315	36	4.1	0.23
29	5d	1.88	35.5	1.495	3.495	3.690	13.6	0.52	3064	2846	26	3.2	0.2
25	5d	1.92	35.5	1.500	3.499	2.322	11.7	0.57	2769	2572	31	3.6	0.22
7	5d	1.94	35.5	1.497	3.491	2.754	11.5	0.52	4129	3835	27	3.4	0.23
26	5d	1.89	35.5	1.495	3.494	3.278	11.8	0.55	3954	3673	24	2.8	0.23
5	5d	1.92	35.5	1.492	3.485	3.722	12.9	0.57	4099	3807	34	4.3	0.21
17	5d	1.98	35.5	1.492	3.485	3.722	12.1	0.52	3551	3298	43	2.2	0.21
Avg:		1.92		1.50	3.49	3.33	12.47	0.52	3355.10	3116.30	31.80	3.38	0.23
COV:		1.88		0.20	0.25	13.72	7.20	6.90	17.71	17.71	23.66	22.95	7.95

Specimen No.		Rings per Inch	Shear Stress--SS-- (Middle Point of Long Side): Gamma	Mu	SS	Adjusted SS for 12%	Shear Stress--SS-- (Middle Point of Short Side): Gamma 1	Mu	SS	Adjusted SS for 12%
					(psi)	(psi)			(psi)	(psi)
28	5d	8	1.9153	3.8893	1542	1538	0.6431	3.8893	1211	1207
42	5d	5	1.9153	3.8893	1253	1255	0.6431	3.8893	984	986
47	5d	6.5	1.9153	3.8893	1637	1688	0.6431	3.8893	1276	1316
13	5d	6	1.9153	3.8893	1160	1181	0.6431	3.8893	907	923
29	5d	4.5	1.9153	3.8893	1435	1469	0.6431	3.8893	1126	1153
25	5d	4.5	1.9153	3.8893	1287	1281	0.6431	3.8893	1008	1003
7	5d	5.5	1.9153	3.8893	1932	1917	0.6431	3.8893	1513	1501
26	5d	5.5	1.9153	3.8893	1853	1847	0.6431	3.8893	1454	1450
5	5d	7	1.9153	3.8893	1933	1960	0.6431	3.8893	1516	1537
17	5d	6	1.9153	3.8893	1675	1678	0.6431	3.8893	1314	1316
Avg:		5.85			1570.68	1581.36			1230.92	1239.27
COV:		18.92			18.09	17.86			18.11	17.87

Length Effect of Torsion Specimens: ASTM (1996a) Small Clear Block Specimens

Specimen No.	MOE	Shearing Area Length	Shearing Area Width	MC	SG	Shear Results Max Load	Shear Results Speed of testing	Shear Stress SS	Shear Stress Adjusted SS 12 %
	(psi)	(in)	(in)	(%)	—	(lbs)	(in/min)	(psi)	(psi)
5	1.92	2.0075	1.9895	12.82	0.53	4650	0.024	1164	1178
7	1.94	2.0025	1.9915	11.03	0.49	3820	0.024	958	944
13	1.97	2.0010	1.9915	12.58	0.45	4490	0.024	1127	1137
17	1.98	2.0015	1.9950	13.73	0.49	4940	0.024	1237	1270
25	1.92	1.9960	1.9890	10.98	0.46	4310	0.024	1086	1069
26	1.89	2.0020	1.9990	11.14	0.47	5030	0.024	1257	1241
28	1.87	1.9990	1.9930	12.02	0.50	4820	0.024	1210	1210
29	1.88	2.0010	1.9915	13.19	0.50	5530	0.024	1388	1413
42	1.91	1.9970	1.9905	11.83	0.43	4960	0.024	1248	1245
47	1.91	1.9990	1.9900	13.43	0.44	5110	0.024	1285	1312
Avg:				12.27	0.48				1201.92
COV (%):				8.36	6.28				10.86

Appendix E
Depth Study Data

E.1 Identification code for the depth study data

- MOE= the modulus of elasticity.
- Ratio= the ratio of beam depth to width. This ratio is used to determine the geometric factors in the Torsion equations, Equation 3.9.
- MC= the moisture content of the specimen at testing.
- SG= the specific gravity of the specimen.
- Calibrated Max Torque= the applied torque as calibrated according to Appendix B.
- Rotation angle= the amount of rotation of the specimen.
- Time to failure= length of time until initial shear failure occurred.
- Rate= the applied strain rate to the specimen.
- Gamma= γ, a geometric factor used in the torsion equations, Equation 3.9.
- Mu=μ, a geometric factor used in the torsion equations, Equation 3.9.
- SS or Shear stress= the shear stress as calculated using the calculated maximum torque and Equation 3.9.
- Adjusted SS for 12%= the shear stress adjusted to the standard moisture content of 12% according to ASTM D 1990-95 (ASTM 1996e).
- Gamma 1= γ_1, a geometric factor used in the torsion equations, Equation 3.9.

- Specimen No.= the first number, which represents the specimen number, and the second number, which represents the board number. Therefore, two specimens that came from the same board will have individual first numbers, but similar second numbers. For example, 2x4 specimens 70, 69, and 78 came from the same board, 26. The following a, b, or c designation separates the specimens.

Depth Effect on Torsion Specimens

2x4

Specimen No.		MOE	Specimen Size/Weight: Length	Width	Depth	Ratio	Weight	MC	SG	Torsion Results: Calibrated Max Torque	Rotation Angle	Time to failure	Rate
		(X 10^6 psi)	(in)	(in)	(in)	of Sides	(lbs)	(%)	---	(in-lb)	(degrees)	(min)	(deg/in/min)
70	26a	1.74	27.9	1.528	3.411	2.2327	2.624	13.9	0.46	2917	28	3.8	0.27
69	26b	1.74	28.0	1.525	3.421	2.2434	2.572	13.6	0.48	2924	39	5.3	0.28
66	25b	1.60	28.0	1.513	3.435	2.2697	2.890	13.5	0.54	2937	23	2.9	0.29
87	1d	1.60	28.0	1.530	3.482	2.2750	3.542	13.0	0.64	3079	24	3.5	0.26
77	24b	1.60	27.9	1.531	3.439	2.2461	2.758	10.7	0.48	2856	32	4.4	0.27
78	26c	1.74	27.9	1.525	3.414	2.2393	2.594	14.1	0.46	2904	31	4.6	0.26
76	24a	1.74	27.9	1.521	3.436	2.2585	2.808	12.9	0.49	3101	25	5.0	0.19
72	3a,b	1.60	27.9	1.516	3.443	2.2717	2.694	13.0	0.50	2976	26	5.1	0.19
73	27a	1.74	27.9	1.523	3.466	2.2766	2.580	13.0	0.46	2194	22	4.1	0.19
80	2b	1.60	28.0	1.505	3.435	2.2816	2.786	13.3	0.51	2727	28	5.2	0.2
Avg:		1.67		1.52	3.44	2.26	2.78	13.09	0.50	2861.52	27.80	4.39	0.24
COV (%):		4.42		0.54	0.64	0.79	10.32	7.15	10.99	8.99	18.40	18.16	17.46

Specimen No.		Rings per Inch	Shear Stress--SS--(Middle Point of Long Side): Gamma	Mu	SS	Adjusted SS for 12%	Shear Stress--SS-- (Middle Point of Short Side): Gamma 1	Mu	SS	Adjusted SS for 12%
					(psi)	(psi)			(psi)	(psi)
70	26a	5	1.9153	3.8893	1443	1484	0.6431	3.8893	1082	1113
69	26b	5	1.9153	3.8893	1448	1483	0.6431	3.8893	1091	1117
66	25b	8	1.9153	3.8893	1471	1505	0.6431	3.8893	1121	1147
87	1d	13	1.9153	3.8893	1488	1510	0.6431	3.8893	1136	1153
77	24b	8	1.9153	3.8893	1395	1369	0.6431	3.8893	1052	1032
78	26c	5	1.9153	3.8893	1442	1487	0.6431	3.8893	1084	1118
76	24a	8	1.9153	3.8893	1537	1558	0.6431	3.8893	1166	1181
72	3a,b	5	1.9153	3.8893	1483	1505	0.6431	3.8893	1131	1148
73	27a	5	1.9153	3.8893	1076	1091	0.6431	3.8893	822	834
80	2b	8	1.9153	3.8893	1380	1408	0.6431	3.8893	1058	1079
Avg:		7.00			1416.38	1440.04			1074.37	1092.31
COV (%):		36.89			9.03	9.29			8.90	9.15

Depth Effect on Torsion Specimens

2x6

Specimen No.		MOE	Specimen Size/Weight: Length	Width	Depth	Ratio	Weight	MC	SG	Torsion Results: Calibrated Max Torque	Rotation Angle	Time to failure	Rate
		(X 10^6 psi)	(in)	(in)	(in)	of Sides	(lbs)	(%)	---	(in-lb)	(degrees)	(min)	(deg/in/min)
49	8a	1.85	44.0	1.518	5.446	3.5869	6.544	15.1	0.48	4468	38	6.24	0.13
51	4a	1.91	44.0	1.519	5.420	3.5691	6.694	12.6	0.48	3563	31	5.40	0.13
52	35a	1.85	44.0	1.507	5.468	3.6287	7.772	12.9	0.58	6327	35	5.78	0.13
53	22a	1.98	44.0	1.516	5.464	3.6050	7.246	13.4	0.53	4643	38	6.37	0.14
54	19b	1.91	44.0	1.523	5.420	3.5580	6.750	14.0	0.48	5671	44	7.30	0.14
55	22b	1.78	44.0	1.499	5.498	3.6671	7.336	13.3	0.51	5465	40	6.52	0.14
57	19a	1.85	44.0	1.519	5.404	3.5574	6.892	13.9	0.49	4523	47	7.44	0.15
62	23a	1.78	44.0	1.528	5.402	3.5362	8.002	13.8	0.59	5302	34	5.42	0.15
63	39a	1.85	44.0	1.528	5.505	3.6035	7.254	13.4	0.52	5735	41	6.36	0.15
64	64b	1.91	44.0	1.518	5.506	3.6274	7.174	13.1	0.52	6160	44	7.07	0.15
Avg:		1.87		1.52	5.45	3.59	7.17	13.55	0.52	5185.72	39.20	6.39	0.14
COV (%):		3.32		0.58	0.75	1.12	6.52	5.19	7.56	16.72	12.77	11.34	6.21

Specimen No.		Rings per Inch	Shear Stress--SS--(Middle Point of Long Side): Gamma	Mu	SS	Adjusted SS for 12%	Shear Stress--SS-- (Middle Point of Short Side): Gamma 1	Mu	SS	Adjusted SS for 12%
					(psi)	(psi)			(psi)	(psi)
49	8a	5	1.9882	4.3970	1287	1348	0.4155	4.3970	965	1011
51	4a	5	1.9882	4.3970	1031	1040	0.4155	4.3970	769	776
52	35a	10	1.9882	4.3970	1844	1867	0.4155	4.3970	1398	1416
53	22a	5.5	1.9882	4.3970	1338	1367	0.4155	4.3970	1008	1030
54	19b	8	1.9882	4.3970	1631	1682	0.4155	4.3970	1213	1251
55	22b	6	1.9882	4.3970	1600	1632	0.4155	4.3970	1226	1250
57	19a	7	1.9882	4.3970	1312	1349	0.4155	4.3970	975	1003
62	23a	5	1.9882	4.3970	1521	1563	0.4155	4.3970	1124	1155
63	39a	6	1.9882	4.3970	1615	1648	0.4155	4.3970	1216	1241
64	64b	6	1.9882	4.3970	1757	1786	0.4155	4.3970	1332	1354
Avg:		6.35			1493.56	1528.27			1122.73	1148.78
COV (%):		25.19			16.56	16.31			17.10	16.82

Depth Effect on Torsion Specimens

2x8

Specimen No.		MOE	Specimen Size/Weight: Length	Width	Depth	Ratio	Weight	MC	SG	Torsion Results: Calibrated Max Torque	Rotation Angle	Time to failure	Rate
		(X 10^6 psi)	(in)	(in)	(in)	of Sides	(lbs)	(%)	---	(in-lb)	(degrees)	(min)	(deg/in/min)
31	6b	1.82	55.0	1.523	7.251	4.7612	11.9640	13.0	0.50	7118	49	8.45	0.11
32	11b	2.01	55.0	1.488	7.333	4.9297	10.4500	13.4	0.52	6713	47	7.40	0.12
33	6a	2.01	55.0	1.522	7.291	4.7915	11.4500	13.4	0.48	6385	47	7.84	0.11
37	13b	1.89	55.1	1.521	7.230	4.7525	12.5840	13.0	0.54	8744	58	9.30	0.11
39	15a	1.78	55.0	1.505	7.311	4.8591	12.5160	13.5	0.53	7673	49	8.63	0.1
41	17a	2.01	55.0	1.522	7.357	4.8337	12.372	12.8	0.53	7660	47	8.08	0.11
42	36b	1.82	55.0	1.517	7.261	4.7856	11.792	12.5	0.52	8634	51	9.16	0.11
44	5a	2.05	55.0	1.502	7.238	4.8191	13.202	13.0	0.56	8203	53	9.14	0.11
45	36a	2.09	55.0	1.532	7.193	4.6965	11.934	12.8	0.53	6763	50	8.64	0.11
46	38a	2.01	55.0	1.522	7.278	4.7818	10.862	12.3	0.45	4431	45	7.59	0.11
Avg:		1.95		1.52	7.27	4.80	11.91	12.99	0.52	7232.39	49.60	8.42	0.11
COV (%):		5.68		0.87	0.69	1.33	6.95	3.07	6.15	17.63	7.56	8.03	4.29

Specimen No.		Rings per Inch	Shear Stress--SS--(Middle Point of Long Side): Gamma	Mu	SS	Adjusted SS for 12%	Shear Stress--SS-- (Middle Point of Short Side): Gamma 1	Mu	SS	Adjusted SS for 12%
					(psi)	(psi)			(psi)	(psi)
31	6b	6.5	1.9973	4.6661	1450	1472	0.3118	4.6661	1078	1094
32	11b	5	1.9973	4.6661	1417	1448	0.3118	4.6661	1090	1114
33	6a	6.5	1.9973	4.6661	1295	1323	0.3118	4.6661	969	989
37	13b	7.5	1.9973	4.6661	1789	1817	0.3118	4.6661	1328	1348
39	15a	23	1.9973	4.6661	1588	1625	0.3118	4.6661	1205	1232
41	17a	6	1.9973	4.6661	1539	1558	0.3118	4.6661	1162	1176
42	36b	6.5	1.9973	4.6661	1769	1782	0.3118	4.6661	1322	1331
44	5a	4	1.9973	4.6661	1721	1748	0.3118	4.6661	1295	1315
45	36a	6	1.9973	4.6661	1373	1390	0.3118	4.6661	1007	1019
46	38a	6	1.9973	4.6661	900	904	0.3118	4.6661	672	675
Avg:		7.70			1484.07	1506.54			1112.60	1129.49
COV (%):		70.88			17.96	18.00			18.02	18.09

Depth Effect on Torsion Specimens

2x10

Specimen No.		MOE	Specimen Size/Weight: Length	Width	Depth	Ratio	Weight	MC	SG	Torsion Results: Calibrated Max Torque	Rotation Angle	Time to failure	Rate
		(X 10^6 psi)	(in)	(in)	(in)	of Sides	(lbs)	(%)	---	(in-lb)	(degrees)	(min)	(deg/in/min)
16	12a	1.99	55.0	1.515	9.209	6.0792	13.530	13.3	0.46	7379	50	7.45	0.13
17	14b	1.80	55.0	1.521	9.277	6.0983	14.890	12.9	0.48	7053	38	4.92	0.14
18	10b	1.68	55.0	1.513	9.154	6.0525	17.056	12.9	0.58	7780	43	6.36	0.12
21	16b	2.22	55.0	1.526	9.305	6.0991	16.034	13.1	0.54	8629	58	8.53	0.13
23	16a	2.16	55.0	1.508	9.273	6.1490	16.580	13.2	0.57	9421	44	6.43	0.13
24	20a	1.89	55.0	1.511	9.308	6.1598	17.132	13.4	0.57	9800	49	6.95	0.13
25	20b	1.99	55.0	1.518	9.294	6.1245	17.412	13.4	0.57	8618	39	6.27	0.11
26	21a	1.89	55.0	1.513	9.147	6.0466	16.880	13.4	0.59	7998	46	7.44	0.11
28	33a	2.16	55.0	1.530	9.190	6.0052	14.980	12.9	0.51	8778	46	7.26	0.12
30	10a	2.16	55.0	1.513	9.177	6.0641	16.632	13.0	0.62	7816	40	6.27	0.12
Avg:		1.99		1.52	9.23	6.09	16.11	13.16	0.55	8327.10	45.30	6.79	0.12
COV (%):		9.03		0.46	0.70	0.79	7.78	1.63	9.46	10.54	13.29	14.30	7.79

Specimen No.		Rings per Inch	Shear Stress--SS--(Middle Point of Long Side): Gamma	Mu	SS	Adjusted SS for 12%	Shear Stress--SS-- (Middle Point of Short Side): Gamma 1	Mu	SS	Adjusted SS for 12%
					(psi)	(psi)			(psi)	(psi)
16	12a	5	1.9998	4.7803	1169	1192	0.2485	4.7803	883	901
17	14b	4	1.9998	4.7803	1100	1115	0.2485	4.7803	833	845
18	10b	7	1.9998	4.7803	1243	1261	0.2485	4.7803	935	948
21	16b	6	1.9998	4.7803	1333	1355	0.2485	4.7803	1011	1027
23	16a	6	1.9998	4.7803	1495	1521	0.2485	4.7803	1143	1163
24	20a	12	1.9998	4.7803	1543	1576	0.2485	4.7803	1182	1207
25	20b	13	1.9998	4.7803	1348	1376	0.2485	4.7803	1026	1048
26	21a	9	1.9998	4.7803	1279	1306	0.2485	4.7803	961	981
28	33a	9	1.9998	4.7803	1365	1384	0.2485	4.7803	1019	1033
30	10a	8	1.9998	4.7803	1245	1264	0.2485	4.7803	938	952
Avg:		7.90			1311.94	1334.93			988.00	1010.41
COV (%):		37.00			10.40	10.52			10.88	11.00

Depth Effect on Torsion Specimens

2x12

Specimen No.		MOE	Specimen Size/Weight: Length	Width	Depth	Ratio	Weight	MC	SG	Torsion Results: Calibrated Max Torque	Rotation Angle	Time to failure	Rate
		(X 10^6 psi)	(in)	(in)	(in)	of Sides	(lbs)	(%)	---	(in-lb)	(degrees)	(min)	(deg/in/min)
1	37a	2.02	55.0	1.486	11.180	7.5246	18.274	12.2	0.52	8874	43	6.88	0.12
4	7a	1.90	54.9	1.494	11.115	7.4408	17.888	13.4	0.50	9999	49	6.74	0.14
5	37b	1.90	55.0	1.474	11.200	7.5999	18.334	12.2	0.53	10061	40	5.37	0.14
6	7b	1.90	55.0	1.512	11.163	7.3835	17.864	13.1	0.49	11529	47	6.48	0.14
7	28a	1.90	55.0	1.491	11.162	7.4845	17.130	13.0	0.47	9768	54	8.17	0.12
8	28b	1.79	55.0	1.509	11.196	7.4180	17.578	13.2	0.49	10169	44	6.47	0.13
11	30a	1.90	55.0	1.500	11.184	7.4546	17.090	13.4	0.47	9306	51	7.38	0.13
12	29	2.16	55.0	1.503	11.127	7.4032	20.676	13.3	0.58	10811	38	5.37	0.13
14	31b	1.96	55.0	1.518	11.098	7.3102	19.098	13.0	0.55	10382	52	7.07	0.14
15	31a	1.96	55.0	1.521	11.110	7.3033	19.510	13.1	0.54	10730	42	5.75	0.14
Avg:		1.94		1.50	11.15	7.43	18.34	12.99	0.52	10164.78	46.00	6.57	0.13
COV (%):		5.05		1.00	0.34	1.23	6.15	3.39	6.97	7.51	11.77	13.58	6.19

Specimen No.		Rings per Inch	Shear Stress--SS--(Middle Point of Long Side): Gamma	Mu	SS	Adjusted SS for 12%	Shear Stress--SS-- (Middle Point of Short Side): Gamma 1	Mu	SS	Adjusted SS for 12%
					(psi)	(psi)			(psi)	(psi)
1	37a	8.5	2.0000	4.8790	1179	1183	0.2015	4.8790	894	897
4	7a	5	2.0000	4.8790	1322	1350	0.2015	4.8790	991	1012
5	37b	10	2.0000	4.8790	1359	1363	0.2015	4.8790	1041	1044
6	7b	5	2.0000	4.8790	1482	1506	0.2015	4.8790	1103	1120
7	28a	5	2.0000	4.8790	1290	1310	0.2015	4.8790	973	988
8	28b	5	2.0000	4.8790	1307	1332	0.2015	4.8790	977	995
11	30a	5	2.0000	4.8790	1212	1237	0.2015	4.8790	911	929
12	29	6	2.0000	4.8790	1410	1438	0.2015	4.8790	1052	1073
14	31b	4	2.0000	4.8790	1331	1351	0.2015	4.8790	981	995
15	31a	4	2.0000	4.8790	1369	1391	0.2015	4.8790	1007	1023
Avg:		5.75			1326.22	1346.01			993.02	1007.79
COV (%):		34.11			6.68	6.84			6.32	6.42

Depth Effect of Torsion Specimens: ASTM (1996a) Small Clear Block Specimen

Specimen	Shear Area				Shear Results		Shear Stress	
No.	Length	Width	MC	SG	Max Load	Speed of testing	SS	Adjusted SS 12 %
NEW	(in)	(in)	(%)	–	(lbs)	(in/min)	(psi)	(psi)
78	2.0010	1.9885	12.87	0.45	4810	0.024	1209	1225
70,69	2.0020	1.9970	12.37	0.47	4470	0.024	1118	1124
66	1.9985	1.9875	12.50	0.48	4120	0.024	1037	1045
87	2.0085	2.0015	12.47	0.54	4790	0.024	1192	1200
76,77	1.9995	1.9800	11.96	0.50	4920	0.024	1243	1242
72	2.0005	1.9990	11.42	0.50	4890	0.024	1223	1212
73	2.0070	1.9955	12.19	0.46	4910	0.024	1226	1229
80	1.9990	1.9900	12.54	0.47	4730	0.024	1189	1199
49	1.9995	1.9965	12.62	0.45	5100	0.024	1278	1289
51	2.0015	1.9935	13.07	0.52	4500	0.024	1128	1146
52	2.0035	1.9950	12.65	0.54	5280	0.024	1321	1334
53	2.0015	1.9950	12.86	0.50	4570	0.024	1145	1159
55	2.0010	1.9950	12.56	0.52	5280	0.024	1323	1334
54	2.0040	1.9950	13.34	0.49	4870	0.024	1218	1243
57	2.0020	1.9865	13.08	0.47	4150	0.024	1044	1060
62	2.0015	1.9875	13.22	0.61	6530	0.024	1642	1672
63	2.0020	1.9950	13.15	0.51	5350	0.024	1340	1363
64	2.0050	1.9925	12.58	0.46	4960	0.024	1242	1252
31,33	2.0000	1.9925	12.03	0.47	4830	0.024	1212	1213
32	2.0020	1.9950	12.50	0.48	5620	0.024	1407	1418
37	2.0010	1.9850	12.07	0.54	5440	0.024	1370	1371
39	2.0050	1.9900	13.08	0.52	5050	0.024	1266	1286
41	2.0000	1.9890	12.26	0.51	5500	0.024	1383	1388
45	1.9990	1.9880	12.36	0.51	4780	0.024	1203	1209
42	2.0025	1.9900	12.10	0.53	5860	0.024	1471	1473
44	2.0020	1.9870	12.43	0.54	5680	0.024	1428	1437
46	2.0075	1.9925	12.21	0.43	4410	0.024	1103	1106
16	2.0035	1.9890	12.89	0.45	3830	0.024	961	974
17	1.9980	1.9960	11.52	0.43	4160	0.024	1043	1036
23	2.0005	1.9840	12.90	0.55	5900	0.024	1487	1507
21	1.9995	1.9930	12.34	0.49	4640	0.024	1164	1170
24	2.0005	1.9955	12.80	0.59	6190	0.024	1551	1569
25	2.0005	1.9915	12.25	0.58	5660	0.024	1421	1426
26	2.0035	1.9935	12.51	0.55	5380	0.024	1347	1357
28	2.0020	1.9750	11.86	0.50	4440	0.024	1123	1121
30	2.0025	1.9970	12.41	0.49	5490	0.024	1373	1381
18	2.0065	1.9975	12.44	0.60	5440	0.024	1357	1366
1	2.0030	1.9905	12.33	0.53	5140	0.024	1289	1295
5	2.0055	1.9915	11.29	0.51	5330	0.024	1335	1321
4	2.0025	1.9895	12.72	0.50	5430	0.024	1363	1378
6	2.0040	1.9975	12.20	0.48	4970	0.024	1242	1245
7	1.9975	2.0060	12.47	0.45	4620	0.024	1153	1161
8	2.0005	1.9965	12.08	0.48	4590	0.024	1149	1151
11	2.0080	1.9915	12.71	0.54	6170	0.024	1543	1559
12	2.0015	1.9915	12.59	0.59	4780	0.024	1199	1210
15	2.0025	1.9940	12.84	0.57	6910	0.024	1731	1752
14	1.9995	1.9960	12.00	0.53	5790	0.024	1451	1451
Avg:			12.46	0.51			1281.61	1290.57
COV (%):			3.61	8.81			12.56	12.71